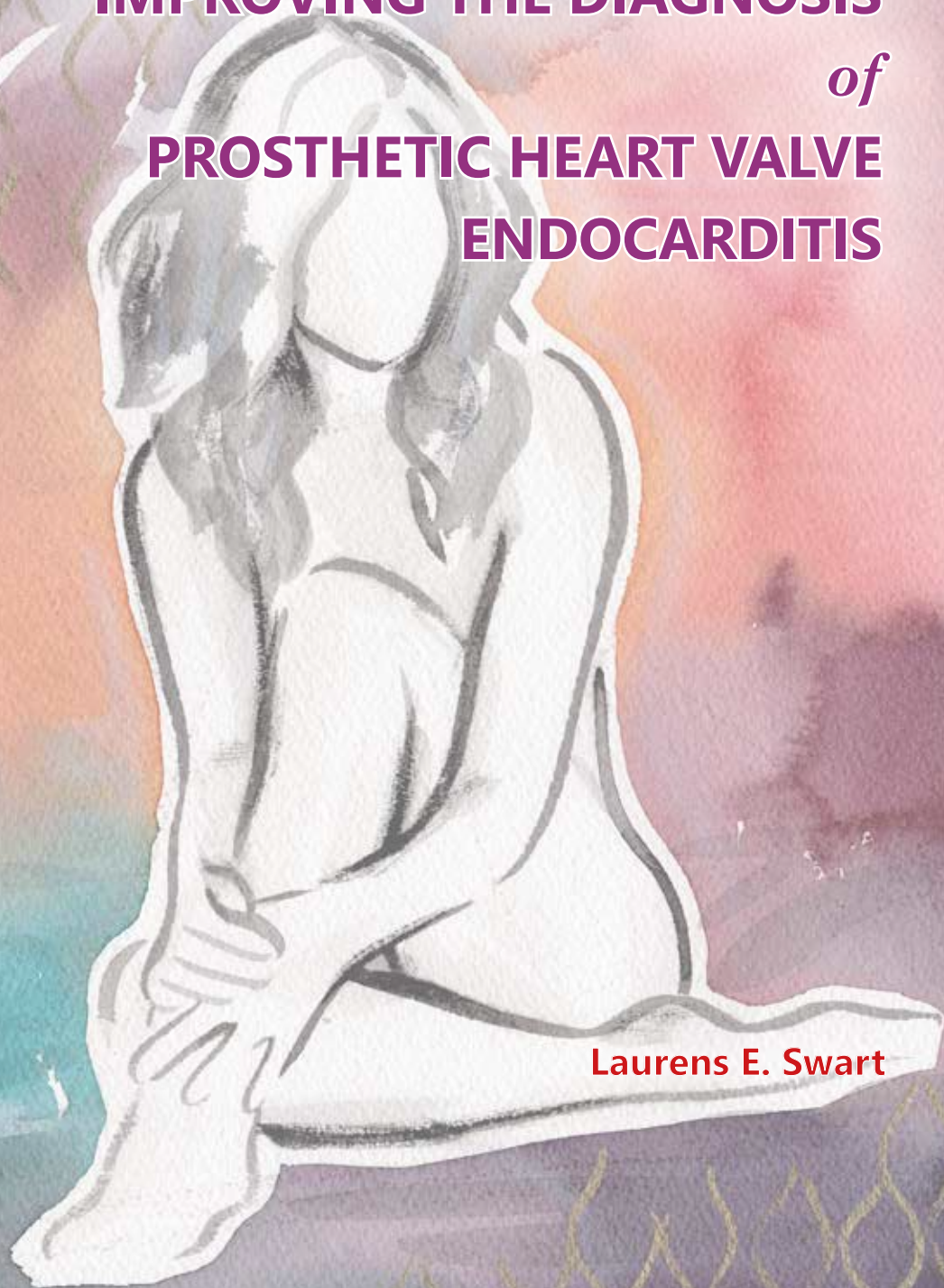


IMPROVING THE DIAGNOSIS
of
PROSTHETIC HEART VALVE
ENDOCARDITIS



Laurens E. Swart

IMPROVING THE DIAGNOSIS *of* **PROSTHETIC HEART VALVE** **ENDOCARDITIS**

Verbetering van de diagnose van kunstklependocarditis

Laurens E. Swart

Improving the Diagnosis of Prosthetic Heart Valve Endocarditis

Printing: ProefschriftMaken | www.proefschriftmaken.nl

Layout/design: Maarten E. Swart

Cover/art: Simone Endert



ISBN: 978-94-6380-321-2



© 2019 - Copyright, Laurens E. Swart
All rights reserved. No parts of this thesis may be reproduced, distributed, stored in a retrieval system or transmitted in any form or by any means without prior permission from the author.

IMPROVING THE DIAGNOSIS *of* PROSTHETIC HEART VALVE ENDOCARDITIS

Verbetering van de diagnose van kunstklependocarditis

Proefschrift

ter verkrijging van de graad van doctor aan de
Erasmus Universiteit Rotterdam
op gezag van de rector magnificus

prof.dr. R.C.M.E. Engels

en volgens besluit van het College voor Promoties.
De openbare verdediging zal plaatsvinden op
4 juni 2019 om 11:30 uur

door

Laurens E. Swart
geboren te Deventer

Promotoren: prof.dr. G.P. Krestin
prof.dr. J.W. Roos-Hesselink

Overige leden: prof.dr. R.H.J.A. Slart
prof.dr. A.J.J.C. Bogers
prof.dr. A. Verbon

Copromotor: dr. R.P.J. Budde

Financial support by the **Netherlands Heart Foundation** for the publication of this thesis is gratefully acknowledged. The research described in this thesis was supported by a grant of the Dutch Heart Foundation (2013-T-071)



*"The diagnostic said there was nothing wrong with the threep,
which may have meant there was something wrong with the diagnostic"*

- John Scalzi (Lock In, 2014)

TABLE OF CONTENTS

INTRODUCTION		9
Chapter 1	General introduction <i>IMAGO 2016;1:11-21</i>	11
PART 1 New imaging techniques in prosthetic heart valve endocarditis		33
Chapter 2	¹⁸ F-FDG PET/CT and CT angiography in prosthetic heart valve endocarditis: from guidelines to clinical practice <i>European Heart Journal 2018;39:3739-49</i>	35
Chapter 3	Improving the diagnostic performance of ¹⁸ F-FDG PET/CT in prosthetic heart valve endocarditis <i>Circulation 2018;138:1412-27</i>	61
Chapter 4	¹⁸ F-FDG PET/CT and CT angiography in endocarditis of percutaneously implanted prosthetic heart valves	89
4.1	Serial ¹⁸ F-FDG PET/CT angiography in transcatheter-implanted aortic valve endocarditis <i>European Heart Journal 2016;37:3059</i>	91
4.2	Hybrid ¹⁸ F-FDG PET/CT angiography in percutaneous pulmonary prosthetic valve endocarditis <i>European Heart Journal – Cardiovascular Imaging 2018;19:1188</i>	94
PART 2 Technical aspects and considerations		99
Chapter 5	Standardized uptake values in FDG PET/CT for prosthetic heart valve endocarditis: a call for standardization <i>Journal of Nuclear Cardiology 2018;25:2084-91</i>	101
Chapter 6	Dual-time-point FDG PET/CT imaging in prosthetic heart valve endocarditis <i>Journal of Nuclear Cardiology 2018;25:1960-7</i>	113
Chapter 7	Confounders in FDG PET/CT imaging of suspected prosthetic valve endocarditis <i>Journal of the American College of Cardiology – Cardiovascular Imaging 2016;9:1462-5</i>	127
Chapter 8	Advanced CT acquisition protocol for comprehensive prosthetic heart valve assessment <i>European Radiology 2018;28:2159-68</i>	137

PART 3	Computed tomography angiography follow-up after heart valve and ascending aortic surgery	157
Chapter 9	Implications of peri-aortic fluid after surgery on the ascending aorta <i>European Journal of Radiology 2017;95:332-41</i>	159
Chapter 10	CT Angiography for depiction of complications after the Bentall procedure <i>British Journal of Radiology 2018</i>	181
EPILOGUE	-	211
	General discussion and conclusions	213
	Summary in Dutch (<i>Nederlandse samenvatting</i>)	229
	Portfolio	241
	Acknowledgements (<i>Dankwoord</i>)	249
	About the author (<i>Curriculum vitae</i>)	255



INTRODUCTION





CHAPTER 1

GENERAL INTRODUCTION

Laurens Swart
Asbjørn Scholtens
Wilco Tanis
Roelf Valkema
Koen Nieman
Gabriel Krestin
Ricardo Budde

Published in: IMAGO 2016:1;11-21

Prosthetic heart valves

Besides coronary artery disease, heart valve conditions are one of the major cardiovascular diseases in our ever-aging population, as most who require heart valve surgery are elderly patients with aortic valve stenosis due to atheromatous calcification or aortic or mitral valve insufficiency (regurgitation). Another small part of heart valve corrections are performed in young patients with congenital heart defects, or those with one or more heart valves that were affected by an infectious or otherwise inflammatory (e.g. rheumatic) process.

As the main treatment for heart valve disease besides surgical repair (plasty), currently, over 300,000 heart valves are replaced by prostheses worldwide every year, and this number is expected to surpass 850,000 by the year 2050.^{1,2} In approximately 50% of all patients, the native valve is excised and replaced by a mechanical prosthetic valve made out of metallic and carbon compounds. Alternatively, a valve made out of biological tissue (usually the bovine or porcine pericardium), often strung up in a metallic frame yet sometimes also stentlessly constructed, is used (*Figure 1*).³ While a mechanical valve is more durable and can last several decades, making it the more opportune choice of valve in younger patients (to prevent high-risk reoperations later on), they require life-long use of anticoagulant therapy (currently warfarin or vitamin-K antagonists) due to their thrombogenic composition and design⁴, and a mechanical “closing click” can be heard by the patient (*Figure 2*). On the other hand, although technological advancements are rapid and new valve replacement techniques such as a tissue-engineered valve –which is merely a biodegradable scaffold around which the body will shape a new ‘native’ valve that should last a life-time– are being developed as we speak, biological valves are more susceptible to degeneration over time, currently having an average lifespan of approximately 15-20 years.⁵

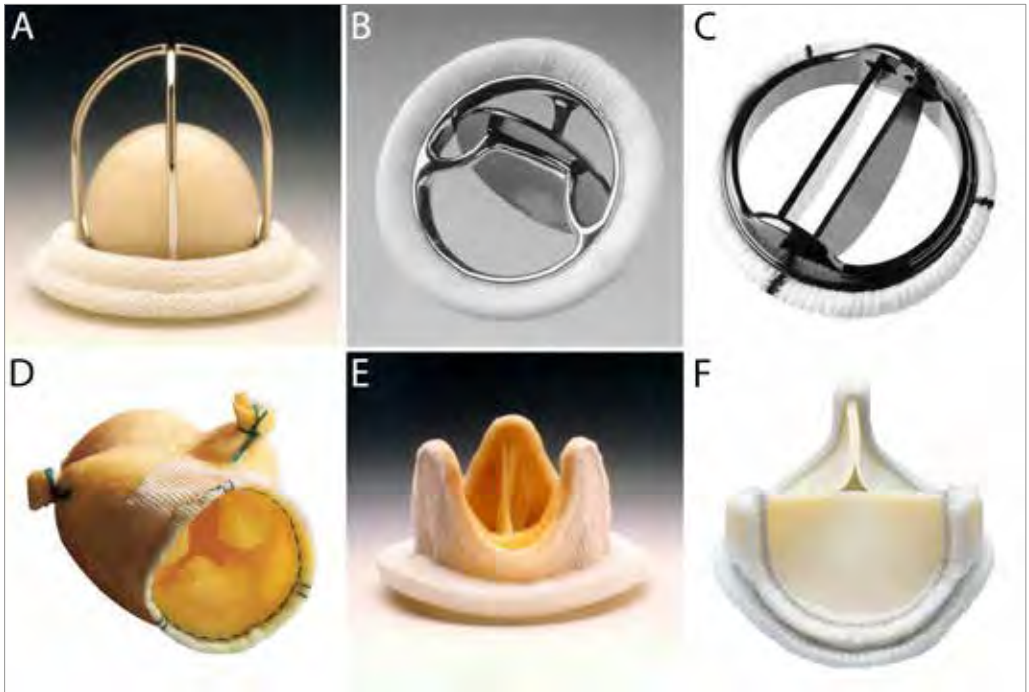


Figure 1 | Examples of different mechanical (A-C) and biological (D-F) heart valve prostheses. (A) Starr-Edwards *Mitral 6120* 'ball-in-cage' prosthetic valve, first described to have been successfully used in a patient over 50 years ago (1968). Discontinued by Edwards Lifesciences in 2007. (B) *Allcarbon* valve prosthesis, the third generation of tilting disc valves by Sorin following the *Monocast* (1977) and *Carbocast* (1986), composed of a completely carbonfilm-coated housing. (C) St. Jude Medical bi-leaflet mechanical *Regent* valve, first introduced in 1977 and still one of the most commonly used aortic and mitral valve prostheses worldwide. (D) Porcine xenograft by Medtronic (*Mosaic*) which includes a portion of the porcine ascending aorta (aortic root). (E) Edwards Lifesciences stented *Duralex* mitral valve made of porcine valve tissue. (F) Carpentier-Edwards *Perimount Magna* valve made of bovine pericardial tissue. Images courtesy of Butany J et al. *Cardiovascular Pathology* 2003;12:322-44, Cohn LH et al. *Cardiac Surgery in The Adult, 4th Edition*, and/or the respective valve manufacturers.



Figure 2 | Opening and closing mechanism of the three main types of mechanical heart valves. (A) Starr-Edwards "ball-in-cage" valve. (B) Medtronic-Hall tilting disc valve. (C) St. Jude Medical bi-leaflet valve. Image (modified) courtesy of Jaron D et al. *The Body Synthetic*.

In 2002, a new type of bioprosthetic valve was introduced that can be implanted percutaneously through delivery via the transfemoral artery, apex of the heart, subclavian artery or directly through the aorta (by a minimally invasive surgical incision). These valves are wrapped inside a stent frame which is folded up around or inside a catheter, and can then either be deployed by expanding a balloon inside the valve stent or releasing it by sliding off the surrounding catheter sheath (in case of a self-expandable stent). Initially, these valves were only used in elderly or critically ill patients with major comorbidities in whom a conventional heart valve replacement was deemed too great of a risk. Lately however, the age threshold for transcatheter aortic valve implantation (TAVI) has gradually become lower as results of long-term outcomes of percutaneously implanted valves are becoming more abundant.⁶⁻⁸ Furthermore, the *Melody* transcatheter pulmonary valve (TPV), approved in Europe in 2006, is nowadays commonly used in patients with a congenital pulmonary valve or right ventricular outflow tract conduit as an alternative to invasive pulmonary valve (e.g. homograft) replacement surgery (*Figure 3*).⁹

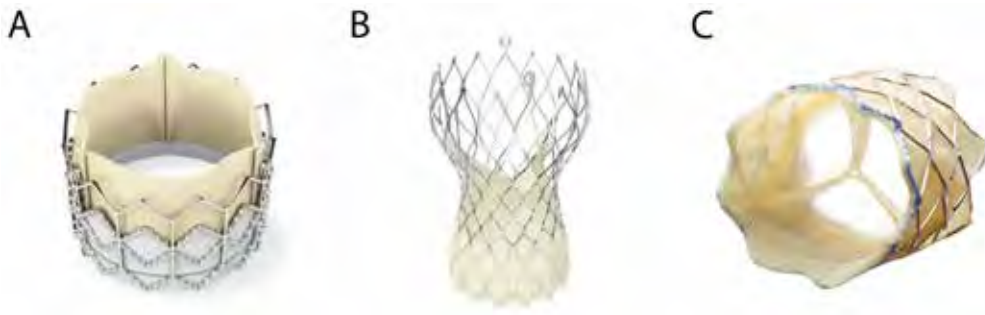


Figure 3 | Examples of different percutaneous aortic (**A, B**) and pulmonic (**C**) valve prostheses. (**A**) Carpentier-Edwards *Sapien 3* transcatheter aortic valve prosthesis, expanded through balloon inflation. (**B**) Medtronic *CoreValve Evolut R* transcatheter aortic valve prosthesis, self-expanding upon release from its sheath. (**C**) Medtronic *Melody* transcatheter pulmonary valve prosthesis, expanded through balloon inflation. Images courtesy of the respective valve manufacturers.

Although heart valve replacement often provides immediate solace, it remains an indefinite cure. Besides the risk of a patient-prosthesis mismatch and other immediate complications (such as a stroke due to dislodging calcifications on the native valve or atrioventricular conduction disorders requiring pacemaker implantation in TAVI procedures^{10,11}) as well as the previously mentioned risk of valve obstruction through thrombus (or pannus) formation¹² and valve degeneration, another major complication with a very high 1-year mortality rate (30-50%)¹³ affects patients with a prosthetic heart valve with an incidence of approximately 0.3-1.2% per patient per year following implantation¹⁴: prosthetic heart valve endocarditis (PVE), an infection of the prosthetic heart valve and/or the surrounding (peri-annular) tissue.

Endocarditis

Endocarditis is an inflammation, sterile or infectious, of the endocardium, usually involving the heart valves. Other structures that may be affected are the chordae tendinae which attach the atrioventricular valves to the myocardium, the interventricular septum (particularly in the presence of atrial or ventricular septal defects), the endocardium of the left or right ventricle wall or any prosthetic intracardiac material (such as prosthetic valves, closure devices or patches, atrial appendage occluders or pacemaker leads).

History

One of the first cases of endocarditis, described in 1646 by Lazare Rivière, professor of medicine in Montpellier, was that of a man who complained of palpitations, swollen feet and legs and an irregular heart rate. The patient rapidly worsened and died shortly thereafter, with the autopsy showing several small outgrowths as large as hazelnuts on the aortic valve.

It was not until 1802 that another French physician named Jean-Nicolas Corvisart, mentor of Théophile Laennec who would later on invent the cylindrical stethoscope and cited Rivière's case report in his work, described "excrescences or soft vegetations" which resembled cauliflower-like lesions found in some venereal diseases, suggesting it may have had something to do with syphilis (*Figure 4*).¹⁵ The connection with syphilis was soon doubted by others though, as these "vegetations" proved to be quite rare and hard to connect to other signs of syphilis.

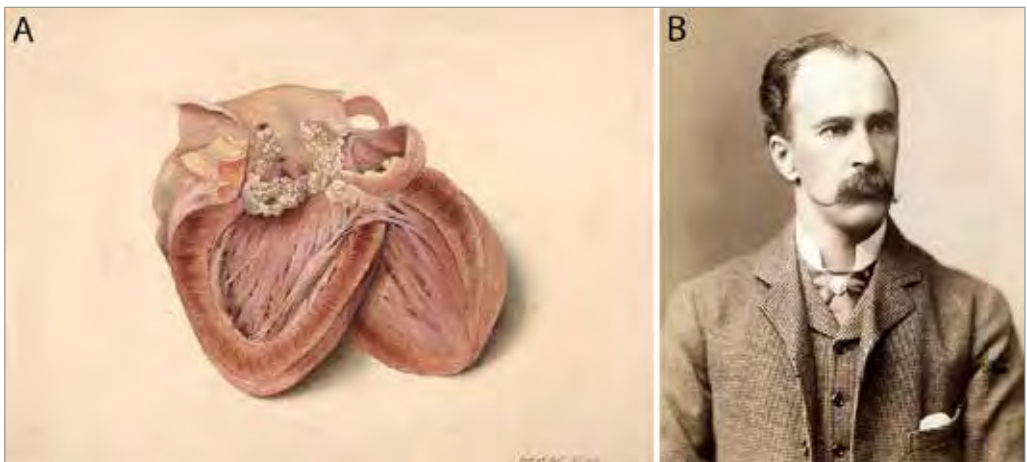


Figure 4 | (A) Water colour drawing of a heart of a patient with ulcerative endocarditis drawn by Thomas Godart (1886). (B) Sir William Osler (1880).

Thirty years later, yet another French physician named Jean-Baptiste Bouillaud found that the inner heart was covered by a membrane which he named the endocardium and deemed “the most likely origin of these organic lesions” previously identified by Laennec and Corvisart. The cause of these lesions however, remained elusive for a little longer up until Emanuel Winge, a Norwegian physician, had a patient of his die due to sepsis caused by a bacterial joint infection and, through his microscope, saw “parasitic organisms” in the vegetations he found in the patient’s heart.¹⁶

It was at that time (around 1885) that Sir William Osler (*Figure 4*), a Canadian physician and founder of the Johns Hopkins Hospital, later described as the “father of modern medicine” and “one of the greatest diagnosticians to wield a stethoscope”, provided the first comprehensive account of the disease in the English language and brought it to the attention of clinicians in his Gulstonian Lectures.¹⁷ He distinguished two broad forms of the disease: an acute form associated with systemic infections, and a chronic form that mainly affected the pericardium, which according to him and opposed to the general consensus at that time that each separate infectious disease was caused by a different specific agent, seemed to be associated with several different micro-organisms as well as certain predisposing factors.

Diagnosis

Evidence of these causative micro-organisms in blood cultures and the presence of these predisposing factors, combined with signs of structural damage to the heart valves or vegetations on the endocardium, are what nowadays make up the diagnostic criteria for infectious endocarditis which were originally proposed by Durack et al. of the Duke University School of Medicine in 1994 and subsequently became known as the Duke criteria.¹⁸ Although initially purely designed for epidemiological studies, their collective sensitivity was >80% in numerous clinical studies with pathological confirmation as the reference standard, and their specificity and negative predictive value were validated as well in a wide spectrum of patients.¹⁹⁻²¹

Nevertheless, the Duke criteria had several shortcomings, mostly because a large group of patients ended up being classified as “possible endocarditis”. Furthermore, these criteria did not address the particularly high relative risk of endocarditis in cases of *Staphylococcus aureus* bacteraemia, the poor diagnostic sensitivity in cases of suspected Q-fever endocarditis as well as the potential role of transoesophageal echocardiography (TEE). Based on these critiques, Durack’s colleagues Li et al. proposed several modifications to the original Duke criteria, reclassifying “possible endocarditis” as requiring at least 1 major criterion or at least 3 minor criteria, removing a vague echocardiographic minor criterion in case of poor echocardiographic images (which were no longer an issue since the introduction of TEE), and adding *S. aureus* bacteraemia as well as positive Q-fever serology as two new major criteria (*Table 1*).²²

Major criteria

Blood cultures positive for endocarditis:

- Typical micro-organisms consistent with infective endocarditis from two separate blood cultures:
 - viridans streptococci; *Streptococcus bovis*, HACEK group, *Staphylococcus aureus*; or
 - community-acquired enterococci, in the absence of a primary focus
- Micro-organisms consistent with IE from persistently positive blood cultures:
 - at least two positive blood cultures drawn >12h apart; or
 - all of three or a majority of ≥4 separate cultures of blood (with first and last sample drawn at least 1h apart)
- Single positive blood culture for *Coxiella burnetii* or antiphase I IgG antibody titer >1:800

Echocardiography positive for endocarditis:

- Oscillating intracardiac mass on valve or supporting structures, in the path of regurgitant jets, or on implanted material in the absence of an alternative anatomic explanation; or
- Abscess; or
- New partial dehiscence of prosthetic valve
- New valvular regurgitation (worsening or changing of pre-existing murmur not sufficient)

Minor criteria

- Predisposition, predisposing heart condition or intravenous drug use
- Fever (temperature >38.0°C)
- Vascular phenomena: major arterial emboli, septic pulmonary infarcts, mycotic aneurysms, intracranial haemorrhage, conjunctival hemorrhages, Janeway's lesions¹
- Immunological phenomena: glomerulonephritis, Osler's nodes², Roth's spots³, rheumatoid factor
- Microbiological evidence: positive blood cultures that do not meet the major criterion as noted above, or serological evidence of active infection with an organism consistent with IE not meeting the major criterion

Table 1 | Modified Duke Criteria according to Li et al.²² **(1)** Non-tender, small (3-5mm in diameter), painless, flat, ecchymotic and erythematous or hemorrhagic nodular lesions on the hand palms or foot soles named after Edward Janeway (1841-1911) who first described these lesions indicative of septic emboli (bacterial deposits) forming micro-abscesses in the smallest peripheral capillaries. **(2)** Red lesions similar to Janeway's lesions, but tender²³ and often painful, caused by immune complex deposition. Approximately 10-25% of patients with infective endocarditis have Osler's nodes. **(3)** Retinal findings first described by Moritz Roth in 1872 as round, oval or flame-shaped hemorrhages with a central white spot, which Roth believed at the time represented disseminated embolic foci of bacterial abscesses originating from infective vegetation on heart valves. Although initially thought to be a sign specific to bacterial embolization, it may occur in many systemic diseases such as leukemia, carbon monoxide poisoning, preeclampsia, diabetic or HIV retinopathy, intracranial hemorrhage or acute reduction of intraocular pressure following trabeculectomy.

Up until 2015, these Modified Duke Criteria acted as reference standard for the diagnosis of both native and prosthetic valve endocarditis with adequate results in studies of mixed cohorts. However, even though the criteria included prosthetic-heart-valve-specific echocardiographic findings (such as new valve dehiscence), in suspected PVE alone, it was soon noted that they lacked sensitivity²⁴⁻²⁵, most likely due to echocardiography being hampered by scattering artefacts due to the metallic components of the prosthesis (*Figure 5*)²⁶, and possibly also due to the fact that PVE is more often caused by atypical micro-organisms that not always immediately show up in initial blood cultures (e.g. *Propionibacterium acnes*).²⁷ These shortcomings, particularly of echocardiography in case of mechanical prosthetic heart valves, are probably the reason why investigations into additional imaging techniques of prosthetic heart valve endocarditis and other conditions such as valve obstruction have been intensively pursued over the past two decades.

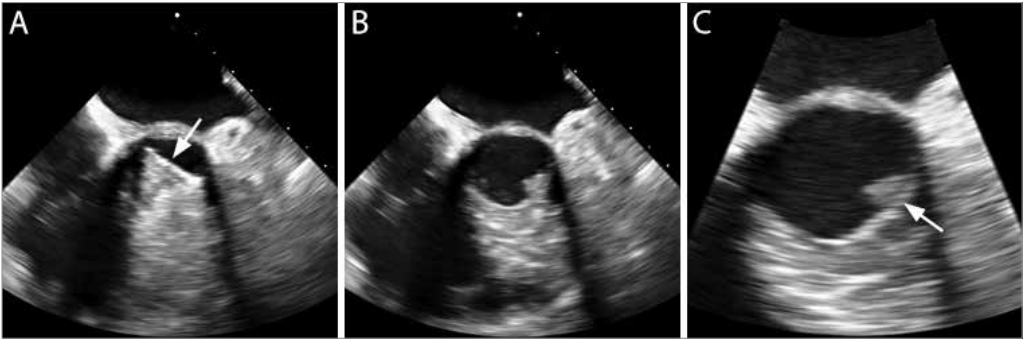


Figure 5 | Transesophageal echocardiogram of the aortic prosthetic valve (posterior side of the valve displayed on top as seen through the oesophagus) of a patient suspected of prosthetic heart valve endocarditis. When the bi-leaflet prosthetic valve is opened during systole (**A**), the echo waves are deflected by the valve surface (**arrow**) resulting in a white streak artefact due to reverberation, which makes the anterior side of the valve and the annular tissue behind it uninterpretable. During diastole (**B, C**) – when the valve is closed – the anterior side of the valve can be depicted much better, and a small mass is identified just below the valve ring (**arrow**).

CT angiography

Multidetector CT angiography (CTA) has shown to be a promising additional imaging technique for the evaluation of prosthetic heart valves, particularly in patients suspected of heart valve obstruction or endocarditis.²⁸⁻³¹ Most types of prosthetic heart valves can, depending on the type of valve and material it consists of, readily be depicted using a state-of-the-art CT scanner, with valves made of cobalt-chrome alloys such as the Björk-Shiley mechanical prosthesis (which is no longer used in most countries nowadays due to vulnerability of the welded struts) being more prone to scatter and blooming artefacts (*Figure 6*).³²⁻³⁴

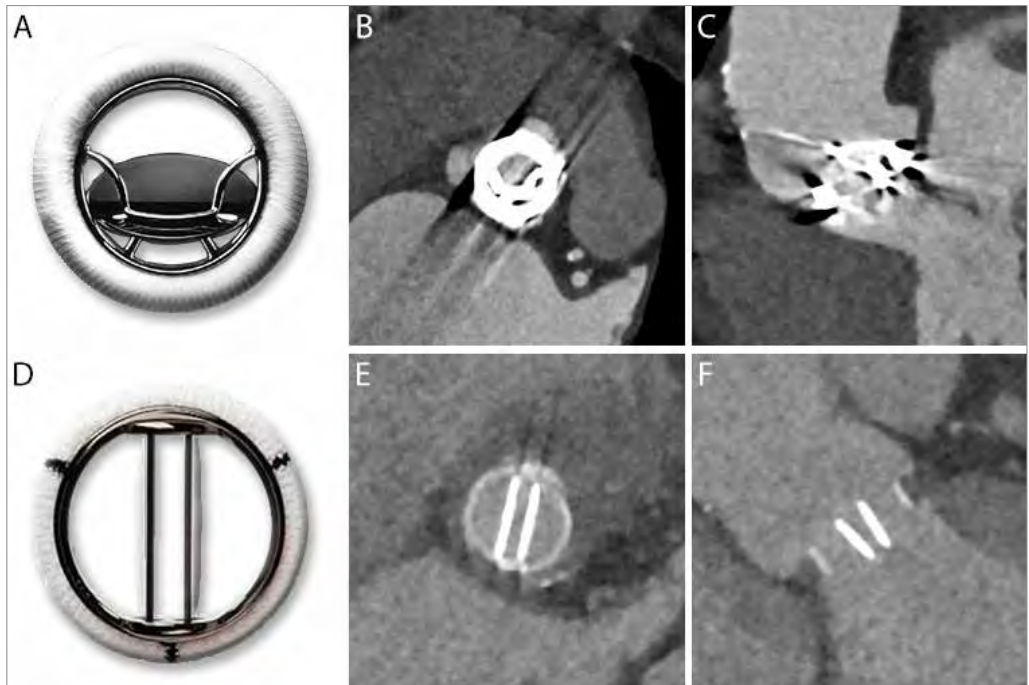


Figure 6 | Short- (**B, E**) and long-axis (**C, F**) CTA images of (**top**) a Björk-Shiley tilting-disc valve (**A**) made of a cobalt-chrome alloy ring and 4 struts which hold a single valve leaflet, causing blooming (the metallic structures seeming thicker than they actually are), beam-hardening (the metal causing bands of black 'shadow') and scatter (white lines spreading from the most bright metallic components in a star-shaped manner; **C**) artefacts; and (**bottom**) an example of a nowadays more commonly used bi-leaflet mechanical valve made of either titanium or nickel analogues, in this case one made by St. Jude Medical (**D**), which, thanks to both the materials it consists of as well as its structure, hardly causes any artefacts.

Besides the detailed anatomical information which is attained about the valve and surrounding structures, current CT scanners are able to acquire dynamic images in all phases of the cardiac cycle, allowing assessment of valve function (opening and closing of the valve leaflets) as well.³⁵ While this (retrospectively ECG-gated) acquisition in all phases of the cardiac cycle is accompanied by a relatively high radiation dose^{28,36}, this seems acceptable in light of the additional information it provides in addition to transoesophageal echocardiography and the mortality associated with missed structural complications of prosthetic heart valve endocarditis. Furthermore, the latest state-of-the-art scanners even allow for prospectively ECG-triggered protocols with iterative reconstruction tailored to the acquisition of prosthetic heart valves which provide images of similar diagnostic quality at a much lower radiation dose (*Chapter 8*).^{37,38}

In case of suspected prosthetic heart valve endocarditis, CTA is of most additional value in the detection of peri-annular complications such as mycotic aneurysms or fistula, as well as small vegetations which are located inside or just beneath the prosthetic valve ring and therefore easily missed by echocardiography.^{39,40} On the other hand, small encapsulated abscesses which may not enhance by a contrast medium or small perforations of a bioprosthetic valve leaflet may be more easily missed by CTA (although a delayed phase scan can provide additional detection of abscesses, see *Chapter 8*)⁴¹, exemplifying the value of a multi-imaging approach as one imaging modality cannot replace the other (*Figure 7*).

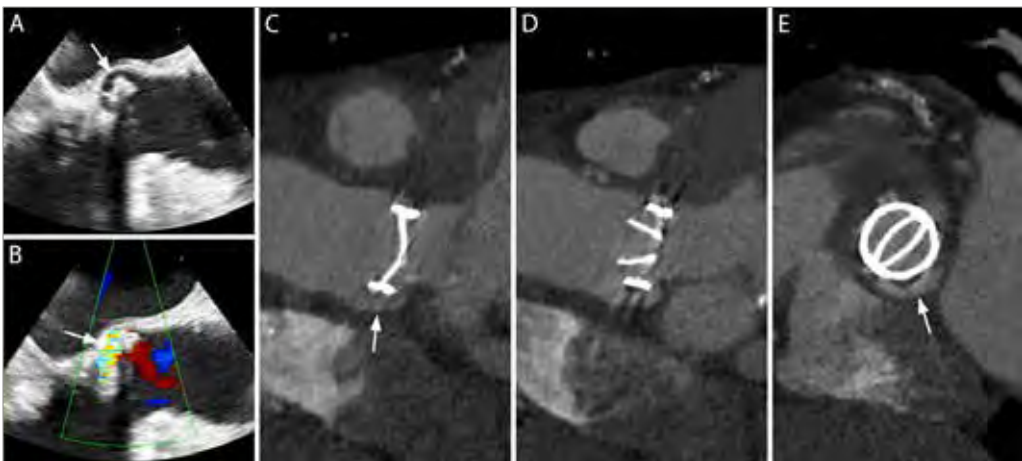


Figure 7 | Transesophageal echocardiography (**A-B**) and CT-angiography (**C-E**) images of a peri-annular extension (arrow) on the posterior side of an aortic prosthetic valve. The echo-lucent extension fills with contrast on CTA and connects the aorta to the left ventricular outflow tract, as shown by the turbulent and rapid blood flow through the extension on Doppler echocardiography (**B**).

Additionally, in case of suspected or known PVE, cardiac CTA acquired for assessment of the prosthetic heart valve, without major changes to the scan protocol, allows simultaneous assessment of the coronary arteries in most patients with non-cobalt-chrome valves. Should a patient with confirmed PVE have an indication for reoperation, evaluation of the coronaries by CT may allow an invasive coronary angiogram to be omitted, especially in patients with suspected large vegetations on the aortic valve (native or prosthetic) in whom invasive angiography may be contraindicated.³⁴

However, despite the high diagnostic accuracy of cardiac CTA for structural complications of PVE and although it can depict signs of inflammation (such as induration, or “fat stranding”, see *Chapter 10*) in some cases, it remains a purely anatomical imaging technique limited by the fact that structural changes are required for a diagnosis. Furthermore, when structural abnormalities are identified, their relation to the infectious state of the patient is not unequivocal, as perivalvular extensions for example may simply be a remnant of a previous native valve endocarditis which wasn't completely surgically repaired, or of a previous episode of PVE which was conservatively treated.⁴² Without a prior CTA acquired in a non-infectious post-surgical state to compare to, the distinction between a loose suture and a small mycotic aneurysm may be hard to draw.⁴³

¹⁸F-FDG PET/CT

In order to depict inflammation without the necessity for structural damage, a relatively new imaging technique called positron-emission tomography (PET), which uses a glucose analogue marked ('labeled') by a radioactive Fluor-isotope (¹⁸F) and was originally developed for oncological imaging in the late 1990s⁴⁴, was first proposed as an additional tool for imaging of infectious disease about a decade ago.⁴⁵ Although originally contested due to potential risks and lacking evidence of its use in the diagnosis of infectious and inflammatory diseases, the European Medicines Agency concluded that the benefits of FDG outweigh its risks and subsequently deemed several indications for the use of FDG in infectious or inflammatory disease appropriate, such as (I) the localization of infectious foci in the presence of fever of unknown origin, (II) the diagnosis of infection in suspected osteomyelitis, spondylodiscitis or other bone infections as well as hip, knee or vascular prostheses, (III) fever in AIDS patients, and (IV) the detection of the extent of inflammation in sarcoidosis, inflammatory bowel disease and vasculitis of the greater vessels.

Working mechanism

The PET imaging technique is based on the principle that proton-rich nuclei in radioactive isotopes decay and thereby emit positrons which, usually within a few millimetres of the site of their origin (average 0.2mm for ^{18}F), collide with nearby electrons resulting in the annihilation of both particles. During this annihilation, energy is released ($E=mc^2$) in the form of two gamma rays emitted in nearly exactly opposite directions ($180 \pm 0.5^\circ$ apart due to the kinetic energy the particles carried at the time of annihilation). In case of a human body, these photons then pass through surrounding tissues with a small chance of scattering or absorption by matter they interact with (resulting in attenuation) before exiting the body after which they can be detected by a PET scanner: a circular array of detectors which can detect the essentially simultaneously arriving photons and thereby determine the line along which the annihilation took place. When an ample amount of gamma rays has been detected, reconstruction of their origins by specific algorithms allows the computing of an image of the distribution of the positron-emitting isotope in the body (*Figure 8*).

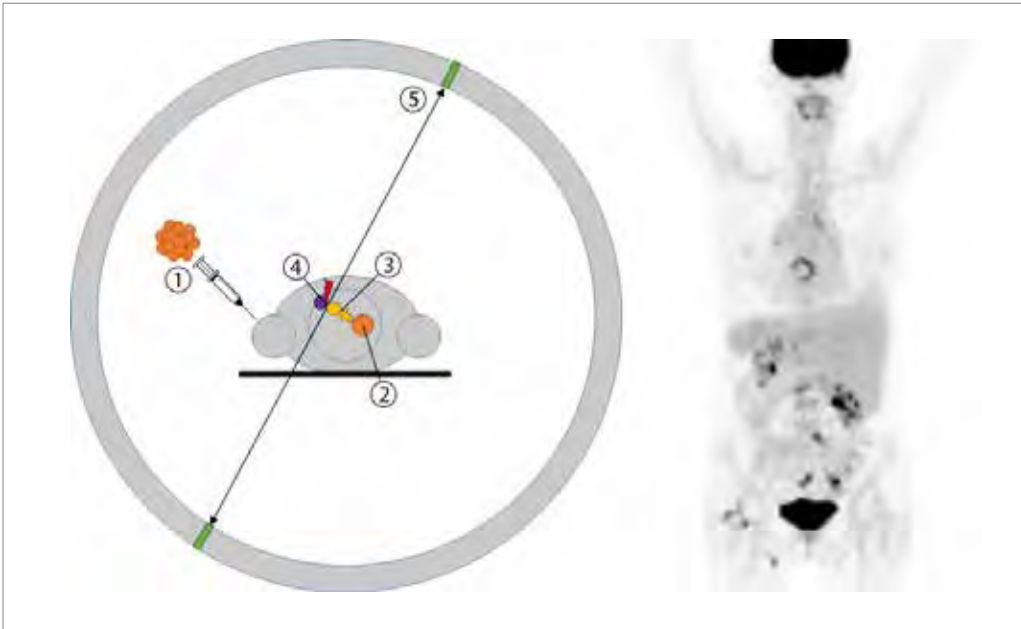


Figure 8 | Schematic of the mechanism of PET imaging. (1) ^{18}F -FDG PET/CT is injected into the patient. Over a period of 1 hour, during which the patient must remain still and strain as few muscles as possible (including the vocal cords), this radiolabeled glucose is, like regular glucose, most absorbed by the most metabolically active cells and organs (including the brain, as seen on the maximum intensity PET projection on the **right**). (2) The radiolabeled glucose decays and emits positrons, (3) which collide with surrounding electrons, resulting in the annihilation of both particles and (4) the emission of two gamma rays in exactly the opposite direction. (5) These simultaneous gamma rays are then detected by the detector ring around the patient, allowing determination of the line along which the origin (i.e. the radiolabeled glucose) must lie.

Although the ^{18}F -FDG is absorbed by all cells in the body (particularly in the brain), partially remains circulating in the blood and is excreted by the kidneys to the bladder (which all light up on the PET scan, see *Figure 8*), it is absorbed most by the cells that are most metabolically active. Areas of inflammation (i.e. a cellular immune response) can thus be detected by identifying areas of increased ^{18}F -FDG uptake, as leukocytes are very metabolically active. However, inflammation should not necessarily be equated with infection, as it is not the bacteria that retain the ^{18}F -FDG, but the leukocytes that respond to the infection which, regrettably, are also attracted to sterile inflammations due to –for example– a foreign-body reaction.

Literature

Half a decade after the first reports on the promising value of ^{18}F -FDG PET/CT in fever of unknown origin⁴⁶, particularly in patients with infected prosthetic joints or vascular prostheses^{47,48}, the first case reports on its use in patients with endocarditis were published.⁴⁹

Initially, myocardial ^{18}F -FDG uptake proved problematic in some patients who were scanned for fever of unknown origin, making authors doubt the value of PET/CT in patients with high myocardial glucose metabolism⁵⁰, although the additional value for early detection of septic emboli and metastatic infections was quickly appraised.⁵¹ Soon though, techniques borrowed from ^{18}F -FDG PET/CT imaging in suspected cardiac sarcoidosis, involving prolonged fasting and a low-carbohydrate preparatory diet, allowed for better visualisation of the heart and heart valves (*Chapter 2*). The focus of most case reports and smaller case series thereafter, however, shifted to the diagnosis of suspected *prosthetic* valve endocarditis rather than endocarditis in general, possibly because the diagnosis of PVE was were most was still to gain.

The first large case series which ‘set the bar’ for PET/CT studies in suspected PVE was the study in 2013 by Saby et al.⁵², who prospectively included 72 consecutive patients suspected of having PVE. Cardiac PET/CT was performed at admission, and the final diagnosis based on clinical or pathological modified Duke criteria determined after a 3-month follow-up. In relation to this (possibly suboptimal) reference standard, PET/CT had a sensitivity, specificity, PPV and NPV of 73% [95% confidence interval 54-87%], 80% [56-93%], 85% [64-95%] and 67% [45-84%] respectively. However, when adding a positive PET/CT scan (based on a visual interpretation of ‘abnormal’ uptake around the prosthetic heart valve which, at that time and even now still, was a vague definition) to the modified Duke criteria as an additional major criterion, the combined sensitivity of the work-up including echocardiography, blood cultures, PET/CT and all the minor diagnostic criteria (*Table 1*) rose to 97% [83-99%].

1

Shortly thereafter, Ricciardi et al.⁵³ published a study of 27 consecutive patients admitted for suspicion of endocarditis in 2014, of whom 25 were concluded to have a final diagnosis of endocarditis based on the modified Duke criteria (18 PVE, 7 native valve endocarditis). ¹⁸F-FDG PET/CT was positive in 16/18 patients with confirmed PVE, yet all seven patients with native valve endocarditis had negative PET/CT findings despite positive echocardiography findings. Possibly these scans were all false negative because of a lower a-priori chance of endocarditis, resulting in prolonged periods of antibiotic therapy for fever of unknown origin –and therefore reduced inflammatory activity, which may be required for an adequate PET/CT scan^{54,55}– before the diagnosis of endocarditis is suspected and a PET/CT is performed, but also possibly because prosthetic material may be a required substrate for infection with more explicit inflammatory activity.

Kestler et al.⁵⁶ subsequently reported another prospective cohort study on 47 patients with definite endocarditis who underwent PET/CT matched with 94 patients who did not. Their study showed a similar poor performance for the diagnosis of valvular uptake in native valves, but still found important additional value by enabling the diagnosis of significantly more infectious complications, thereby reducing the number of relapses by more than 50%.

Finally, in 2015 the largest prospective study still to date by Pizzi et al.⁵⁷, ninety-two patients admitted for suspected prosthetic valve or cardiac implantable electronic device (i.e. pacemaker or ICD) infection underwent ¹⁸F-FDG PET/CT while 76 also underwent cardiac CT angiography. The final diagnosis was based on consensus by an expert team. Sensitivity, specificity, PPV and NPV of PET/CT were 86%, 88%, 90% and 83%, respectively. When adding CT angiography (*Figure 9*), mostly for the purpose of discerning un-suppressed physiological myocardial FDG uptake from pathological perivalvular uptake (as opposed to using the imaging technique's ability to depict perivalvular extensions or vegetations as a source of additional diagnostic information), these values increased to 91%/91%/93%/88%.

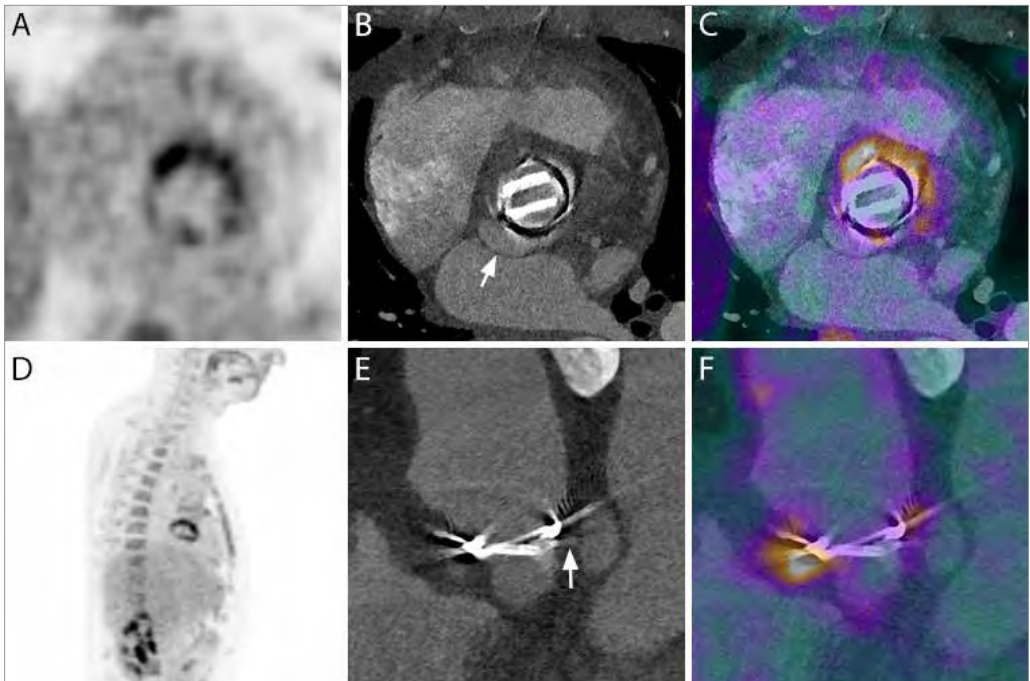


Figure 9 | Example of combined PET and CT angiography. Double-oblique short-axis PET (**A**), CTA (**B**) and fused PET/CTA (**C**) images, a lateral maximum intensity PET projection (**D**), as well as double-oblique long-axis CTA (**E**) and PET/CTA (**F**) images of an infected prosthetic aortic valve, as demonstrated by the intense ^{18}F -FDG uptake around the anterior and lateral side of the prosthesis (**C**, **E**). CTA shows signs of a perivalvular extension (**B**, **arrow**) which fills with contrast through a tiny connection arising from the left ventricular outflow tract (**E**, **arrow**) yet is not FDG-avid. These findings were compared to routine CTA images post-implantation, on which the perivalvular extension was already visible, hence allowing this patient to be conservatively treated in this instance as there were no signs of new perivalvular complications. This particular case nicely illustrates the ability of CTA to depict perivalvular extensions, but its inability to distinguish between sterile abnormalities (e.g. a loose suture or remnants of a previous infectious endocarditis or previous valve surgery) and infectious ones.

Despite the limited number of studies and small numbers of patients, these findings nevertheless led to the last-minute addition of both PET/CT and CTA to the recommended imaging techniques in suspected PVE of the 2015 ESC guidelines.⁵⁸ The updated guidelines stated that both imaging techniques should be considered alternatives to the major diagnostic criterion of abnormalities found on echocardiography, now to be collectively considered as imaging abnormalities, but –probably due to the study by Ricciardi et al.– *only* in patients with suspected *prosthetic* heart valve endocarditis, and only when initial testing (i.e. blood cultures and transoesophageal echocardiography) remained inconclusive.

Outline of this thesis

This thesis further explores the additional diagnostic value of ^{18}F -FDG PET/CT and CT angiography in suspected prosthetic heart valve endocarditis, how and when these imaging techniques may or should be employed, and how their use –and thereby their diagnostic accuracy– can be improved.

In *Part I*, a review of current literature (and mostly its limitations) up until this thesis is provided (*Chapter 2*), followed by the results of our large multicentre trial that seeks to address some of these limitations in previous literature (*Chapter 3*). Finally, two pilot case reports of patients with infected *percutaneously* implanted heart valves, one in a patient with a transcatheter-implanted aortic valve and one in a patient with a percutaneously implanted pulmonary valve, –both the first reports in literature of these imaging techniques being used in these conditions– are put forward (*Chapter 4*).

Part II addresses several technical aspects to be taken into account. First, in concordance with our previously mentioned review, an overview of the literature on the quantitative assessment of ^{18}F -FDG PET/CT and the lack of standardization herein is presented, calling for more standardization in both image acquisition (including unified calibration of PET/CT scanners) and measurement techniques (*Chapter 5*). Second, our findings regarding a possible adaptation to the standard ^{18}F -FDG PET scanning protocol which was directly adopted from scanning protocols for oncological purposes are put forward (*Chapter 6*). Although there had been several reports of more accurate imaging of infection with adapted PET acquisition times in previous studies, our study showed a poorer performance of a delayed acquisition in patients suspected of PVE. Third, in a pictorial essay, several other possible confounders that may need to be taken into account when evaluating ^{18}F -FDG PET/CT images in suspected PVE are presented (*Chapter 7*). These images further demonstrate some of the gaps in our knowledge regarding certain findings such as specific FDG uptake patterns which future research may find to be able to provide a distinction between pathological uptake indicating infection and physiological uptake indicating sterile (e.g. foreign-body) inflammation. Finally, a CT angiography scanning protocol tailored to the acquisition of prosthetic heart valves which seeks to address some of the limitations of CTA in previous literature (and our own clinical experience) is proposed (*Chapter 8*).

Lastly, in *Part III*, results of our study regarding post-operative findings on CT angiography following a combined replacement of the aortic valve and ascending aorta (i.e. a Bentall-procedure) are presented. In this study, we aimed to both acquire an idea of a normal post-operative CTA image after such an extensive procedure, as well as to evaluate the significance of an often-seen abnormality in this kind of scans that is the accumulation of fluid (e.g. edema) in the fatty tissue around the prosthetic heart valve and prosthetic ascending aorta, often called ‘fat stranding’, which may also be seen in inflammation due to infection (*Chapter 9*). Finally, an extensive pictorial review of both the spectrum of normal findings that may be seen on CT angiography after this kind of major cardiothoracic surgery, as well as an overview of all possible complications that may be identified by this imaging technique is provided (*Chapter 10*).

References

1. Butchart EG, Gohlke-Bärwolf C, Antunes MJ, et al. Recommendations for the management of patients after heart valve surgery. *Eur Heart J*. 2005;26:2463–71.
2. Yacoub MH, Takkenberg JJ. Will heart valve tissue engineering change the world? *Nat Clin Pract Cardiovasc Med*. 2005;2:60–1.
3. Baumgartner H, Falk V, Bax JJ et al. 2017 ESC/EACTS Guidelines for the management of valvular heart disease. *Eur Heart J*. 2017;38:2739–91.
4. Edmunds LH. Is prosthetic valve thrombogenicity related to design or material? *Tex Heart Inst J*. 1996;23:24–27.
5. Hoffmann G, Lutter G, Cremer J. Durability of bioprosthetic cardiac valves. *Dtsch Arztebl Int*. 2008;105:143–148.
6. Lüscher TF. Managing aortic stenosis with TAVI or surgery: risk assessment and long-term outcome. *Eur Heart J*. 2017;38:3327–9.
7. Long-term outcomes of transcatheter aortic valve implantation (TAVI): a systematic review of 5-year survival and beyond. *Ann Cardiothorac Surg*. 2017;6:432–43.
8. Wendler O, Schymik G, Treede H, et al. SOURCE 3: 1-year outcomes post-transcatheter aortic valve implantation using the latest generation of the balloon-expandable transcatheter heart valve. *Eur Heart J*. 2017;38:2717–26.
9. Cheatham JP, Hellenbrand WE, Zahn EM, et al. Clinical and hemodynamic outcomes up to 7 years after transcatheter pulmonary valve replacement in the US melody valve investigational device exemption trial. *Circulation*. 2015;131:1960–70.
10. Muralidharan A, Thiagarajan K, van Ham R, et al. Meta-analysis of perioperative stroke and mortality in transcatheter aortic valve implantation. *Am J Cardiol*. 2016;118:1031–45.
11. Shin DI, Merx MW, Kirmanoglou K, et al. Baseline HV-interval predicts complete AV-block secondary to transcatheter aortic valve implantation. *Acta Cardiol*. 2015;70:574–80.
12. Tanis W, Habets J, van den Brink RB, et al. Differentiation of thrombus from pannus as the cause of acquired mechanical prosthetic heart valve obstruction by non-invasive imaging: a review of the literature. *Eur Heart J Cardiovasc Imaging*. 2014;15:119–29.
13. Lalani T, Chu VH, Park LP, et al. In-hospital and 1-year mortality in patients undergoing early surgery for prosthetic valve endocarditis. *JAMA Intern Med*. 2013;173:1495–504.
14. Baddour LM, Wilson WR, Bayer AS, et al. Infective endocarditis: diagnosis, antimicrobial therapy, and management of complications. *Circulation*. 2005;111:e394–e434.
15. Barnett R. Infective endocarditis. *Lancet*. 2016;388:1148.
16. Contrepois A. Towards a history of infective endocarditis. *Med Hist*. 1996;40:25–54.
17. Pruitt RD. William Osler and his Gulstonian Lectures on malignant endocarditis. *Mayo Clin Proc*. 1982;57:4–9.
18. Durack DT, Lukes AS, Bright DK. New criteria for diagnosis of infective endocarditis: utilization of specific echocardiographic findings. Duke Endocarditis Service. *Am J Med*. 1994;96:200–9.
19. Bayer AS, Ward JI, Ginzton LE, et al. Evaluation of new clinical criteria for the diagnosis of infective endocarditis. *Am J Med*. 1994;96:211–9.

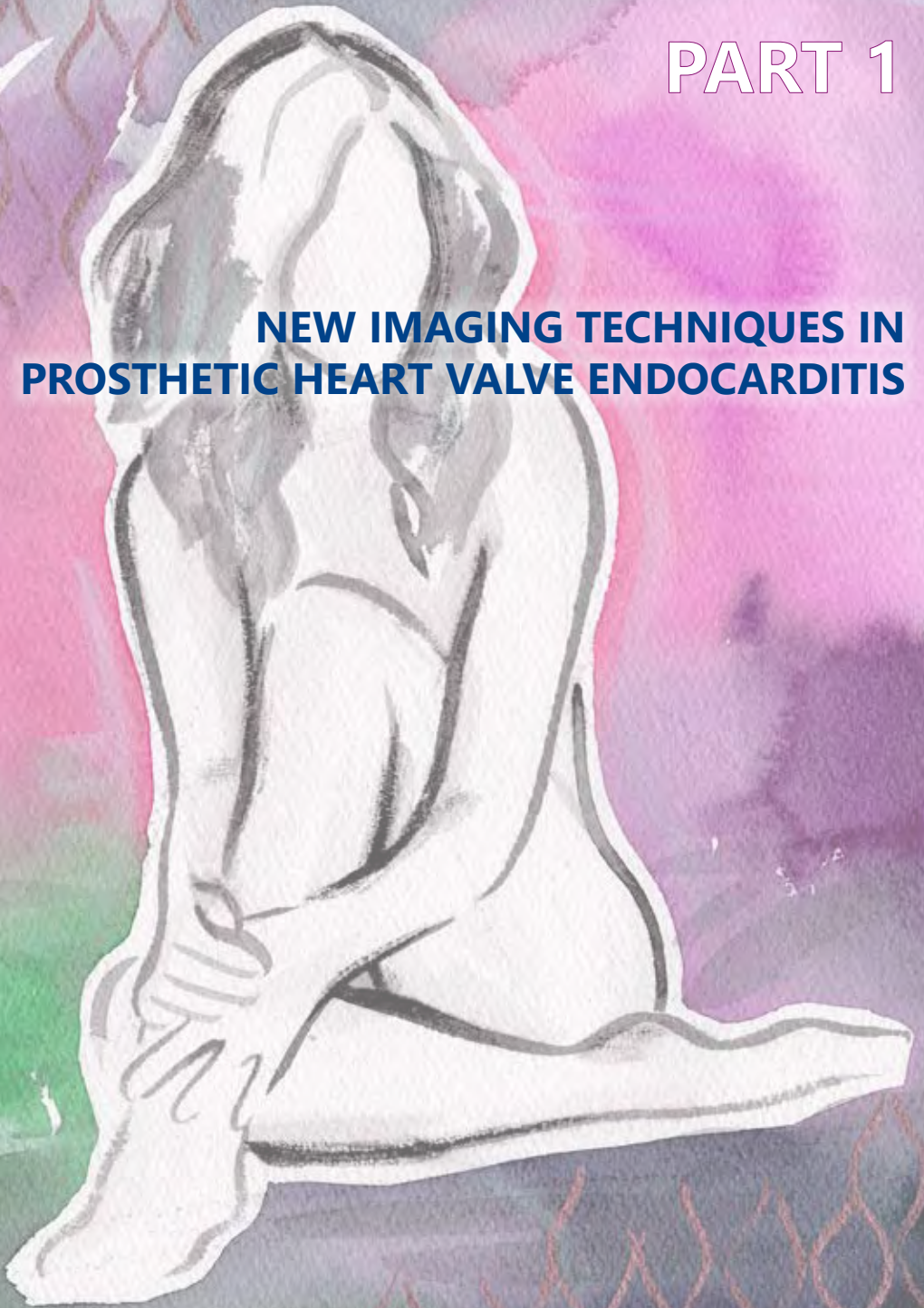
20. Hoen B, Selton-Suty C, Danchin N, et al. Evaluation of the Duke criteria versus the Beth Israel criteria for the diagnosis of infective endocarditis. *Clin Infect Dis.* 1995;21:905–9.
21. Cecci E, Parrini I, Chinaglia A, et al. New diagnostic criteria for infective endocarditis, a study of sensitivity and specificity. *Eur Heart J.* 1997;18:1149–56.
22. Li JS, Sexton DJ, Mick N, et al. Proposed modifications to the Duke criteria for the diagnosis of infective endocarditis. *Clin Infect Dis.* 2000;30(4):633–8.
23. Farrior JB, Silverman ME. A consideration of the differences between a Janeway's lesion and an Osler's node in infective endocarditis. *Chest* 1976;70:239–43.
24. Pérez-Vázquez A, Fariñas MC, García-Palomo JD, et al. Evaluation of the Duke criteria in 93 episodes of prosthetic valve endocarditis: could sensitivity be improved? *Arch Intern Med.* 2000;160:1185–91.
25. Nettles RE, McCarty DE, Corey GR, Li J, Sexton DJ. An evaluation of the Duke criteria in 25 pathologically confirmed cases of prosthetic valve endocarditis. *Clin Infect Dis.* 1997;25:1401–3.
26. Mahesh B, Angelini G, Caputo M, et al. Prosthetic Valve Endocarditis. *Ann Thorac Surg.* 2005;80:1151–8.
27. Van Valen R, de Lind van Wijngaarden RA, et al. Prosthetic valve endocarditis due to *Propionibacterium acnes*. *Interact Cardiovasc Thorac Surg.* 2016;23:150–5.
28. Suchá D, Symersky P, van den Brink RB, et al. Diagnostic evaluation and treatment strategy in patients with suspected prosthetic heart valve dysfunction: The incremental value of MDCT. *J Cardiovasc Comput Tomogr.* 2016;10:398–406.
29. Tanis W, Budde RP, van der Bilt IA, et al. Novel imaging strategies for the detection of prosthetic heart valve obstruction and endocarditis. *Neth Heart J.* 2016;24:96–107.
30. Suchá D, Symersky P, Tanis W, et al. Multimodality imaging assessment of prosthetic heart valves. *Circ Cardiovasc Imaging.* 2015;8:e003703.
31. Tanis W, Habets J, van den Brink RB, et al. Differentiation of thrombus from pannus as the cause of acquired mechanical prosthetic heart valve obstruction by non-invasive imaging: a review of the literature. *Eur Heart J Cardiovasc Imaging.* 2014;15:119–29.
32. Habets J, Mali WP, Budde RP. Multidetector CT angiography in evaluation of prosthetic heart valve dysfunction. *Radiographics.* 2012;32:1893–905.
33. Habets J, Symersky P, Leiner T, et al. Artifact reduction strategies for prosthetic heart valve CT imaging. *Int J Cardiovasc Imaging.* 2012;28:2099–108.
34. Habets J, van den Brink RB, Uijlings R, et al. Coronary artery assessment by multi-detector computed tomography in patients with prosthetic heart valves. *Eur Radiol.* 2012;22:1278–86.
35. Chenot F, Montant P, Goffinet C, et al. Evaluation of anatomic valve opening and leaflet morphology in aortic valve bioprosthesis by using multidetector CT: comparison with transthoracic echocardiography. *Radiology.* 2010;255:377–85.
36. Habets J, Tanis W, van Herwerden LA, et al. Cardiac computed tomography angiography results in diagnostic and therapeutic change in prosthetic heart valve endocarditis. *Int J Cardiovasc Imaging.* 2014;30:377–87.
37. Symersky P, Habets J, Westers P, et al. Prospective ECG triggering reduces prosthetic heart valve-induced artefacts compared with retrospective ECG gating on 256-slice CT. *Eur Radiol.* 2012;22:1271–7.

38. Faure ME, Swart LE, Dijkshoorn ML, et al. Advanced CT acquisition protocol with a third-generation dual-source CT scanner and iterative reconstruction technique for comprehensive prosthetic heart valve assessment. *Eur Radiol.* 2018;28:2159–68.
39. Tsai IC, Lin YK, Chang Y, et al. Correctness of multi-detector-row computed tomography for diagnosing mechanical prosthetic heart valve disorders using operative findings as a gold standard. *Eur Radiol.* 2009;19:857–67.
40. Wong D, Rubinshtein R, Keynan Y. Alternative Cardiac Imaging Modalities to Echocardiography for the Diagnosis of Infective Endocarditis. *Am J Cardiol.* 2016;118:1410–8.
41. Koneru S, Huang SS, Oldan J, et al. Role of preoperative cardiac CT in the evaluation of infective endocarditis: comparison with transesophageal echocardiography and surgical findings. *Cardiovasc Diagn Ther.* 2018;8:439–49.
42. Tanis W, Scholtens A, Habets J, et al. CT angiography and ¹⁸F-FDG-PET fusion imaging for prosthetic heart valve endocarditis. *JACC Cardiovasc Imaging.* 2013;6:1008–13.
43. Agrifoglio M, Filippini S, Roberto M, et al. Non-infective severe aortic paravalvular leakage 7 years after surgery: the role of suture technique. *J Cardiothorac Surg.* 2011;6:60.
44. Townsend DW. Combined PET/CT: the historical perspective. *Semin Ultrasound CT MR.* 2008;29:232–35.
45. Glaudemans AWJM, Signore A. FDG-PET/CT in infections: the imaging method of choice? *Eur J Nucl Med Mol Imaging.* 2010;37:1986–91.
46. Tseng J-R, Chen K-Y, Lee M-H, et al. Potential usefulness of FDG PET/CT in patients with sepsis of unknown origin. *PLoS One.* 2013;8:e66132.
47. Keidar Z, Engel A, Nitecki S, et al. PET/CT using 2-deoxy-2-[¹⁸F]fluoro-D-glucose for the evaluation of suspected infected vascular graft. *Mol Imaging Biol.* 2003;5:23–5.
48. Stádler P, Bilohlávek O, Spacek M, Michálek P. Diagnosis of vascular prosthesis infection with FDG-PET/CT. *J Vasc Surg.* 2004;40:1246–7.
49. Vind SH, Hess S. Possible role of PET/CT in infective endocarditis. *J Nucl Cardiol.* 2010;17:516–9.
50. Simons KS, Pickkers P, Bleeker-Rovers CP, Oyen WJ, van der Hoeven JG. F-18-fluorodeoxyglucose positron emission tomography combined with CT in critically ill patients with suspected infection. *Intensive Care Med.* 2010;36:504–11.
51. Van Riet J, Hill EE, Gheysens O, et al. (18)F-FDG PET/CT for early detection of embolism and metastatic infection in patients with infective endocarditis. *Eur J Nucl Med Mol Imaging.* 2010;37:1189–97.
52. Saby L, Laas O, Habib G, et al. Positron emission tomography/computed tomography for diagnosis of prosthetic valve endocarditis: increased valvular 18F-fluorodeoxyglucose uptake as a novel major criterion. *J Am Coll Cardiol.* 2013;61:2374–82.
53. Ricciardi A, Sordillo P, Ceccarelli L, et al. 18-Fluoro-2-deoxyglucose positron emission tomography-computed tomography: an additional tool in the diagnosis of prosthetic valve endocarditis. *Int J Infect Dis.* 2014;28:219–24.
54. Balink H, Veeger NJ, Bennink RJ, et al. The predictive value of C-reactive protein and erythrocyte sedimentation rate for 18F-FDG PET/CT outcome in patients with fever and inflammation of unknown origin. *Nucl Med Commun.* 2015;35:604–9.
55. Tsai HY, Lee MH, Wan CH, et al. C-reactive protein levels can predict positive 18F-FDG PET/CT findings that lead to management changes in patients with bacteremia. *J Microbiol Immunol Infect.* 2018. doi: 10.1016/j.jmii.2018.08.003.

56. Kestler M, Muñoz P, Rodríguez-Crèixems M, et al. Role of (18)F-FDG PET in Patients with Infectious Endocarditis. *J Nucl Med*. 2014;55:1093–8.
57. Pizzi MN, Rogue A, Fernández-Hidalgo N, et al. Improving the Diagnosis of Infective Endocarditis in Prosthetic Valves and Intracardiac Devices With 18F-Fluorodeoxyglucose Positron Emission Tomography/Computed Tomography Angiography: Initial Results at an Infective Endocarditis Referral Center. *Circulation*. 2015;132:1113–26.
58. Habib G, Lancellotti P, Antunes MJ, et al. 2015 ESC Guidelines for the management of infective endocarditis: The Task Force for the Management of Infective Endocarditis of the European Society of Cardiology (ESC). *Eur Heart J*. 2015;36:3075–128.

PART 1

**NEW IMAGING TECHNIQUES IN
PROSTHETIC HEART VALVE ENDOCARDITIS**



CHAPTER 2

¹⁸F-FDG PET/CT AND CT ANGIOGRAPHY IN PROSTHETIC HEART VALVE ENDOCARDITIS: FROM GUIDELINES TO CLINICAL PRACTICE

Laurens Swart
Asbjørn Scholtens
Wilco Tanis
Koen Nieman
Ad Bogers
Fred Verzijlbergen
Gabriel Krestin
Jolien Roos-Hesselink
Ricardo Budde

2

Published in: European Heart Journal 2018;39:3739-49

Abstract

The timely diagnosis of prosthetic heart *valve* endocarditis remains challenging yet of utmost importance. ^{18}F -fluorodeoxyglucose (^{18}F -FDG) positron emission/computed tomography (PET/CT) and cardiac computed tomography angiography (CTA) were recently introduced as additional diagnostic tools in the most recent ESC guidelines on infective endocarditis. However, how to interpret PET/CT findings with regard to what is to be considered abnormal, what the potential confounders may be, as well as which patients benefit most from these additional imaging techniques and how to best perform them in these often-complex patients, remains unclear. This review focusses on factors regarding patient selection and image acquisition that need to be taken into account when employing ^{18}F -FDG PET/CT and CTA in daily clinical practice, and the importance of a multidisciplinary Endocarditis Team herein. Furthermore, it emphasizes the need for standardized acquisition protocols and image interpretation, especially now that these techniques are starting to be widely embraced by the cardiovascular society.

Introduction

Over 300 000 prosthetic heart valves (PHVs) are implanted worldwide every year. Besides the immediate risk of prosthesis-patient mismatch and the long-term risk of well-known complications such as thromboembolic events and structural valve deterioration, another serious condition with a very high mortality rate (30–50%) affects patients with PHVs at an incidence of approximately 0.3–1.2% per patient-year: prosthetic heart valve endocarditis (PVE).^{1–3}

Despite ongoing advances in echocardiographic imaging and diagnostic microbiology, the diagnosis of PVE remains challenging, mostly because echocardiography and blood cultures (as mainstays of the Modified Duke Criteria)⁴ are inconclusive in more than 20% of PVE episodes, especially in the early stages of the disease.⁵ Combined with an atypical clinical presentation, the consequent delay or inappropriateness of treatment can lead to extensive perivalvular structural damage and systemic complications, worsening patient outcomes, and increasing risk of recurrence.⁶

¹⁸F-fluorodeoxyglucose (¹⁸F-FDG) positron emission/computed tomography (PET/CT) and cardiac computed tomography angiography (CTA) were recently introduced as additional tools to diagnose PVE, and added to the diagnostic criteria in the most recent ESC guidelines for infective endocarditis.⁶ The two largest prospective studies to date have shown decent diagnostic accuracy of PET/CT alone, and an improved performance of the entire diagnostic workup when PET/CT and CTA were added to it.^{7,8}

However, randomized controlled trials are lacking, and how to interpret PET findings with regard to what is to be considered abnormal, what the potential confounders may be, as well as which patients benefit most from these additional imaging techniques and how to best perform them in these often-complex patients, remains unclear. This review focusses on factors regarding patient selection and image acquisition that need to be taken into account when employing ¹⁸F-FDG PET/CT and CTA in daily clinical practice, and emphasizes the need for standardized acquisition protocols and image interpretation, especially now that these techniques are starting to be widely embraced by the cardiovascular society.

Implementation in the diagnostic work-up of suspected prosthetic heart valve endocarditis

The 2015 ESC Guidelines on Endocarditis recommend using additional imaging modalities when echocardiography and blood cultures are inconclusive (i.e. result in a 'possible' diagnosis of endocarditis, or a 'rejected' diagnosis with persisting high suspicion). Three techniques may be employed: CTA to depict perivalvular complications, cerebral magnetic resonance imaging (MRI), and/or whole-body CT or PET/CT to depict embolic events, and—only in case of PHVs—¹⁸F-FDG PET/CT to evaluate abnormal metabolic activity around the site of prosthetic valve implantation,⁶ as evidence on the use of ¹⁸F-FDG PET/CT in patients with native valve endocarditis is merely limited and non-supporting. For PHVs, no distinction is made between biological and mechanical prosthetic valves, as PET/CT performance does not differ between the two valve types.^{7,8} Evidence of its use in patients suspected of transcatheter-replaced aortic valves (TAVR) endocarditis is still limited to case reports,⁹ but may soon become relevant as the incidence of TAVR endocarditis has been increasing over the past decade and mortality is high.¹⁰

The ESC guidelines recommend cardiac CTA and ¹⁸F-FDG PET/CT only to be employed when diagnostic uncertainty remains after the usual diagnostic work-up comprising echocardiography and blood cultures.⁶ One problem with this approach is the consequential delay of additional imaging, sometimes after several weeks of antibiotic therapy. The resulting decrease in inflammatory activity directly affects the intensity of ¹⁸F-FDG uptake around the infected prosthetic valve.¹¹ Moreover, there are other valid reasons to consider both PET/CT and CTA, even when the Modified Duke criteria have already been met (*Figure 1*).

For PET/CT, these reasons include the possibility of depicting metastatic infections and septic emboli, identification of the focus of infection (port of entry), evaluation of involvement of other valves or cardiac implanted electronic devices, and identification of other foci of infection should PVE be ruled out, all of which may guide treatment strategies. For CTA, besides the ability to depict oedema as an early sign of inflammation (seen as stranding of the fatty tissue around the annulus and ascending aorta), the detailed anatomical depiction in all cardiac phases offers superior detection of perivalvular extensions such as abscesses and pseudoaneurysms.^{12,13} Since the presence and extent of such perivalvular extensions often guides the decision to surgically intervene, clear depiction of these life-threatening complications is of the utmost importance and simultaneously provides valuable anatomical information for planning of the surgical approach.²

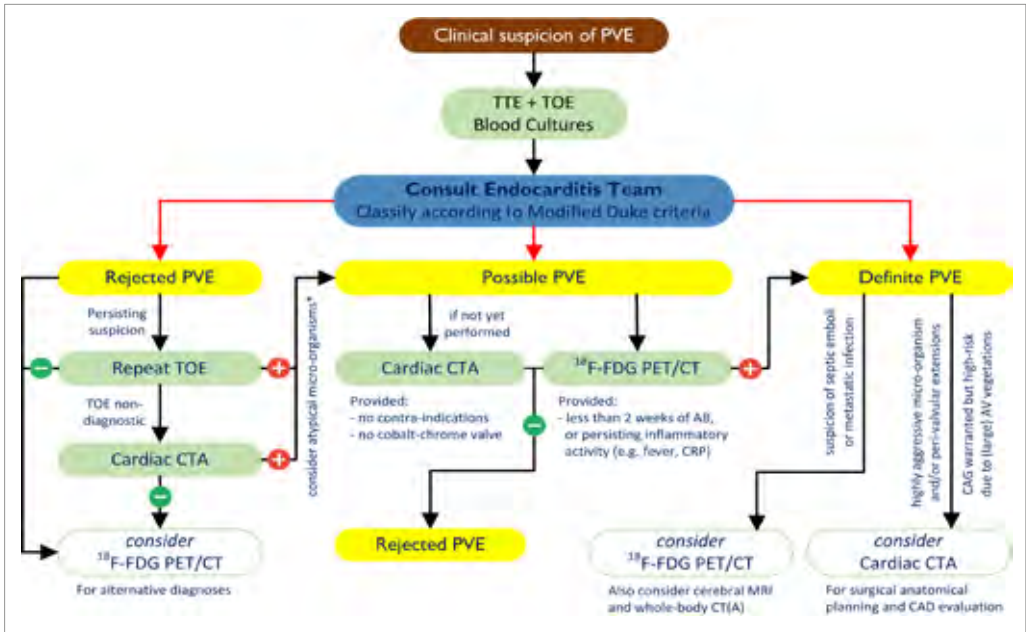


Figure 1 | Flowchart of the proposed diagnostic work-up of (suspected) prosthetic heart valve endocarditis, including an early consultation of the multidisciplinary Endocarditis Team and early employment of additional imaging techniques. AB, antibiotic therapy; AV, aortic valve; CAD, coronary artery disease; CAG, coronary angiography; CRP, C-reactive protein; CTA, computed tomography angiography; PCR, polymerase chain reaction; PVE, prosthetic heart valve endocarditis; TTE, transthoracic echocardiography; TOE, transoesophageal echocardiography; ^{18}F -FDG PET/CT, ^{18}F -fluorodeoxyglucose positron emission/computed tomography. *Consider serology and/or PCR for known atypical causative micro-organisms in culture-negative endocarditis (e.g. *Coxiella burnetii*, *Tropheryma whippelii*, *Bartonella henselae*, *Brucella*, *Legionella*, etc. depending on clinical suspicion).

Either technique, but ^{18}F -FDG PET in particular, can detect inflammation before structural changes (i.e. vegetations, perivalvular extensions, etc.), which are required for echocardiographic detection of PVE, ensue, while also allowing for early detection of septic emboli and metastatic infections before these become clinically apparent.^{14–16} This further increases the importance of their early implementation in the diagnostic work-up, as they may allow for diagnosis and initiation of appropriate antibiotic therapy in the earlier stages of the disease, before extensive damage (or vegetational growth) that may require a major surgical (re)intervention has occurred.

The optimal timing of employment of PET/CT and CTA however, is not absolute, and the benefits of the additional information gained should be weighed against the downsides of exposure to radiation and intravenous contrast, however small these may often be in light of the morbidity associated a missed diagnosis or an unidentified complication. Acquiring a PET-scan in a critically ill patient may, just like TEE, be problematic, in which case assessment by CTA alone for complications requiring immediate care may be preferential, further underlining the importance of a patient-tailored diagnostic approach in every case of suspected PVE. Combined with the expertise, advanced scanning equipment and broad reference framework required for the acquisition and interpretation of PET/CT and CTA images in suspected PVE, this emphasizes the need for a multi-disciplinary Endocarditis Team in surgical reference centres.⁶ Early consultation with—or referral to—this team is essential for any patient suspected of endocarditis, particularly in case of suspected PVE, and should take place as soon as the initial diagnostic work-up comprising a clinical evaluation, blood cultures and (transthoracic and transoesophageal) echocardiography has been completed (*Figure 1*).

Methods of acquisition

Some of the largest studies performed to date have simply adopted the oncological total-body PET protocol, in which, after a 6-h fast, a dose of ¹⁸F-FDG based on the patients' body weight is injected 60 min prior to image acquisition. Although alternative post-injection acquisition timings have been suggested for the detection of PVE, there is no substantial evidence that supports an earlier or a delayed acquisition.^{17,18} However, to adequately assess the heart, some other important adaptations are required.

PET patient preparation

Fasting and low-carbohydrate diet

Under normal circumstances, the heart metabolizes both carbohydrates and free fatty acids (FFAs), thus also taking up an ample amount of ¹⁸F-FDG which often makes evaluation of (prosthetic) heart valves and the peri-annular areas difficult and cannot sufficiently be prevented by regulation of blood glucose levels alone.¹⁹ Prolonged fasting (up to 18h) and a low-carbohydrate diet suppress myocardial ¹⁸F-FDG uptake as they reduce the amount of glucose available for myocardial metabolism, making FFAs the predominant cardiac energy source.²⁰ However, no standardized preparatory protocol exists.

The duration of the pre-scan fasting period and the way in which a preparatory diet (if any) was applied, varied widely within studies performed to date. From a number of studies on the use of ¹⁸F-FDG PET/CT in cardiac sarcoidosis however, it seems the longer the fasting period, the better the myocardial suppression²¹, and combined fasting for at least 12h and a 24-h low-carbohydrate diet is likely superior to either one alone (*Figure 2*).²²

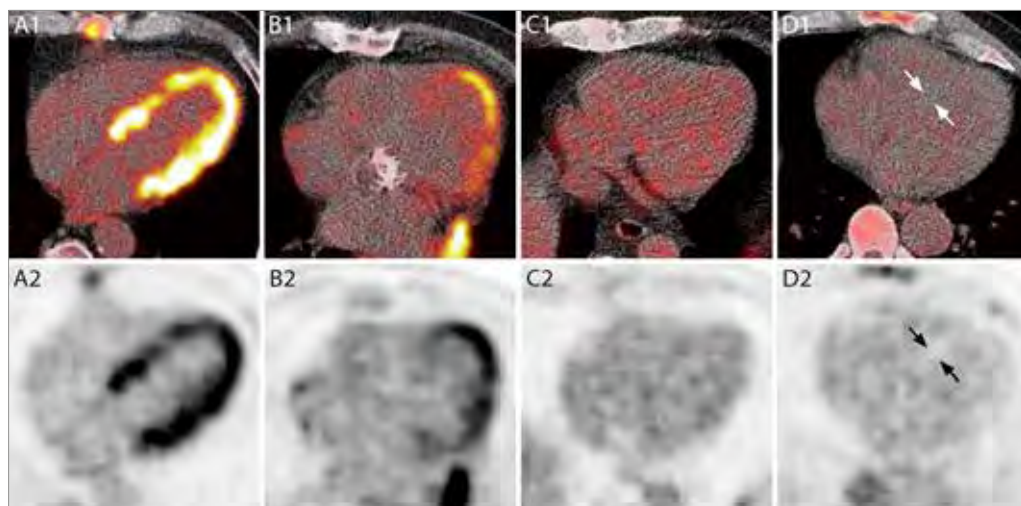


Figure 2 | Fused positron emission/computed tomography (1) and positron emission tomography only (2) images of grades of myocardial suppression in four patients with different preparation prior to ^{18}F -fluorodeoxyglucose administration. (A) Six hour fast only: poor suppression; (B) 6-h fast and 24-h low-carb diet: fair suppression (more than blood pool, but less than liver); (C) ~12-h fast and 24-h low-carb diet: good suppression (equal to blood pool); (D) ~6-h fast, 24-h low-carb diet and 50 IU/kg of i.v. unfractionated heparin 15min prior to fluorodeoxyglucose administration: excellent suppression (less than blood pool; myocardium indicated by **arrows**).

Intravenous heparin injection

To further decrease myocardial ^{18}F -FDG uptake, intravenous heparin has been proposed.²³ Unfractionated heparin promotes the release of FFAs into the bloodstream, thereby shifting myocardial metabolism further towards their oxidation. While the minimal dose for significant reduction of myocardial ^{18}F -FDG uptake remains unknown, injection of 50 IU/kg of unfractionated heparin approximately 15min before ^{18}F -FDG administration has shown to provide distinguishable additional suppression (*Figure 2*).^{24,25}

CT angiography

The low-dose localization CT acquired on the PET/CT-scanner cannot be used for diagnostic purposes. Since depiction of PHVs requires contrast enhancement, ECG-gating and a high temporal resolution, an additional CTA is required. Although co-registration on one integrated scanner with breathing- and ECG-gated PET is preferred as it provides more reliable image fusion and is feasible on current state-of-the-art PET/CT scanners, the required CTA image quality and temporal resolution may require a separate scan with post hoc fusion on a high-end dedicated CTA scanner in centres with less advanced PET/CT equipment.

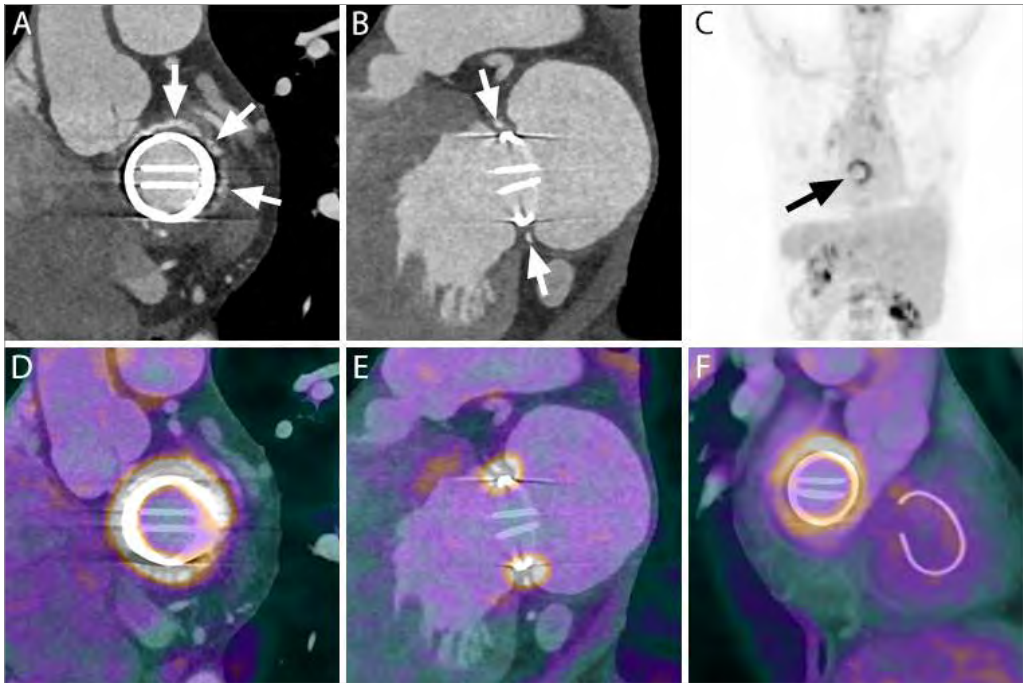


Figure 3 | CTA (**A, B**), maximum intensity projection PET (**C**) and fused PET/CTA (**D-F**) of another patient with a mechanical mitral valve (St. Jude Medical, St. Paul MN, USA) and a tricuspid valve ring (plasty). Although the short axis view of the prosthetic valve may give the impression of extensive perivalvular extensions around the entire valve (**A, arrows**), the perpendicular view shows that there is no paravalvular connection (**B, arrows**) and that these areas therefore most likely represent surgical felt pledgets (see *Figure 5*; a non-contrast enhanced scan was not performed in this patient). The fused PET/CTA images however, clearly show diffuse highly increased ^{18}F -FDG uptake around the entire mitral valve prosthesis, confirming the diagnosis of PVE, while the tricuspid valve ring is completely unaffected. This patient was found to have chronic Q-fever and was treated conservatively.

Fusion of PET and CTA images allows for better anatomical correlation (*Figure 3*), and can help differentiate sterile paravalvular extensions⁹ (e.g. those that are a result of surgery or previous endocarditis) from mycotic aneurysms and abscesses (*Figure 4*), which may help guide the surgical approach in case a reoperation is required.

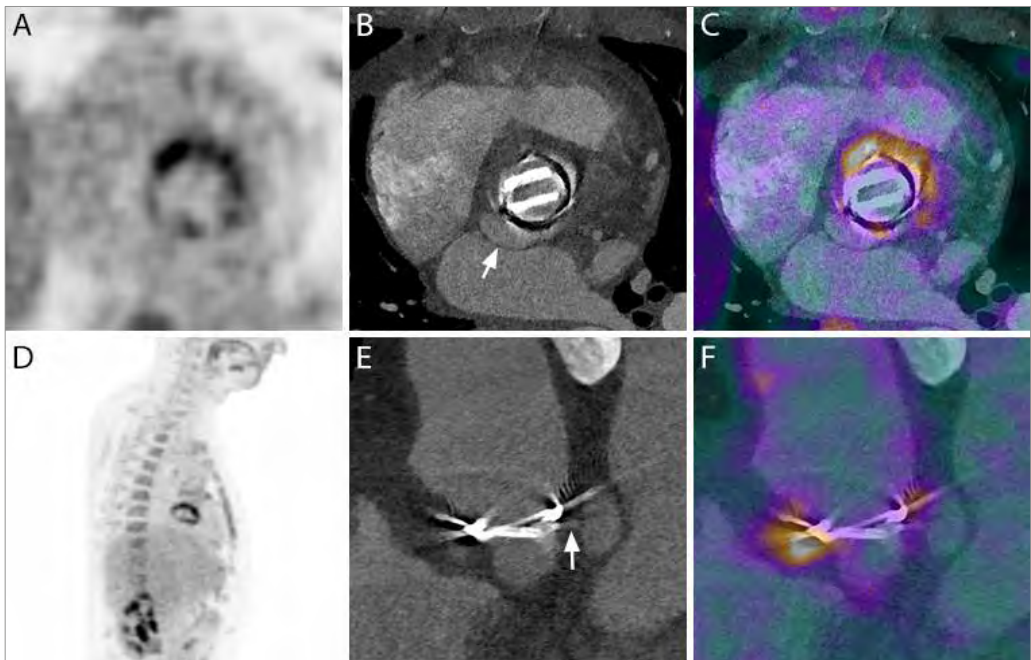


Figure 4 | PET (A, D), CTA (B, E) and fused PET/CTA (C, F) images of a patient with a combined aortic valve and ascending aortic prosthesis following a Bentall procedure for *Staphylococcus aureus* endocarditis, who was diagnosed with recurrent endocarditis, this time of *Streptococcal* origin. CTA showed a pseudo-aneurysm on the posterior side of the aortic prosthetic valve that was however PET-negative, and therefore most likely a remainder of the previous episode of endocarditis (CTA had not been performed after the Bentall procedure). The patient was reoperated upon and the perivalvular extension, which was surgically corrected, did not show any signs of active infection according to the cardiothoracic surgeon.

Most PHVs cause only limited artefacts on CT images.²⁶ Adjusted double-oblique planes provide short-axis views of the prosthetic valve, as well as perpendicular views of the valve leaflets that allow for a more detailed assessment of vegetations and mechanical valve function (e.g. opening and closing angles of bi-leaflet valves).^{26,27} In most patients, even the presence of coronary artery disease and the patency of coronary bypass grafts can readily be evaluated,²⁸ which is of particular importance in aortic PVE that requires reoperation, as vegetations may be dislodged due to catheter manipulation during invasive coronary angiography (*Figure 5*).

While the contrast-enhanced acquisition is the most important, an additional non-contrast-enhanced acquisition may be helpful to assess calcifications and suture pledgets. A prospectively ECG-triggered scan of the PHV, similar to a calcium score scan, at 45% of the RR interval is often sufficient (*Figure 5*). Finally, a delayed venous-phase acquisition of the entire chest may be helpful to detect wall enhancement of abscesses and differentiate thrombus from slow flow, but can be challenging to acquire and has not been sufficiently validated yet.

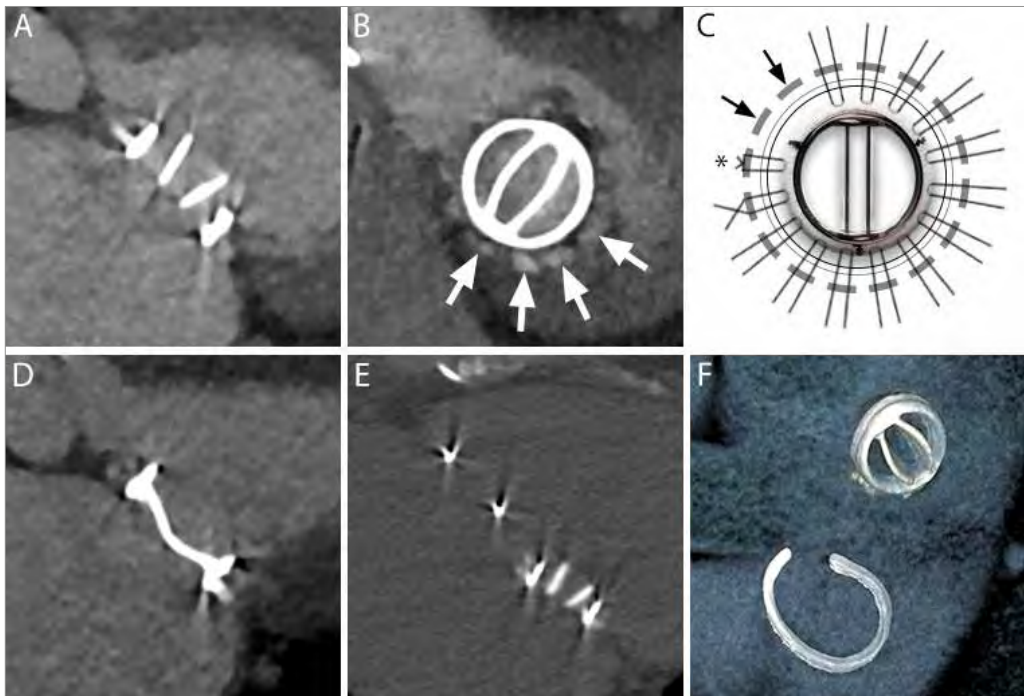


Figure 5 | Comprehensive computed tomography angiography evaluation of a prosthetic mitral valve and tricuspid valve ring for suspicion of prosthetic heart valve endocarditis. Multiplanar reconstructions perpendicular (**A**) and parallel (**B**) to the valve plane in the open (**A**) and closed (**D**) phase, allowing for evaluation of valve function (compared with normal opening and closing angles provided by the manufacturer) and assessment of (sub)-valvular masses, such as vegetations, thrombus, or pannus. Often during implantation, surgical felt pledgets (**arrows**) may be used to strengthen the annulus (**C**) onto which the prosthetic heart valve is sutured (**asterisk**), which have a similar density as iodinated contrast on computed tomography angiography and may therefore mimic perivalvular extensions (**B, arrows**). An additional non-contrast enhanced scan (**E**) will allow differentiation between the two. On a three-dimensional volumetric rendering (**F**), a visual impression of valve function and possible 'rocking' of the valve (in case of dehiscence) can be gained.

Total radiation dose

With the average PET/CT radiation dose varying from approximately 5–15mSv (depending on the administered amount of ^{18}F -FDG) and an approximate dose of 5–10mSv for a dynamically ECG-gated or triggered CTA of the heart, the total radiation dose approaches 15–20mSv,⁸ which is high but, in light of the mortality associated with PVE and (missed) perivalvular extensions in particular, seems acceptable when considering the possible benefits of early diagnosis and adequate treatment that can be achieved by combining these imaging modalities. Future technological advancements, new (iterative) reconstruction techniques and prospective CTA protocols specifically tailored for the acquisition of PHVs may allow further reduction of this radiation dose.^{29,30}

Image interpretation

Scatter-corrected PET-images with and without correction for attenuation by surrounding tissues and scattering (based on the low-dose CT) can be viewed separately in all planes, as a maximum intensity projection or fused with the low-dose CT images. Besides the full-body assessment of any pathological ^{18}F -FDG uptake, both a visual and a (semi-)quantitative evaluation of the PHV(s) should be performed. Finally, there are several patient and acquisition related factors that could result in either false positive or false negative misinterpretations and need to be taken into account.

Qualitative assessment

Through visual analysis, regions with pathological ^{18}F -FDG uptake are identified as areas of increased signal intensity, i.e. a higher intensity than may be expected, usually shown as bright or 'hot' colours on fused images. Based on the density of tissues around the point of interest as determined by the low-dose CT, the signal is amplified depending on the amount of attenuating material between the source (i.e. the location of the ^{18}F -FDG) and the PET camera (attenuation correction). In case of PHV, the metallic components are identified as having a very high density, which may result in over-amplification of the signal originating from regions around or 'behind' the prosthetic valve. Therefore, when an abnormal focus of ^{18}F -FDG uptake is identified surrounding a prosthetic heart valve, correlation with the non-attenuation-corrected images is advised, as the combination of visual assessment of both the corrected and non-corrected images has the highest diagnostic accuracy for PVE.³¹ As long as the pathological uptake remains distinguishable from the surrounding background on the non-attenuation-corrected images, the intensity of the signal seems to be less relevant for diagnostic purposes.³¹

Alternatively, metal-artefact reducing algorithms have recently been suggested to help reduce the erroneous overcorrection for attenuation in case of cardiac implantable electronic devices³², but these have not yet been tested with PHV.

The assessment of abnormal ^{18}F -FDG uptake around PHV is not dichotomous. Different patterns of uptake with different intensities can be found, and always have to be evaluated in light of clinical parameters such as the duration of antibiotic therapy prior to imaging since the clinical relevance of these different patterns is not yet fully understood (*Figure 6*).³³

In bioprosthetic valves with struts, slightly increased ^{18}F -FDG uptake around these metallic components is sometimes observed, possibly due to chronic tension or friction exerted on these anchor points.^{34,35}

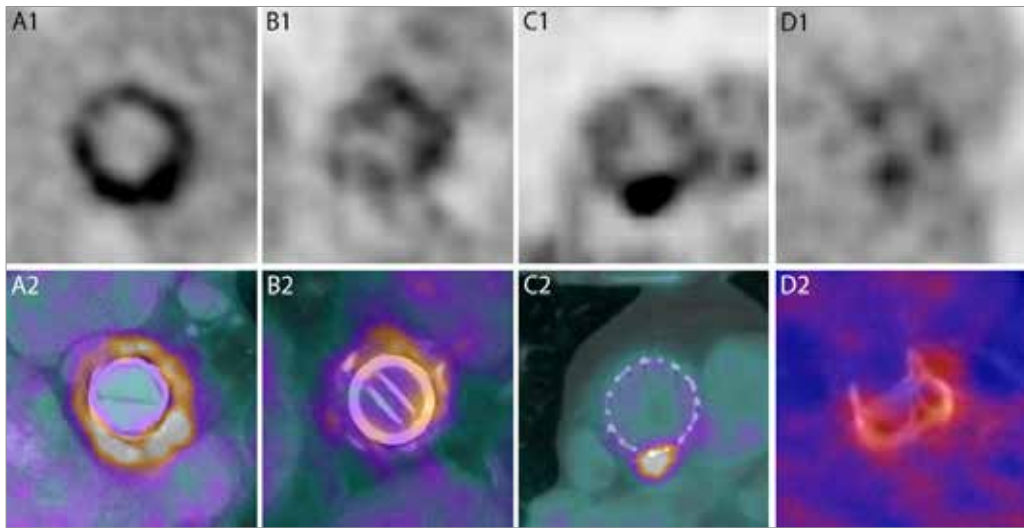


Figure 6 | Attenuation-corrected positron emission tomography (**top**) fused positron emission/computed tomography (**A2–C2**) and three-dimensional maximum-intensity projection positron emission/computed tomography (**D2**) images of different patterns and intensities of ^{18}F -FDG uptake around prosthetic heart valves: a surgically confirmed case of prosthetic aortic valve endocarditis in its acute stage showing diffuse and intense uptake (**A**); a mechanical aortic valve prosthesis infected by *Streptococcus equinus* in a patient that had already been treated with intravenous antibiotics for 14 days showing less intense, semi-circular ^{18}F -FDG uptake (**B**); a very focal and intense pattern of ^{18}F -FDG uptake in a definite case of a transcatheter-implemented aortic valve endocarditis⁹ (**C**); and a semi-recently implanted (63 days) bioprosthetic valve showing mild multi-focal uptake of ^{18}F -FDG around the three metallic struts (**D**).

Quantitative assessment

To reduce observer subjectivity, several studies to date have attempted to add a quantitative analysis to the visual evaluation of PHVs for suspicion of PVE. Standardized uptake values are commonly used in PET-imaging to express the amount of ^{18}F -FDG uptake in a particular region of interest relative to the amount of injected radioactivity (assuming an even distribution throughout the body; corrected for body mass index or lean body mass).

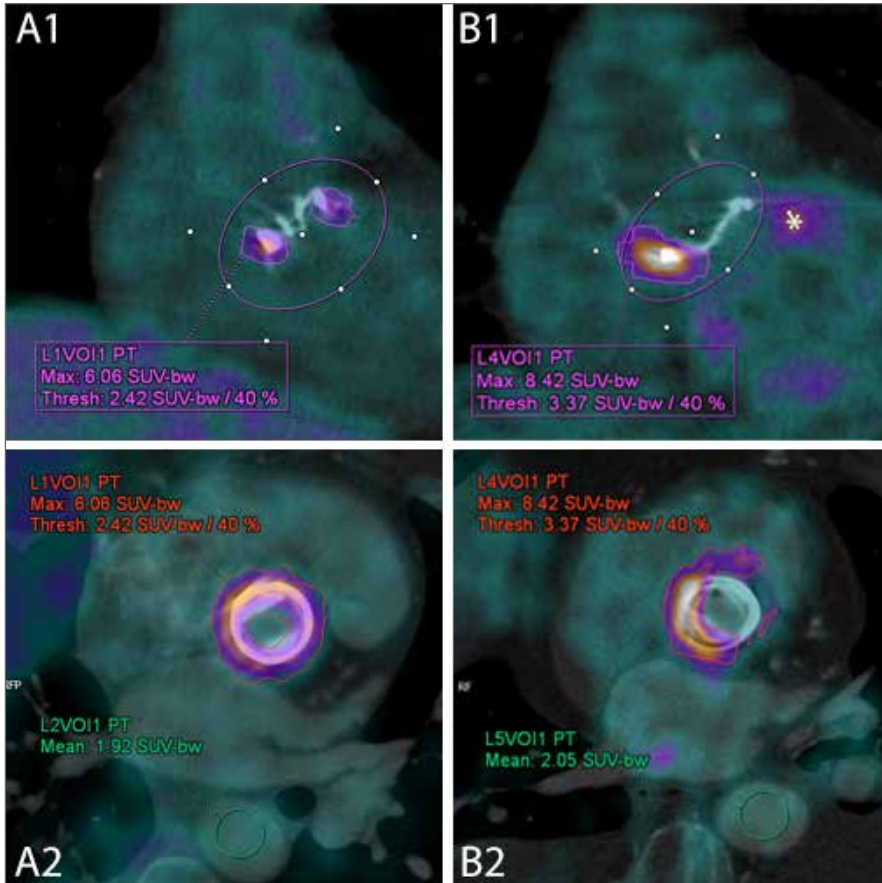


Figure 7 | Semi-quantitative analysis of periprosthetic ^{18}F -fluorodeoxyglucose uptake in a patient with excellent suppression of myocardial ^{18}F -FDG uptake (**A**) and a patient with some residual myocardial ^{18}F -fluorodeoxyglucose uptake (**B**). Through a combination of manual avoidance of unsuppressed myocardium (**asterisk, B1**), and the use of an automated volume of interest created as an isocontour of all voxels that have an intensity of at least 40% of the voxel with the highest intensity in the selected area (**bottom**), the maximum standardized uptake value around the prosthetic heart valve is reliably and reproducibly measured. The maximum standardized uptake value is then divided by the mean standardized uptake value of a small spherical volume of interest placed in the blood pool of the descending aorta at the level of the prosthetic valve (small enough to guarantee exclusion of any aortic wall) to calculate the ratio of standardized uptake value (**bottom**). SUV, standardized uptake value.

Use of a spherical volume of interest around the prosthetic heart valve to measure the maximum signal intensity may prove troublesome when this volume includes any residual ^{18}F -FDG uptake in the myocardium or ascending aorta. An automated volume of interest expanding to a certain percentage (e.g. 40%) of the amount of ^{18}F -FDG uptake measured at the point of maximum intensity, with manual correction if necessary, may therefore be a more sensible approach (*Figure 7*).

Several studies attempted to establish cut-off values for the measured maximum intensity around the PHV (SUV_{max}). However, since the SUV_{max} is dependent on a number of variables including the amount of injected ^{18}F -FDG in relation to the body weight of the patient, the camera of the scanner and scanning parameters (such as time per bed position), an alternative measure of relative ^{18}F -FDG uptake has also been advocated, which is not affected as much by these parameters: the ratio of the uptake around the PHV to the background activity measured in the blood pool (e.g. in the descending aorta or adjacent venous system). Even this $\text{SUV}_{\text{ratio}}$ still lacks generalizability though, mostly due to differences in cameras, imaging protocols and reconstruction methods between centres, hence the widely spread suggested cut offs for both parameters (see *Tables 1* and *2*).

To partially overcome this issue, a standardized calibration and reconstruction method has been introduced by the European Association of Nuclear Medicine Research Ltd (EARL) which adapts the quantified uptake relative to the uptake measured in a phantom. Over 150 centres currently have their accreditation.

Study	PVE	Controls ^a	Average or median SUV _{max} for PVE	Average or median SUV _{max} for controls	ROC AUC	Cut off ^b	Sensitivity	Specificity
Saby et al. ⁷	30	20	4.7 [3.6-6.0]	3.3 [2.8-4.3] (p=0.02)	n/a	n/a	n/a	n/a
Tanis et al. ⁴⁶	7	1	8.4 [7.2-9.7]	2.2	n/a	n/a	n/a	n/a
Rouzet et al. ³⁸	13	6	6.5 (3.9-14.7)	4.9 (3.3-6.2) (p=0.08)	n/a	6.2	n/a	100%
Pizzi et al. ⁸	52	35	7.4 [5.4-10.5]	0.5 [0.5-3.7]	0.89	3.7	91%	79%
Jiménez-Ballvé et al. ³¹	24 ^c	13 ^c	6.4 ± 2.3 (3.1-13.3)	4.3 ± 0.9 (2.8-6.1) (p=0.004)	0.82	4.5	79%	69%
Fagman et al. ⁴²	8	19	5.8 [3.5-6.5]	3.2 [2.5-3.7] (p<0.001)	0.90	3.3	88%	68%
Salomäki et al. ⁴³	6	3 ^d	5.8 (4.1-9.0)	3.0 (2.9-3.0)	n/a	4.0	100%	100%
Mathieu et al. ³⁵	0	54	n/a	3.5 (2.1-8.0)	n/a	n/a	n/a	n/a

Table 1 | Overview of SUV_{max} values reported in literature for patients with PVE and controls. Average and median SUV_{max} values for patients with definite PVE and controls, with the diagnostic performance and optimal cut-off values suggested in different studies. Values shown as mean ± standard deviation (range), median [interquartile range], or median (range). PVE, prosthetic heart valve endocarditis; ROC AUC, area under the receiver-operator curve; PET/CT, positron emission/computed tomography; SUV_{max}, maximum standardized uptake value. **(a)** Patients with a final diagnosis of ‘possible PVE’ according to the Modified Duke Criteria and/or expert team consensus were excluded in this table. **(b)** Assuming sensitivity and specificity are equally important. **(c)** Jiménez-Ballvé et al.³¹ reported PET/CT findings per area (i.e. prosthetic valve) suspected of PVE, as opposed to a per-patient analysis. We performed a new analysis on the data they provided (excluding all cardiac implanted electronic devices) which included 24 prosthetic valves with definite PVE and 13 valves with a rejected diagnosis of PVE. **(d)** Salomäki et al.⁴³ reported that two scans were false-positive, one due to a foreign body reaction, the other most likely due to recent valve implantation (6 weeks). These two scans, with respective SUV_{max} values of 7.1 and 7.8, were excluded in this table.

Study	PVE	Controls ^a	Average or median SUV _{ratio} for PVE	Average or median SUV _{ratio} for controls	ROC AUC	Cut off ^b	Sensitivity	Specificity
Saby et al. ⁷	30	20	2.0 [1.7-2.8]	1.6 [1.3-2.1] (p=0.16)	n/a	n/a	n/a	n/a
Tanis et al. ⁴⁶	7	1	4.2 [3.8-5.9]	1.4	n/a	2.2	100%	100%
Rouzet et al. ³⁸	13	6	4.1 (2.3-7.8)	3.4 (2.4-4.4) (p=0.24)	n/a	4.4	n/a	100%
Pizzi et al. ⁸	52	35	3.9 [2.8-5.9]	0.3 [0.2-2.1]	0.89	1.7	91%	76%
Jiménez-Ballvé et al. ³¹	24c	13c	3.3 (1.7-6.0)e	2.0 (1.4-2.9)e	0.87	1.9	92%	69%
Fagman et al. ⁴²	8	19	2.4 [1.7-3.0]e	1.45 [1.3-1.6]e (p<0.001)	0.90	1.6	88%	84%
Salomäki et al. ⁴³	6	3§	2.3 (1.9-3.8)	1.5 (1.3-1.7)	n/a	1.8	100%	100%
Mathieu et al. ³⁵	0	54	n/a	2.0 (1.3-6.6)	n/a	n/a	n/a	n/a

Table 2 | Overview of SUV_{ratio} values reported in literature for patients with PVE and controls. Legend as Table 1, but for SUV_{ratio} in stead of SUV_{max}* (e) Target-to-background SUV_{ratios} were calculated by dividing the SUV_{max} of the PHV by the SUV_{max} of the mediastinal blood pool (as opposed to the mean SUV in the blood pool).

Positive confounding factors

Recent valve implantation

Increased ^{18}F -FDG uptake due to (physiological) inflammation after recent surgery, irradiation, or chemotherapy, is a well-known pitfall causing false positive misinterpretations in oncological PET imaging.³⁶ For PHV surgery, the duration and characteristics (i.e. uptake pattern, *Figure 6*) of postoperative periprosthetic inflammation remains unclear. Some cases of increased ^{18}F -FDG uptake around recently (<2months) implanted valves have been reported (*Figure 8A*).³⁷ Therefore, the ESC guidelines do not currently recommend ^{18}F -FDG PET/CT for suspicion of PVE within 3months of PHV implantation. More recently however, the arbitrariness of this three-month grace period was underlined, as many true negatives have been reported even within 1month of valve implantation, as well as several false positives beyond the first three post-operative months,¹⁸ further exemplifying the need for future research to elucidate the exact duration and especially the characteristics of postoperative inflammation on PET/CT, as well as its influencing factors (i.e. valve type, implantation technique, etc.).

As an alternative imaging technique to ^{18}F -FDG PET/CT that is also mentioned in the ESC guidelines,⁶ radiolabeled leucocyte scintigraphy employs in-vitro labelling of autologous leucocytes with radioactive markers such as $^{99\text{m}}$ -Technetium analogues to detect inflammation. In a study that compared both techniques in 39 patients with suspected PVE, PET/CT had a low specificity and positive predictive value of 71% and 68% respectively.³⁸ However, all of the six false positive results were identified in patients who had undergone open-chest cardiac surgery <2 months prior to ^{18}F -FDG PET/CT imaging. Radiolabeled leucocyte scintigraphy was not affected by postoperative inflammation and was thus true-negative in all of these patients, suggesting a sequential strategy consisting of both modalities could be feasible in patients with suspicion of a false positive PET/CT result due to recent valve implantation. Radiolabeled leucocyte scintigraphy did, however, substantially compromise sensitivity in this study and is generally very time-consuming and labour-intensive, which limits clinical applicability.

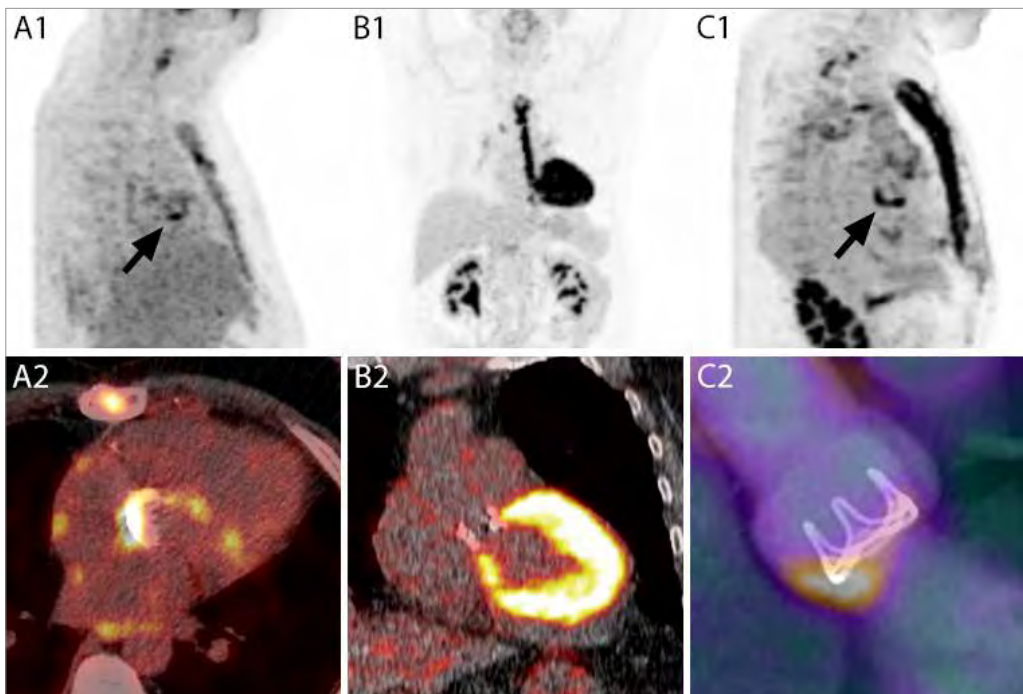


Figure 8 | Positron emission tomography maximum intensity projections (**A1**, **B1**, **C1**) and fused positron emission/computed tomography (**A2**, **B2**), or positron emission tomography/computed tomography angiography (**C2**) images of false positive positron emission tomography scans due to recent valve implantation of a mechanical aortic valve (27 days prior to positron emission/computed tomography imaging) (**A**, **arrow**); inadequate suppression of myocardial ^{18}F -fluorodeoxyglucose uptake in a patient who did not adhere to the dietary instructions, making assessment of the perivalvular area of this mechanical aortic valve nearly impossible (**B**); and prior use of certain fluorodeoxyglucose-avid surgical adhesives in this patient who underwent a Bentall procedure with biological aortic valve prosthesis 3 years prior to positron emission tomography imaging, during which BioGlue (CryoLife Inc., Kennesaw, GA, USA) had been applied in a small area of the artificial annulus (**C**, **arrow**).

Inadequate suppression of myocardial glucose metabolism

Inadequate suppression of myocardial ^{18}F -FDG uptake can result in uninterpretable or false positive exams (*Figure 2*). Especially the basal lateral and septal wall may often show persisting myocardial ^{18}F -FDG uptake despite prolonged fasting that, when close to a prosthetic aortic or mitral valve, can possibly mimic uptake also observed in cases of PVE (*Figure 8B*).^{22,25} Semi-quantitative analyses using spherical volumes of interest around these PHV are practically unfeasible.³⁴ Fusion with CTA may provide improved delineation of the prosthetic valve and allow for better differentiation of pathological periprosthetic ^{18}F -FDG uptake from residual myocardial ^{18}F -FDG uptake.⁸

Surgical adhesives

Surgical adhesives used during cardiac surgery can be very FDG-avid for undetermined but extended periods of time, possibly due to an inflammatory foreign body reaction (*Figure 8C*). They have previously been reported to result in false positive PET misinterpretations after aortic root surgery³⁹ and heart valve replacement.³⁴

Other patient and image processing related artefacts

Movement of the heart and the patient during PET acquisition, as well as erroneous fusion of PET and CT images, may displace or spread extracardiac (e.g. pulmonary) or unsuppressed myocardial ¹⁸F-FDG uptake and project it adjacent to a PHV, resulting in false positive misinterpretations. As stated earlier, both overcorrection due to beam hardening next to a PHV as well as 'normal' slightly increased uptake due to possible strain exerted by sutures or PHV struts can also lead to false-positive misinterpretations.

Negative confounding factors

Prolonged antibiotic therapy

In the prospective cohort study by Saby et al.,⁷ eight out of 30 (26%) patients with a definite final diagnosis of PVE had negative PET/CT results. Echocardiography was positive for endocarditis in all eight patients, but blood cultures were negative in three. None of the reported variables were statistically significant predictors of a negative PET/CT, yet the authors stated that these false negative results could be attributed to lower inflammatory activity and PET/CT being performed after extended periods of antibiotic therapy in these cases.⁷

One could even argue that the PET-scan is not false negative, but in fact true negative for active infection, as the inflammation is suppressed by the antibiotics. Thus, a certain level of inflammatory activity is required for accurate PET results, as illustrated by two studies that showed significantly improved diagnostic accuracy of PET for fever of unknown origin when C-reactive protein levels were elevated.^{40,41} Early implementation of PET/CT(A) in the diagnostic work-up of patients with suspected PVE may therefore not just improve outcome by allowing for a timelier diagnosis, but may also prevent missed diagnoses due to extended periods of antibiotic therapy.

Vegetations

Isolated, small, or mobile vegetations have been reported to be missed by ¹⁸F-FDG PET/CT due to its limited temporal and spatial resolution⁴², and because vegetations mostly consist of dense fibrous residue which shields the pathogen from a cellular immune response⁴³, as illustrated by some cases of larger vegetations also being PET-negative.⁴⁴ This further underlines the need for a multimodality approach in which each imaging modality covers the other's possible shortcomings, as vegetations are readily detected on CTA.

Metastatic infections and incidental findings

Before ^{18}F -FDG PET/CT was introduced for the diagnosis of infective endocarditis itself, it was already being used to detect septic emboli— particularly asymptomatic ones—and metastatic infections.¹⁵ In fact, septic emboli detected by additional imaging techniques including ^{18}F -FDG PET, whole body CT(A) and (cerebral) MRI have now been added as a minor diagnostic criterion in the latest guidelines.⁶ Any extracardiac focus is likely to be identified by ^{18}F -FDG PET/CT if performed in the early stage, before prolonged antibiotic therapy.⁴⁶ Moreover, when no pathological ^{18}F -FDG uptake is identified around a PHV, ^{18}F -FDG PET/CT may provide an alternative diagnosis in up to 54% of the patients with a rejected diagnosis of PVE.⁸

Interpretation of findings and decision-making: role of the 'Endocarditis Team'

The PET/CT and CTA findings should be correlated to clinical and other diagnostic findings. Ideally—and according to the most recent ESC guidelines⁶—, findings of blood cultures, (transthoracic and transoesophageal) echocardiography, CT angiography, PET/CT, and other imaging modalities tailored to suspicion of complications such as septic emboli (e.g. abdominal or whole-body CT, brain CT or MR) are to be discussed in a multidisciplinary 'Endocarditis Team'. This team (in a tertiary care centre with cardiothoracic surgical capabilities) should have regular meetings and consist of at least a cardiologist, cardiothoracic surgeon, microbiologist and/or infectious disease specialist, radiologist and/or nuclear medicine physician.⁴⁷

Due to the complexity of the disease itself, and the acquisition and interpretation of often-required additional imaging in particular, referral to a reference centre with such an expert team should—besides in cases of complicated endocarditis, as the guidelines recommend—readily be considered in any case of PVE.

Future perspectives

The possibilities of using PET as a tool to follow-up on antibiotic therapy and possibly even guide decisions such as treatment prolongation (or a surgical approach) have been debated in other studies employing PET for the detection of infectious or inflammatory disease.^{48,49} However, keeping in mind the negative confounding effect of prolonged antibiotic therapy on the diagnosis of PVE using PET, it remains questionable whether it can in fact accurately distinguish suppressed infection from complete eradication.¹¹ Alternatively, some case reports have shown that even in successful antibiotic treatment of PVE, follow-up PET/CT may still, albeit less intense, show abnormal ¹⁸F-FDG uptake around the PHV despite uneventful clinical follow-up, once more exemplifying that inflammation does not necessarily imply infection.⁹

Lack of an adequate reference standard has been problematic in all trials to date. With an estimated sensitivity and specificity of the Modified Duke Criteria in PVE of approximately 60–70%, the diagnostic performance of PET can hardly be adequately assessed, while an alternative reference standard based on expert consensus, as in the largest prospective cohort studies to date, results in a substantial incorporation bias due to the experts not being blinded to PET/CT findings.

The goal should not be to replace routine PVE diagnostics, but rather to employ PET/CT and CTA on top of the current standard of care. However, it should not be reserved just for the most complicated cases in which current diagnostics fall short and uncertainty remains. Prospective trials that employ standardized acquisition methods in the early diagnostic work-up of patients with PVE can then assess the true diagnostic accuracy of PET/CT, and may even be able to determine possible cut-off (i.e. maximum SUV or SUV_{ratio}) values for quantitative PET analysis.

Conclusion

¹⁸F-FDG PET/CT is a very promising novel diagnostic tool for patients suspected of having PVE, as it allows for a most accurate and timely diagnosis. When combined or even fused together with cardiac CT angiography, it provides a complete assessment of structural and functional abnormalities, as well as any concomitant coronary artery disease and the optimal surgical approach, should a reoperation be required.

All studies to date have mostly been limited by both the lack of an adequate reference diagnostic and the absence of standardized image acquisition and interpretation methods, either of which may have even resulted in underestimation of the true diagnostic accuracy of these imaging modalities. Early—if not routine—implementation in the clinical work-up combined with standardization of imaging protocols and both visual and quantitative analysis will allow future larger, prospective, multicentre studies to further evaluate the full diagnostic potential of ¹⁸F-FDG PET/CT(A) in patients with suspected PVE, and allow for better generalizability of their results to daily clinical practice.

References

1. Butchart EG, Gohlke-Bärwolf C, Antunes MJ, et al. Recommendations for the management of patients after heart valve surgery. *Eur Heart J*. 2005;26:2463–71.
2. Lalani T, Chu VH, Park LP, et al. In-hospital and 1-year mortality in patients undergoing early surgery for prosthetic valve endocarditis. *JAMA Intern Med*. 2013;173:1495–504.
3. Baddour LM, Wilson WR, Bayer AS, et al. Infective endocarditis: diagnosis, antimicrobial therapy, and management of complications. *Circulation*. 2005;111:e394–e434.
4. Li JS, Sexton DJ, Mick N, et al. Proposed modifications to the Duke criteria for the diagnosis of infective endocarditis. *Clin Infect Dis*. 2000;30:633–8.
5. Dilsizian V, Achenbach S, Narula J. Adding or selecting imaging modalities for incremental diagnosis: a case study of 18FDG PET/CT in prosthetic valve endocarditis. *JACC Cardiovasc Imaging*. 2013;6:1020–1.
6. Habib G, Lancellotti P, Antunes MJ, et al. 2015 ESC Guidelines for the management of infective endocarditis: The Task Force for the Management of Infective Endocarditis of the European Society of Cardiology (ESC). *Eur Heart J*. 2015;36:3075–128.
7. Saby L, Laas O, Habib G, et al. Positron emission tomography/computed tomography for diagnosis of prosthetic valve endocarditis: increased valvular 18F-fluorodeoxyglucose uptake as a novel major criterion. *J Am Coll Cardiol*. 2013;61:2374–82.
8. Pizzi MN, Roque A, Fernández-Hidalgo N, et al. Improving the diagnosis of infective endocarditis in prosthetic valves and intracardiac devices with 18F-fluorodeoxyglucose positron emission tomography/computed tomography angiography: initial results at an infective endocarditis referral center. *Circulation*. 2015;132: 1113–26.
9. Swart LE, Scholtens AM, Liesting C, Mieghem NMDA. V, Krestin GP, Roos-Hesselink JW, Budde RPJ. Serial 18F-fluorodeoxyglucose positron emission tomography/CT angiography in transcatheter-implanted aortic valve endocarditis. *Eur Heart J*. 2016;37:3059.
10. Regueiro A, Linke A, Latib A, et al. Association between transcatheter aortic valve replacement and subsequent infective endocarditis and in-hospital death. *JAMA*. 2016;316:1083.
11. Scholtens AM, Aarnhem EEHL. V, Budde RP. Effect of antibiotics on FDG-PET/CT imaging of prosthetic heart valve endocarditis. *Eur Hear J Cardiovasc Imaging*. 2015;16:1223.
12. Feuchtner GM, Stolzmann P, Dichtl W, et al. Multislice computed tomography in infective endocarditis. comparison with transesophageal echocardiography and intraoperative findings. *J Am Coll Cardiol*. 2009;53:436–44.
13. Fagman E, Perrotta S, Bech-Hanssen O, et al. ECG-gated computed tomography: a new role for patients with suspected aortic prosthetic valve endocarditis. *Eur Radiol*. 2012;22:2407–14.
14. Gomes A, Glaudemans AWJM, Touw DJ, et al. Diagnostic value of imaging in infective endocarditis: a systematic review. *Lancet Infect Dis*. 2016;0:269–89.
15. van Riet J, Hill EE, Gheysens O, et al. (18)F-FDG PET/CT for early detection of embolism and metastatic infection in patients with infective endocarditis. *Eur J Nucl Med Mol Imaging*. 2010;37:1189–97.

16. Orvin K, Goldberg E, Bernstine H, et al. The role of FDG-PET/CT imaging in early detection of extra-cardiac complications of infective endocarditis. *Clin Microbiol Infect*. 2015;21:69–76.
17. Scholtens AM, Swart LE, Verberne HJ, et al. *J Nucl Cardiol*. 2017; doi:10.1007/s12350-017-0902-3.
18. Scholtens AM, Budde RPJ, Lam MGEH, Verberne HJ. FDG PET/CT in prosthetic heart valve endocarditis: there is no need to wait. *J Nucl Cardiol*. 2017;24:1540–1.
19. Tiwari B, Kand P. Myocardial uptake of F-18-fluorodeoxyglucose in whole body positron emission tomography studies. *Indian J Nucl Med*. 2012;27:69.
20. Harisankar CNB, Mittal BR, Agrawal KL, et al. Utility of high fat and low carbohydrate diet in suppressing myocardial FDG uptake. *J Nucl Cardiol*. 2011;18:926–36.
21. Morooka M, Moroi M, Uno K, et al. Long fasting is effective in inhibiting physiological myocardial 18F-FDG uptake and for evaluating active lesions of cardiac sarcoidosis. *EJNMMI Res*. 2014;4:1.
22. Kumar P, Patel CD, Singla S, Malhotra A. Effect of duration of fasting and diet on the myocardial uptake of F-18-2-fluoro-2-deoxyglucose (F-18 FDG) at rest. *Indian J Nucl Med*. 2014;29:140–5.
23. Minamimoto R, Morooka M, Kubota K, et al. Value of FDG-PET/CT using unfractionated heparin for managing primary cardiac lymphoma and several key findings. *J Nucl Cardiol*. 2011;18:516–20.
24. Ishimaru S, Tsujino I, Takei T, et al. Focal uptake on 18F-fluoro-2-deoxyglucose positron emission tomography images indicates cardiac involvement of sarcoidosis. *Eur Heart J*. 2005;26:1538–43.
25. Scholtens AM, Verberne HJ, Budde RPJ, Lam M. Additional heparin preadministration improves cardiac glucose metabolism suppression over low carbohydrate diet alone in 18F-FDG-PET imaging. *J Nucl Med*. 2016;57:568–74.
26. Habets J, Mali WP, Budde RPJ. Multidetector CT angiography in evaluation of prosthetic heart valve dysfunction. *Radiographics*. 2012;32:1893–905.
27. Suchá D, Daans CG, Symersky P, et al. Reliability, agreement, and presentation of a reference standard for assessing implanted heart valve sizes by multidetector-row computed tomography. *Am J Cardiol*. 2015;116:112–20.
28. Habets J, van den Brink RB, Uijlings R, et al. Coronary artery assessment by multidetector computed tomography in patients with prosthetic heart valves. *Eur Radiol*. 2012;22:1278–86.
29. Habets J, Symersky P, de Mol BA, et al. A novel iterative reconstruction algorithm allows reduced dose multidetector-row CT imaging of mechanical prosthetic heart valves. *Int J Cardiovasc Imaging*. 2012;28:1567–75.
30. Suchá D, Willeminck MJ, de Jong PA, et al. The impact of a new model-based iterative reconstruction algorithm on prosthetic heart valve related artifacts at reduced radiation dose MDCT. *Int J Cardiovasc Imaging*. 2014;30:785–93.
31. Jiménez-Ballvé A, Pérez-Castejón MJ, Delgado-Bolton RC, et al. Assessment of the diagnostic accuracy of 18F-FDG PET/CT in prosthetic infective endocarditis and cardiac implantable electronic device infection: comparison of different interpretation criteria. *Eur J Nucl Med Mol Imaging*. 2016;43:2401–12.
32. Ahmed FZ, James J, Tout D, et al. Metal artefact reduction algorithms prevent false positive results when assessing patients for cardiac implantable electronic device infection. *J Nucl Cardiol*. 2015;22:219–20.

33. Pizzi MN, Roque A, Cuéllar-Calabria H, Fernández-Hidalgo N, et al. 18F-FDG-PET/CTA of prosthetic cardiac valves and valve-tube grafts: infective versus inflammatory patterns. *JACC Cardiovasc Imaging*. 2016;9:1224–7.
34. Scholtens AM, Swart LE, Verberne HJ, et al. Confounders in FDG-PET/CT imaging of suspected prosthetic valve endocarditis. *JACC Cardiovasc Imaging*. 2016;9:1462–5.
35. Mathieu C, Mikail N, Benali K, et al. Characterization of 18 F-fluorodeoxyglucose uptake pattern in noninfected prosthetic heart valves. *Circ Cardiovasc Imaging*. 2017;10:e005585.
36. Griffeth LK. Use of PET/CT scanning in cancer patients: technical and practical considerations. *Proc (Bayl Univ Med Cent)*. 2005;18:321–30.
37. Abidov A, D’Agnolo A, Hayes SW, et al. Uptake of FDG in the area of a recently implanted bioprosthetic mitral valve. *Clin Nucl Med*. 2004;29:848.
38. Rouzet F, Chequer R, Benali K, et al. Respective performance of 18F-FDG PET and radiolabeled leukocyte scintigraphy for the diagnosis of prosthetic valve endocarditis. *J Nucl Med*. 2014;55:1980–5.
39. Schouten LR, Verberne HJ, Bouma BJ, et al. Surgical glue for repair of the aortic root as a possible explanation for increased F-18 FDG uptake. *J Nucl Cardiol*. 2008;15:146–7.
40. Tseng J-R, Lin C-W, Chen S-H, et al. Clinical usefulness of 18F-FDG PET/CT for the detection of infections of unknown origin in patients undergoing maintenance hemodialysis. *J Nucl Med*. 2015;56:681–7.
41. Crouzet J, Boudousq V, Lechiche C, et al. Place of 18F-FDG-PET with computed tomography in the diagnostic algorithm of patients with fever of unknown origin. *Eur J Clin Microbiol Infect Dis*. 2012;31:1727–33.
42. Fagman E, Essen M van, Fredén Lindqvist J, et al. 18F-FDG PET/CT in the diagnosis of prosthetic valve endocarditis. *Int J Cardiovasc Imaging*. 2016;32:679–86.
43. Salomäki SP, Saraste A, Kemppainen J, et al. 18F-FDG positron emission tomography/computed tomography in infective endocarditis. *J Nucl Cardiol*. 2017;24:195–206.
44. Ricciardi A, Sordillo P, Ceccarelli L, et al. 18-Fluoro-2-deoxyglucose positron emission tomography-computed tomography: an additional tool in the diagnosis of prosthetic valve endocarditis. *Int J Infect Dis*. 2014;28:2–7.
45. McCormick JK, Tripp TJ, Dunny GM, Schlievert PM. Formation of vegetations during infective endocarditis excludes binding of bacterial-specific host antibodies to *Enterococcus faecalis*. *J Infect Dis*. 2002;185:994–7.
46. Tanis W, Scholtens A, Habets J, et al. CT angiography and 18F-FDG-PET fusion imaging for prosthetic heart valve endocarditis. *JACC Cardiovasc Imaging*. 2013;6:1008–13.
47. Erba PA, Habib G, Glaudemans AWJM, Miro JM, Slart RHJA. The round table approach in infective endocarditis & cardiovascular implantable electronic devices infections: make your e-Team come true. *Eur J Nucl Med Mol Imaging*. 2017; 44:1107–8.
48. Glaudemans AW, de Vries EF, Galli F, et al. The use of (18)F-FDG-PET/CT for diagnosis and treatment monitoring of inflammatory and infectious diseases. *Clin Dev Immunol*. 2013;2013:623036.
49. Basu S. 18F-FDG PET/CT as a sensitive and early treatment monitoring tool: will this become the major thrust for its clinical application in infectious and inflammatory disorders? *J Nucl Med*. 2012;53:165-6.

CHAPTER 3

IMPROVING THE DIAGNOSTIC PERFORMANCE OF ^{18}F -FDG PET/CT IN PROSTHETIC HEART VALVE ENDOCARDITIS

Laurens Swart¹

Anna Gomes¹

Asbjørn Scholtens¹

Bhanu Sinha

Wilco Tanis

Marnix Lam

Maureen van der Vlugt

Sebastian Streukens

Erik Aarntzen

Jan Bucerius

Sander van Assen

Chantal Bleeker-Rovers

Peter Paul van Geel

Gabriel Krestin

Joost van Melle

Jolien Roos-Hesselink

Riemer Slart²

Andor Glaudemans²

Ricardo Budde²



Published in: Circulation 2018;138:1412–27

Abstract

Background

¹⁸F-Fluorodeoxyglucose (FDG) positron-emission tomography/computed tomography (PET/CT) was recently introduced as a new tool for the diagnosis of prosthetic heart valve endocarditis (PVE). Previous studies reporting a modest diagnostic accuracy may have been hampered by unstandardized image acquisition and assessment, and several confounders, as well. The aim of this study was to improve the diagnostic performance of FDG PET/CT in patients in whom PVE was suspected by identifying and excluding possible confounders, using both visual and standardized quantitative assessments.

Methods

In this multicentre study, 160 patients with a prosthetic heart valve (median age, 62 years [43–73]; 68% male; 82 mechanical valves; 62 biological; 9 transcatheter aortic valve replacements; 7 other) who underwent FDG PET/CT for suspicion of PVE, and 77 patients with a PV (median age, 73 years [65–77]; 71% male; 26 mechanical valves; 45 biological; 6 transcatheter aortic valve replacements) who underwent FDG PET/CT for other indications (negative control group), were retrospectively included. Their scans were reassessed by 2 independent observers blinded to all clinical data, both visually and quantitatively on available European Association of Nuclear Medicine Research Ltd–standardized reconstructions. Confounders were identified by use of a logistic regression model and subsequently excluded.

Results

Visual assessment of FDG PET/CT had a sensitivity/specificity/positive predictive value/negative predictive value for PVE of 74%/91%/89%/78%, respectively. Low inflammatory activity (C-reactive protein <40 mg/L) at the time of imaging and use of surgical adhesives during prosthetic heart valve implantation were significant confounders, whereas recent valve implantation was not. After the exclusion of patients with significant confounders, diagnostic performance values of the visual assessment increased to 91%/95%/95%/91%. As a semiquantitative measure of FDG uptake, a European Association of Nuclear Medicine Research Ltd–standardized uptake value ratio of ≥ 2.0 was a 100% sensitive and 91% specific predictor of PVE.

Conclusions

Both visual and quantitative assessments of FDG PET/CT have a high diagnostic accuracy in patients in whom PVE is suspected. FDG PET/CT should be implemented early in the diagnostic workup to prevent the negative confounding effects of low inflammatory activity (e.g. attributable to prolonged antibiotic therapy). Recent valve implantation was not a significant predictor of false-positive interpretations, but surgical adhesives used during implantation were.

Introduction

Prosthetic heart valve (PV) endocarditis (PVE) is a life-threatening complication with a 1-year mortality of up to 50% that affects up to 5% of patients per year following valve implantation.¹ Unfortunately, timely diagnosis of PVE before the occurrence of severe complications such as perivalvular abscesses or valve dehiscence, which usually require high-risk reoperation, is difficult. Echocardiography, as one of the mainstays of the modified Duke criteria,² can only visualize structural damage, and the sensitivity and specificity of these criteria, additionally including microbiological and clinical evidence of infection, are substantially lower in PVE than in native valve endocarditis.³

Clinical guidelines^{4,5} were recently updated following newly available data on the additional value of ¹⁸F-fluorodeoxyglucose (FDG) positron-emission tomography (PET)/computed tomography (CT) in PVE.^{6,7} FDG PET/CT aids in the diagnosis of both intracardiac and extracardiac infectious foci by functional visualization of inflammation, even before structural damage occurs.⁷ However, FDG PET/CT findings have been reported to be influenced by several confounders such as myocardial FDG uptake, low inflammatory activity (e.g. attributable to prolonged antibiotic therapy), prior use of surgical adhesives, and recent valve implantation.^{8,9} The first 3 possible confounders can be mitigated with adequate patient preparation, timely implementation of FDG PET/CT in the diagnostic workup, and evaluation of the surgical report,¹⁰ whereas evidence for the influence of recent valve implantation is scarce and inconsistent.¹¹

Besides a visual evaluation, FDG uptake can also be measured (semi)quantitatively, and potential cutoffs for the maximum measured intensity around a PV (standardized uptake value [SUV]max), and target-to-background ratios (SUVratio), as well, have been reported.^{12,13} However, these reported cutoffs vary widely because of differences in calibration between scanners, and measurement and reconstruction techniques, as well.^{10,12–15} Therefore, the European Association of Nuclear Medicine Research Ltd (EARL) has provided a standardized calibration and reconstruction method that is currently applied in >150 centres in Europe.¹⁶

The aim of this study was to investigate the diagnostic performance of FDG PET/CT in a large multicentre cohort of patients in whom PVE was suspected by identifying and subsequently excluding potential confounders using both visual and EARL-standardized quantitative assessments. In addition, a cohort of patients with PVs but without suspicion of PVE, who underwent PET/CT imaging for other (i.e. oncological) indications, was included as negative controls.

Methods

In this multicentre study, patients of 6 cardiothoracic centres in the Netherlands who had ≥ 1 PVs in situ and underwent FDG PET/CT imaging for any indication were retrospectively included. The study was approved and informed consent was waived by the local Medical Ethics Committees of all participating centres. The data, analytic methods, and study materials have been made available to other researchers for purposes of reproducing the results or replicating the procedure.¹⁷

Patient identification and selection

All patients with a PV (including percutaneously implanted valves, but excluding valvuloplasties) who underwent an FDG PET/CT scan between January 1, 2010, and March 31, 2016, were included. For all patients, at least 1 year of follow-up was available. No distinction was made between scans that were performed after first PV implantations or reimplantations.

Data collection

Demographic and clinical data of the included patients and technical data of the included scans were entered into a collaborative database. To prevent possible confounding by follow-up scans during an active or after a previous endocarditis episode, only the first scan for suspicion of PVE was included in the analysis. No patients had undergone both a scan for suspicion of PVE and one for another (i.e. oncological) indication.

Patient data

Demographic data and the type of PVs and implantation dates, as well, were retrieved. In case of multiple replacement surgeries of the same valve, the most recent valve implantation date was used. A history of diabetes mellitus and previous endocarditis was also noted.

Echocardiographic findings from the same clinical admission as the FDG PET/CT scan were recorded for the presence of vegetation (per valve), abscesses, fistulas, new dehiscence of the PV, or paravalvular leakage. If multiple echocardiograms were available, abnormalities on transoesophageal echocardiography were considered leading, and, in case of multiple transoesophageal echocardiographies, the reported presence of abnormal findings on one would overrule their reported absence on another to ensure an accurate reference standard and modified Duke classification.

Evidence of cardiac device or lead infection was recorded, and results of blood cultures were scored as positive if at least 1 blood culture had been positive directly before or during the clinical admission, and the causative microorganism was recorded. Results of serology and polymerase chain reaction were recorded separately. Based on these data and clinical follow-up, the modified Duke classification² was calculated. As a measure of inflammatory activity, C-reactive protein (CRP) and leukocyte levels were recorded if obtained close to the FDG PET/CT scan (maximum 7 days before or after the date of the scan).

Scan data

Based on the original clinical question of the FDG PET/CT scan (derived from the report), the indication for imaging was categorized as suspicion of PVE versus other (i.e. oncological) indications.

We recorded the scan date and acquisition protocol, including preparatory measures such as a fasting period of >6 hours, a low-carbohydrate diet for at least 24 hours and a heparin injection, and the administered FDG dose (in MBq), as well as the blood glucose level at the time of FDG injection, the time interval of scan acquisition after FDG injection, and whether the scanner was EARL-accredited and an EARL-standardized reconstruction was available. In case of missing images or insufficient clinical data for a reliable final diagnosis, the scan was excluded from further analyses.

Patient classification

Patients with an FDG PET/CT scan performed for other (i.e. oncological) indications were considered controls by default, because these patients had no clinical suspicion of an infection. To ensure a reliable diagnostic accuracy representative of daily clinical practice, these negative controls were primarily used for the evaluation of causes of false-positive FDG PET/CT scans, and were not included in the analysis on the diagnostic performance of PET in patients in whom PVE was suspected.

For patients who did undergo FDG PET/CT for suspicion of PVE, the final diagnosis of PVE was established through expert consensus based on all available clinical and diagnostic data, and at least 1 year of follow-up, as well. The modified Duke criteria were scored as well,² with the exception that echocardiographic findings unrelated to the PV were not included in the final diagnosis of PVE (e.g., a vegetation on 1 of the native valves would not count as a major criterion in the final Duke classification regarding PVE), and data on minor Duke criteria (e.g. vascular or immunologic stigmata) were often missing.

Expert consensus was achieved through a stepwise approach in which patients were discussed by a multidisciplinary group of physicians from the Departments of Cardiology, Infectious Diseases, Medical Microbiology, Radiology, and Nuclear Medicine (the Endocarditis Team) when the diagnosis was neither confirmed by surgery/histopathology nor rejected by an uneventful 1-year follow-up regarding infectious disease without further antibiotic treatment.

Image acquisition and analysis

Depending on the centre, images had originally been acquired on a Biograph mCT (Siemens Healthcare) or a Gemini TF PET/CT (Philips Medical Systems).

Image quality

All scans were evaluated for image quality (sharpness/noise) and classified as good, moderate, or poor by 2 independent observers. Scans that were classified as being of poor quality were excluded from further analyses. Furthermore, the quality of myocardial FDG-uptake suppression was assessed by visually comparing the maximum intensity of FDG in the myocardium to the blood pool (of the descending aorta) and the liver, and classified as I, less than blood pool; II, equal to blood pool; III, less than liver but more than blood pool; IV, more than liver; and V, intense (i.e. similar to brain).

Qualitative analysis of PVE

All images were analysed on commercially available software (Syngo.via, Siemens) by 2 nuclear medicine physicians blinded to the original scan report and any clinical data of the patient. Each observer had several years of experience in reading FDG PET/CT scans for suspicion of PVE, device infections, and infectious diseases in general. Based on both the attenuation-corrected and noncorrected images, both observers assessed the presence of any uptake around the PV and gave a final verdict on the abnormality of this uptake (consistent with infection), taking known normal variations into account.⁹ In case of disagreement, a consensus reading was performed.

(Semi)quantitative analysis of PVE

The SUV_{max} around the PV was measured on EARL-accredited, attenuation-corrected reconstructions. A volume of interest was defined automatically as an isocontour of 40% of the maximum measured signal intensity, which included the blood pool within and some of the soft tissue adjacent to the PV (*Figure 1*). When there was a visual impression of unsuppressed myocardial FDG uptake within the automatically generated volume of interest, this area was manually removed from the measurement. The SUV_{max} was divided by the mean SUV of the blood pool in the descending aorta (at the level of the PV) to calculate the SUV_{ratio} . This was measured within a spherical volume of interest with a maximum diameter of the lumen of the aorta (excluding the vessel wall). For all semi-quantitative analyses, the average of the measurements of the 2 observers was used.

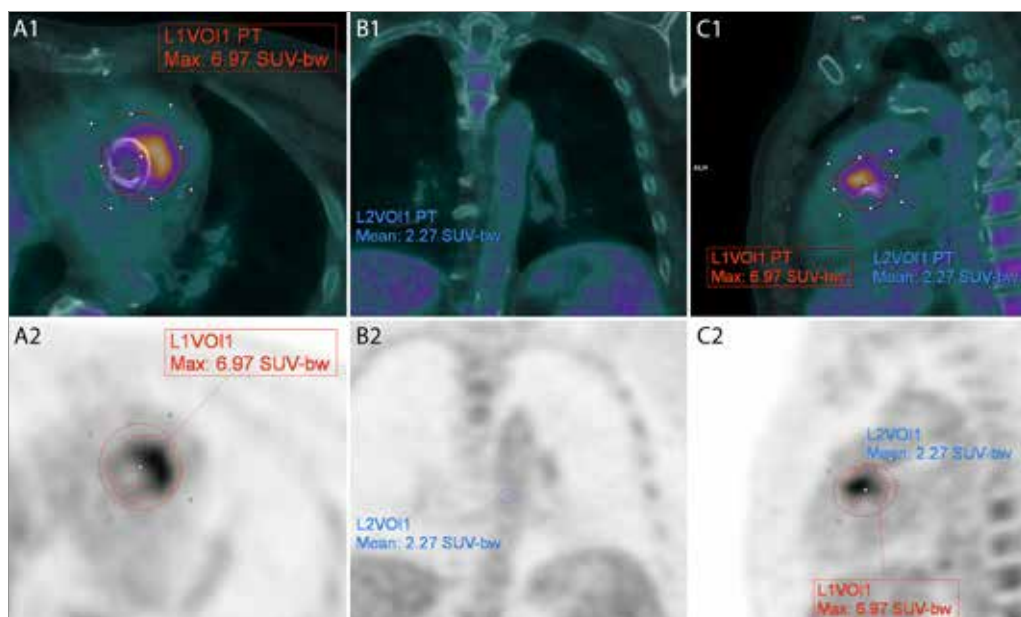


Figure 1 | Semiquantitative analysis of periprosthetic FDG uptake in a patient with definite PVE. Fused PET/CT (**1**) and PET-only (**2**) images shown. (**A**) Horizontal view of a measurement of the SUV_{max} around the PV by using an automated volume of interest based on an isocontour (**red line**) encompassing all voxels with an intensity of at least 40% of the voxel with the highest intensity in the spherical selected area (**red ellipse**). (**B**) Coronal view of a measurement of the mean SUV in the blood pool of the descending aorta using a small spherical volume of interest (**blue circle**), drawn with particular care not to include the aortic wall. (**C**) Combined sagittal view of both measurements. The SUV_{ratio} is calculated by dividing the SUV_{max} around the PV by the mean SUV in the blood pool: $6.97/2.27=3.07$. FDG indicates ^{18}F -fluorodeoxyglucose; PV, prosthetic heart valve; PVE, prosthetic heart valve endocarditis; SUV_{max} , maximum standardized uptake value; and SUV_{ratio} , standardized uptake value ratio.

In case of multiple PVs, each valve was assessed and scored separately. Because the definition of case (PVE) versus control (no PVE) was set on a patient level rather than on a valve level, only the affected PV was included for the analyses of diagnostic performance and thresholds for SUV_{max} and SUV_{ratio} to prevent erroneously classifying the scan as false-negative for the other valves. In patients with multiple valves without PVE (all negative on FDG PET/CT), the most commonly implanted valve was considered the primary valve (i.e. in the following order: aortic, mitral, pulmonary, and tricuspid valve). Only the SUV_{max} around the primary valve was included in the analysis. Scans that were not acquired on an EARL-accredited scanner or did not include an EARL-accredited reconstruction were not included in the semiquantitative analyses.

Confounders

The effect of possible confounders on the diagnostic accuracy was assessed by identification of statistically significant differences between patients with false-positive or false-negative interpretations and those with correctly interpreted scans using a logistic regression model including all demographic and clinical variables. In particular, the effect of the previously described potential positive (i.e. recent valve implantation and surgical adhesives) and negative (i.e. low inflammatory activity attributable to prolonged antibiotic therapy and isolated vegetation) confounders was evaluated. The effect of poor myocardial FDG-uptake suppression was evaluated both as a possible predictor of false-positive (i.e. uptake that mimics an infectious pattern) and false-negative (i.e. diffuse myocardial uptake that masks an underlying infectious pattern) scans. Subsequently, all patients or scans with statistically significant predictors of a negative or positive confounding effect were excluded to evaluate possible improvement of diagnostic accuracy.

Statistics

Accuracy of FDG PET/CT for the diagnosis of PVE was assessed by comparing the final imaging diagnosis (based on visual analysis) with the reference standard of expert consensus based on all available clinical data. For comparisons between groups, the Student *t* test or Mann-Whitney *U* test was used for normally distributed and nonparametric data, respectively. For all statistical analyses, a significance level of $\alpha=0.05$ and 95% CIs were used. SPSS v25.0 (IBM Corp) was used for all analyses, with the exception of CIs for C-statistics, for which MedCalc v18.2.1 (MedCalc Software) was used. Unless otherwise indicated, the interquartile range or CI is denoted in square brackets.

The interobserver agreement on quantitative analyses was evaluated by using an absolute-agreement 2-way mixed intraclass correlation coefficient.¹⁸ Receiver-operator curves were used to analyze diagnostic distinctiveness (as area under the curve, AUC), and the optimal cutoff values for both SUV_{max} and SUV_{ratio} were determined by using the Youden J statistic, assuming that sensitivity and specificity are equally important. Outcomes of the quantitative analyses were adjusted for the same confounders identified in the visual assessment through exclusion of the same scans.

Results

Patient characteristics

Between January 2010 and March 2016, 390 FDG PET/CT scans had been acquired in 289 patients with at least 1 PV. After exclusion of scans that were irretrievable, that had a poor image quality, or for which sufficient clinical data were lacking, and after exclusion of all follow-up scans, 237 FDG PET/CT scans remained (*Figure 2*).

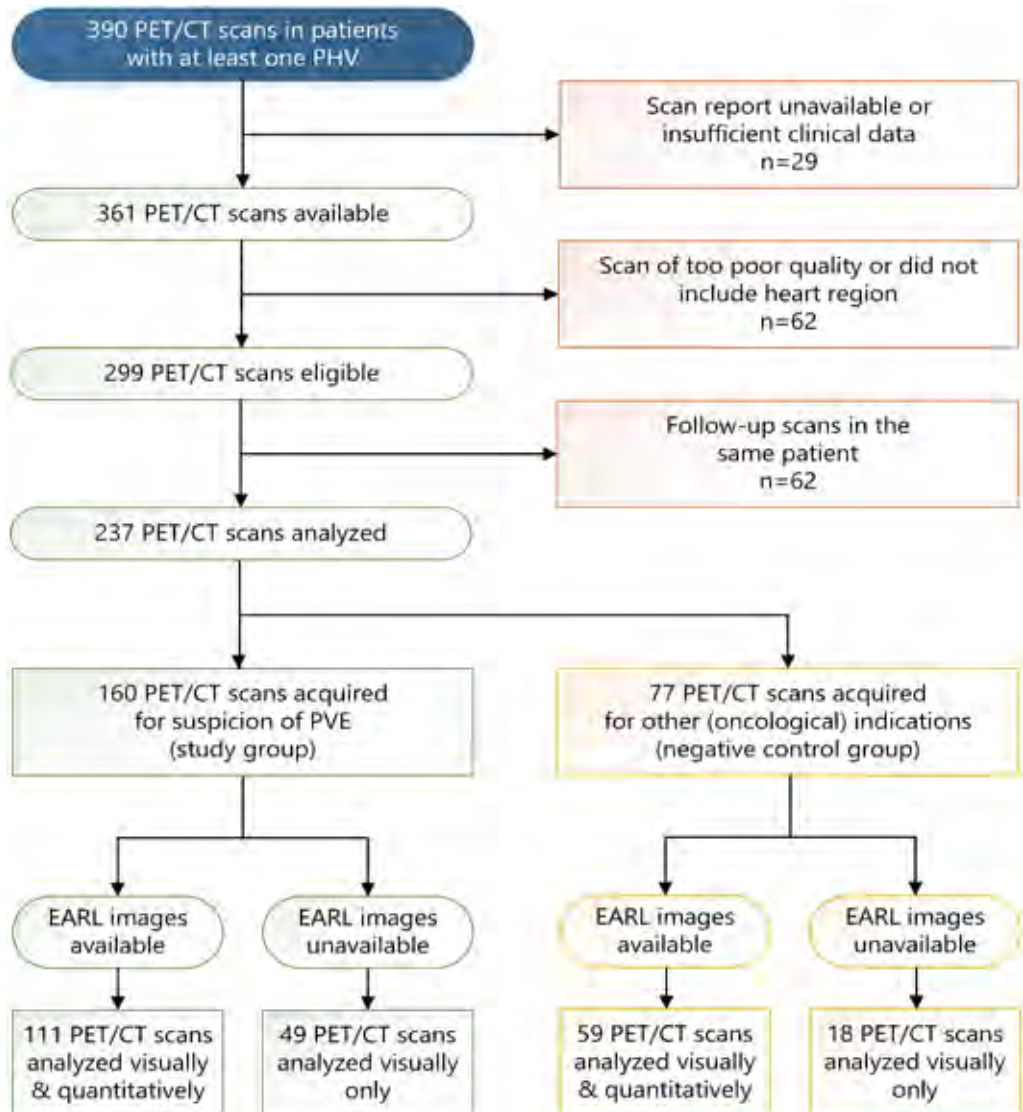


Figure 2 | Inclusion and exclusion flowchart. EARL indicates European Association of Nuclear Medicine Research Ltd; PET/CT, positron-emission tomography/computed tomography; PHV, prosthetic heart valve; and PVE, prosthetic heart valve endocarditis.

One hundred sixty scans were performed for suspicion of PVE, whereas 77 scans were acquired for other, mostly oncological indications. Clinical parameters including blood cultures and results of echocardiography at the time of these scans are listed in *Table 1*. Of the 160 patients in whom PVE was suspected, 80 had a final diagnosis of PVE, whereas the other 80 were deemed not to have PVE.

	Suspicion of PVE (n=160)			No PVE (scan for other indication)
	All scans for suspicion of PVE	PVE*	No PVE (after initial suspicion)*	
Demographics	n=160	n=80	n=80	n=77
Age (median [IQR], years)	62 [43-73]	52 [35-68] ²	68 [53-75] ¹	73 [65-77]
Gender (male)	108 (68%)	49 (61%)	59 (74%)	55 (71%)
BMI (mean ±SD, kg/m ²)	25.2 ±5.0	24.9 ±5.4	25.6 ±4.6	26.3 ±4.7
Diabetes	23 (14%)	10 (13%)	13 (16%)	18 (23%)
Prior history of endocarditis	33 (21%) ²	15 (19%) ²	18 (23%) ²	5 (6%) ¹
Mortality during follow-up	27 (17%) ²	10 (13%) ²	17 (21%) ²	28 (36%) ¹
Primary valve location**				
Aortic	132 (83%)	61 (75%)	71 (90%)	70 (91%)
Mitral	12 (8%)	6 (7%)	6 (8%)	6 (8%)
Pulmonary	14 (9%)	13 (16%)	1 (1%) ¹	0 (0%) ¹
Tricuspid	2 (1%)	1 (1%)	1 (1%)	1 (1%)
Primary valve type**				
Mechanical	82 (51%)	43 (54%) ²	39 (49%) ^{1,2}	26 (34%) ¹
Biological	62 (39%)	34 (43%)	28 (35%)	45 (58%)
TAVI	9 (6%)	1 (1%)	8 (10%) ¹	6 (8%)
Homograft	4 (3%)	2 (3%)	2 (3%)	0 (0%)
Autologous	3 (2%)	0 (0%)	3 (4%)	0 (0%)
Including replacement of ascending aorta (i.e. Bentall)	21 (13%)	15 (19%)²	6 (8%)	2 (3%)¹
Time since valve implantation (median [IQR], days)	685 [82-2216]	939 [370-2282]	226 [39-1923]^{1,2}	1104 [299-2268]
Valves implanted <3 month ago	43 (27%) ^{1,2}	8 (10%)	32 (40%) ^{1,2}	4 (5%)
Valves implanted <1 month ago	18 (11%) ²	2 (3%)	16 (20%) ^{1,2}	2 (3%)
Secondary prosthetic valve	21 (13%)	9 (11%)	12 (15%)	7 (9%)
Aortic + Mitral	12 (8%)	3 (4%)	9 (11%)	7 (9%)
Aortic + Pulmonary	9 (6%)	6 (8%)	3 (4%)	0 (0%)
Cardiac implantable electronic device	17 (11%)	8 (10%)	9 (11%)	5 (6%)
Echocardiography data available	130 (81%)²	77 (96%)²	53 (66%)^{1,2}	0 (0%)¹
Signs of PVE ^Δ	58 (44%)	50 (65%)	8 (15%) ¹	n/a
Vegetation ^Δ	35 (27%) [‡]	32 (42%) [‡]	3 (6%) ^{1,‡}	n/a
Aortic ^Δ	24 (18%)	24 (31%)	0 (0%) ¹	n/a
Mitral ^Δ	6 (5%)	5 (6%)	1 (2%) [‡]	n/a
Pulmonary ^Δ	6 (5%)	5 (6%)	1 (2%) [‡]	n/a
Tricuspid ^Δ	2 (2%)	1 (1%)	1 (2%) [‡]	n/a
Abscess ^Δ	18 (14%)	17 (22%)	1 (2%) [‡]	n/a
Fistula ^Δ	1 (1%)	1 (1%)	0 (0%)	n/a
Prosthetic valve dehiscence ^Δ	1 (1%)	1 (1%)	0 (0%)	n/a
Paravalvular leakage ^Δ	12 (9%)	8 (10%)	4 (8%) [‡]	n/a
Cardiac implantable device infection ^Δ	3 (2%)	2 (3%) ^β	1 (2%) ^β	n/a

Blood cultures available†	160 (100%)^{2,§}	80 (100%)²	80 (100%)²	0 (0%)¹
Positive blood cultures	86 (54%)	62 (78%)	24 (30%) ¹	n/a
<i>Staphylococcus aureus</i>	28 (18%)	19 (24%)	9 (11%)	n/a
Enterococci	15 (9%)	9 (11%)	6 (8%)	n/a
Coagulase-negative staphylococci	7 (4%)	4 (5%)	3 (4%)	n/a
<i>Viridans streptococci</i>	21 (13%)	17 (21%)	4 (5%) ¹	n/a
HACEK***	5 (3%)	5 (6%)	0 (0%)	n/a
<i>Cutibacterium acnes</i> ◊	5 (3%)	5 (6%)	0 (0%)	n/a
Other	5 (3%)	3 (4%)	2 (3%)	n/a
PCR and/or serology positive^{†,}	5 (3%)	5 (6%)	0 (0%)	0 (0%)¹
<i>Coxiella burnetii</i> (Q-fever)	2 (1%)	2 (2%)	0 (0%)	n/a
<i>Bartonella henselae</i>	1 (1%)	1 (1%)	0 (0%)	n/a
<i>Tropheryma whipplei</i>	1 (1%)	1 (1%)	0 (0%)	n/a
<i>Haemophilus parainfluenzae</i>	1 (1%)	1 (1%)	0 (0%)	n/a
Modified Duke classification				
PVE rejected	57 (36%)	5 (6%)	52 (65%) ¹	n/a
Possible PVE	45 (28%)	19 (24%)	26 (33%)	n/a
Definite PVE	58 (36%)	56 (70%)	2 (3%) ¹	n/a
Surgical/histopathological confirmation of PVE	40 (25%)	40 (50%)	0 (0%)¹	n/a
Days of i.v. antibiotic therapy (median [IQR])	11 [6-20]	12 [6-18]	9 [6-23]	n/a
CRP (median [IQR], mg/L)	54 [20-96]	51 [26-70]	63 [17-145]	n/a
Leukocytes (median [IQR], x10 ⁹ /L)	9.6 [7.3-11.2]	8.6 [6.3-11.0]	9.8 [7.5-11.8]	n/a

Table 2 | Clinical data at time of FDG PET/CT imaging. (1) Statistically significantly different from the PVE group ($p < 0.05$, only calculated for No PVE groups). (2) Statistically significantly different from the scans performed for other indications ($p < 0.05$, calculated for all scans for suspicion of PVE). (*) Final diagnosis based on surgical findings (if reoperated), expert opinion and follow-up. (**) The primary valve was defined as either the valve involved in -or suspected of- PVE, or in case of controls, based on the order of most common occurrence (AV, MV, PV, TV). (¥) Three patients had a vegetation on both their prosthetic AV and their prosthetic MV. (***) HACEK: *Haemophilus* species, *Aggregatibacter* (*Actinobacillus*) species, *Cardiobacterium hominis*, *Eikenella corrodens*, *Kingella* species. (◊) Formerly known as *Propionibacterium*. (†) For blood cultures, PCR and serology, even if they were no longer positive at the time of FDG PET/CT imaging, these were classified as positive if they had been positive during the clinical episode preceding the scan. (‡) The mitral valve vegetation was deemed a remainder of previous endocarditis, while the pulmonary and tricuspid vegetation were later concluded to have probably been small thrombi. The one abscess found in a patient concluded not to have PVE was found to be a remainder of previous endocarditis prior to PHV implantation, as it had decreased in size in comparison with imaging before surgery. Four pre-existing paravalvular leakages were found in this control group. (Δ) Percentages of abnormal echocardiographic findings are relative to the number of available echocardiograms. (β) Two patients were deemed to have both PVE and a cardiac implantable electric device infection. One patient was concluded to have a pacemaker lead infection but not PVE, based on absence of abnormalities on echocardiography, CT angiography and PET/CT. (||) Only PCRs and serologies that newly identified a causative micro-organism are reported. (§) In two patients, blood cultures were not performed or data about these could not be retrieved from the electronic patient file.

Acquisition parameters and image quality

Acquisition parameters of the 237 FDG PET/CT scans are shown in *Table 2*. Overall image quality was good in 161 and moderate in 76 scans. All patients had fasted for at least 6 hours, whereas 88 of the patients in whom PVE was suspected (55%) had also been on a low-carbohydrate diet for at least 24 hours before FDG injection, of whom 20 (12%) had additionally received a heparin injection (50 IU/kg) 15 minutes before the FDG injection. One patient in the negative control group who underwent FDG PET/CT for suspicion of cardiac sarcoidosis had also been on a low-carbohydrate diet for >24 hours.

	All scans (n=237)	Scans for sus- picion of PVE (n=160)	Scans for oth- er indications (n=77)
Amount of FDG administered (mean ± SD, MBq)	193 ± 69	192 ± 76	198 ± 55
Glucose blood levels at time of injection (mean ± SD, mmol/L)	5.7 ± 1.4	5.3 ± 1.3	6.2 ± 1.5
Time between FDG injection and image acquisition (mean ± SD, minutes)	61 ± 5	61 ± 4	61 ± 6
EARL standardization	170 (72%)	111 (69%)	59 (77%)
At least 6 hours of fasting	237 (100%)	160 (100%)	77 (100%)
Low-carbohydrate diet	88 (37%)	87 (55%)	1 (1%) ^{†*}
Heparin iv.	20 (8%)	20 (12%)	0 (0%) [†]

Table 2 | Acquisition parameters of all FDG PET/CT scans. (†) Statistically different from the scans acquired for suspicion of PVE ($p < 0.001$). (*) This scan had been acquired for suspicion of cardiac sarcoidosis, hence the low-carbohydrate diet.

The preparatory low-carbohydrate diet (n=88) significantly reduced the average grade of physiological myocardial FDG uptake from 3.0 to 2.0 on a 1 to 5 scale in comparison with the patients who were not instructed to adhere to this diet for 24 hours ($P < 0.001$, *Table 3*). An additional intravenous heparin injection (n=20) reduced the average grade of myocardial FDG uptake further, from 2.0 to 1.6 ($P = 0.02$). Both methods individually led to a significantly lower percentage of scans in which the observers indicated that myocardial uptake may have negatively influenced their quantitative measurements of FDG uptake, and combined, they reduced the amount of possibly affected measurements from 31% to 12% ($P < 0.001$, *Table 3*).

	>6-h fast (n=237)	>6-h fast + 24-h diet (n=88)	>6-h fast + 24-h diet + heparin (n=20)
Mean visual myocardial uptake grading (five-point scale, mean \pm SD)	3.0 \pm 1.4	2.0 \pm 0.8 (p<0.001)*	1.6 \pm 0.6 (p=0.02) [†]
1. Less than blood pool	95 (40%)	57 (64%)	15 (71%)
2. Equal to blood pool	18 (8%)	8 (9%)	2 (14%)
3. More than blood pool, less than liver	15 (6%)	7 (8%)	2 (10%)
4. More than liver	36 (15%)	5 (6%)	0 (0%)
5. Intense	73 (31%)	11 (13%)	1 (5%) [‡]
Physiological myocardial uptake may have influenced quantitative measurements (on EARL-reconstructions only)	52/170 (31%)	10/57 (18%) (p<0.001)	2/17 (12%) (p=0.03)

Table 3 | Influence of patient preparation on myocardial glucose metabolism suppression. (*) Significant difference when compared to the 149 patients who only fasted for >6 hours and had an average visual myocardial uptake grade of 3.5 ± 1.6 . (†) Significant difference when compared to the 68 patients who fasted and followed a 24-h low-carbohydrate diet but did not get an i.v. heparin injection prior to FDG administration and had an average visual myocardial uptake grade of 2.2 ± 0.8 . (‡) The adherence of this patient to the low-carbohydrate was later questioned by the attending physician.

Visual assessment

Visual assessment of FDG uptake by 2 independent blinded observers resulted in 66 positive and 171 negative PET/CT scans. After a consensus reading of 23 scans (10%), there were no remaining discrepancies between the 2 observers in the evaluation of pathological FDG uptake.

In the 160 PET/CT scans performed for suspicion of PVE, PET was positive in 59 of the 80 patients with PVE, and negative in 74 of 80 patients without PVE. The sensitivity, specificity, positive predictive value (PPV), and negative predictive value (NPV) of scans acquired for suspicion of PVE, without any correction, were 74%, 91%, 89%, and 78%, respectively. When only looking at patients with a surgically or histopathologically confirmed diagnosis, PET was positive in 32 of 40 patients (80%). The sensitivity of echocardiography for PVE was 50 of 77 (65%; Table 1). In 24 of the 27 cases of PVE in which echocardiography was negative, the FDG PET/CT scan was positive. Thus, when adding FDG PET/CT to the diagnostic workup, the combined sensitivity increased to 96%. Of the 53 patients deemed not to have PVE for whom an echocardiogram report was available, echocardiography showed signs of endocarditis in 8 (specificity 85%). None of them had a positive FDG PET/CT scan (combined specificity 100%).

False-negative interpretations

Overall, 21 scans of patients with PVE (26%) were false-negative based on the visual analysis. Fourteen of these patients had a definite diagnosis of PVE according to the modified Duke criteria, whereas 7 had a possible PVE classification.

As a measure of inflammatory activity, the average CRP at the time of PET imaging was lower in these 21 patients than in those with a true positive scan (25.0 ± 24.5 versus 73.7 ± 59.9 mg/L; $P=0.001$). At the time of these 21 scans, 17 patients (81%) had a CRP of <40 mg/L ($4 \times$ upper normal limit), which was a statistically significant predictor of a false-negative FDG PET/CT scan ($P=0.016$, *Figure 3A*). When excluding all 69 scans of patients with a CRP of <40 mg/L at the time of imaging ($n=91$), the sensitivity, specificity, PPV, and NPV of visual PET analysis for PVE (in patients with a CRP of >40 mg/L) improved to 91%, 91%, 91%, and 91%, respectively. None of the other variables (including leukocyte levels at the time of imaging) were significant predictors of a false-negative scan, although longer intravenous antibiotic treatment was associated with lower inflammatory activity (Spearman correlation coefficient of -0.36 mg/L CRP for every day of antibiotic therapy; $P<0.001$). Specific species of micro-organisms were not associated with lower inflammatory activity at the time of PET/CT imaging or with a false-negative FDG PET/CT scan.

Of the 4 patients with a false-negative visual interpretation of their FDG PET/CT scan despite higher CRP levels, 3 had an isolated vegetation on their aortic PV without any signs of structural damage to the peri-annular tissue. The fourth patient with a false-negative FDG PET/CT had negative blood cultures, but was deemed to have PVE by expert consensus because of echocardiographic signs of a peri-annular extension, for which, however, the patient was not reoperated because of a too high estimated procedural risk. Thus, absolute certainty about the diagnosis of PVE in these patients could not be achieved, but they were all pragmatically antibioticly treated for at least 6 weeks despite a negative FDG PET/CT scan.

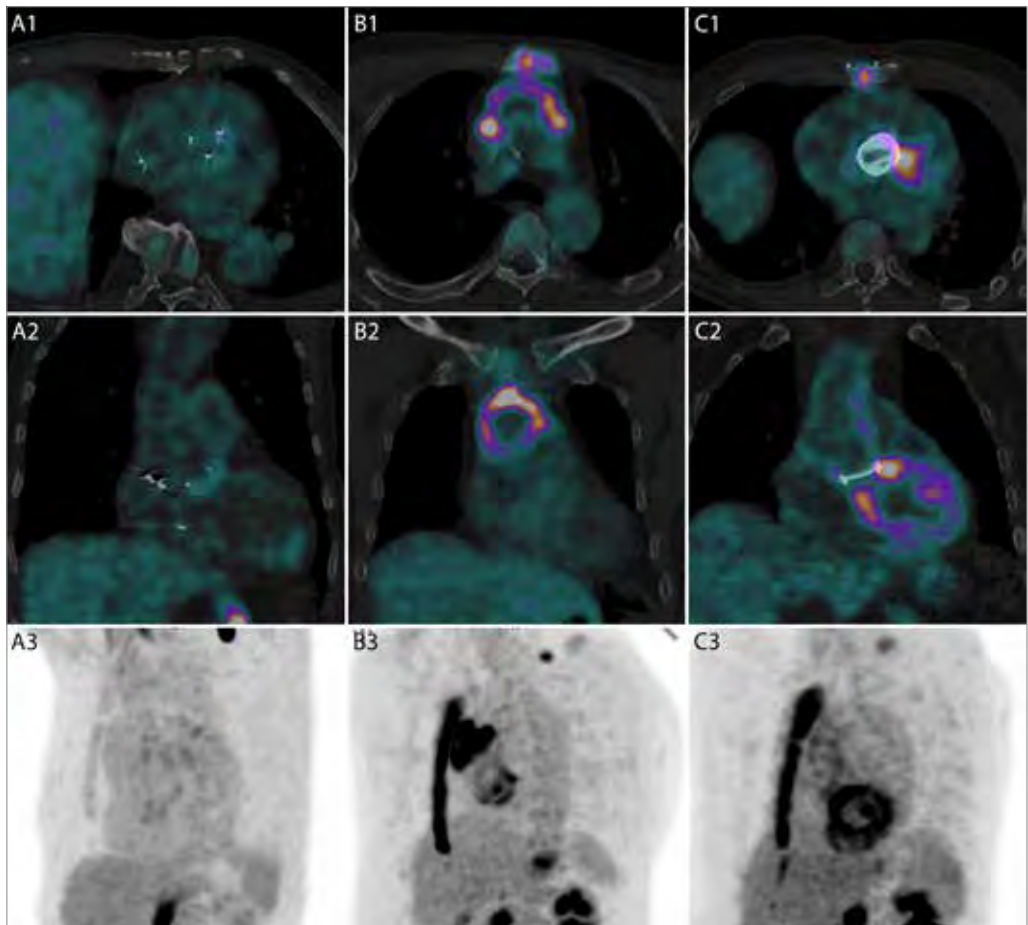


Figure 3 | Three examples of scans affected by confounding factors. Horizontal (**1**), coronal (**2**), and sagittal (**3**) view of fused FDG PET/CT (**1, 2**) and maximum-intensity PET (**3**) projections shown. (**A**) An 80-year-old male patient with definite *Enterococcus faecalis* PVE of a biological aortic PV, who had already been treated with antibiotics for 65 days before FDG PET/CT imaging (CRP was 14 mg/L), and despite a negative scan (SUV_{ratio} 1.68), was reoperated 5 days later because of persisting vegetation with new septic emboli. PVE was intraoperatively macroscopically and subsequently histopathologically confirmed. (**B**) A 57-year-old male patient with a biological aortic valve and ascending aorta replacement (Bentall procedure) who underwent FDG PET/CT imaging for oncological indications (myocardial suppression was good, possibly thanks to prolonged >12-hour fasting), showing intense uptake of FDG (SUV_{ratio} 6.78) in the areas where surgical adhesives had been applied, particularly surrounding the distal seam of the ascending aortic graft. (**C**) A 46-year-old male patient with a mechanical aortic valve who underwent FDG PET/CT imaging for suspicion of PVE, but in whom PVE was ruled out by negative blood cultures, negative echocardiography, and an alternative diagnosis of upper urinary tract infection, showing circular FDG uptake (**C3**, SUV_{ratio} 3.66) in the basal septal and anterior myocardial wall (**C2**), which could have been mistaken for a sign of periannular infection (**C1**), but was most likely caused by insufficient adherence to the low-carbohydrate diet. CRP indicates C-reactive protein; CT, computed tomography; FDG, ^{18}F -fluorodeoxyglucose; PET, positron-emission tomography; PV, prosthetic heart valve; PVE, prosthetic heart valve endocarditis; and SUV_{ratio} , standardized uptake value ratio.

False-positive interpretations

Six scans in patients in whom PVE was suspected but who had a final rejected diagnosis (8%) were false-positive.

In 3 of these patients, the surgical report of the PV implantation mentioned use of surgical adhesives (i.e. BioGlue [CryoLife Inc]), which was the only statistically significant predictor of a false-positive scan in the logistic regression model. The area of increased FDG uptake was consistent with the description of the area the surgical adhesive had been applied to in the surgical report of all 3 patients (*Figure 3B*). There were no negative scans in patients in whom the use of surgical adhesives had been reported (n=4). Excluding scans affected by this confounder increased the specificity and PPV of PET in patients in whom PVE was suspected to 96% (74/77) and 95% (58/61), respectively.

In 2 other patients, the PV had been implanted 11 and 18 days before FDG PET/CT imaging, respectively. However, 16 other patients who underwent imaging within 1 month of PV implantation had a true-negative FDG PET/CT scan. Overall, in 20 patients, the PV had been implanted <1 month before FDG PET/CT imaging, with only 2 false-positive FDG PET/CT scans (10%). Two other patients with an implantation this shortly before FDG PET/CT imaging were deemed to have PVE: 1 scan was true positive, and the other was false negative. Twenty-seven scans had been acquired in patients with a PV implantation between 1 and 3 months before imaging, with only 2 false-positive FDG PET/CT scans in this group as well (7%). One of these false positives within 1 to 3 months after surgery was also attributed to the use of BioGlue, bringing the total number of false-positive scans in patients with a PV implantation <3 months before FDG PET/CT imaging to 3 of 47 (6%). Neither the number of days since PV implantation, nor an implantation within 1 or 3 months, were significant predictors of a false-positive scan.

In the last patient in whom PVE was suspected who had a false-positive scan, and in the 1 patient with a false-positive scan that had been acquired for oncological indications, as well, myocardial FDG uptake had been classified by both observers as more than liver and intense, respectively, which may have hampered the visual assessment (*Figure 3C*). Neither patient had been prepared by means of a low-carbohydrate diet. However, because poor myocardial suppression occurred in many more correctly evaluated FDG PET/CT scans, this was not a statistically significant confounder either.

Diagnostic performance adjusted for significant confounders

Following the exclusion of scans influenced by low inflammatory activity at the time of imaging and those influenced by prior use of surgical adhesives, the sensitivity, specificity, PPV, and NPV of FDG PET/CT in patients in whom PVE was suspected increased to 91%, 95%, 95%, and 91%, respectively. Recent valve implantation (within 1 or within 3 months before FDG PET/CT imaging) was not a significant confounder.

Quantitative analysis

Of the 237 included scans, 170 had an EARL-accredited reconstruction available for (semi)quantitative analyses: 55 in the PVE group and 115 in the control groups. The mean SUV_{max} and SUV_{ratio} (average of both observers) in the PVE group were significantly higher than in both the group of patients in whom PVE was suspected with a final rejected diagnosis and the negative control group (Table 4, Figure 4).

	Suspicion of PVE (n=111)		No PVE (scans for other indications)
	PVE*	No PVE (after initial suspicion)*	
All EARL-standardized scans	n=55	n=56	n=59
SUV_{max} (mean \pm SD [range])	4.7 \pm 1.6 [2.3-9.9]	3.3 \pm 1.3 [1.3-9.1] (p<0.001) ^β	3.4 \pm 0.7 [2.1-6.7] (p<0.001) ^β
SUV_{ratio} (mean \pm SD [range])	2.8 \pm 0.9 [1.4-5.3]	1.9 \pm 0.8 [0.9-6.8] (p<0.001) ^β	1.9 \pm 0.7 [1.3-6.4] (p<0.001) ^β
Scans with sufficient myocardial suppression[†]	n=45	n=42	n=31
SUV_{max} (mean \pm SD [range])	4.8 \pm 1.6 [2.3-9.9]	3.2 \pm 1.2 [1.3-9.1] (p<0.001) ^β	3.0 \pm 0.5 [2.1-4.7] (p<0.001) ^β
SUV_{ratio} (mean \pm SD [range])	2.8 \pm 0.9 [1.4-5.3]	1.8 \pm 0.9 [0.9-6.8] (p<0.001) ^β	1.6 \pm 0.2 [1.3-2.1] (p<0.001) ^β
Excluding significant confounders[‡]	n=30	n=34	n=10
SUV_{max} (mean \pm SD [range])	5.3 \pm 1.6 [3.0-9.9]	3.0 \pm 0.6 [1.8-4.3] (p<0.001) ^β	3.6 \pm 0.7 [2.8-4.9] (p=0.003) ^β
SUV_{ratio} (mean \pm SD [range])	3.2 \pm 0.8 [2.0-5.3]	1.7 \pm 0.3 [1.1-2.6] (p<0.001) ^β	1.9 \pm 0.3 [1.5-2.3] (p<0.001) ^β

Table 4 | Quantification of FDG uptake (averages of both observers, range in square brackets) in all EARL-standardized scans (n=170). CRP indicates C-reactive protein; EARL, European Association of Nuclear Medicine Research Ltd; FDG, ¹⁸F-fluorodeoxyglucose; PV, prosthetic heart valve; PVE, prosthetic heart valve endocarditis; SUVmax, maximum standardized uptake value; and SUVratio, standardized uptake value ratio. (*) Final diagnosis based on surgical findings (if re-operated), expert opinion, and follow-up. (β) Significantly lower than the average measurements in the PVE group. (†) Excluding measurements that were indicated as having possibly included unsuppressed myocardial FDG uptake by both observers (n=52, Table 3). (‡) Excluding scans of patients in whom CRP was <40 mg/L at the time of imaging or surgical adhesives had been used during PV implantation.

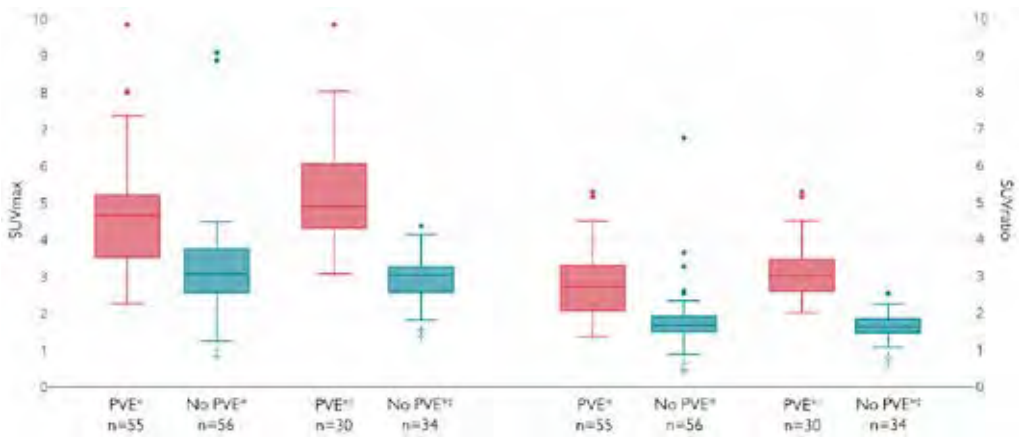


Figure 4 | Differences in SUV_{max} and SUV_{ratio} between the PVE and no-PVE group. Box plots for the 2-observer average measured SUV_{max} (**left**) and SUV_{ratio} (**right**) in cases (red) and controls (green) in all EARL-standardized scans acquired for suspicion of PVE ($n=111$), and (**†**) after exclusion of scans in patients with low inflammatory activity (CRP <40 mg/L) at the time of imaging or reported use of surgical adhesives during PV implantation ($n=64$). CRP indicates C-reactive protein; EARL, European Association of Nuclear Medicine Research Ltd; PV, prosthetic heart valve; PVE, prosthetic heart valve endocarditis; SUV_{max} , maximum standardized uptake value; and SUV_{ratio} , standardized uptake value ratio. (*****) Final diagnosis based on surgical findings (if reoperated), expert opinion, and follow-up. (**†**) Significantly different from adjacent PVE group ($P < 0.001$).

Only looking at EARL-standardized scans obtained for suspicion of PVE ($n=111$) and assuming sensitivity and specificity are equally important, the optimal threshold was 4.2 for SUV_{max} (sensitivity 60%, specificity 91%, PPV 87%, NPV 70%, AUC 0.81 [0.73–0.88]) and 2.1 for SUV_{ratio} (sensitivity 75%, specificity 86%, PPV 84%, NPV 77%, AUC 0.83 [0.75–0.89]; **Figure 5A**).

When excluding scans in patients with either a CRP of <40 mg/L or prior use of surgical adhesives ($n=64$ remaining), the diagnostic performance of both cutoff values improved substantially, with an optimal cutoff value of 3.3 for SUV_{max} (sensitivity 97%, specificity 79%, PPV 81%, NPV 96%, AUC 0.95 [0.87–0.99]) and 2.0 for SUV_{ratio} (sensitivity 100%, specificity 91%, PPV 91%, NPV 100%, AUC 0.99 [0.93–1.00]; **Figure 5B**). Adjusted for confounders, a SUV_{ratio} of 2.6 had a specificity (and PPV) of 100% for PVE (**Figure 5B**).

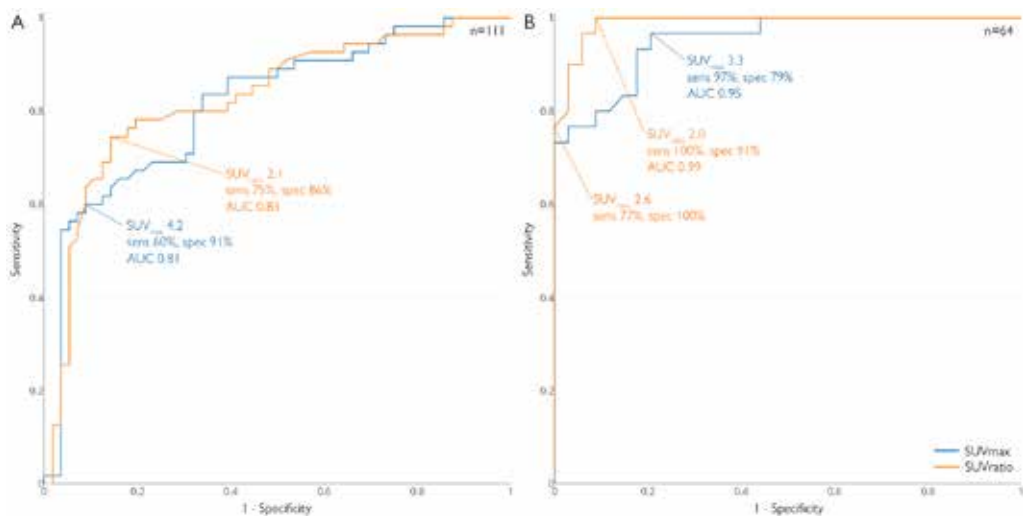


Figure 5 | Diagnostic performance of the semiquantitative analyses of FDG uptake. ROCs for SUV_{max} and SUV_{ratio} (averages of both observers) in all EARL-standardized scans of patients suspected of PVE (n=111; **A**) and excluding scans in patients with low inflammatory activity at the time of FDG PET/CT imaging (CRP<40 mg/L) or reported use of surgical adhesives during PV implantation (n=64; **B**). AUC indicates area under the curve; CRP, C-reactive protein; EARL, European Association of Nuclear Medicine Research Ltd; FDG, ¹⁸F-fluorodeoxyglucose; PET/CT, positron-emission tomography/computed tomography; PV, prosthetic heart valve; PVE, prosthetic heart valve endocarditis; ROC, receiver-operator curve; sens, sensitivity; spec, specificity; SUV_{max}, maximum standardized uptake value; and SUV_{ratio}, standardized uptake value ratio.

When verifying these cut-off values in the negative control group without any suspicion of PVE, 4 of 59 scans had an SUV_{ratio} of >2.0 (specificity 93%), whereas none were >2.6. Three of these 4 measurements had been done in oncological scans with intense myocardial uptake due to a lack of adequate patient preparation, which may have influenced these measurements. The fourth had an SUV_{ratio} of 2.1.

Interobserver variability

Overall, in the EARL-standardized scans (n=170), the differences between SUV_{max} and SUV_{ratio} measurements of both observers were relatively small (mean SUV_{max} difference -0.04; 95% CI, -0.35 to 0.28; *P*=0.82; mean SUV_{ratio} difference 0.04; 95% CI, -0.16 to 0.25; *P*=0.70). The 2-way mixed intraclass correlation coefficient of absolute agreement for single SUV_{max} measurements (0.82; 95% CI, 0.76–0.86) and SUV_{ratio} measurements (0.84; 95% CI, 0.78–0.88) indicated a good-to-excellent agreement between the observers on both variables. Excluding scans with unsuppressed myocardial FDG uptake that may have hampered these measurements increased interobserver reliability to excellent for both variables, with intraclass correlation coefficients of 0.94 (95% CI, 0.91–0.96) and 0.95 (95% CI, 0.92–0.96) for SUV_{max} and SUV_{ratio}, respectively.

Discussion

To our knowledge, this multicenter study reports the largest patient cohort on the diagnostic performance of FDG PET/CT in PVE to date, including a negative control group of patients with a PV who underwent FDG PET/CT imaging for other indications than suspected PVE. Although several authors have reported the possible influence of prolonged antibiotic therapy and surgical adhesives, to our knowledge, this study is the first to identify these factors as significant confounders and to assess the true diagnostic accuracy of FDG PET/CT by excluding scans that were affected by them. Finally, in this study, standardized quantification of FDG uptake after exclusion of these confounders allowed for identification of a reliable diagnostic cutoff for PVE that can be used in any center with an EARL-calibrated scanner (currently > 150 centers in Europe¹⁶).

The diagnostic performance of the visual assessment of FDG PET/CT scans in patients in whom PVE was suspected in our study, not adjusted for confounders, was reasonable and comparable to previous studies^{12,19}, with a sensitivity, specificity, PPV, and NPV of 74%, 91%, 89%, and 78%, respectively. As previously mentioned, low inflammatory activity at the time of FDG PET/CT imaging and prior use of surgical adhesives during PV implantation were identified, respectively, as significant predictors of false-negative or false-positive misinterpretations in a logistic regression model. Excluding scans affected by these 2 significant confounders significantly improved the diagnostic performance values of the visual assessment in patients in whom PVE was suspected to 91%, 95%, 95%, and 91%.

Confounding factors

Low inflammatory activity

Several authors of previous studies regarding FDG PET/CT in suspected PVE have suggested the influence of low inflammatory activity, measured by CRP or white blood cell count, or prolonged antibiotic therapy on false-negative PET interpretations.^{8,19} However, no studies to date had corrected for this confounder, even though several studies on the value of FDG PET/CT for the detection of infections of unknown origin have shown that high inflammatory activity is a significant predictor of, and may be a requirement for, an adequate FDG PET/CT scan.^{20,21}

The drastic increase in sensitivity observed when adding FDG PET/CT to echocardiography (from 65% of echocardiography alone to 96% of both imaging techniques combined), without even adjusting for low inflammatory activity, is probably caused by the fact that the patients with negative echocardiograms are often also the patients that were scanned early in the disease process, before structural damage or vegetation ensued. It is in these patients that levels of inflammatory activity are still high and that FDG PET/CT is most reliable.

Whether initial or empirical antibiotic therapy should be ceased for diagnostic purposes, however, in case inflammatory parameters have already diminished without a certain diagnosis, remains questionable in light of the risks associated with unsuccessfully treated PVE. In our opinion, a pragmatic antibiotic treatment of a possible PVE is preferable over a PET-confirmed definite PVE that has to be reoperated because of the

cessation of antibiotic therapy. Although a CRP level of <4 times the upper normal limit (<40 mg/L) was a significant and major predictor of false-negative interpretations in this study, FDG PET/CT may still be considered when inflammatory parameters are low if the diagnosis of PVE has significant therapeutic consequences. In our study, FDG PET/CT was positive in 13 of 28 (46%) patients with a CRP of <40 mg/L and a definite diagnosis of PVE.

Surgical adhesives

Surgical adhesives are known to be very FDG avid, with several case reports on patients who underwent lung surgery, aortic surgery, or heart valve surgery showing intense FDG uptake in areas where they had been applied, which can persist for several years if not indefinitely.⁹ In our study, we evaluated the surgical reports of all patients, of which 4 mentioned the use of a surgical adhesive during PV implantation. All 4 of these patients (3 without PVE, 1 with PVE) had a positive FDG PET/CT scan, and, as far as could be determined from the surgical report, the areas of FDG uptake were consistent with the areas that these adhesives had been applied to.

Recent valve implantation

Current European Society of Cardiology (ESC) guidelines recommend not to perform FDG PET/CT within 3 months of PV implantation.⁴ The reasoning behind this 3-month grace period was the assumed likelihood of false-positive findings attributable to sterile inflammation, as seen in recent lung cancer resection surgery,²² based on expert opinion and a case report of increased FDG uptake around a biological mitral PV implanted 2 months before FDG PET/CT imaging.

In the largest study on FDG PET/CT in suspected PVE before the 2015 update of the ESC guidelines, Saby et al.¹⁹ excluded patients with a PV implanted <1 month before admission to avoid false-positive results related to early postoperative inflammation. They also referred to the same case report, but described no false positives that could have been attributed to PV implantation between 2 and 3 months before imaging. In another study by Rouzet et al.,²³ in which FDG PET/CT was compared with radiolabeled leukocyte scintigraphy in patients in whom PVE was suspected, 6 patients in whom a PV had been implanted <2 months before imaging had a false-positive FDG PET/CT result, whereas leukocyte scintigraphy was not affected by this sterile inflammation.

Since the publication of this study and the 2015 update of the ESC guidelines, however, several studies that included patients scanned within 3 months of implantation, some even within 2 weeks, have explicitly described true-negative findings.¹¹ Moreover, Mathieu et al.²⁴ recently described a cohort of 51 patients without PVE, and showed that the mean amount of FDG uptake was not significantly different between patients scanned within 3 months of implantation or thereafter, and that elevated FDG uptake may occur as late as 8 years after PV implantation without any clinical suspicion of PVE.

In our study, recent valve implantation was not a significant predictor of false-positive interpretations, and we cannot substantiate the ESC guideline recommendation. We believe performing FDG PET/CT early after surgery poses no significant diagnostic difficulties based on our findings and the evidence available from previous studies.

Myocardial FDG uptake

Visual assessment of FDG uptake around the PV was not significantly hampered by unsuppressed myocardial uptake in this study, even though the myocardial uptake had been classified as more than liver or intense in a substantial number of scans. In particular, in patients who had not been prepared with a low-carbohydrate diet before the scan, myocardial FDG uptake was frequently intense. Unsuppressed myocardial FDG uptake did not hamper the quantitative measurements as much as we had initially anticipated, either, as demonstrated by the merely slight change in average SUV_{max} and SUV_{ratio} when excluding scans with myocardial uptake that may have possibly affected the observers' measurements. However, it did significantly decrease interobserver reliability, and should always be minimized as much as possible by using at least a >6-hour fast (in our own experience, preferably at least 12 hours) and a 24-hour low-carbohydrate diet to allow for easy distinction of periprosthetic FDG uptake.^{10,15}

An additional intravenous injection of 50 IU/kg of unfractionated heparin 15 minutes before FDG administration (on top of the prolonged fasting and low-carbohydrate diet) slightly further reduced myocardial FDG uptake (*Table 3*), but the sample size was too small to show a clinically meaningful difference, and the small potential additional benefit of this should always be weighed against the possible adverse effects.²⁵⁻²⁷ Without a low-carbohydrate diet or extensive fasting (>18 hours), however, the additional value of intravenous heparin seems limited and does not result in sufficient myocardial suppression.²⁸ Furthermore, patients already on low-molecular-weight heparin or warfarin therapy (e.g. all patients with mechanical valves) most likely already benefit from the incremental suppression that these drugs provide, and do not need an additional unfractionated heparin bolus injection.²⁹

Quantitative analysis

Quantification of FDG uptake, expressed as SUV_{max} or SUV_{ratio} , showed reasonable diagnostic performance with an AUC for SUV_{max} of 0.81 and an AUC for SUV_{ratio} of 0.83, but lacked sufficient sensitivity. However, after exclusion of the previously mentioned significant confounders, the diagnostic performance drastically increased, and more reliable cutoffs could be identified.

Pizzi et al.¹² reported an AUC for SUV_{max} and SUV_{ratio} of 0.89 in a prospective study comprising 92 patients in whom PVE was suspected, with a sensitivity/specificity for their cutoffs ($SUV_{max} \geq 3.7$, $SUV_{ratio} \geq 1.69$) of 91%/79% and 91%/76%, respectively. Their measurements had not been performed on EARL-standardized reconstructions. After exclusion of scans affected by confounders, we found slightly different cutoffs for both measures ($SUV_{max} \geq 3.3$, $SUV_{ratio} \geq 2.0$) with a sensitivity/specificity of 97%/79% and 100%/91%, respectively. SUV_{ratio} was the most reliable and predictive measure, possibly because it was less dependent on patient characteristics and scanning parameters, with a 91% PPV for a SUV_{ratio} of ≥ 2.0 and a 100% PPV for a SUV_{ratio} of ≥ 2.6 .

As a confirmation of validity, there were no significant differences in measured SUV_{max} or SUV_{ratio} between the group of patients in whom PVE was initially suspected with a final rejected diagnosis and the negative control group of patients who underwent FDG PET/CT imaging for other indications.

Some authors have suggested calculating the SUV_{ratio} by dividing by the mean SUV in the atrial or mediastinal blood pool (as opposed to the blood pool in the descending aorta) because some patients may show increased FDG uptake in the aortic wall because of aortic calcifications or active plaque.^{13,14} In our study, we took particular care not to include the vessel wall in the volume of interest in the descending aorta, and preferred to adhere to the most commonly used measurement method for comparison.¹⁰ In addition, in case of valvular regurgitation or atrial fibrillation, the atrial wall may similarly show increased FDG uptake.

Interobserver reliability

Interobserver agreement for quantitative measurements of FDG uptake was good to excellent in our study, and significantly improved when excluding scans with poorly suppressed myocardial FDG uptake. This shows that quantification of perivalvular FDG uptake is a reliable tool with diagnostic cutoff values applicable to all centers with EARL accreditation, which allows for less-subjective image evaluation. There were, however, some discrepancies between the observers in the initial visual assessment of a number of scans (10%), for which a consensus reading was performed. In the majority of these, experience with normal variations of perivalvular uptake, which 1 observer arguably had less than the other, was key to a correct interpretation, exemplifying that the visual assessment of paravalvular FDG uptake is not always black and white and probably subject to a learning curve. Although the exact role of the pattern and distribution of FDG uptake around a PV (e.g. heterogeneous, diffuse, or focal) is still unclear, some patterns such as diffuse, slightly increased FDG uptake have been attributed to physiological inflammation processes around the PV.²⁴

Limitations

Our study had a number of potential limitations. Most importantly, besides the regular limitations of a retrospective study design, our study may have been influenced by the availability of the FDG PET/CT results to the expert team determining the final diagnosis, which may have introduced an incorporation bias. This is, however, the case in all studies to date regarding novel imaging techniques for suspected PVE, and is hard to circumvent. Even when investigators are blinded to the FDG PET/CT results, the subsequent clinical course of action will usually reveal the implications that the FDG PET/CT findings had. Ideally, although imaginably difficult and possibly unethical to realize, the diagnostic performance of FDG PET/CT would be evaluated in a prospective trial in which even the physicians remain blinded to its findings. In addition, although we strongly believe that FDG PET/CT may aid in the timely diagnosis of PVE, the impact of an early diagnosis of PVE by FDG PET/CT on morbidity and mortality remains uninvestigated, and would require large randomized controlled trials to be elucidated.

Next, all FDG PET/CT scans were reassessed by 2 independent observers with several years of experience in FDG PET/CT imaging of suspected PVE, who were blinded to all clinical data. The external validity of a fully blinded assessment of FDG PET/CT in suspected PVE could be contested, because clinical information is often important for the interpretation of possibly pathological FDG uptake. In clinical practice, results of the FDG PET/CT scan would be interpreted in a multidisciplinary setting in the context

of the clinical presentation, microbiological and echocardiographic findings, and the results of other imaging techniques, as well, such as CT angiography. Furthermore, the blinding may have been imperfect in the presence of obvious findings such as large malignancies, biasing the interpretation by revealing an alternate diagnosis, especially because the observers were aware of our study design. This bias did not, however, have any effect on the calculation of diagnostic accuracy in our study, because oncological scans were not included in these analyses.

Finally, the exclusion of scans affected by significant confounders may have limited the clinical applicability and generalizability of our findings. However, the confounders identified in this study can most likely be identified and mitigated in clinical practice as well, most importantly by implementing FDG PET/CT early in the diagnostic workup of PVE to prevent imaging after extended periods of antibiotic therapy, while insight in the surgical report may help to identify increased FDG uptake attributable to use of surgical adhesives.

Clinical implications

Our findings may have several important clinical implications. First, our study shows that FDG PET/CT should preferably be implemented early in the diagnostic workup of suspected PVE to prevent the negative confounding effect of low inflammatory activity, ideally while CRP levels are >40 mg/L (Figure 6). Moreover, if implemented early, FDG PET/CT can detect PVE before structural damage occurs, allowing timely appropriate antibiotic treatment that could possibly prevent a reoperation, while also preventing missed diagnoses because echocardiography may be negative in these early stages of the disease.¹⁰ In any patient with a PV and positive blood cultures, particularly if the micro-organism is known to be aggressive (e.g. *Staphylococcus aureus*),³⁰ FDG PET/CT should readily be considered in the absence of clear alternative diagnoses.

Second, if performed in a timely manner, and taking into account possible confounders, EARL-standardized quantification of FDG uptake around PVs (as SUV_{ratio}) has a very high predictive value for PVE at a cutoff of ≥ 2.0 (100% sensitivity, 91% specificity), which can immediately be applied in daily clinical practice in all EARL-accredited centers.

Third, the interpreting nuclear physician has to be explicitly made aware of prior use of surgical adhesives during PV implantation.

Fourth, although myocardial FDG uptake did not substantially influence our results, adequate suppression by at least a low-carbohydrate diet is essential for reliable PV assessment, and easy to achieve.

And finally, our results do not corroborate ESC guideline recommendations to avoid FDG PET/CT in patients with a recently implanted PV. The possibility of periprosthetic FDG uptake because of physiological inflammation should always be taken into account, although future studies on the distribution and patterns of FDG uptake may identify characteristics that further aid the distinction between inflammation and infection.

Most importantly, however, the goal should never be to replace routine PVE diagnostics (eg, echocardiography, blood cultures, computed tomography angiography), but rather to combine all these modalities, each with their specific strengths and weaknesses, to achieve optimal diagnostic accuracy (Figure 6).

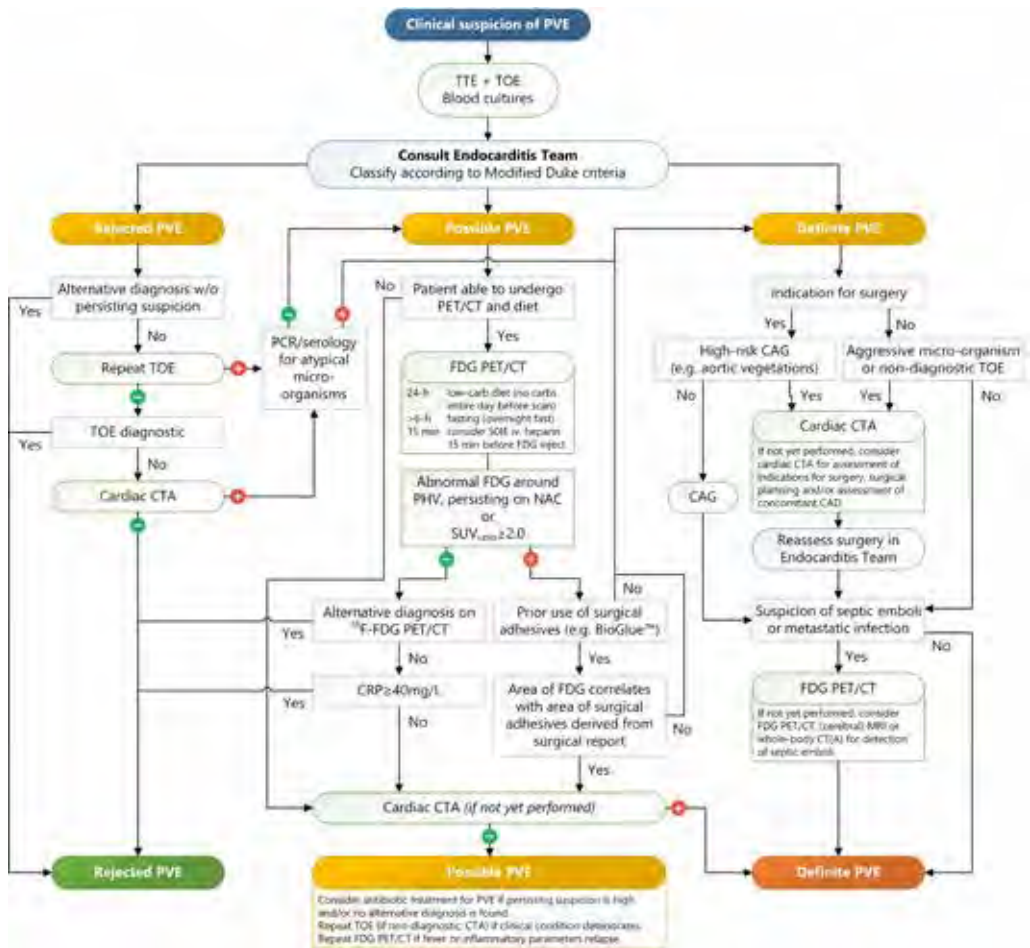


Figure 6 | Flowchart for the proposed diagnostic workup of suspected PVE. CAD indicates coronary artery disease; CAG, coronary angiography; CRP, C-reactive protein; CTA, computed tomography angiography; FDG, 18-fluorine-fluorodeoxyglucose; IE, international units; NAC, nonattenuation corrected reconstructions; PCR, polymerase chain reaction; PET/CT, positron-emission tomography/computed tomography; PHV, prosthetic heart valve; PVE, prosthetic heart valve endocarditis; SUV_{ratio}, standardized uptake value ratio; TOE, transesophageal echocardiography; and TTE, transthoracic echocardiography.

Conclusions

Both visual and quantitative assessment of FDG PET/CT have a high diagnostic accuracy in patients in whom PVE is suspected when implemented early in the diagnostic workup to prevent the negative confounding effect of low inflammatory activity (e.g. because of prolonged antibiotic therapy). As a quantitative measure of FDG uptake, an EARL-standardized SUV_{ratio} of ≥ 2.0 is a 100% sensitive and 91% specific predictor of PVE. Recent valve implantation did not significantly influence the diagnostic performance of FDG PET/CT in our study, but surgical adhesives used during implantation did.

References

1. Sohail MR, Martin KR, Wilson WR, et al. Medical versus surgical management of Staphylococcus aureus prosthetic valve endocarditis. *Am J Med.* 2006;119:147–54.
2. Li JS, Sexton DJ, Mick N, et al. Proposed modifications to the Duke criteria for the diagnosis of infective endocarditis. *Clin Infect Dis.* 2000;30:633–8.
3. Habib G, Derumeaux G, Avierinos JF, et al. Value and limitations of the Duke criteria for the diagnosis of infective endocarditis. *J Am Coll Cardiol.* 1999;33:2023–9.
4. Habib G, Lancellotti P, Antunes MJ, et al. 2015 ESC Guidelines for the management of infective endocarditis: The Task Force for the Management of Infective Endocarditis of the European Society of Cardiology (ESC). *Eur Heart J.* 2015;36:3075–128.
5. Nishimura RA, Otto CM, Bonow RO, et al. 2014 AHA/ACC guideline for the management of patients with valvular heart disease: a report of the American College of Cardiology/American Heart Association Task Force on Practice Guidelines. *Circulation.* 2014;129:e521–e643.
6. Habets J, Tanis W, Reitsma JB, et al. Are novel non-invasive imaging techniques needed in patients with suspected prosthetic heart valve endocarditis? A systematic review and meta-analysis. *Eur Radiol.* 2015;25:2125–33.
7. Gomes A, Glaudemans AWJM, Touw DJ, et al. Diagnostic value of imaging in infective endocarditis: a systematic review. *Lancet Infect Dis.* 2017;17:e1–e14.
8. Scholtens AM, van Aarnhem EE, Budde RP. Effect of antibiotics on FDG PET/CT imaging of prosthetic heart valve endocarditis. *Eur Heart J Cardiovasc Imaging.* 2015;16:1223.
9. Scholtens AM, Swart LE, Verberne HJ, et al. Confounders in FDG-PET/CT imaging of suspected prosthetic valve endocarditis. *JACC Cardiovasc Imaging.* 2016;9:1462–5.
10. Swart LE, Scholtens AM, Tanis W, et al. 18F-fluorodeoxyglucose positron emission/computed tomography and computed tomography angiography in prosthetic heart valve endocarditis: from guidelines to clinical practice. *Eur Heart J.* 2018; doi: 10.1093/eurheartj/ehx784.
11. Scholtens AM, Budde RPJ, Lam MGEH, Verberne HJ. FDG PET/CT in prosthetic heart valve endocarditis: there is no need to wait. *J Nucl Cardiol.* 2017;24:1540–1.
12. Pizzi MN, Roque A, Fernández-Hidalgo N, et al. Improving the diagnosis of infective endocarditis in prosthetic valves and intracardiac devices with 18F-fluorodeoxyglucose positron emission tomography/computed tomography angiography: initial results at an infective endocarditis referral center. *Circulation.* 2015;132:1113–26.
13. Jiménez-Ballvé A, Pérez-Castejón MJ, Delgado-Bolton RC, et al. Assessment of the diagnostic accuracy of 18F-FDG PET/CT in prosthetic infective endocarditis and cardiac implantable electronic device infection: comparison of different interpretation criteria. *Eur J Nucl Med Mol Imaging.* 2016;43:2401–12.
14. Fagman E, van Essen M, Fredén Lindqvist J, et al. 18F-FDG PET/CT in the diagnosis of prosthetic valve endocarditis. *Int J Cardiovasc Imaging.* 2016;32:679–86.
15. Scholtens AM, Swart LE, Kolste HJT, et al. *J Nucl Cardiol.* 2017; doi: 10.1007/s12350-017-0932-x.
16. Kaalep A, Sera T, Oyen W, et al. EANM/EARL FDG-PET/CT accreditation - summary results from the first 200 accredited imaging systems. *Eur J Nucl Med Mol Imaging.* 2018;45:412–22.

17. Swart LE, Gomes A, Scholtens AM, et al. Retrospective Multicenter Study on the Diagnostic Accuracy of 18-F FDG PET/CT for suspected Prosthetic Valve Endocarditis. *Zenodo*. 2018; doi: 10.5281/zenodo.1208421.
18. Mehta S, Bastero-Caballero RF, Sun Y, et al. Performance of intraclass correlation coefficient (ICC) as a reliability index under various distributions in scale reliability studies. *Stat Med*. 2018;37:2734–52.
19. Saby L, Laas O, Habib G, et al. Positron emission tomography/computed tomography for diagnosis of prosthetic valve endocarditis: increased valvular 18F-fluorodeoxyglucose uptake as a novel major criterion. *J Am Coll Cardiol*. 2013;61:2374–82.
20. Tseng JR, Lin CW, Chen SH, et al. Clinical usefulness of ¹⁸F-FDG PET/CT for the detection of infections of unknown origin in patients undergoing maintenance hemodialysis. *J Nucl Med*. 2015;56:681–7.
21. Crouzet J, Boudousq V, Lechiche C, et al. Place of (18)F-FDG-PET with computed tomography in the diagnostic algorithm of patients with fever of unknown origin. *Eur J Clin Microbiol Infect Dis*. 2012;31:1727–33.
22. Griffeth LK. Use of PET/CT scanning in cancer patients: technical and practical considerations. *Proc (Bayl Univ Med Cent)*. 2005;18:321–30.
23. Rouzet F, Chequer R, Benali K, et al. Respective performance of 18F-FDG PET and radiolabeled leukocyte scintigraphy for the diagnosis of prosthetic valve endocarditis. *J Nucl Med*. 2014;55:1980–5.
24. Mathieu C, Mikail N, Benali K, et al. Characterization of 18F-fluorodeoxyglucose uptake pattern in noninfected prosthetic heart valves. *Circ Cardiovasc Imaging*. 2017;10:e005585.
25. Scholtens AM, Verberne HJ, Budde RP, Lam MG. Additional heparin preadministration improves cardiac glucose metabolism suppression over low-carbohydrate diet alone in ¹⁸F-FDG PET imaging. *J Nucl Med*. 2016;57:568–73.
26. Masuda A, Naya M, Manabe O, et al. Administration of unfractionated heparin with prolonged fasting could reduce physiological 18F-fluorodeoxyglucose uptake in the heart. *Acta Radiol*. 2016;57:661–8.
27. Osborne MT, Hulten EA, Murthy VL, et al. Patient preparation for cardiac fluorine-18 fluorodeoxyglucose positron emission tomography imaging of inflammation. *J Nucl Cardiol*. 2017;24:86–99.
28. Gormsen LC, Christensen NL, Bendstrup E, et al. Complete somatostatin-induced insulin suppression combined with heparin loading does not significantly suppress myocardial 18F-FDG uptake in patients with suspected cardiac sarcoidosis. *J Nucl Cardiol*. 2013;20:1108–15.
29. Giorgetti A, Marras G, Genovesi D, et al. Effect of prolonged fasting and low molecular weight heparin or warfarin therapies on 2-deoxy-2-[¹⁸F]-fluoro-D-glucose PET cardiac uptake. *J Nucl Cardiol*. 2017; doi: 10.1007/s12350-017-0800-8.
30. Berrevoets MAH, Kouijzer IJE, Aarntzen EHJG, et al. 18F-FDG PET/CT optimizes treatment in staphylococcus aureus bacteremia and is associated with reduced mortality. *J Nucl Med*. 2017;58:1504–10.





CHAPTER 4

¹⁸F-FDG PET/CT AND CT ANGIOGRAPHY IN ENDOCARDITIS OF PERCUTANEOUSLY IMPLANTED PROSTHETIC HEART VALVES

Laurens Swart
Asbjørn Scholtens
Christa Liesting
Roelf Valkema
Karin Schurink
Nicolas van Mieghem
Gabriel Krestin
Jolien Roos-Hesselink
Ricardo Budde

4

*Published in: European Heart Journal 2016;37:3059
and European Heart Journal Cardiovascular Imaging 2018;19:1188–9*

Introduction

As an alternative to heart valves that had to be implanted through conventional cardiothoracic surgery, which is a large and, particularly for elderly patients, very-high-risk procedure, in 2002 a new type of bioprosthetic valve was introduced that can be implanted percutaneously through delivery via the transfemoral artery, apex of the heart, subclavian artery or directly through the aorta (by a minimally invasive surgical incision). These valves are wrapped inside a stent frame which is folded up around or inside a catheter, and can then either be deployed by expanding a balloon inside the valve stent or releasing it by sliding off the surrounding catheter sheath (in case of a self-expandable stent). Initially, these valves were only used in elderly or critically ill patients with major comorbidities in whom a conventional heart valve replacement was deemed too great of a risk. Lately however, the age threshold for transcatheter aortic valve implantation (TAVI) has gradually become lower as results of long-term outcomes of percutaneously implanted valves are becoming more abundant.¹⁻³ Furthermore, the *Melody* transcatheter pulmonary valve (TPV), approved in Europe in 2006, is nowadays commonly used in patients with a congenital pulmonary valve or right ventricular outflow tract conduit as an alternative to invasive pulmonary valve (e.g. homograft) replacement surgery (*Figure 1*).⁴

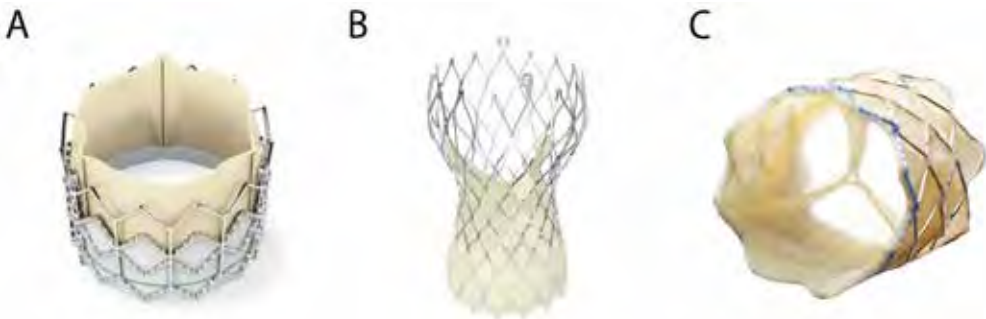


Figure 1 | Examples of different percutaneous aortic (**A**, **B**) and pulmonic (**C**) valve prostheses. (**A**) Carpentier-Edwards *Sapien 3* transcatheter aortic valve prosthesis, expanded through balloon inflation. (**B**) Medtronic *CoreValve Evolut R* transcatheter aortic valve prosthesis, self-expanding upon release from its sheath. (**C**) Medtronic *Melody* transcatheter pulmonary valve prosthesis, expanded through balloon inflation. Images courtesy of the respective valve manufacturers.

Endocarditis of a percutaneously implanted valve has been thought to be a rare entity, with only a couple of case reports showing up in early literature following the introduction of these new valve types. More recently however, most likely because the number of TAVI procedures has dramatically increased over the past decade, its incidence has increased probably at least as rapid, with the latest reports estimating a 1.1% risk per patient per year.^{5,6} In a registry of over 20,000 TAVI patients, the median time from TAVI to the first signs of endocarditis was 5.3 months, with more than 75% of all endocarditis episodes occurring within the first year of implantation. Risk factors associated with an increased risk of PVE were younger age, male sex, history of diabetes mellitus, and moderate to severe residual aortic regurgitation. The in-hospital and 2-year mortality rates were 36% and 66%, respectively.⁶

For percutaneously implanted pulmonary valves such as the Melody (Medtronic) valve, the incidence of PVE is probably even higher, estimated at approximately 3% per patient per year.^{7,8} The diagnosis of PVE in all these studies was established by employment of the modified Duke criteria, with the value of ¹⁸F-FDG PET/CT and CT angiography only recently being first acknowledged in small case series.⁹ This chapter presents two case reports, one of a patient with endocarditis of a TAVI valve and one of a patient with endocarditis of a Melody valve, in which we first described the additional value of combined (i.e. fused, or 'hybrid') ¹⁸F-FDG PET/CT and CT angiography in suspected PVE of these valve types.

Case I: Percutaneous aortic valve endocarditis

A 75-year-old woman was referred to our centre for suspicion of endocarditis. Six months earlier, she had undergone an uncomplicated transcatheter aortic valve implantation (TAVI; Medtronic CoreValve Evolut R). For several days prior to admission, she had been experiencing symptoms of drowsiness, malaise, and a spiking fever. Blood cultures were positive for *Staphylococcus aureus*, and echocardiography revealed a small, slightly oscillating structure within the distal TAVI stent frame, without signs of perivalvular extensions or paravalvular leakage. Additional cardiac computed tomography angiography (CTA) and ¹⁸F-fluorodeoxyglucose (¹⁸F-FDG) positron emission tomography (PET) scans were performed in accordance with the most recent guidelines.

Computed tomography angiography confirmed the presence of a small structure at the craniodorsal side of TAVI stent (*Figure 2* Panel I-C), and demonstrated some stranding of the periaortic fatty tissue, slightly above the level of the suspected vegetation (*Figure 2* Panel I-A; *Figure 3*), while PET revealed intense uptake of ¹⁸F-FDG in the same area (*Figure 2* Panels I-B and I-D). The maximum standardized uptake value (SUV_{max}; a quantitative measure of uptake) and the ratio between the SUV_{max} and the mean SUV in the bloodpool (target-to-background ratio, TBR) were 8.00 and 3.92, respectively (*Figure 4* Panel A). The patient was treated conservatively and was started on flucloxacillin and gentamicin.

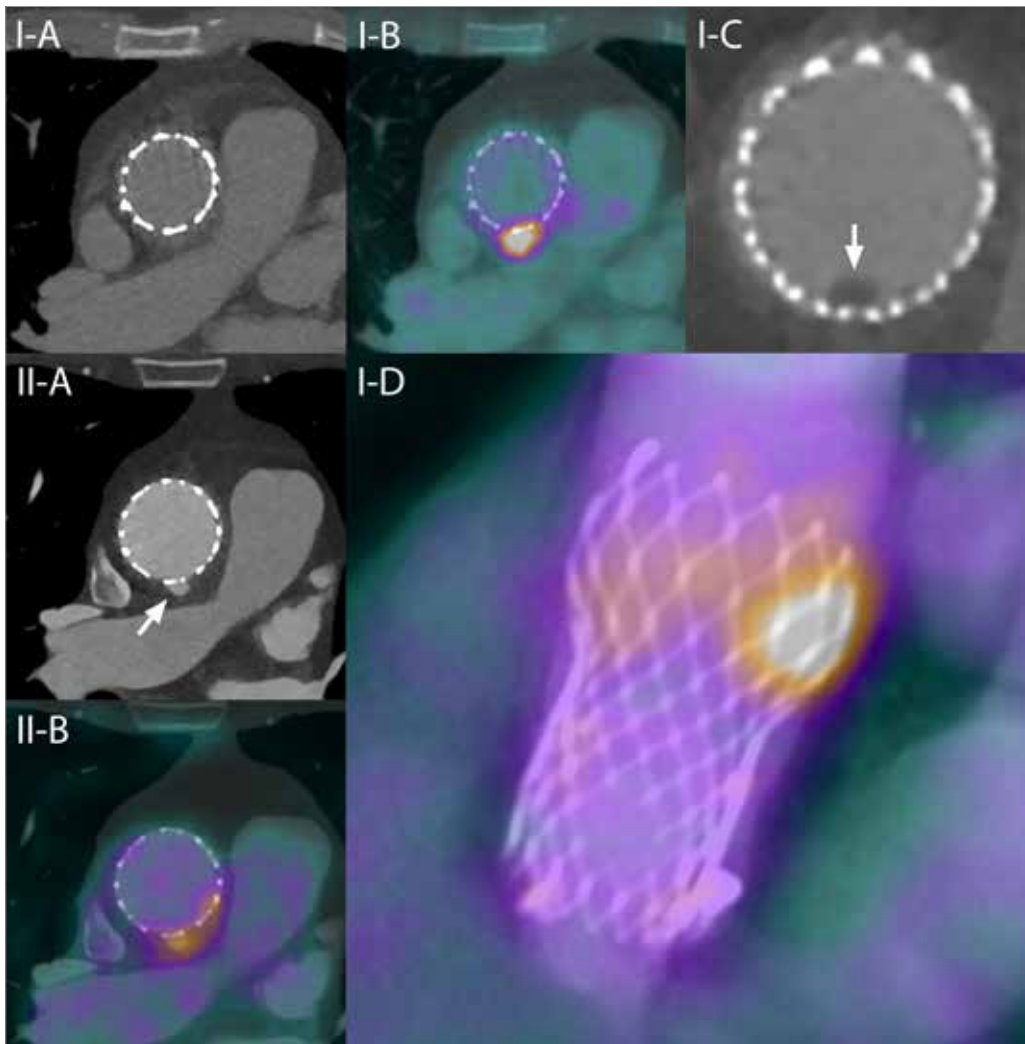


Figure 2 | **(I-A)** Double-oblique CTA image of the distal TAVI stent showing some slight induration around the prosthesis, particularly on the dorsal side. **(I-B)** Fused PET/CTA showing intense focal FDG uptake on the dorsal side of the distal TAVI stent. **(I-C)** Enlarged slightly more proximal slice of the distal TAVI stent showing a tiny area without contrast, indicating a possible vegetation. **(I-D)** Fused PET/CTA 3D maximum-intensity projection showing the entire TAVI prosthesis and the localization of the FDG uptake. **(II-A)** Follow-up CTA after 6 weeks of antibiotic treatment, showing a small mycotic aneurysm or ulcer at the site of increased FDG uptake. **(II-B)** Follow-up fused PET/CT showing FDG uptake that has diminished but not completely disappeared.

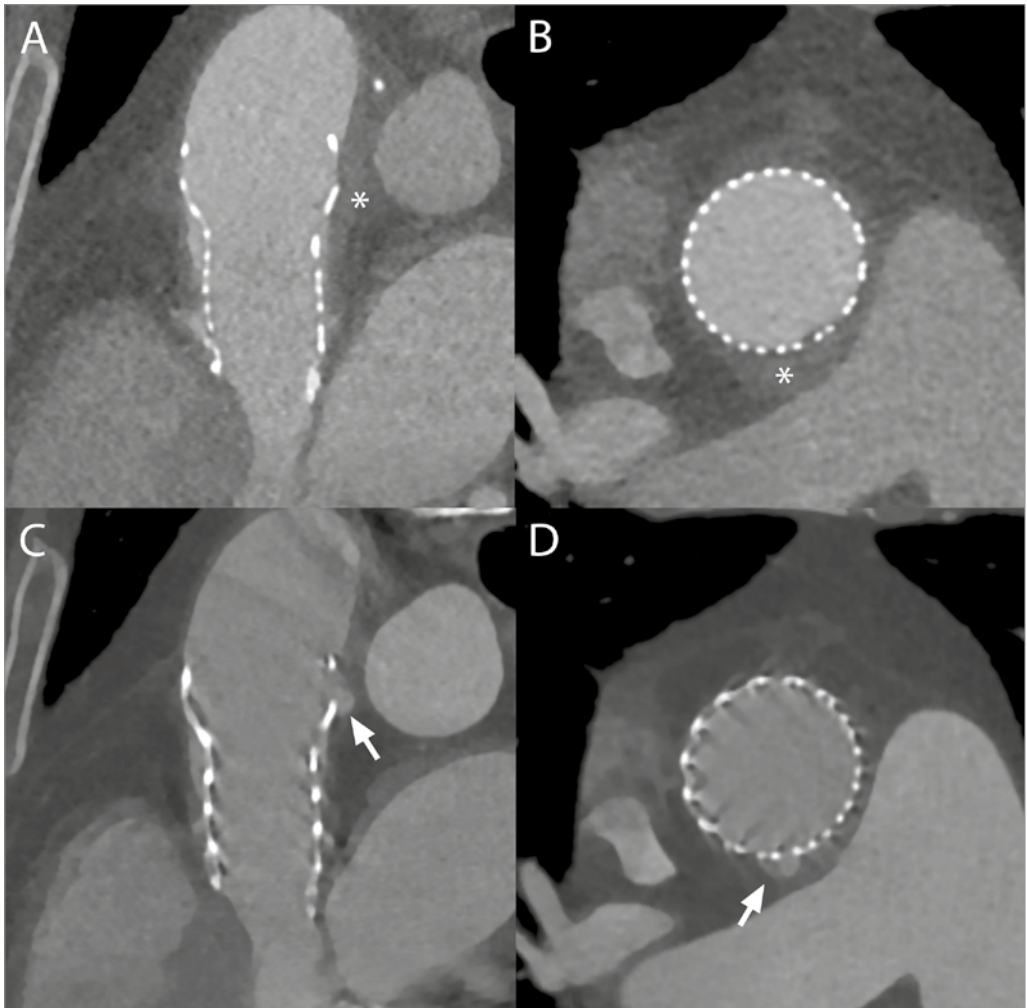


Figure 3 | (A, B) Additional long- and short-axis CTA images of the TAVI prosthesis at presentation, showing induration (*) dorsally of the distal prosthesis. (C, D) Follow-up CTA showing a newly formed small mycotic aneurysm (ulcus, **arrow**) at the same localization as the earlier described stranding.

During 6 weeks of antibiotic treatment, the patient quickly recovered and blood cultures as well as inflammatory markers normalized. After a 5-day 'grace period' off antibiotics, PET/CTA was repeated. Although increased ^{18}F -FDG uptake was still distinguishable (Figure 2 Panel II-B), the intensity had decreased significantly (SUVmax 4.32, TBR 1.88; Figure 4 Panel B). However, CTA now revealed a small mycotic aneurysm at the same location (Panel II-A). The patient was discharged under close, weekly monitoring. A follow-up CTA was acquired 4 weeks later, which showed no changes (Figure 3). It was therefore considered likely that the small mycotic aneurysm was not a sign of unsuccessful antibiotic therapy, but rather something that occurred during the active stage of the disease and did not progress thanks to adequate therapy.

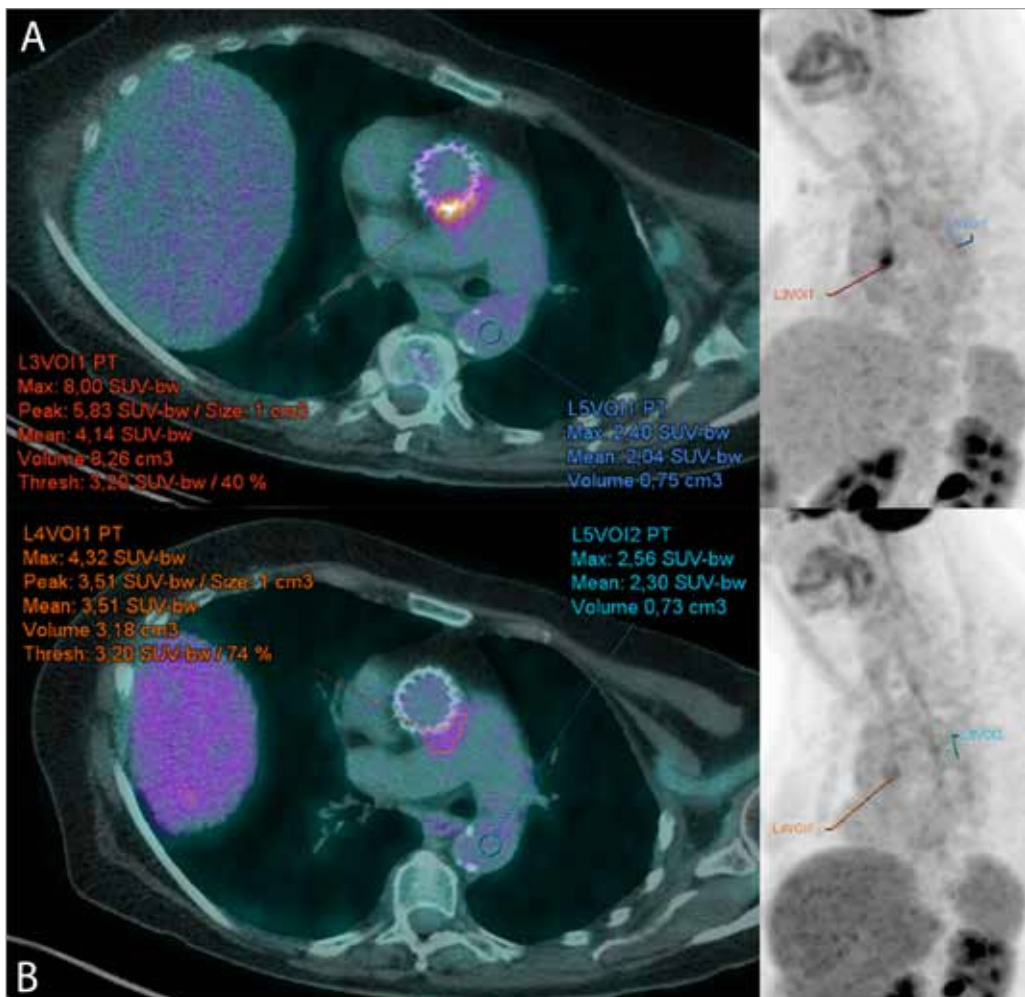


Figure 4 | Quantitative analysis of the FDG-uptake surrounding the TAVI prosthesis. **(A)** Fused PET/CTA (**left**) and PET maximum intensity projection (**right**) of the first PET/CT at presentation, with an SUV_{max} of 8.00 and a SUV_{ratio} of $8.00/2.04=3.92$. **(B)** Follow-up PET/CTA after 6 weeks of antibiotic treatment, showing decreased FDG uptake (SUV_{max} 4.32, SUV_{ratio} 1.88).

Case II: Percutaneous pulmonary valve endocarditis

A 25-year-old man with a history of pulmonary atresia combined with a ventricular septal defect was referred to our centre for suspicion of prosthetic heart valve endocarditis. Three years ago, a percutaneous pulmonary valve (Melody®, Medtronic) had been implanted to replace his homograft because of severe pulmonary insufficiency.

At admission, his temperature was 40°C, oxygen saturation 93% (with 3L O₂), and parameters of infection were elevated (CRP 177mg/L, WBC 18x10⁹/L). Blood cultures were positive for *Staphylococcus aureus* within a day.

Both transthoracic and transoesophageal echocardiography, however, did not show any signs of endocarditis or changes in valve function (*Figure 5* Panel G). The patient was started on flucloxacillin 12g/day and an ^{18}F -fluorodeoxyglucose (^{18}F -FDG) positron emission tomography/CT (PET/CT) and pulmonary CT angiography (CTA) were performed in accordance with the most recent European Society of Cardiology (ESC) guidelines.

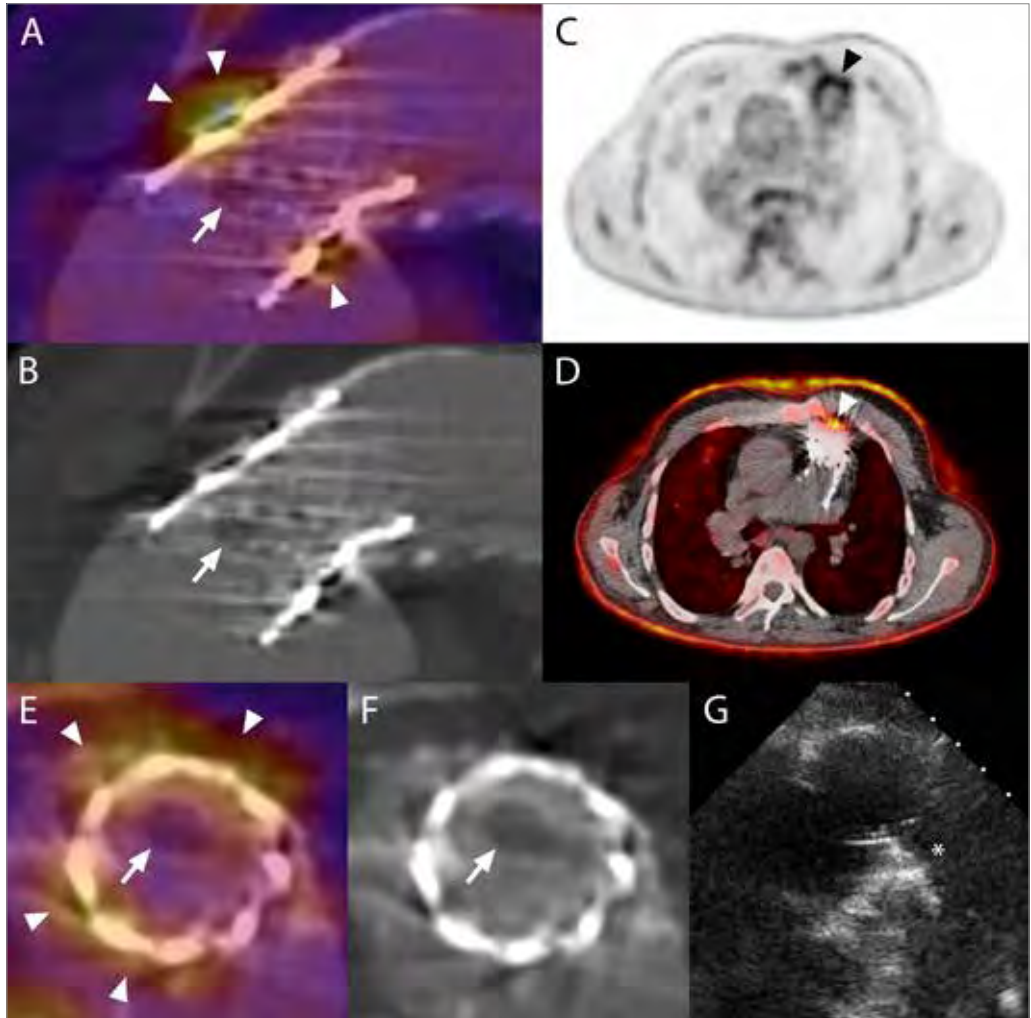


Figure 5 | Fused PET/CTA (**A**, **C**) and CTA (**B**, **F**) long- and short-axis images of the Melody pulmonary valve prosthesis, showing multifocal intense FDG uptake surrounding the mid-section of the prosthesis (**arrowheads**) as well as a vegetation on one of the valve leaflets (**arrow**), which was missed on echo (**G**). (**C**, **D**) Conventional non-attenuation-corrected (NAC) PET and PET/CT images. (*) Melody valve prosthesis.

There were no signs of pulmonary emboli, but a vegetation of approximately 8mm was identified on the valve leaflets (*Figure 5* Panels B and F, arrows). Moreover, PET/CT (Panel C) revealed intense ^{18}F -FDG uptake around the prosthetic valve at the level of the valve leaflets (*Figure 5* Panels A and E, arrowheads), which persisted on the non-attenuation-corrected images (*Figure 5* Panel D), thereby ruling out metal-induced attenuation-correction artefacts and confirming the diagnosis. The maximum standardized uptake value (SUV_{max}) and ratio between the SUV_{max} and the mean SUV in the blood pool were 3.07 and 3.23, respectively (*Figure 6*).

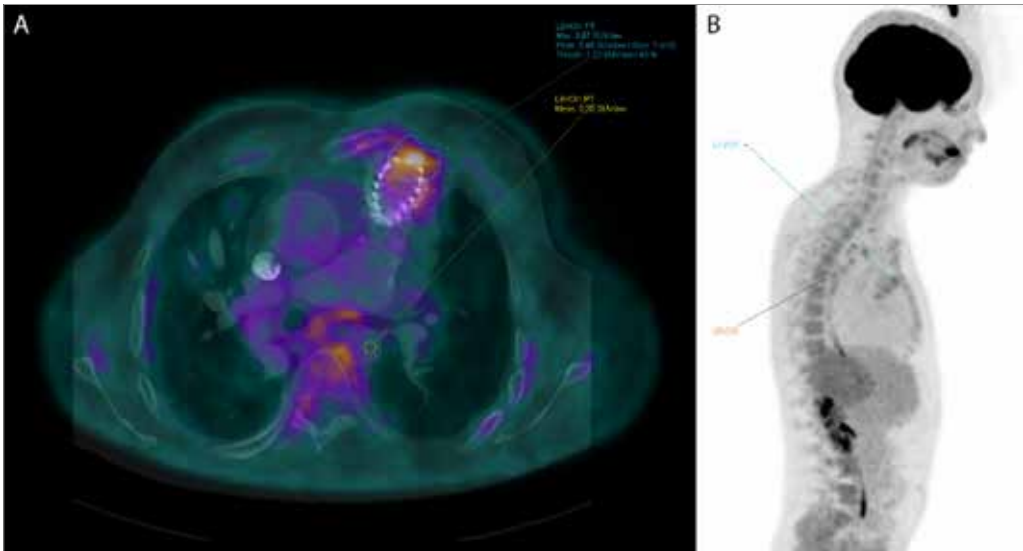


Figure 6 | Quantification of FDG uptake around the Melody valve prosthesis on fused PET/CTA (**A**) images, measuring an SUV_{max} of 3.07 and an $\text{SUV}_{\text{ratio}}$ of 3.23. (**B**) Lateral maximum intensity projection illustrating the location at which the volumes of interest were selected.

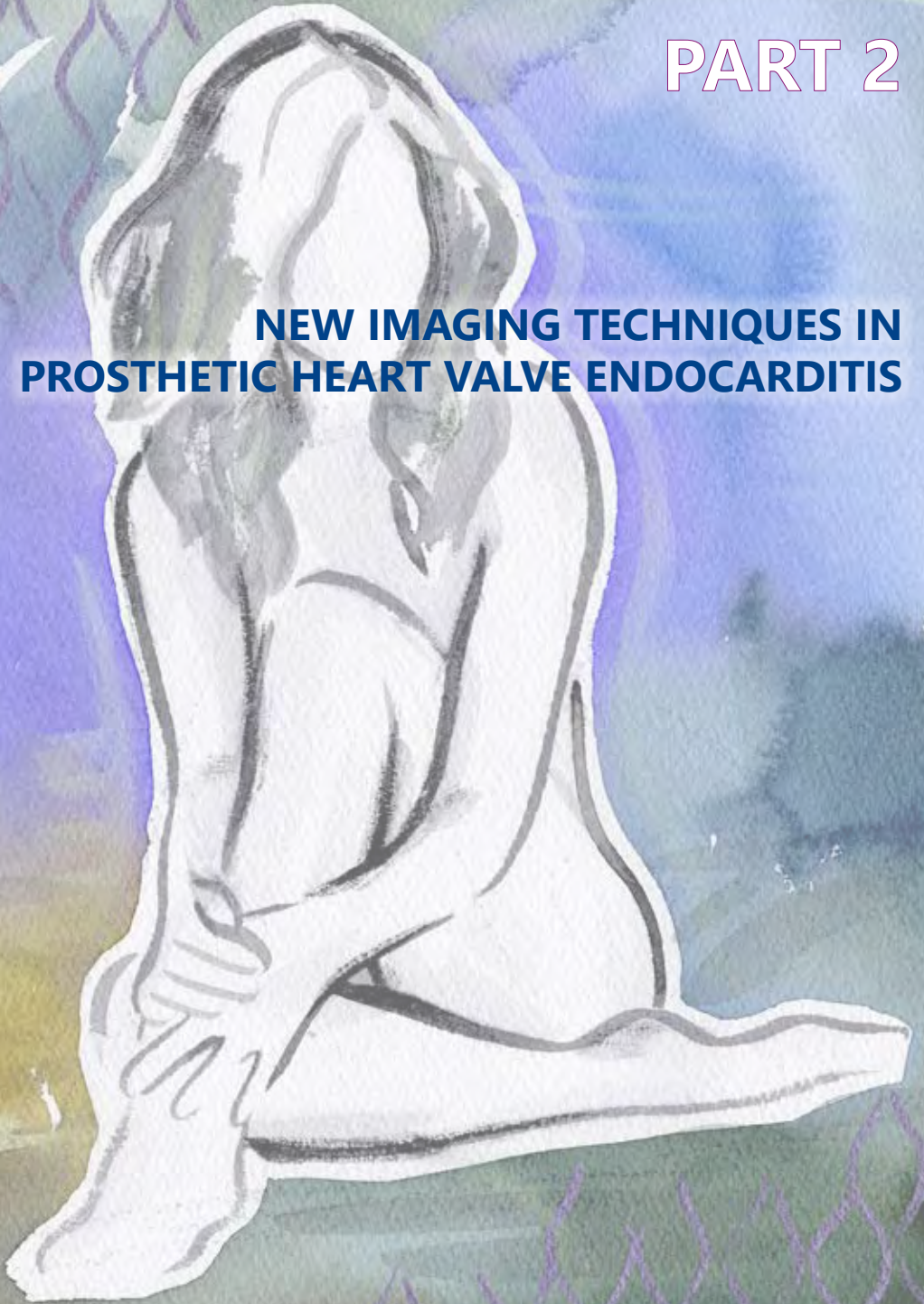
Because of many previous cardiothoracic interventions, haemodynamic stability, absence of structural damage, and a good preliminary response to antibiotics, a conservative treatment was deemed most appropriate by our multidisciplinary Endocarditis Team, and 600mg of rifampicin twice daily was added. In this case, where echocardiography fell short, combined PET/CTA allowed for a swift and comprehensive diagnosis.

References

1. Lüscher TF. Managing aortic stenosis with TAVI or surgery: risk assessment and long-term outcome. *Eur Heart J*. 2017;38:3327–9.
2. Long-term outcomes of transcatheter aortic valve implantation (TAVI): a systematic review of 5-year survival and beyond. *Ann Cardiothorac Surg*. 2017;6:432–43.
3. Wendler O, Schymik G, Treede H, et al. SOURCE 3: 1-year outcomes post-transcatheter aortic valve implantation using the latest generation of the balloon-expandable transcatheter heart valve. *Eur Heart J*. 2017;38:2717–26.
4. Cheatham JP, Hellenbrand WE, Zahn EM, et al. Clinical and hemodynamic outcomes up to 7 years after transcatheter pulmonary valve replacement in the US melody valve investigational device exemption trial. *Circulation*. 2015;131:1960–70.
5. Olsten NT, De Backer O, Thyregod HG, et al. Prosthetic valve endocarditis after transcatheter aortic valve implantation. *Circ Cardiovasc Interv*. 2015;8:e001939.
6. Regueiro A, Linke A, Latib A, et al. Association Between Transcatheter Aortic Valve Replacement and Subsequent Infective Endocarditis and In-Hospital Death. *JAMA* 2016;316:1083–92.
7. McElhinney DB, Benson LN, Eicken A, et al. Infective endocarditis after transcatheter pulmonary valve replacement using the Melody valve: combined results of 3 prospective North American and European studies. *Circ Cardiovasc Interv*. 2013;6:292–300.
8. Malekzadeh-Milani S, Ladouceur M, Iserin L, et al. Incidence and outcomes of right-sided endocarditis in patients with congenital heart disease after surgical or transcatheter pulmonary valve implantation. *J Thorac Cardiovasc Surg*. 2014;148:2253–9.
9. Salaun E, Sportouch L, Barral P-A, et al. Diagnosis of infective endocarditis after TAVR: value of a multimodality imaging approach. *JACC Cardiovasc Imaging*. 2018;11:143–6.

PART 2

NEW IMAGING TECHNIQUES IN PROSTHETIC HEART VALVE ENDOCARDITIS



CHAPTER 5

STANDARDIZED UPTAKE VALUES IN FDG PET/CT FOR PROSTHETIC HEART VALVE ENDOCARDITIS: A CALL FOR STANDARDIZATION

Asbjørn Scholtens
Laurens Swart
Henryk te Kolste
Ricardo Budde
Marnix Lam
Hein Verberne

Published in: Journal of Nuclear Cardiology 2018;25:2084-91

Abstract

Background

The significance of and threshold values for the standardized uptake value (SUV) in FDG PET/CT to diagnose prosthetic heart valve (PHV) endocarditis (PVE) are unclear at present.

Methods

A literature search was performed in the PubMed and EMBASE medical databases, comprising the following terms: (FDG OR *fluorode* OR *fluoro-de*) AND (endocarditis OR prosthetic heart valve OR valve replacement). Studies reporting SUVs correlated to the diagnosis of PVE were selected for analysis.

Results

8 studies were included, with a total of 330 PHVs assessed. SUVs for PVE varied substantially across studies due to differences in acquisition, reconstruction, and measurement protocols, with median SUVmax values for rejected PVE ranging from 0.5 to 4.9 and for definite PVE ranging from 4.2 to 7.4.

Conclusions

Reported SUV values for PVE are not interchangeable between sites, and further standardization of quantification is desirable. To this end, optimal protocols for patient preparation, image acquisition, and reconstruction and measurement methods need to be standardized across centres.

Introduction

In recent years, ^{18}F -fluorodeoxyglucose positron emission tomography with computed tomography-based attenuation correction (FDG PET/CT) has been used increasingly in the setting of infection detection in general and prosthetic heart valve (PHV) endocarditis (PVE) in particular. FDG PET/CT has been proposed as a new criterion for the modified Duke classification¹ and has been added to the European Society of Cardiology guidelines for the diagnosis and management of infective endocarditis.²

Most of the available studies on FDG PET/CT for PVE focus on the visual interpretation of images to differentiate between normal and pathological findings. FDG PET/CT is also able to semi-quantitatively measure the amount of metabolic activity of a lesion in the form of the standardized uptake value (SUV). This concept is appealing since it might offer objective cut-off values to discriminate normal from pathological uptake levels, relying less on subjective interpretation. However, SUV is dependent on a large number of variables regarding acquisition and reconstruction parameters, rendering the true applicability of the term "standardized" somewhat questionable.

Further standardization of the SUV has been proposed in a number of ways^{3,4}, including the European Association of Nuclear Medicine Research Ltd. (EARL) accreditation. We performed a review of the available literature to ascertain whether a range of normal values for FDG PET/CT for PVE could be established.

Methods

A literature search was performed in the PubMed and EMBASE medical databases, comprising the following terms: (FDG OR *fluorode* OR *fluoro-de*) AND (endocarditis OR prosthetic heart valve OR valve replacement). Search results were screened to comply with the following predetermined criteria: English language only; no single case reports, case series acceptable; patient group with cardiac valve replacement; SUV values reported as median and ranges or individual values and compared to diagnosis. Eligible articles were read in full by one researcher (AMS) and their references screened for possible additional studies which fit the criteria, but none were found.

Results

Out of 154 results of our initial literature search, 8 studies were found to be eligible under the predetermined criteria.^{1,5-11} Four studies were performed on EARL-accredited systems.^{6,8,9,11} In total, 330 PHVs were assessed. Study characteristics are described in *Table 1* and boxplot representations of the SUV_{max} findings for each study are shown in *Figure 1*.

Study	Nó. of pts.	Nó. of PHVs	Patient preparation	FDG dose (MBq/kg)	Time to acquisition (min)	Reconstruction method	EARL-accr.	Camera type
Mathieu et al. 2017	51	54	6h fast*	4	60	3D TOF OSEM	Yes	GE Discovery 690
Jiménez-Ballvé et al. 2016	41	42	48h HFCL diet 12h fast 50IU/kg heparin		45-60	Iterative reconstruction	No	Siemens BioGraph 6 TruePoint
Salomäki et al. ⁹ 2015	23	16	24h LC diet 10h fast		72	OSEM	Yes	GE Discovery VCT
Fagman et al. ⁸ 2015	30	30	1 HFCL meal 18h fast (n=11) 6h fast (n=19)†		60	Default iterative	Yes	Siemens BioGraph TruePoint 64
Pizzi et al. ⁷ 2015	92	65	12h fast 50IU/kg heparin		60	Iterative TrueX TOF	No	Siemens BioGraph mCT 645
Rouzet et al. ⁶ 2014	39	45	1 HFCL meal 12h fast		60	Iterative 3D reconstruction	Yes	GE Discovery 690
Bartoletti et al. ⁵ 2014	6	6	n/a		n/a	n/a	No	n/a
Saby et al. ¹ 2013	72	72	1 HFCL meal 12h fast		60	OSEM	No	GE Discovery ST

Table 1 | Study characteristics. (*) Scans with intense, homogeneous uptake in myocardium excluded from analysis. (†) Controls based on oncologic scan protocols. HFCL indicates high-fat low-carbohydrate; LC, low-carbohydrate; IU, international units; MBq, Megabecquerel; TOF, time of flight; OSEM, ordered-subsets expectation maximization.

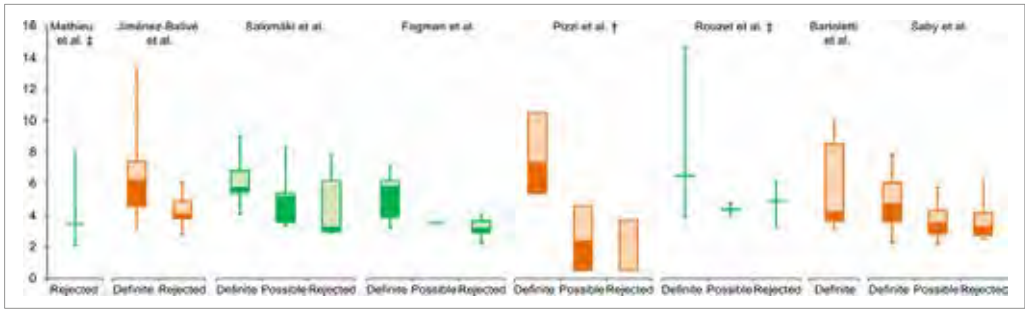


Figure 1 | Reported SUVs in the eligible studies as median, interquartile ranges and total ranges unless noted otherwise. Green values were reported by EARL-accredited centres. (‡) Values reported as median with total ranges. (†) Values reported as median with quartile ranges.

In the seminal publication by Saby et al.¹, 72 patients suspected of PVE were prospectively included. Findings on FDG PET/CT were compared to the final diagnosis, defined according to the modified Duke criteria after a follow-up period of 3 months. Visual analysis was based on hypermetabolism in prosthetic and periprosthetic areas on both attenuation-corrected (AC) and non-AC (NAC) images. SUV_{max} was measured as the average of 3 measurements from 3 volumes of interest (VOI) of 5mm^3 at equal distances from each other. Additionally, a 35mm^3 VOI was placed in the right atrium blood pool in a location without significant metabolic activity from myocardium, and target-to-background ratio (TBR) was calculated as (SUV_{max} valve/ SUV_{max} atrial blood pool). The reported sensitivity, specificity, positive predictive value (PPV), negative predictive value (NPV), and global accuracy for visual assessment were 73%, 80%, 85%, 67%, and 76%, respectively. By adding FDG PET/CT to the modified Duke criteria, sensitivity increased to 97%.

Bartoletti et al.⁵ only included patients with proven PVE in their case series of 6 patients. They did not describe the measurement method for the reported values. They found a large variation in SUV_{max} with several relatively low values (median 4.2, range 3.2–10.0). In patients with the lowest values, antibiotic therapy had been started before FDG PET/CT with resolution of fever and other symptoms of infection.

Rouzet et al.⁶ included 39 patients with a total of 45 PHVs in their study on FDG PET/CT and radiolabeled leukocyte scintigraphy in PVE. Visual analysis and SUV measurement were performed based on the same methods as reported by Saby et al. and final diagnosis was also based on modified Duke criteria after 3 months follow-up. The reported sensitivity, specificity, PPV, NPV, and global accuracy for visual assessment were 93%, 71%, 68%, 94%, and 80% respectively. SUVs for patients classified as 'rejected' by the modified Duke criteria were relatively high (median 4.9, range 3.3–6.2), but patients with no visually discernible uptake of FDG in the region of the prosthetic valve were excluded from the semi-quantitative analysis. Since it is reasonable to assume that these would have represented lower SUV_{max} values, the reported SUV_{max} values will therefore most likely be skewed to the higher end of the spectrum.

5

The study by Pizzi et al.⁷ included both patients with PHVs and cardiac implantable electronic devices (CIEDs). The reported sensitivity, specificity, PPV, and NPV for the total group were 84%, 75%, 81%, and 78%, respectively when compared to the modified Duke criteria at 3 months. For the purpose of this review only the values of the patients with PHVs were included. Visual analysis was comparable to the methods outlined by Saby et al.¹, but SUV analysis differed in that SUV_{max} was measured at any abnormal area, and blood pool measurement was based on the mean standardized uptake value (SUV_{mean}) as obtained with a 30 mm³ VOI at the thoracic descending aorta. TBR was calculated as (SUV_{max} prosthesis/ SUV_{mean} blood pool). The region of interest in scans without visually detectable uptake near the prosthetic valve was placed around the metallic components of the valve alone, without inclusion of the adjacent tissues and blood pool, which most likely resulted in a lower SUV_{max} and may explain the exceptionally low values found in the 'rejected' category (median 0.5).

Fagman et al.⁸ included 11 patients scanned for suspected PVE. Additionally, 19 normal controls were added in the form of patients with prosthetic heart valves scanned for malignancy. Visual analysis, comparable to the methods described by Saby et al.¹, resulted in a sensitivity of 75% and specificity of 84%, based on patients with definite (N = 8) or without (N = 19) PVE. Semi-quantitative analysis was performed measuring SUV_{max} in or directly adjacent to the prosthetic aortic valve. Blood pool values were determined by measuring SUV_{max} in five circular ROIs on consecutive slices in the lumen of the descending aorta at the level of carina, avoiding inclusion of potential uptake in the wall of the aorta. TBR was calculated as (prosthetic valve SUV_{max} / SUV_{max} descending aorta).

In their study, Salomäki et al.⁹ included both native valves and PHVs suspected of endocarditis, confirming that FDG PET/CT is less capable of diagnosing native valve endocarditis (only 1 out of 6 cases detected). For the purpose of this review only the data of the 16 patients with PHVs were considered. Visual analysis was performed as described by Saby et al.¹, resulting in a reported sensitivity of 100% (6/6 cases) but a specificity of only 60%. SUV_{max} was measured in a VOI covering the valve or prosthesis area based on co-registered CT images. The mean blood pool values were measured in the ascending aorta excluding the vessel wall (mean radioactivity in a VOI of 6.8 cm³) to calculate TBR. Two noticeably high values (7.8 and 7.2) skewed the overall findings in the 'rejected' category (N = 5) upwards (median 4.8, range 2.9-7.8), with one value reported as being this high due to a foreign body reaction and one due to imaging relatively early after implantation (6 weeks).

Jiménez-Ballvé et al.¹⁰ compared different interpretation criteria in their cohort consisting of patients with PHVs and/or CIEDs compared to the Duke pathological criteria if tissue was available or the decision of an endocarditis expert team after a minimum of 4 months follow-up. Using criteria comparable to those used by Saby et al.¹ in the whole group, visual analysis resulted in reported sensitivity, specificity, PPV, NPV, and global accuracy of 100%, 73%, 80%, 100%, and 87%, respectively. Again, for this review only the data in PHV patients compared to the final diagnosis were included. SUV_{max} was measured in the area under suspicion and was compared to physiological uptake (also measured as SUV_{max}) in the mediastinal blood pool, calculated by measuring a VOI with 3 mm diameter in the ascending aorta, and in the liver, calculated by measuring a VOI with 3 cm diameter drawn in the right hepatic lobe excluding any areas of inhomogeneous or focally increased uptake. As in the study by Rouzet et al, patients with no visually discernible uptake of FDG in the region of the prosthetic valve were

excluded from the semi-quantitative analysis, probably skewing reported SUV_{max} values to the higher end of the spectrum.

Mathieu et al.¹¹ recently studied 51 patients with 54 PHVs with no suspicion of PVE to define normal variants and values of FDG uptake. Indications for PET were oncology (N = 26), suspicion of prosthetic valve endocarditis subsequently excluded (N = 17), and history of vasculitis (N = 11). Visual analysis was descriptive, with FDG uptake described as absent, homogeneous, or focal in 13%, 80%, and 7% of AC images and 44%, 50%, and 6% of NAC images, respectively. SUV measurements were performed according to the protocol as described by Saby et al.¹ and Rouzet et al.⁶, resulting in a median SUV_{max} of 3.5 (range 2.1-8.0). In subgroup analysis, values were higher in patients referred with a history of vasculitis (median 4.7, range 3.0-8.0) than in the other patients referred for oncologic indications (median 3.3, range 2.1-5.7) or rejected PVE (median 3.5, range 2.1-4.7), even though metabolic activity in the wall of the ascending aorta did not differ significantly between groups.

Discussion

In general, the included studies show that higher SUVs are reported for patients with PVE than those without. However, the great variations in median values and their ranges are a concern, and proof that reported values cannot heedlessly be extrapolated into clinical practice.

The numerous patient- and preparation-related variables that influence the uptake of FDG in the region of the heart make interpreting FDG PET/CT images in the setting of PVE a challenging task. The use of antibiotics or corticosteroids can lead to false-negative results, foreign body reactions may be falsely interpreted as infection, and other confounders may influence the interpretation as well.¹² Knowing this, we cannot expect the SUV to be the only distinguishing variable. Nevertheless, there is much to be gained by performing FDG PET/CT in a uniform way with truly standardized SUV measurements. As our review of the literature shows, there is currently very little standardization of how FDG PET/CT is performed in PVE, both regarding acquisition and reconstruction protocols as well as the definition of the region in which the uptake is to be quantified.

Although the different studies may have used different criteria to define the diagnosis of PVE, this can be argued to be a lesser concern in the context of this article. Even if the diagnostic criteria had been perfectly equal across the studies, the reported values would still be incomparable due to the differences in methodology of measurement and parameters of acquisition.

EARL-accredited reconstruction is a logical step towards better reproducibility of reconstruction parameters. The SUV_{ref} method, in which camera- and reconstruction-specific filter parameters are applied to produce images with standardized properties for SUV measurements⁴ is another option, which may have the added benefit of being applicable to non-EARL-accredited sites in retrospect.

The potential negative effect of EARL-accredited reconstructions is its relatively high level of smoothing of images, resulting in lower reported SUV_{max} measurements than on images based on contemporary reconstruction methods incorporating Time-of-Flight and other parameters, especially in the higher ranges. For this reason it may be desirable to add EARL-reconstructions only for the purpose of standardized mea-

5
surements, using vendor- and camera-optimized reconstructions for visual analysis and clinical implementation.

To be able to reliably measure values in the region of PHVs, it is important that the physiological glucose metabolism (and by proxy FDG uptake) of the myocardium be suppressed. Many patient preparation protocols exist, with the optimal solution still up for debate.¹³ Based on our own experiences, a low carbohydrate fat-allowed diet for 24 hours, 12-hour fast and unfractionated heparin bolus pre-administration results in adequate suppression¹⁴ and shorter fasting periods should be avoided. Centres should strive for a protocol that reliably yields suppression in >80% of patients.¹³ Recently, Giorgetti et al. published their findings on increased myocardial suppression in patients receiving low molecular weight heparin or warfarin therapy¹⁵, and patients receiving such therapy likely do not need additional unfractionated heparin bolus administration.

Regarding measurement methods, a number of studies excluded valves with no visual abnormalities from semi-quantitative measurement, thus introducing a potential reporting bias in the values for normal valves and rejected PVE. As these excluded measurements likely had values close to blood pool values, the true median may be expected to be lower than reported. To reduce potential reporting bias we would recommend that SUV be measured and reported in all PHVs, not just in visually abnormal ones, with the same methodology used in all measurements. To improve ease of measurement (and hence reproducibility) we suggest reporting the SUV_{max} obtained from a single VOI encompassing the entire prosthesis where possible, rather than creating mean values from multiple SUV_{max} measurements in multiple VOIs.

By creating reproducible results, recommendations based on SUV measurements could become interchangeable between sites, and research data from various hospitals could safely be pooled into a larger dataset. The latter should be of particular interest, since the incidence of PVE is relatively low even in specialized centres. To allow for truly large studies with significant statistical power, it is inevitable to include multiple centres, which is inappropriate without better standardization of FDG PET/CT.

Once the process of FDG PET/CT imaging is comparable between sites, including every step from patient preparation to image interpretation and measurement, we can begin to understand the effects of the other variables based on reliable interpretation and measurement standards.

Recommendations

SUVs for PVE reported in the literature are highly dependent on acquisition, reconstruction, and measurement protocols, and further standardization is needed before values are interchangeable between centres. To improve uniformity in measurements, we recommend patient preparation with a carbohydrate-restricted diet and a prolonged fast coupled with heparin bolus administration preceding the administration of FDG.¹⁴ Reported measurements should be performed on reconstructions according to the EARL accreditation, and should include whole-valve or whole-prosthesis measurements of the SUV_{max} (with VOI excluding physiological myocardial uptake) as well as a measurement of the SUV_{mean} of the blood pool in the descending aorta (VOI excluding vessel wall) to calculate a target-to-background ratio (example in *Figure 2*). VOI measurements of SUV_{mean} in the right atrium and the liver may be of additional value to ascertain the optimal region for TBR calculation.

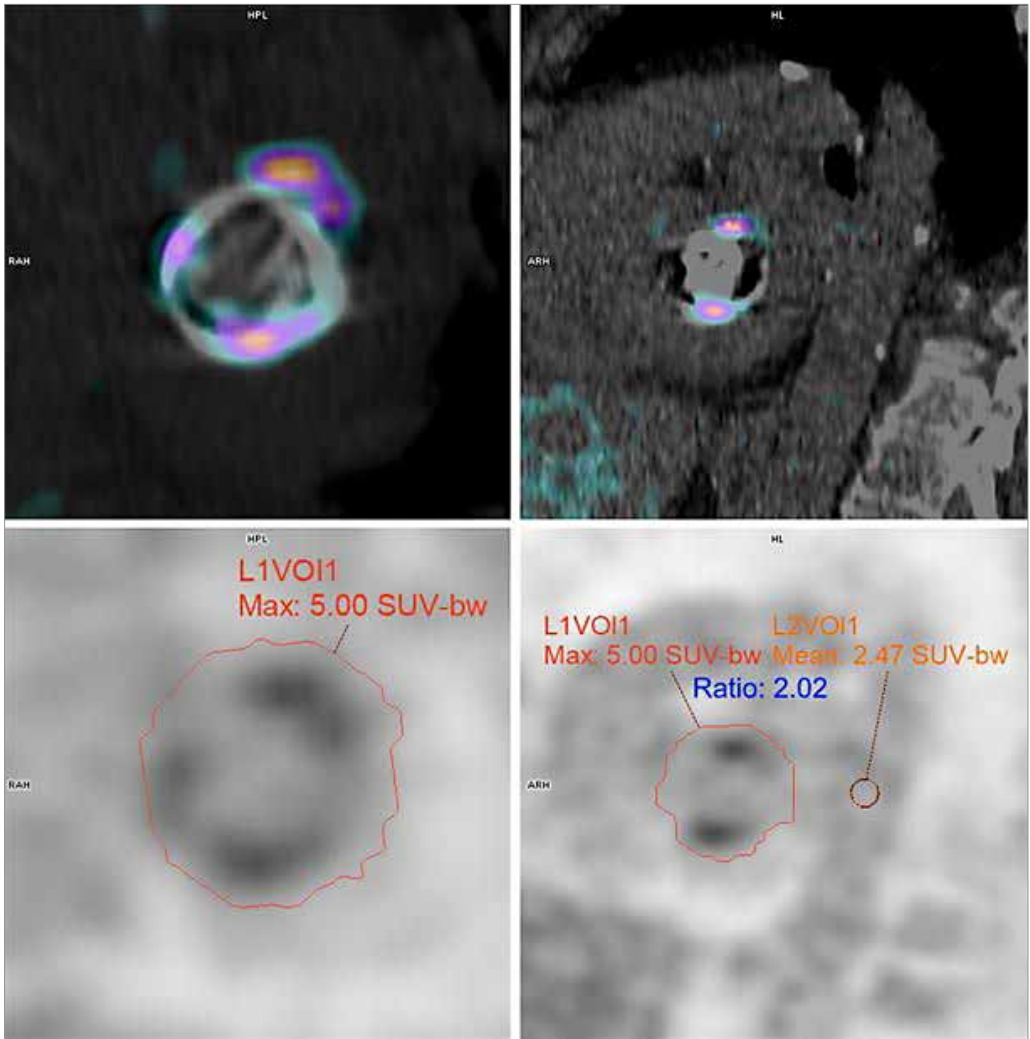


Figure 2 | Example of proposed measurement standardization in a mitral valve prosthesis. Fused PET/CT images (upper row) and corresponding attenuation-corrected PET images (below) showing whole-valve measurement VOI (in this case a self-expanding VOI set to include voxels $\geq 40\%$ of maximum) and VOI sphere in the descending aorta (lower right). Uptake in myocardium (hardly present here) and the aortic wall are excluded. VOI indicates volume of interest; SUV, standardized uptake value.

Conclusion

SUVs reported in the current literature on FDG PET/CT in PVE vary according to acquisition, reconstruction, and measurement methods, emphasizing the need for a uniform protocol to allow for better comparison of results between different centres. Although not without drawbacks, standardized measurements on EARL-accredited reconstructions seem a sensible and feasible starting point.

References

1. Saby L, Laas O, Habib G, Cammilleri S, et al. Positron emission tomography/computed tomography for diagnosis of prosthetic valve endocarditis: Increased valvular 18F-fluorodeoxyglucose uptake as a novel major criterion. *J Am Coll Cardiol*. 2013;61:2374–82.
2. Habib G, Lancellotti P, Antunes MJ, et al. 2015 ESC Guidelines for the management of infective endocarditis: The Task Force for the Management of Infective Endocarditis of the European Society of Cardiology (ESC). *Eur Heart J*. 2015;36:3075–3128.
3. Boellaard R. Standards for PET image acquisition and quantitative data analysis. *J Nucl Med*. 2009;50:11S–20S.
4. Kelly MD, Declerck JM. SUVref: Reducing reconstruction-dependent variation in PET SUV. *EJNMMI Res* 2011;1:16.
5. Bartoletti M, Tumietto F, Fasulo G, et al. Combined computed tomography and fluorodeoxyglucose positron emission tomography in the diagnosis of prosthetic valve endocarditis: A case series. *BMC Res Notes*. 2014;7:32.
6. Rouzet F, Chequer R, Benali K, et al. Respective performance of 18F-FDG PET and radiolabeled leukocyte scintigraphy for the diagnosis of prosthetic valve endocarditis. *J Nucl Med*. 2014;55:1980–5.
7. Pizzi MN, Roque A, Fernandez-Hidalgo N, et al. Improving the diagnosis of infective endocarditis in prosthetic valves and intracardiac devices with 18F-fluorodeoxyglucose positron emission tomography/computed tomography angiography: Initial results at an infective endocarditis referral center. *Circulation*. 2015;132:1113–26.
8. Fagman E, van Essen M, Freden Lindqvist J, et al. F-FDG PET/CT in the diagnosis of prosthetic valve endocarditis. *Int J Cardiovasc Imaging*. 2016;32:679–86.
9. Salomäki SP, Saraste A, Kempainen J, et al. F-FDG positron emission tomography/computed tomography in infective endocarditis. *J Nucl Cardiol*. 2017;24:195–206.
10. Jiménez-Ballvé A, Pérez-Castejon MJ, Delgado-Bolton RC, et al. Assessment of the diagnostic accuracy of 18F-FDG PET/CT in prosthetic infective endocarditis and cardiac implantable electronic device infection: Comparison of different interpretation criteria. *Eur J Nucl Med Mol Imaging*. 2016;43:2401–12.
11. Mathieu C, Mikail N, Benali K, et al. Characterization of 18F-fluorodeoxyglucose uptake pattern in noninfected prosthetic heart valves. *Circ Cardiovasc Imaging*. 2017;10:e005585.
12. Scholtens AM, Swart LE, Verberne HJ, et al. Confounders in FDG-PET/CT imaging of suspected prosthetic valve endocarditis. *JACC Cardiovasc Imaging*. 2016;9:1462–5.
13. Osborne MT, Hulten EA, Murthy VL, et al. Patient preparation for cardiac fluorine-18 fluorodeoxyglucose positron emission tomography imaging of inflammation. *J Nucl Cardiol*. 2017;24:86–99.
14. Scholtens AM, Verberne HJ, Budde RP, Lam M. Additional heparin pre-administration improves cardiac glucose metabolism suppression over low carbohydrate diet alone in 18F-FDG-PET imaging. *J Nucl Med*. 2016;57:568–73.
15. Giorgetti A, Marras G, Genovesi D, et al. Effect of prolonged fasting and low molecular weight heparin or warfarin therapies on 2-deoxy-2-[18F]-fluoro-D-glucose PET cardiac uptake. *J Nucl Cardiol*. 2017; doi: 10.1007/s12350-017-0800–8.



CHAPTER 6

DUAL-TIME-POINT FDG PET/CT IMAGING IN PROSTHETIC HEART VALVE ENDOCARDITIS

Asbjørn Scholtens
Laurens Swart
Hein Verberne
Ricardo Budde
Marnix Lam

6

Published in: Journal of Nuclear Cardiology 2018;25:1960-7

Abstract

Purpose

FDG PET/CT has been of increasing interest in the diagnostic workup of prosthetic heart valve endocarditis (PVE). Some reports advocate later imaging time points to improve the diagnostic accuracy for PVE. In this study, we compared standard and late FDG PET/CT images in patients with a clinical suspicion of PVE.

Materials and methods

Fourteen scans in 13 patients referred for FDG PET/CT for suspicion of PVE performed at standard (60 min post injection) and late (150 min post injection) time points were scored based on visual interpretation and semi-quantitatively with SUV_{max} and target-to-background ratio (TBR, defined as $[SUV_{max} \text{ valve}/SUV_{mean} \text{ blood pool}]$). Final diagnosis was based on surgical findings in all cases of infection (n=6) and unremarkable follow-up in all others (n=8).

Results

Late images were more prone to false positive interpretation for both visual and semi-quantitative analyses. Visual analysis of the standard images yielded 1 false negative and 1 false positive result. On the late images, no scans were false negative but 5 scans were false positive.

Conclusions

Late FDG PET/CT imaging for PVE seems prone to false positive results. Therefore, late imaging should be interpreted with caution.

Introduction

Prosthetic heart valve (PHV) implantation is performed at an increasing rate, due to the prevalence of heart valve disease increasing in tandem with the growing aging population, with over 800,000 annual procedures estimated to be performed worldwide by the year 2050.¹ Prosthetic heart valve (PHV) endocarditis (PVE) is a relatively uncommon complication, with an incidence of 0.3-1.0% per patient per year², but is associated with an alarmingly high mortality rate, especially when *Staphylococcus aureus* is the pathogen involved.^{2,3} PVE can be difficult to diagnose, with echocardiography unable to identify signs of the disease in up to 30% of cases.^{4,5}

Computed tomography angiography (CTA) of the valve area has been shown to be of complementary value to clinical routine workup in suspected PVE⁶, although it can be difficult to distinguish between non-infectious postoperative anatomical variation and infectious complications in select cases.

Fluorine-18 fluorodeoxyglucose positron emission tomography with CT-based attenuation correction (FDG PET/CT) is gaining momentum as a tool in the diagnosis of

suspected PVE⁷⁻¹⁰, due to its ability to image inflammation activity as opposed to the aforementioned modalities that image anatomy only. Recently, FDG PET/CT was added as a diagnostic modality in the guidelines of the European Society of Cardiology for the diagnosis and management of infectious endocarditis.¹¹

However, the optimal imaging protocol for FDG PET/CT in PVE is still unclear, with preparatory protocols and timing of image acquisition still subjects of debate. In standard oncological FDG PET/CT protocols, images are acquired 60 minutes after injection of the tracer. However, for the detection of infection and inflammation, both earlier and later imaging have been proposed; the former based on the fast influx of glucose into inflammatory cells followed by efflux based on active glucose-6-phosphatase¹², the latter based on persistent influx in inflammation and further clearance of glucose from the blood pool leading to higher contrast between activity in infectious foci and background.¹³

Based on earlier reports, delayed imaging may be of additional value in diagnosing infection of cardiovascular implants.^{13,14} We performed both standard and delayed acquisitions of FDG PET/CT images in a number of patients referred for possible PVE under the assumption that the delayed images may improve diagnostic accuracy.

Methods

Based on earlier reports^{13,14}, we added delayed acquisition at 150 minutes post injection of the radiotracer to our clinical protocol for FDG PET/CT for suspicion of PVE, in keeping with the innovation and development stages as described by the IDEAL framework.¹⁵ Thirteen patients with 14 scans referred for FDG PET/CT with suspected PVE in the University Medical Center Utrecht were imaged at standard and late time points after giving informed consent. The local ethical committee waived review of this study.

FDG PET/CT

All patients were prepared according to our protocol for suppression of physiological myocardial glucose metabolism (low-carbohydrate diet for 12 hours followed by a 12-hour fast and 50 IU/kg heparin IV 15 minutes prior to FDG administration).¹⁶ After injection of 2 MBq/kg FDG via an antecubital vein, PET/CT images were acquired according to the standard protocol at approximately 60 minutes and additionally of the thorax at approximately 150 minutes post injection. All scans were performed on the same FDG PET/CT system (Biograph mCT, Siemens, Erlangen, Germany). Prior to the PET acquisitions, non-contrast CT images were obtained for attenuation correction (AC). PET images were obtained using 3D acquisition, field of view 216 mm, and 3 minutes per bed position scan time; low-dose CT acquisition for attenuation correction was obtained with a pitch of 1.0, slice thickness 10 mm, 120 kV, and 40 mAs. PET/CT data were reconstructed using ordered subset expectation maximization (OSEM) iterative reconstruction (Gaussian filter, 4 iterations, 21 subsets).

All images were read on commercially available software (Syngo.Via, Siemens, Erlangen, Germany). Volumes of Interest (VOIs) were placed to ascertain semi-quantitative measurements of glucose metabolism as follows: (I) Automated growing VOI algorithm set to include pixels within 40% of maximum measured standardized uptake value (SUV_{max}) containing the PHV, (II) VOI sphere within the lumen of the descending aorta (maximum possible size without including vessel wall).

Care was taken to exclude non-suppressed myocardial uptake and uptake in the aortic wall. From these VOIs, the SUV_{max} in the region of the PHV and the mean standardized uptake value (SUV_{mean}) in the aortic blood pool were obtained. Target-to-background ratios (TBR) were calculated as SUV_{max} (PHV) divided by SUV_{mean} (blood pool).⁸

Visual analysis was based on elevated uptake of FDG at or near the implanted PHV, taking into account normal variations and potential confounders.¹⁷ Elevated uptake at the PHV or adjacent structures that exceeded that of the surrounding blood pool and could not be ascribed to a normal variant was deemed suspect for PVE. Lesions on AC images were confirmed on non-AC images to rule out possible AC artifacts. Scoring was dichotomous into either no/unlikely PVE or likely/certain PVE.

Diagnosis

The final diagnosis of infected versus uninfected PHV was based on surgical findings in all cases of infection and based on unremarkable follow-up after clinically rejected diagnosis of endocarditis (median 17.9 months, range 9.7-22.6 months) in all others.

Analysis

Comparisons of means between the normally distributed semi-quantitative values for infected and uninfected PHVs were performed with paired Student's *t*-test. Statistical analyses were performed on Statistical Package for Social Sciences (SPSS) software version 22. Additional ROC analysis was performed with MedCalc software version 16.4.3.

Results

Scans were performed for suspected PVE of one mitral valve replacement, one pulmonic valve replacement, and 11 aortic valve replacements. In two patients, the aortic valve replacement was part of a Bentall graft of the aortic root and ascending aorta. Median time from implantation to FDG PET/CT was 654 days (range 21-4992 days). Two patients were scanned within the first six weeks after implantation. Standard images were acquired at a mean of 65 minutes post injection (range 56-80 minutes), and late images were acquired at a mean of 144 minutes post injection (range 120-195 minutes). The time between standard and late scans ranged from 57 to 115 minutes. One patient was scanned twice: once during antibiotic therapy to exclude other foci, and once when cessation of antibiotic therapy led to an increase in symptoms and the return of fever. Suppression of physiological myocardial glucose metabolism was acceptable in all but one patient. PVE was diagnosed and surgically confirmed in 6 out of 13 patients. Patient characteristics are listed in *Table 1* and their respective PET/CT results are listed in *Table 2*.

Pt. nr.	Age	Valve type	Valve pos.	Implantation/ complications	Days since implant	CRP mg/L	WBC x10 ⁹ /L	PVE
1	72	Mechanical	MV	Uncomplicated implantation	4992	43	10.1	No
2	46	Mechanical	AV	Bentall procedure. Postoperative haematoma requiring re-thoracotomy and re-suturing of the graft	28	9	7.8	No
3	65	Mechanical	AV	Uncomplicated implantation	645	71	10.5	No
4	84	Biological	AV	Uncomplicated implantation	21	154	11.7	No
5	82	Mechanical	AV	Postoperative pneumothorax; no complications involving the valve	922	184	12.7	No
6	83	Biological	AV	Uncomplicated implantation; combined with CABG	63	10	7.5	No
7	71	Biological	AV	Uncomplicated implantation	150	89	11.1	No
8	57	Mechanical	AV	Uncomplicated implantation	2694	35	7.8	No
9	49	Biological	AV	Bentall procedure; uncomplicated implantation	1769	35	11.5	Yes
10	75	Biological	AV	Postoperative pneumothorax; no complications involving the valve; combined with CABG	143	43	7.6	Yes
11	78	Biological	AV	Uncomplicated implantation; combined with CABG	101	2	4.1	Yes
12	23	Biological	PV	Uncomplicated implantation	2501	43	8.2	Yes
13	68	Biological	AV	Uncomplicated implantation	662	30	9.5	Yes
					710	8	7.9	Yes

Table 1 | Patient characteristics. MV indicates mitral valve; AV, aortic valve; CABG, coronary artery bypass graft surgery; CRP, C-reactive protein; WBC, white blood cell count; PVE, prosthetic heart valve endocarditis.

Pt. nr.	PVE	Visual FDG PET/CT interpretation		SUV _{max}		TBR	
		Standard	Late	Standard	Late	Standard	Late
1	No	True negative	False positive	3.37	3.92	1.57	3.21
2	No	False positive	False positive	5.38	6.30	2.96	5.63
3	No	True negative	False positive	3.33	3.23	1.71	2.36
4	No	True negative	True negative	2.68	2.39	2.14	2.60
5	No	True negative	True negative	2.38	2.26	1.71	2.31
6	No	True negative	False positive	3.01	3.74	2.39	3.43
7	No	True negative	False positive	3.31	4.64	1.91	4.22
8	No	True negative	True negative	3.58	4.11	2.29	3.95
9	Yes	True positive	True positive	4.83	6.76	3.45	7.95
10	Yes	True positive	True positive	4.27	4.51	3.26	4.65
11	Yes	True positive	True positive	3.23	3.13	1.78	3.16
12	Yes	True positive	True positive	3.99	3.88	3.05	4.26
13	Yes	True positive	True positive	6.16	7.92	5.01	8.43
	Yes	False negative	True positive	3.20	3.40	2.41	3.66

Table 2 | FDG PET/CT results. PVE indicates prosthetic heart valve endocarditis; SUV, standardized uptake value; TBR, target-to-background ratio.

For the group as a whole, late images had significantly higher TBR values compared to the standard images, mostly due to a decrease in measured activity in the blood pool (SUV_{max} PHV standard 3.77 ± 1.06 vs. late 4.30 ± 1.64 , $P = 0.02$; TBR standard 2.55 ± 0.93 vs. late 4.27 ± 1.89 , $P = 0.0001$).

Contingency tables for visual interpretation of standard and late images are shown in **Table 3**. Sensitivity, specificity, positive predictive value and negative predictive value were 83%, 88%, 83%, and 88% respectively for the standard images and 100%, 38%, 55%, and 100%, respectively, for late images. Although late images correctly identified the single false negative result in the standard images, false positive results increased from 1 scan (7%) to 5 scans (36%).

	Standard		Late	
	PET/CT +	PET/CT -	PET/CT +	PET/CT -
PVE +	5	1	6	0
PVE -	1	7	5	3

Table 3 | Contingency tables of the visual analysis. PVE indicates prosthetic heart valve endocarditis.

Standard SUV_{max} in the region of the PHV was higher in patients with PVE (median 4.13, interquartile range [IQR] 3.42-4.69) than in those without (median 3.32, IQR 2.93-3.42), but not significantly so ($P = 0.12$). The same was true for late SUV_{max} , but with even more overlap between the values (PVE median 4.20, IQR 3.52-6.20; non-PVE median 3.83, IQR 3.02-4.24. $P = 0.23$). In two scans of patients with PVE, the SUVs were comparatively low, probably due to effective antibiotic therapy at the time of imaging (based on normalized laboratory parameters and abated symptoms); when these scans were excluded from the analysis, standard SUV_{max} differed significantly ($P = 0.02$), while the difference in late SUV_{max} was still only trending towards significance ($P = 0.07$). When patients under adequate antibiotic therapy were regarded as a separate group, their values were more comparable to those in the disease-free group (Figure 1).

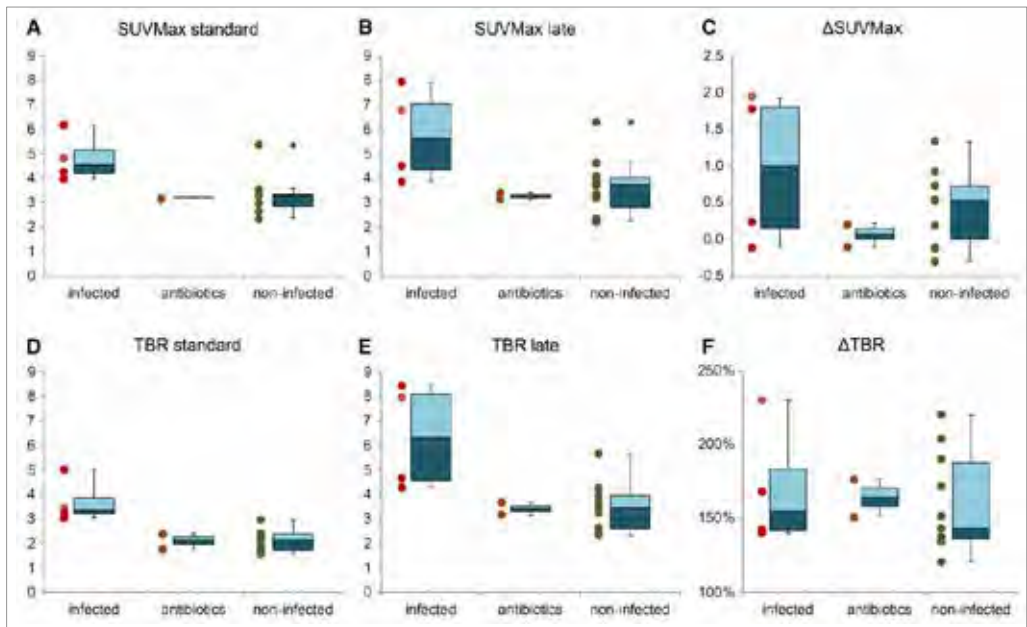


Figure 1 | Semi-quantitative measurements. Values for standard SUV_{max} (A), late SUV_{max} (B), changes in SUV_{max} from standard to late (ΔSUV_{max}) (C) as well as standard and late Target-to-background ratios (TBR) and changes in TBR (D, E, and F respectively) with boxplot representations of median values, interquartile ranges, and total ranges. * Statistical outlier.

Only the TBR at the standard acquisition time was significantly different between infected and uninfected PHVs ($P = 0.027$), with sensitivity, specificity, positive predictive value, and negative predictive value of 83%, 88%, 83%, and 88%, respectively, at a threshold of 2.4 equalling the visual interpretation. Comparison of receiver operating characteristic curves showed a greater area under the curve for standard TBR (0.87) compared to late TBR (0.79), although the difference was not statistically significant ($P = 0.22$).

Discussion

With the aim to improve our imaging protocol in patients with suspected PVE, according to the IDEAL criteria, we compared standard and late acquisition of FDG PET/CT images in suspected PVE in a small cohort of patients. The most important finding of our study was that delayed images did not compare favorably to standard images, as delayed images were more prone to false positive results. Changes in SUV_{max} and TBR between standard and late images showed great variation in both the PVE group and the non-PVE group, and almost complete overlap between the two groups. Although delayed images did show a higher contrast between target and background, due mostly to a decrease in activity in the blood pool, this higher contrast did not lead to better differentiation between infected and uninfected PHVs.

These findings may indicate that even in uninfected PHVs, a variable amount of sterile inflammation, likely a mild foreign body reaction, is present which may be indistinguishable from indolent or low-grade infection. As no histological data were retrieved from any non-infected PHVs, we cannot be certain about the underlying cause or why some PHVs show more inflammation than others.

In two patients, standard FDG PET/CT showed very low uptake of FDG around the PHV, even though both patients were diagnosed with PVE (*Table 2*, patient 11 and second scan of patient 13). However, both patients were free of signs and symptoms and had normalized laboratory parameters for infection after antibiotic treatment at the time of PET/CT acquisition. It is likely that FDG PET/CT showed the true effect of therapy in these patients, as the subsequent and final diagnosis of PVE was made at surgery after signs, symptoms, and laboratory values had increased following cessation of antibiotic therapy. As we have described earlier¹⁸, an initial response to antibiotic therapy does not necessarily imply eradication of the causative pathogen. In one of these two patients, the delayed images did show increased uptake where the standard images did not, but this also occurred in the late images of several patients without PVE and should therefore be interpreted with caution (*Figure 2*).

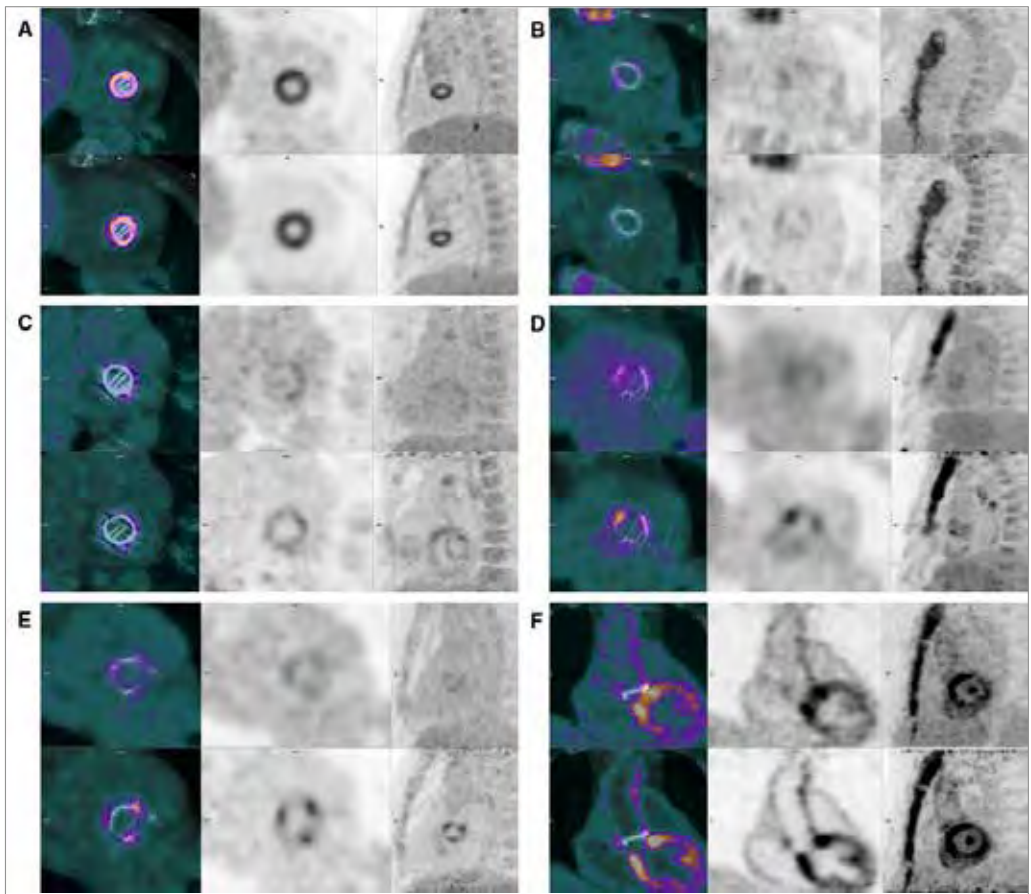


Figure 2 | Examples of standard (top row) and late (bottom row) FDG PET/CT images in six patients. **(A)** True positive uptake surrounding a mechanical aortic PHV in both phases. **(B)** True negative images with hardly any uptake near the biological aortic PHV in either phase. **(C)** True negative standard images with minimal uptake surrounding the mechanical mitral PHV, clearly delineated in the late image. **(D)** True positive late phase with focal uptake near the strut of the biological aortic PHV near the right coronary that is not apparent on standard images. Note accumulation of uptake in mediastinal lymph nodes. **(E)** False positive late images with exaggerated uptake near all struts of a biological aortic PHV with normal uptake on standard images. **(F)** False positive uptake in both phases surrounding the prosthesis after semi-recent Bentall procedure complicated by haematoma. Note the unsuppressed physiological uptake in the myocardium.

Conversely, standard PET/CT was false positive in one patient, with high SUV_{max} and TBR values compared to the other values in the uninfected group (*Table 2*, patient ^{max} 2). This scan was performed 4 weeks after a Bentall procedure complicated by bleeding, which necessitated a re-sternotomy to drain 400 ml of haematoma and re-suturing of the graft. It is likely that imaging relatively shortly after such a complicated procedure visualized sterile inflammation as part of the immune response to the haematoma. Delayed images did not contribute to the differentiation of sterile inflammation from infection.

These cases stress the importance of being well informed about the patient history before interpreting FDG PET/CT in patients with suspected PVE, as many factors including details about the implantation, current signs and symptoms, medication, and changes in inflammatory laboratory parameters over time may considerably influence the interpretation of findings.

In the other four scans with negative standard and positive late images, two patients had positive blood cultures with *Staph. aureus* and were receiving antibiotic treatment at the time of imaging, which could potentially have led to false negative interpretation of the standard images. However, as both cases had well-defined infectious foci elsewhere (presteral wound infection in one and infected knee prosthesis in the other) which were clearly visible on FDG PET/CT and responded well to local therapy, PVE was not diagnosed clinically and we believe it is more likely that the late images were false positive. The other two patients had negative blood cultures and were not receiving antibiotics, further corroborating that false positive late images in the absence of PVE do occur.

Current opinion on the timeframe after surgery after which FDG PET/CT can be reliably performed varies, with indications that sterile postoperative inflammation may persist as long as two months after surgery.¹⁰ In our cohort, true negative images were obtained as early as three weeks after surgery whereas false positive late images occurred more than 13 years after implantation. In our experience, scans may be performed as early as a few weeks after uncomplicated surgery. If complications occurred during or after surgery (as in the Bentall procedure described above) sterile inflammation may persist for longer.

In this study, only the standard TBR showed a statistically significant difference between infected and uninfected PHVs; standard SUVmax trended towards but did not reach significance, likely due to the small number of patients and the confounding factors mentioned above.

Defining threshold values on a cohort as small as ours should be done with extreme caution, but TBR at the standard acquisition time at a threshold of 2.4 did perform as well as visual analysis, with equal sensitivity, specificity, and positive and negative predictive values. Perhaps of greater clinical value is the finding that all scans with TBR >3.0 were infected. Still, some confounders such as surgical adhesive and lipomatous hypertrophy of the interatrial septum show intense uptake of FDG¹⁷ and would probably score above this threshold, and our data show that scans performed under adequate antibiotic therapy will be underestimated.

When comparing our data to the aforementioned earlier reports, the case presented by Calderella et al.¹³ fits with our findings, basically mirroring the one case in our series that was false negative on standard images and true positive on late images (Figure 2D). However, our data suggest that applying this approach to every negative standard FDG PET/CT would lead to an unwarranted number of false positive late scans. Leccisotti et al.¹⁴ found added value for late images in diagnosing cardiac implantable electronic device lead infection, which is likely to have a different presentation compared to PVE. False positive findings did occur for lead infection, but did not increase on late images, as opposed to our results in patients with PVE. Therefore, these findings are not necessarily at odds with each other. It may very well be that delayed images have added value in diagnosing lead infection because of the high false negative rate on standard images and the apparent lack of physiologically increased uptake due to sterile inflammation, as opposed to imaging in PVE.

Our findings are limited by the small number of patients included in a single centre, and the retrospective nature of the data. Ideally, our findings should be corroborated by a prospective study powered for statistical analysis. In these early stages of development of FDG PET/CT protocols specifically applicable to PVE diagnosis, we essentially find ourselves moving from stage 1 of the IDEAL framework (Idea) to stage 2a (Development) where the details about a new procedure become more defined.¹⁵ Regardless of its limitations, our data show a clinically important risk of false positive PVE findings if late images at 150 minutes post injection are allowed to guide treatment decisions, which should be taken into account in possible future studies and their design. It is possible that the ideal time point for FDG PET/CT imaging in PVE lies somewhere between our two chosen time points.

Delayed imaging at 150 minutes post injection does not seem to improve the interpretation of FDG PET/CT in PVE as it seems prone to false positive findings. Imaging at the standard oncology protocol acquisition time outperformed delayed imaging both in visual and semi-quantitative analysis. Based on our current data, we cannot recommend the use of delayed FDG PET/CT imaging in PVE, whether as substitution for or as an adjunct to standard images, as we believe the risk of false positive interpretation is too high in either scenario.

References

1. Yacoub MH, Takkenberg JJ. Will heart valve tissue engineering change the world? *Nat Clin Pract Cardiovasc Med.* 2005;2:60–1.
2. Thuny F, Grisoli D, Collart F, et al. Management of infective endocarditis: Challenges and perspectives. *Lancet.* 2012;379:965–75.
3. Choussat R, Thomas D, Isnard R, et al. Perivalvular abscesses associated with endocarditis; clinical features and prognostic factors of overall survival in a series of 233 cases. Perivalvular abscesses french multicentre study. *Eur Heart J.* 1999;20:232–41.
4. Vieira ML, Grinberg M, Pomerantzeff PM, et al. Repeated echocardiographic examinations of patients with suspected infective endocarditis. *Heart.* 2004;90:1020–4.
5. Hill EE, Herijgers P, Claus P, Vanderschueren S, et al. Abscess in infective endocarditis: The value of TEE and outcome: A 5-year study. *Am Heart J.* 2007;154:923–8.
6. Habets J, Tanis W, van Herwerden LA, et al. Cardiac computed tomography angiography results in diagnostic and therapeutic change in prosthetic heart valve endocarditis. *Int J Cardiovasc Imaging.* 2014;30:377–87.
7. Saby L, Laas O, Habib G, et al. Positron emission tomography/computed tomography for diagnosis of prosthetic valve endocarditis: Increased valvular 18F-FDG uptake as a novel major criterion. *J Am Coll Cardiol.* 2013;61:2374–82.
8. Tanis W, Scholtens A, Habets J, et al. CT angiography and (18)F-FDG-PET fusion imaging for prosthetic heart valve endocarditis. *JACC Cardiovasc Imaging.* 2013;6:1008–13.
9. Ricciardi A, Sordillo P, Ceccarelli L, et al. 18-fluoro-2-deoxyglucose positron emission tomography-computed tomography: An additional tool in the diagnosis of prosthetic valve endocarditis. *Int J Infect Dis.* 2014;28:219–24.
10. Rouzet F, Chequer R, Benali K, et al. Respective performance of 18F-FDG PET and radiolabeled leukocyte scintigraphy for the diagnosis of prosthetic valve endocarditis. *J Nucl Med.* 2014;55:1980–5.
11. Habib G, Lancellotti P, Antunes MJ, et al. 2015 ESC Guidelines for the management of infective endocarditis: The Task Force for the Management of Infective Endocarditis of the European Society of Cardiology (ESC). *Eur Heart J.* 2015;36:3075–128.
12. Van Riet J, Hill EE, Gheysens O, et al. (18)F-FDG PET/CT for early detection of embolism and metastatic infection in patients with infective endocarditis. *Eur J Nucl Med Mol Imaging.* 2010;37:1189–97.
13. Caldarella C, Leccisotti L, Treglia G, Giordano A. Which is the optimal acquisition time for FDG PET/CT imaging in patients with infective endocarditis? *J Nucl Cardiol.* 2013;20:307–9.
14. Leccisotti L, Perna F, Lago M, et al. Cardiovascular implantable electronic device infection: Delayed vs standard FDG PET-CT imaging. *J Nucl Cardiol.* 2014;21:622–32.
15. McCulloch P, Altman DG, Campbell WB, et al. No surgical innovation without evaluation: The IDEAL recommendations. *Lancet.* 2009;374:1105–12.
16. Scholtens AM, Verberne HJ, Budde RP, Lam M. Additional heparin pre-administration improves cardiac glucose metabolism suppression over low carbohydrate diet alone in 18F-FDG-PET imaging. *J Nucl Med.* 2015;36:3075–128.
17. Scholtens AM, Swart LE, Verberne HJ, et al. Confounders in FDG-PET/CT imaging of suspected prosthetic valve endocarditis. *JACC Cardiovasc Imaging.* 2016;9:1462–5.

18. Scholtens AM, van Aarnhem EE, Budde RP. Effect of antibiotics on FDG-PET/CT imaging of prosthetic heart valve endocarditis. *Eur Heart J Cardiovasc Imaging*. 2015;16:1223.



CHAPTER 7

CONFOUNDERS IN FDG PET/CT IMAGING OF SUSPECTED PROSTHETIC VALVE ENDOCARDITIS

Asbjørn Scholtens
Laurens Swart
Hein Verberne
Wilco Tanis
Marnix Lam
Ricardo Budde

7

*Published in: Journal of the American College of Cardiology
– Cardiovascular Imaging 2016;9:1462-5.*

Introduction

Recently, ^{18}F -fluorodeoxyglucose positron-emission tomography with low-dose computed tomography for attenuation correction and anatomical correlation (^{18}F -FDG-PET/CT) has seen increasing use to help diagnose prosthetic heart valve (PHV) endocarditis. Based on the available evidence, ^{18}F -FDG-PET/CT has even been incorporated in the latest European Society of Cardiology Endocarditis Guidelines.¹ As this is still a novel indication for ^{18}F -FDG-PET/CT, the boundaries between normal and abnormal findings are relatively undefined. We present a number of variations (*Figures 1-6*) that could lead to misdiagnosis and need to be taken into account when reading ^{18}F -FDG-PET/CT in patients suspected for PHV endocarditis. Awareness of these variants specifically in the context of suspected PHV endocarditis and cardiovascular infection in a broader sense is pivotal, as this may prevent false-positive or false-negative ^{18}F -FDG-PET/CT readings.

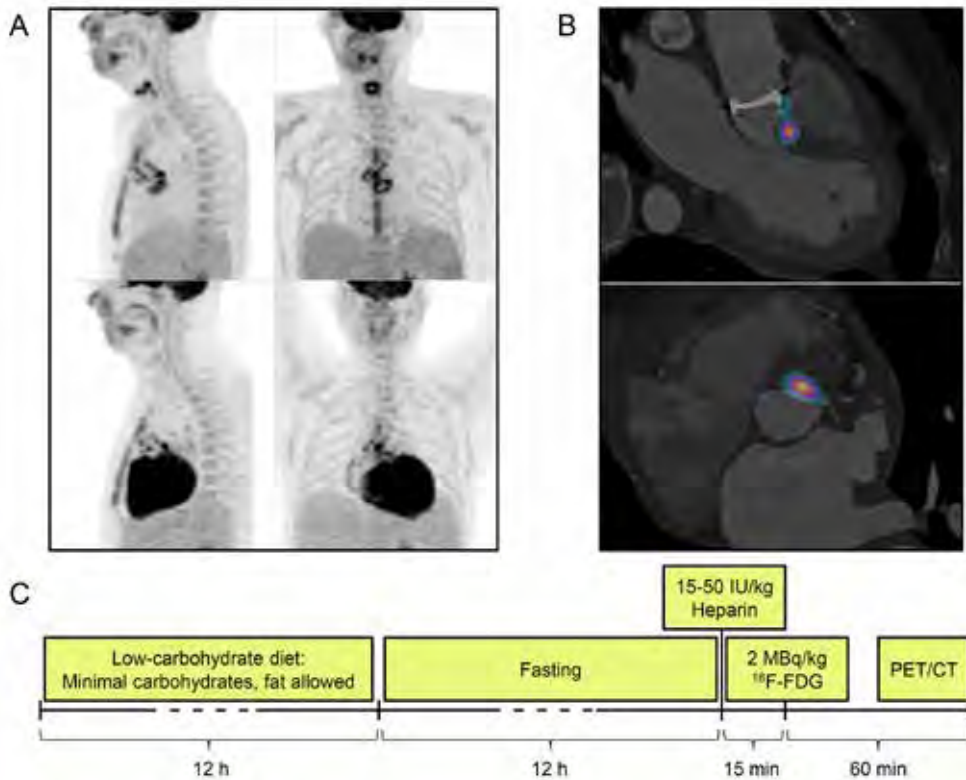


Figure 1 | Importance of adequate suppression of myocardial ^{18}F -FDG uptake. **(A)** Maximum intensity projection positron emission tomography (PET) images in sagittal and coronal views of 2 scans (interval 35 days) in the same patient with endocarditis of a St. Jude mechanical prosthetic heart valve (St. Jude Medical, St. Paul, Minnesota) implanted 1 year earlier, with and without additional preparatory measures. The intense physiological uptake in the myocardium after the standard 6-h fast makes it difficult to delineate uptake caused by the infection (**lower panels**), whereas after the preparatory protocol, the myocardial metabolism has switched to free fatty acids and only the infectious process surrounding the prosthetic heart valve ring and ascending aorta shows uptake of ^{18}F -FDG (**B**), easily delineated from other structures (**A, upper panels**). In some cases, unsuccessful suppression can be very focal in the basal anteroseptum, directly adjacent or close to prosthetic valves and seem suspect for infection. **(C)** Our preparatory protocol, combining a low-carbohydrate diet, prolonged fasting and heparin pre-administration to maximize myocardial suppression (**2**). CT indicates computed tomography; IU, international units.

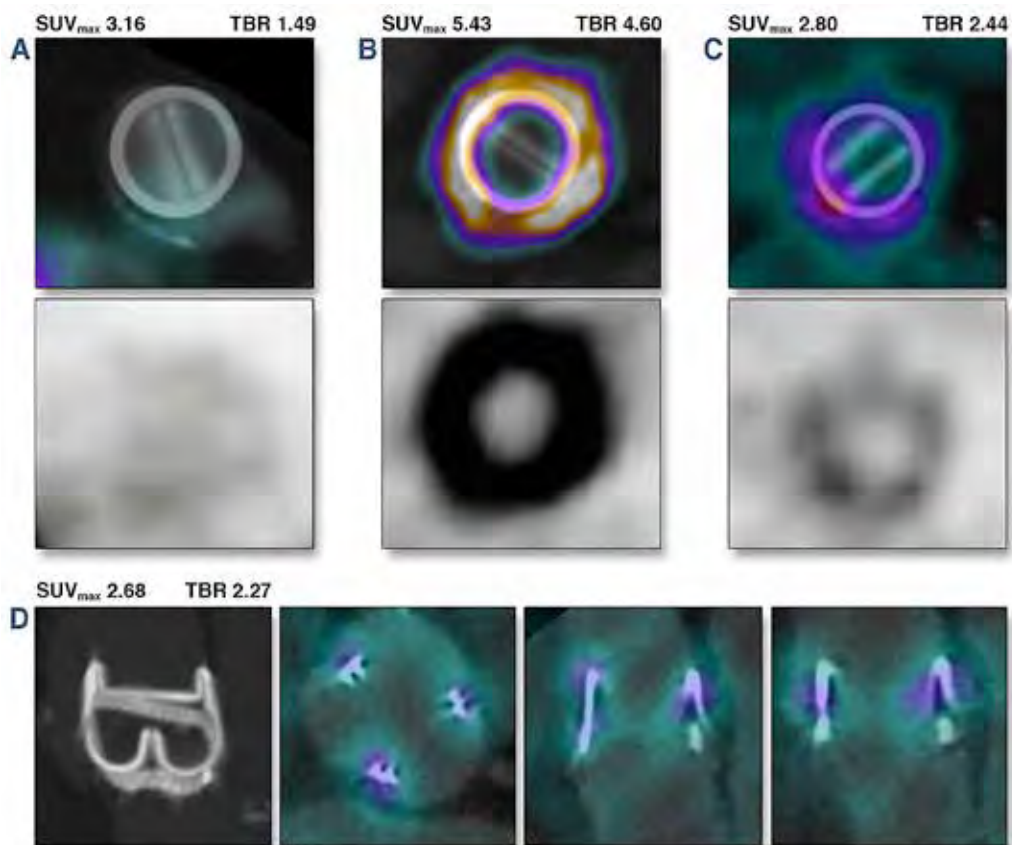


Figure 2 | ^{18}F -FDG PET/CT in PHV endocarditis: how much is too much? PET/CT images of the valvular plane in 3 different patients with a mechanical prosthetic heart valve (PHV) (**A-C**) and a patient with a Carpentier-Edwards bioprosthesis (Edwards Lifesciences, Irvine, California), with maximum standard uptake values (SUV_{max}) and target-to-background ratios (TBR) (SUV_{max} PHV divided by SUV_{mean} aortic blood pool). (**A**) Images show no significant ^{18}F -FDG uptake surrounding the PHV in a patient without endocarditis. (**B**) Images show intense uptake of ^{18}F -FDG in surgically confirmed infection of the aortic root surrounding the PHV ring. (**C**) Images show mild to moderate uptake of ^{18}F -FDG surrounding and confined to the PHV ring, in a patient confirmed by follow-up to have no PHV endocarditis. (**D**) Images show mild, symmetrical ^{18}F -FDG uptake at or near the struts to which the leaflets are fastened (shown in detail in the first CT–maximum intensity projection image), typical of this type of prosthesis. A mild to moderate amount of ^{18}F -FDG uptake around a PHV is a normal variant, possibly due to a mild foreign body reaction or strain on the aortic wall.

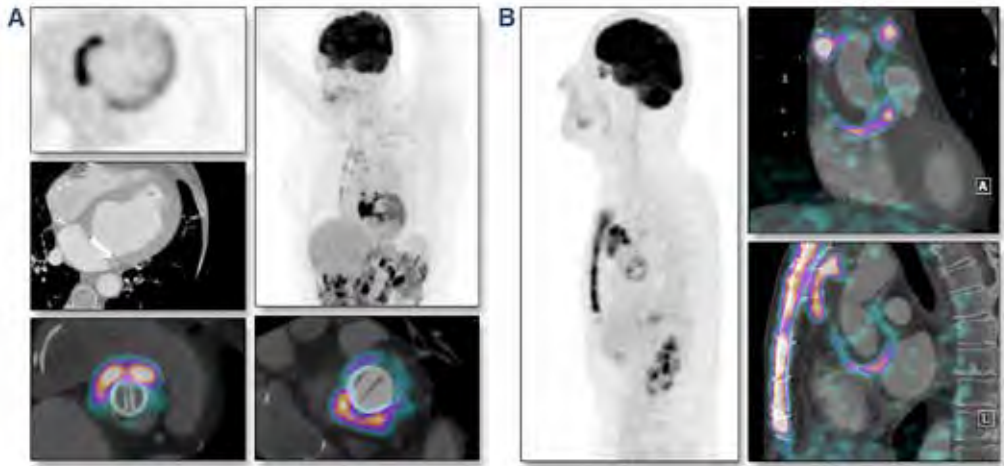


Figure 3 | Infection versus inflammation. **(A)** Images show a patient with both aortic and mitral mechanical PHV with intense ^{18}F -FDG uptake in the entire basal septum extending to both PHV. Minor uptake in the lateral wall is physiological based on incomplete suppression. Antibiotics did not change the clinical presentation, and re-evaluation of biopsy samples led to the diagnosis of sterile granuloma, possibly sarcoidosis. Symptoms diminished under corticosteroid therapy. **(B)** Images show a patient with suspicion of endocarditis of biological PHV and Bentall prosthesis. There is intense accumulation of ^{18}F -FDG surrounding the implant (aortic valve and ascending aorta), indicative of widespread inflammation. During implantation, surgical adhesive had been applied to ensure hemostasis. The accumulation of ^{18}F -FDG is most likely based on sterile inflammation due to the surgical adhesive and not due to infective endocarditis. This was confirmed during unrelated thoracic surgery. These images highlight the inability to reliably differentiate between infection and sterile inflammatory processes.

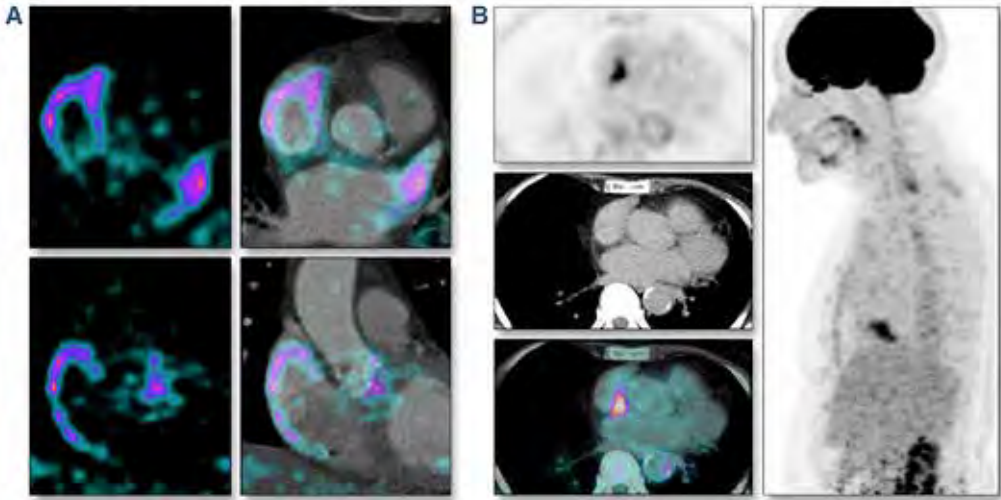


Figure 4 | Atrial variants. In atrial fibrillation, the uncoordinated contraction of the atrial myocardium leads to high energy consumption and a consequent up-regulation of glucose metabolism leading to increased uptake of ^{18}F -FDG, even though the ventricular myocardial glucose metabolism may be completely suppressed. Such accumulation of ^{18}F -FDG in the atrial myocardium may lie adjacent to PHV and may be hard to differentiate from infectious foci (**A**). Lipomatous hypertrophy of the interatrial septum is associated with moderately to intensely increased uptake of ^{18}F -FDG, presented here in a patient without a PHV (**B**). Especially in patients with PHV in the aortic position, lipomatous hypertrophy of the interatrial septum may be located adjacent to the valve. Typical barbell-shape and fatty density without stranding on CT images are arguments against infection.

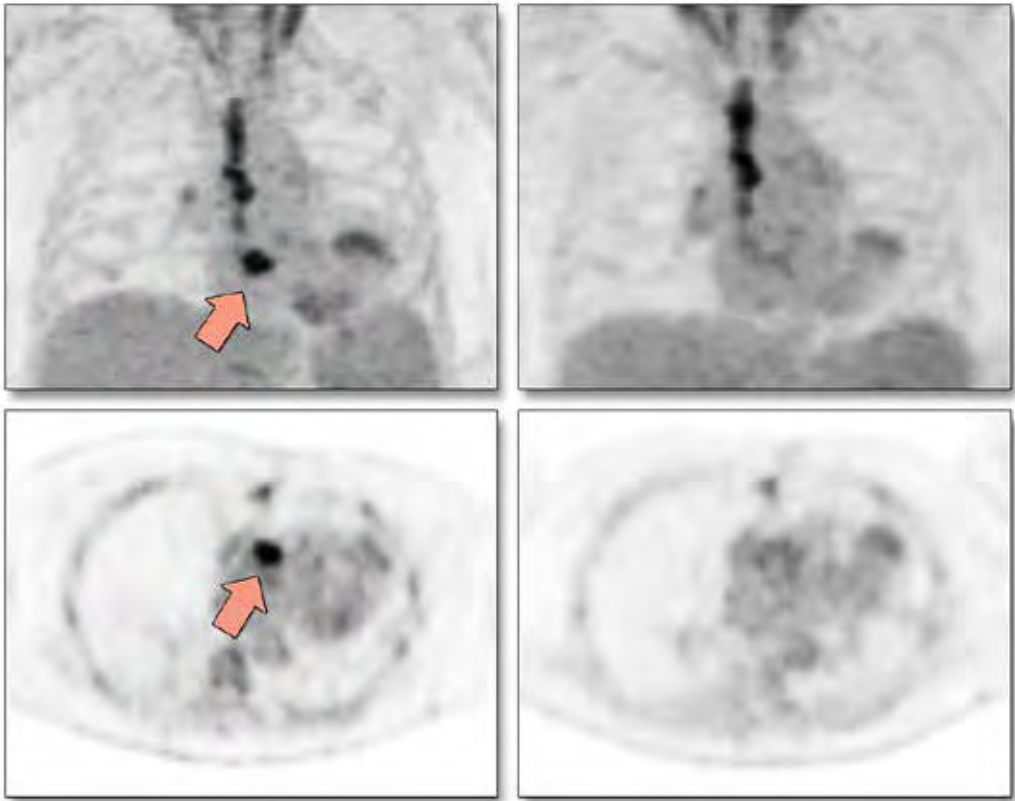


Figure 5 | The effect of antibiotic therapy. Maximum intensity projection and transaxial PET images before (**left**) and during (**right**) antibiotic therapy in the same patient. The initial scan shows focal activity at the implanted aortic PHV (**arrows**). At the end of antibiotic therapy, repeat imaging shows only minimal residual ^{18}F -FDG activity around the PHV, suggesting the infection was treated successfully. However, signs and symptoms of infection returned after cessation of antibiotic therapy, with subsequent surgery showing focal persistence of infection. Although the follow-up scan could therefore be argued to be false negative, it is probably true negative with regard to disease activity, as all clinical and laboratory parameters had also normalized. As this case shows, this does not necessarily imply the complete eradication of pathogens as ^{18}F -FDG PET/CT imaging visualizes leukocyte activity rather than the presence of pathogens themselves.

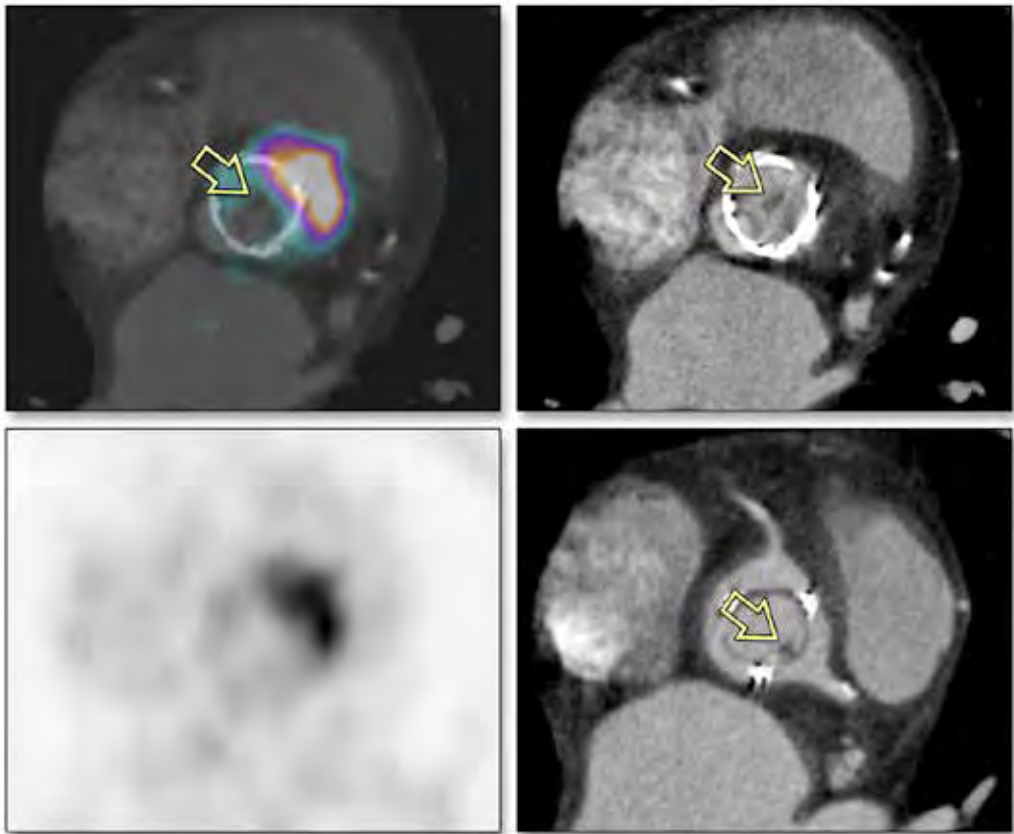


Figure 6 | False-negative ^{18}F -FDG PET/CT in valve vegetation. ^{18}F -FDG PET/CT is not capable of excluding vegetations on PHV, as they are likely to be false negatives. PET shows pathological hyperactivity in the aortic wall, but not in the vegetation (**arrows**) visible on CT angiography (diastolic phase upper right, systolic phase lower right). Several factors may contribute to low levels of activity in vegetations, from the limited spatial resolution of ^{18}F -FDG PET/CT to a lesser cellular component in the inflammatory response to vegetations. ^{18}F -FDG PET/CT should always be combined with echocardiography or CT angiography of the valve to rule out solitary vegetations.

References

1. Habib G, Lancellotti P, Antunes MJ, et al. 2015 ESC Guidelines for the management of infective endocarditis: The Task Force for the Management of Infective Endocarditis of the European Society of Cardiology (ESC). *Eur Heart J*. 2015;36:3075–128.
2. Scholtens AM, Verberne HJ, Budde RPJ, Lam MG. Additional heparin preadministration improves cardiac glucose metabolism suppression over low carbohydrate diet alone in ^{18}F -FDG PET imaging. *J Nucl Med*. 2016;57:568-73.



CHAPTER 8

ADVANCED CT ACQUISITION PROTOCOL FOR COMPREHENSIVE PROSTHETIC HEART VALVE ASSESSMENT

Marguerite Faure
Laurens Swart
Marcel Dijkshoorn
Jos Bekkers
Marcel van Straten
Koen Nieman
Paul Parizel
Gabriel Krestin
Ricardo Budde

Abstract

Objectives

Multidetector CT (MDCT) is a valuable tool for functional prosthetic heart valve (PHV) assessment. However, radiation exposure remains a concern. We assessed a novel CT-acquisition protocol for comprehensive PHV evaluation at limited dose.

Methods

Patients with a PHV were scanned using a third-generation dual-source CT scanner (DSCT) and iterative reconstruction technique (IR). Three acquisitions were obtained: a non-enhanced scan; a contrast-enhanced, ECG-triggered, arterial CT angiography (CTA) scan with reconstructions at each 5 % of the R-R interval; and a delayed high-pitch CTA of the entire chest. Image quality was scored on a five-point scale. Radiation dose was obtained from the reported CT dose index (CTDI) and dose length product (DLP).

Results

We analysed 43 CT examinations. Mean image quality score was 4.1 ± 1.4 , 4.7 ± 0.5 and 4.2 ± 0.6 for the non-contrast-enhanced, arterial and delayed acquisitions, respectively, with a total mean image quality of 4.3 ± 0.7 . Mean image quality for leaflet motion was 3.9 ± 1.4 . Mean DLP was 28.2 ± 17.1 , 457.3 ± 168.6 and 68.5 ± 47.2 mGy·cm for the non-contrast-enhanced (n=40), arterial (n=43) and delayed acquisition (n=43), respectively. The mean total DLP was 569 ± 208 mGy·cm and mean total radiation dose was 8.3 ± 3.0 mSv (n=43).

Conclusion

Comprehensive assessment of PHVs is possible using DSCT and IR at moderate radiation dose.

Introduction

Prosthetic heart valve (PHV) dysfunction is an uncommon but important and potentially life-threatening complication after PHV implantation.¹ In daily practice, the most commonly used imaging modality for evaluating PHVs is transthoracic echocardiography (TTE).² TTE has known limitations such as a high interobserver variability, the possibility of poor acoustic windows and acoustic shadowing. Hence, evaluation of PHV abnormalities often also requires transoesophageal echocardiography (TEE), which is a semi-invasive procedure associated with certain risks and complications, and is also affected by some of the TTE limitations, albeit to a lesser extent.³

More recently, multidetector computed tomography (MDCT) has been shown to provide complementary information for PHV assessment and is useful to identify the cause of PHV dysfunction, including obstructive masses (such as pannus and thrombus), prosthesis-patient mismatch, paravalvular regurgitation, as well as infective endocarditis and its complications.⁴⁻⁵ Most often, a retrospectively ECG-gated CT angiography (CTA) acquisition is used to assess PHV dysfunction since it allows for reconstructions at each 5–10 % of the R-R interval needed to dynamically assess valve leaflet motion and anatomy. Such acquisitions are associated with a relatively high radiation dose as reported in multiple studies (mean 11.6 mSV [interquartile range (IQR) 10.8–14.4]⁶, 11.8 mSV [IQR 11.2–12.8]⁷ and 18.8 ± 3.8 mSV⁸). Ideally, a CT acquisition protocol for PHV assessment would not only include a dynamic CTA but also a non-enhanced scan of the valve region to assess calcifications and suture pledgets, as well as a delayed phase of the entire chest for possible abscesses, septic pulmonary emboli and overall thoracic anatomy, which would increase radiation dose even further⁹. Third-generation dual-source scanners allow for several dose-reduction strategies that are advantageous for PHV assessment. We examined whether a novel, moderate radiation dose three-phase CT acquisition protocol for third-generation dual-source CT (DSCT) allows comprehensive ECG-triggered PHV assessment with both static and dynamic reconstructions to assess the PHV region as well as the entire chest.

Materials and methods

Patients

All consecutive patients with a PHV that underwent a CT scan with this specific acquisition protocol in our department between December 2014 and November 2016 were included. The acquisition was a part of the routine clinical workup, and data were gathered retrospectively. No additional acquisitions were made specifically for this study. Patient data were retrieved from the electronic patient files. A waiver for retrospective evaluation of the data was obtained from the medical ethics committee.

CT scan protocol

Image acquisition was performed on a third-generation DSCT (SOMATOM Force, Siemens, Erlangen, Germany). Image acquisition included three consecutive scans (*Table 1, Figure 1*).

Protocol parameter	Non-enhanced scan	Contrast-enhanced, ECG-triggered CTA	Delayed high-pitch CTA of the entire chest
Scan start	2cm above valve	Center	2cm above arch
Scan end	2cm below valve	Valve	Bottom of heart
Scan length	Variable	Fixed 14cm (3 stacks)	Variable
Scan type	Prospective step-and-shoot	Prospective step-and-shoot	Prospective high-pitch spiral flash
Collimation	Adapted to scan length	192x0.6mm	192x0.6mm
Rotation time (ms)	250	250	250
Pitch	n/a	n/a	3.2
Feed/rot (mm)	Variable	48	184
Reference mAs/rot	80	180	180
mA modulation	CARE DOSE 4D	CARE DOSE 4D	CARE DOSE 4D
Reference kVp	120	120	120
kVp modulation	CARE kV semi 102	CARE kV semi 120	CARE kV semi 120
Tissue of interest	Non-contrast	Vascular	Vascular
Betablocker/nitrates	No	No	No
ECG padding	45%-45%	0-1500ms	n/a
ECG pulsing	Off	50-500ms	n/a
Contrast	No	Yes	Yes
Type		Iodixanol* 320mg l/ml	
Bolus		80ml at 5ml/sec	
Chaser (30% mix ratio)		20ml at 3.5ml/sec	
Delay		Bolustracking	70sec post-injection
Slice width (mm)	3.0	0.75	0.75
Slice increment (mm)	3.0	0.4	0.4
Kernel	Qr36	Bv40	Bv40
ADMIRE strength	3	3	3
ECG phase (%)	45%	10-100% at 5% intervals	30% at trachial carina
ECG phase (ms)	n/a	Best systolic (com- puted)	n/a

Table 1 | Prosthetic heart valve scan protocol. (*) Visipaque, GE Healthcare. CTA indicates CT angiography; ADMIRE, advanced modeled iterative reconstruction; CARE kV, automatic tube voltage modulation technique by SIEMENS; CARE DOSE 4D, automatic exposure control system by SIEMENS.

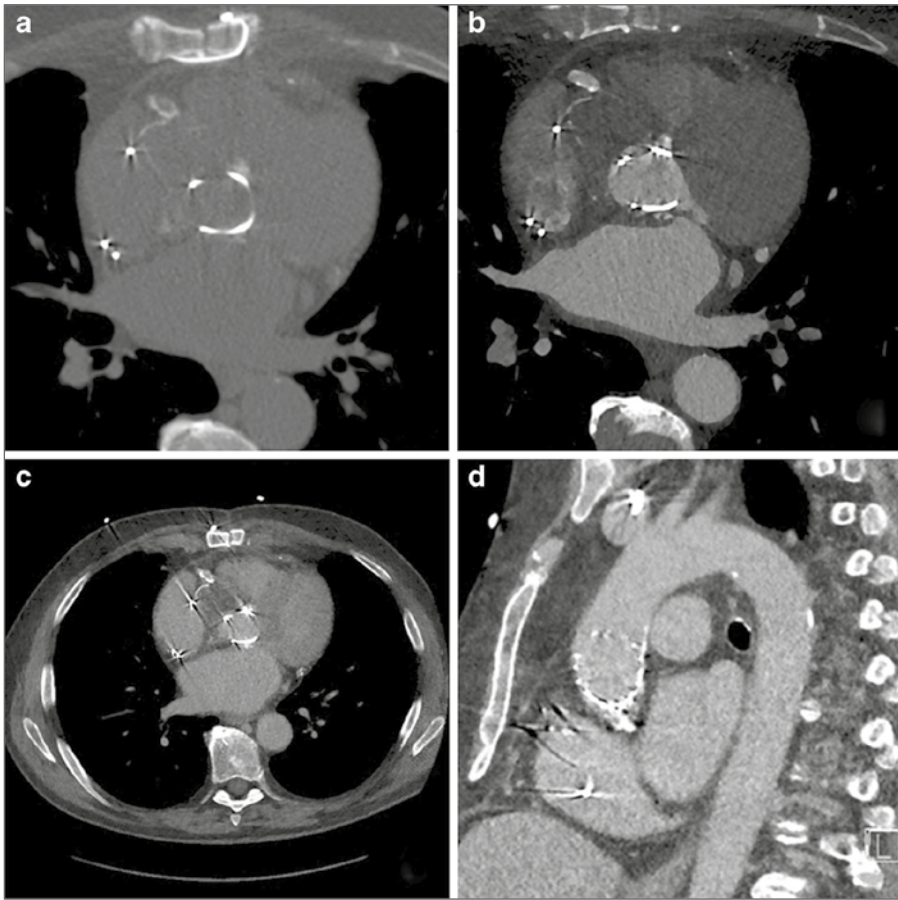


Figure 1 | Image acquisition includes three sequential acquisitions: A non-contrast-enhanced scan (A); a contrast-enhanced arterial CT angiography (CTA) with reconstructions at each 5 % of the R-R interval (B); and a delayed high pitch CTA of the entire chest (C), which allows for evaluation of the complete thoracic aorta as shown on this sagittal view (D).

First, a non-enhanced prospectively ECG-triggered scan of the PHV region alone was performed with the following acquisition parameters: fixed tube voltage 120 kV, reference effective tube load 80 mAs, collimation adapted to fit scan length, and gantry rotation time 250 ms. Data were acquired and reconstructed (slice thickness 3 mm, increment 3 mm, Qr36 kernel) for the 45 % phase of the R-R interval with iterative reconstruction (IR) (Admire Level 3, Siemens).

Secondly, a prospectively ECG-triggered wide-pulsing window sequential CT angiography (CTA) was performed with the following parameters: fixed tube voltage of 120 kV, reference effective tube load 180 mAs, collimation 192×0.6 mm and gantry rotation time of 250 ms. This prospectively ECG-triggered sequential scan was made with three, five or seven stacks. Care was taken to centre the middle stack on the prosthetic valve to avoid any stack artefacts at the level of the valve. For three stacks, the scan length in the z-axis was set at 14 cm, to allow for a maximum coverage per stack in the longitudinal direction (*Figure 2, Figure 3*). Reducing the scan length will reduce the coverage of each of the three stacks evenly until the coverage can be accommodated by two stacks, thereby increasing the risk of stack artefacts. For this CTA, we used an ECG-trigger based on an absolute delay time after an R-peak instead of a relative (%) R-R trigger delay. Irrespective of heart rate, a fixed 'scan-on-scan-off' padding setting from 0–1,500 ms with 50–500 ms ECG-pulsing was used, which resulted in a scan acquisition window that is guaranteed to provide the fastest onset of radiation after an R-peak. After 500 ms, tube current (and thus radiation) decreased from 100 % to 20 % of the set level. Radiation was then maintained for 1,500 ms (which is a full heart cycle at 40 bpm) or cut off when the next R-peak occurred. Reconstructions were made at each 5 % of the R-R interval, with a slice thickness of 0.75 mm, an increment of 0.4 mm and Bv40 kernel (*Figure 2, Figure 3*). An iterative reconstruction technique was used (Admire level 3, Siemens).



Figure 2 | CT angiography (CTA) acquisition: Effect of scan range length in CTA: With prospective protocols in third-generation dual-source CTA the collimation is adapted to the set scan length. In regular cardiac examinations, this helps to avoid overscanning and results in an interpatient variability of the coverage per stack. When scanning heart valves full heart coverage is not always necessary and a shorter range may be sufficient. Special care should be taken in planning the scan range, however, so the largest possible z coverage per stack is obtained to avoid stack artefacts at the valve level. **(A)** A short scan range consisting of two stacks will result in potential stack artefacts through the valve. **(B)** A slightly longer scan range will result in three thin collimate stacks with the valve in the middle of the mid stack. Heart motion and respiratory variability might still move the valve into the potential stack artefacts. **(C)** Opening the scan length to exactly 14 cm will result in three stacks with maximum stack coverage ensuring valve images without ECG stack artefacts.

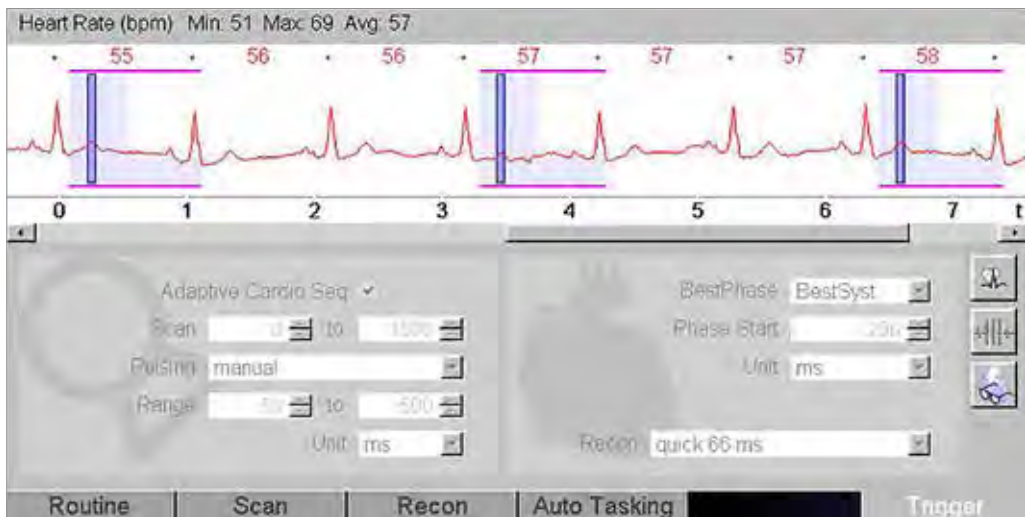


Figure 3 | Screenshot from scanner console. The ECG-trigger in this CTA acquisition is based on absolute millisecond (ms) time instead of a relative (%) R-R-trigger. A 'scan-on-scan-off' padding setting from 0–1,500 ms with 50–500 ms ECG-pulsing results in a scan acquisition window that is guaranteed to provide the fastest onset of radiation after an R-peak (minimum delay is ± 100 ms, which is 10 % at 60 bpm). Radiation is maintained for 1,500 ms (which is a full heart cycle at 40 bpm) or is cut off when the next R-peak occurs. This means that independent of the heart rate, a full heart cycle (starting from 100 ms) is guaranteed.

Thirdly and finally, a low-dose high-pitch CTA of the entire chest was performed, which was triggered in such a way that the scan reaches the trachial carina level at 30 % of the R-R interval. The scan was made with the following parameters: automatically selected tube voltage, reference effective tube load 180 mAs at 120 kV, collimation 192 × 0.6 mm, and a pitch of 3.2. Reconstructions were made with an increment of 0.4 mm, a slice thickness of 0.75 mm in Bv40 kernel and iterative reconstruction (ADMIRE level 3, Siemens).

A single biphasic contrast administration protocol was used in which a total amount of 100 ml of contrast was given with an iodine concentration of 320 mg/ml (Visipaque 320®, GE Healthcare, Cork, Ireland). First, 80 ml of contrast was injected at a rate of 5.0 ml/s, followed by 20 ml of contrast at 3.5 ml/s and a saline flush of 25 ml at 2.5 ml/s. A region of interest was defined in the ascending aorta and data acquisition was initialized when the threshold of 100 HU was reached. The delayed acquisition was obtained 70 s after contrast injection. No beta blockers or nitroglycerin were administered since they may be contraindicated in patients with valvular pathology.

Radiation dose was obtained from the reported CT dose index (CTDI) and dose length product (DLP) and converted to an effective dose, using a conversion factor of 0.0145 mSv/mGy*cm.¹⁰ Heart rate during the acquisitions was obtained from the automatically generated information stored with the DICOM images.

Image analysis

Assessment of the CT examinations was performed on a dedicated workstation (Philips Intellispace Portal, v6.0.3.12200). Using multiplanar reformation, images were reconstructed in plane with the PHV and perpendicular to the PHV and valve leaflets. Cine mode was used to dynamically evaluate PHV leaflet motion in all reconstructed phases of the R-R interval. Image quality was scored separately for each of the three acquisitions in the same way, using a 5-point scale, adapted from a 4-point scoring system used in a previous study by our group.¹¹

The criteria for the different scores were formulated as follows: 1 – no discernible detail, no diagnostic information can be obtained; 2 – only limited visualization of the region of interest, no accurate measurements can be made; 3 – image quality is moderate, measurements and diagnosis are possible; 4 – image quality is good, no diagnostic or measurement problems; 5 – image quality is excellent. Furthermore, image quality of PHV leaflet motion was scored in the same way: 1 – leaflet motion not assessable; 2 – leaflet motion assessable, no reliable measurements can be made; 3 – leaflet motion assessable with the ability to measure opening and closing angles; 4 – good image quality of the leaflet motion; 5 – excellent assessment of leaflet motion possible. Scoring was performed by two radiologists (RB and MF) who had 10 and 2 years of experience with cardiac CT, respectively. The best image quality phase for assessing PHV could be variable among patients. Therefore, for each acquisition, the best cardiac phase was selected for scoring image quality. All images were clinically assessed for PHV-related pathology such as paravalvular leakage, thrombus and/or pannus formation, left ventricular outflow tract (LVOT) obstruction and abscesses.

Data analysis

Descriptive statistics were used to analyse the study data. Mean values and standard deviations were calculated. Interobserver variability was analysed by weighted kappa statistics based on Cohen's statistic.

Results

Patient characteristics

A total of 43 CT examinations acquired in 41 patients were included (mean age 60 ± 23 years, 22 males). One patient who was imaged on three separate occasions was included three times. PHVs were positioned in the aortic ($n=35$), mitral ($n=6$) and pulmonary position ($n=3$). One patient had two PHVs. Of all 44 PHVs examined, 21 were mechanical valves and 23 were biological valves (*Table 2*). The main indications for referral were suspicion or follow-up of endocarditis ($n=22$), increased pressure gradient or suspicion of valve obstruction ($n=10$), suspicion or follow-up of paravalvular leakage ($n=4$). Other indications were follow-up after coarctation repair ($n=2$), after tetralogy of Fallot repair ($n=1$), follow-up of Marfan's disease ($n=1$), after a Bentall procedure ($n=1$), after closure of a pseudo-aneurysm ($n=1$) and newly diagnosed pleural effusion ($n=1$).

Patient characteristics	(n=41)
Male (n=41)	22 (54%)
Age	60 ± 23
Prosthetic heart valve characteristics	(n=44)
Position*	
- Aortic	35 (80%)
- Mitral	6 (14%)
- Pulmonary	3 (7%)
Type	
- Mechanical	21 (48%)
- Biological	12 (27%)
- TAVI	11 (25%)
Brand/model	
- St. Jude Medical	19 (43%)
- Carpentier-Edwards Perimount	6 (14%)
- Medtronic CoreValve	6 (14%)
- Sorin/Carbomedics	2 (5%)
- Boston Scientific Lotus	3 (7%)
- Björk-Shiley	1 (2%)
- Medtronic Perigon	1 (2%)
- Edwards SAPIEN	2 (5%)
- Homograft	4 (9%)

Table 2 | Patient and heart valve characteristics. (*) Three patients had an aortic and a mitral valve prosthesis.

CT parameters

The non-enhanced acquisition was not performed in three patients. In all other patients (n=40), the three acquisitions were obtained. Mean heart rate during scanning was 70 ± 19 bpm for the non-enhanced scan, 69 ± 13 bpm for the ECG-triggered CTA and 75 ± 25 bpm for the high-pitch CTA. Heart rate variability was calculated for the different stacks of the non-contrast-enhanced scan and the CTA, using 1 standard deviation of the mean heart rate. This was 2.3 bpm for the non-contrast-enhanced scan and 2.8 bpm for the CTA. The maximum heart rate variability was 24 bpm for the non-enhanced scan and 32.3 bpm for the CTA. The number of stacks used was 1 (n=10), 2 (n=23), 3 (n=5) and 4 (n=2) for the non-enhanced scan and 3 (n=41), 5 (n=1) and 7 (n=1) for the ECG-triggered CTA. Stack artefacts were seen in one out of 30 non-contrast enhanced CT scans (ten non-contrast scans were scanned with only one stack, so artefacts could not occur) and in two out of 43 ECG-triggered CTAs. In all these examinations, the artefacts did not appear at the valve position. In the delayed acquisition with automatic tube voltage selection, in one of 43 scans (2 %) the reference voltage of 120 kV was chosen, in three scans (7 %) the tube voltage was 100 kV, in four scans (9 %) 70 kV, in nine scans (21 %) 90 kV and in most of the scans (26 scans, 61 %) 80 kV was chosen.

Radiation dose

Mean CTDI was 3.13 ± 1.28 , 30.92 ± 9.6 and 2.31 ± 0.94 mGy for the non-enhanced (n=40), CTA (n=43) and delayed acquisitions (n=43), respectively. Mean DLP was 28.2 ± 17.1 , 457.3 ± 168.6 and 68.5 ± 47.2 mGy·cm for the non-contrast-enhanced (n=40), arterial (n=43) and delayed acquisition (n=43), respectively. The mean total DLP was 569 ± 208 mGy·cm. Mean total radiation dose was 8.3 ± 3.0 mSv (range 3–17, n=43) (Table 3). In one study, the arterial CTA had seven stacks, with a wider scan range due to coronary artery bypass grafting (CABG), which resulted in a total dose of 16.7 mSv. In two studies, the abdomen was included in the high-pitch acquisition with a total radiation dose of 16.8 mSv and 6.7 mSv, respectively. Furthermore, one study had an additional high-pitch acquisition with a total radiation dose of 12.7 mSv.

Dose parameter	Non-enhanced scan	Contrast-enhanced, ECG-triggered CTA	Delayed high-pitch CTA of the entire chest
CTDI (mean±SD, mGy)	3.13 ± 1.27	31.01 ± 9.57	2.32 ± 0.93
DLP (mean±SD, Gy·cm)	28.1 ± 16.9	458.3 ± 166.7	68.7 ± 46.7
Dose (mean±SD, mSv)	0.41 ± 0.23	6.65 ± 2.42	1.00 ± 0.68

Table 3 | Radiation dose overview of the different acquisitions. CTDI, CT dose index; DLP, dose length product.

Image quality scores

The mean image quality score was 4.1 ± 1.4 , 4.7 ± 0.5 and 4.2 ± 0.6 for the non-enhanced, arterial CTA and delayed acquisition, respectively, with a total mean image quality of 4.3 ± 0.7 (Figure 4). Mean image quality for leaflet motion was 3.9 ± 1.4 . Only one non-enhanced scan had a score of 1 and was not interpretable due to the presence of a cobalt- and chromium-containing mechanical heart valve (Björk-Shiley valve), which gives substantial artefacts. Another non-enhanced scan had a score of 2 with limited image quality due to a too short scan length with incomplete visualization of the heart. Overall, 124 out of 126 (98%) acquisitions (40 non-contrast-enhanced, 43 CTA and 43 delayed acquisitions) had an image quality score of ≥ 3 . Regarding leaflet motion, four scans had a score of 1 and were non-diagnostic and four had a score of 2 with only poor image quality. These were five transcatheter valves (four CoreValves and one Sapien valve) and three conventional biological valves. Thirty-four scans had an image quality score of ≥ 3 (81 %) with respect to leaflet motion.

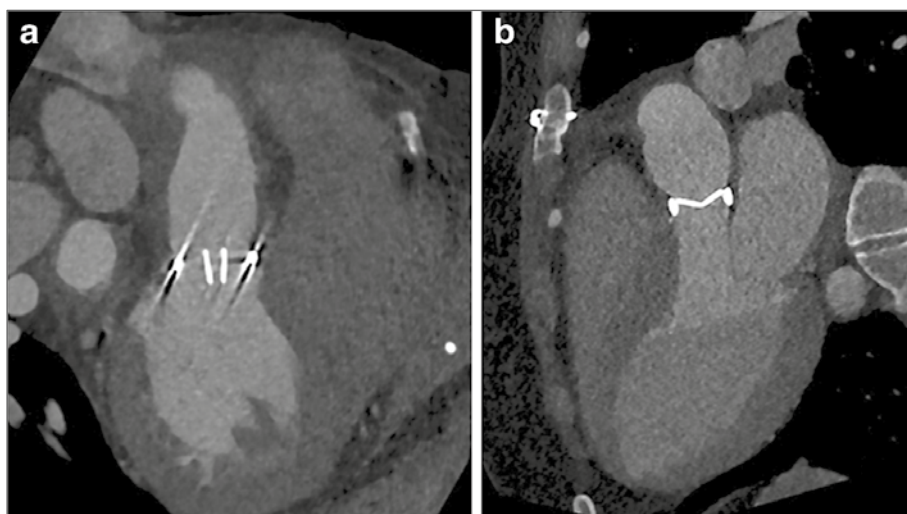


Figure 4 | Image quality. Example of CT angiography (CTA) reconstruction in systole and diastole showing excellent image quality of a bi-leaflet prosthetic heart valve in the aortic position with valve in open (A) and closed (B) position.

Out of 43 examinations, 16 showed no PHV-related abnormalities. Five examinations revealed a false aneurysm at the aortic root. Three examinations showed a clear paravalvular leakage (PVL) and four had possible PVL (*Figure 5*). Five examinations showed pannus or thrombus under the PHV and six examinations showed vegetations/structures inside the PHV. Abscess formation was found in one examination. Five examinations showed a cavity under the PHV. Three examinations revealed thrombus in the left atrial appendage. On the other hand, two patients had suboptimal filling of the left atrial appendage at the CTA, but thrombus could be excluded with the delayed scan.

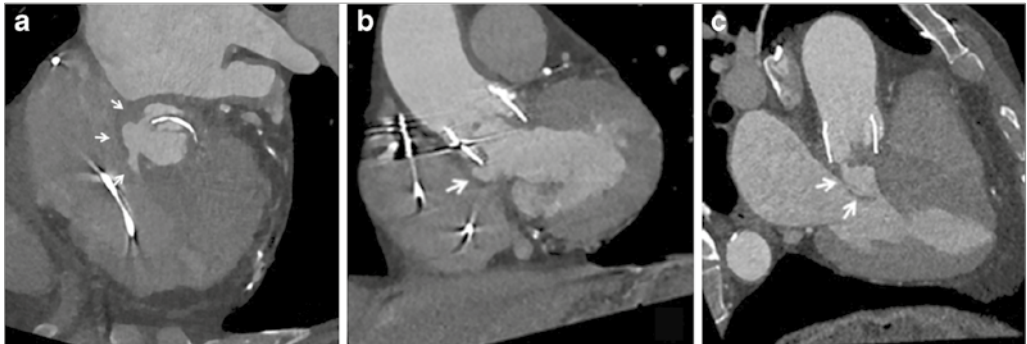


Figure 5 | Patient with aortic prosthetic heart valve (PHV) (TAVR, type Lotus valve) with suspected endocarditis. CT shows PVL and false aneurysm formation. **(A)** Axial contrast-enhanced ECG-triggered CT image shows paravalvular leakage (arrows). **(B)** (coronal) and **(C)** (sagittal) contrast-enhanced ECG-triggered CT images nicely show the PHV in the aortic position and the false aneurysm formation underneath (arrows).

Interobserver agreement

The weighted kappa value for the image quality scores of both observers was 0.74 for the non-contrast-enhanced scan, 0.87 for the CTA and 0.80 for the delayed high-pitch scan. For scoring image quality of leaflet motion the kappa value was 0.80. This means there was a good interobserver agreement for the non-enhanced scan and a good-to-excellent agreement for the other acquisitions and for scoring image quality of leaflet motion.

Discussion

Several studies have demonstrated the potential and incremental value of MDCT in patients with suspected PHV dysfunction.⁶⁻⁸ However, these studies used retrospective ECG-gating CT angiography with a relatively high mean radiation dose of well over 10 mSv for a single arterial phase acquisition only.

Utilizing the capabilities of a modern dual-source scanner, we devised a comprehensive multiphase acquisition protocol for PHV assessment that aims to reduce radiation dose but at the same time increase coverage and assessment potential in multiple phases. Our study shows that this acquisition protocol was associated with good overall image quality and a moderate radiation dose of 8.3 ± 3.0 mSv while making three consecutive acquisitions. Furthermore, leaflet motion, which is an essential part of PHV evaluation with CT, could be visualized using the cine mode with a mean image quality of 3.9 ± 1.4 .

The use of three subsequent acquisitions offers a wide range of diagnostic possibilities and also provides essential information for planning possible re-interventions. Although the additional acquisition phases may not necessarily change the diagnosis per se, they may be helpful in interpretation and increase confidence. This, however, is difficult to quantify and therefore not included quantitatively in this study.

The first, non-enhanced, scan shows the presence and extent of (peri)valvular calcifications. In case of endocarditis, calcifications in pseudoaneurysms around the aortic root allow discrimination between a chronic instead of an active endocarditis, as was the case in one of our patients. Moreover, this non-enhanced scan can identify sutures with polytetrafluorethylene felt pledgets, which were used in eight (19%) of our patients. These pledgets can be isodense to contrast and mimic paravalvular leakage on CTA, thus a non-enhanced scan can be helpful to differentiate between the two (*Figure 6*).¹²

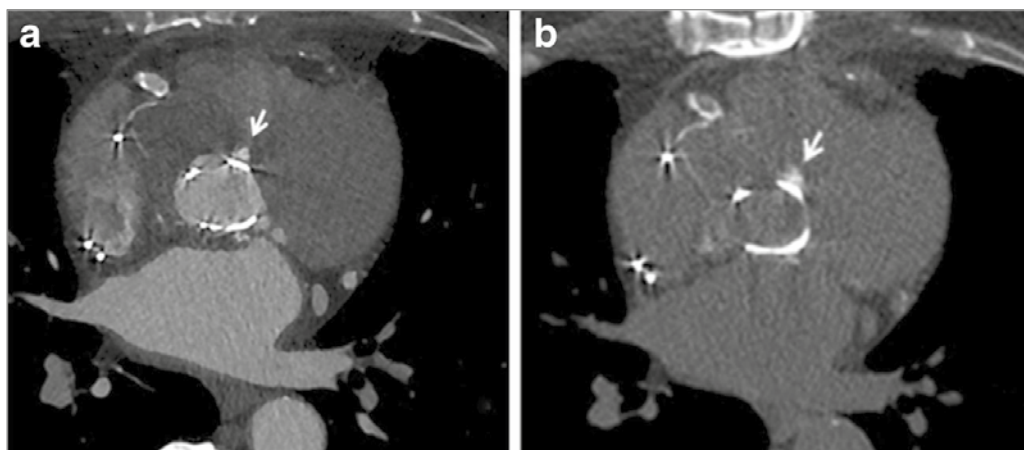


Figure 6 | The non-contrast scan can identify sutures with polytetrafluorethylene felt pledgets. These pledgets can be isodense to contrast and mimic paravalvular leakage (PVL) on CT angiography (CTA) (**A**) and a non-contrast scan (**B**) can thus be helpful to differentiate between the two. The **arrow** indicates possible PVL on the CTA and confirms the hyperdense nature of the pledget on the non-contrast scan.

The goal of the second CTA acquisition is to evaluate valve position and valve dynamics as well as to look for possible leakage, obstruction, pannus tissue, thrombus or signs of endocarditis. We used prospective ECG-triggering with three stacks for our CTA acquisition, which lowered the dose by more than 20 % in comparison to retrospective ECG-triggering at the cost of a short lack of data in the first 100 ms after the R-peak of the cardiac cycle.⁶⁻⁸

By setting the scan length to exactly 14 cm, three stacks were obtained with maximum individual stack coverage to ensure images were without stack artefacts at the level of the valve, as shown by our results (only two out of 44 CTAs had stack artefacts, none of them affecting the valve). One might consider scanning a single stack only for the valve. However, the advantage of using three stacks is that the coronary arteries are completely visualized, which may allow an additional coronary angiography to be omitted in case of re-operation. Furthermore, it gives a good overview of the left ventricular outflow tract.

In this acquisition, we used an ECG-trigger based on absolute millisecond (ms) time instead of a relative (%) RR-trigger. A 'scan-on-scan-off' padding setting from 0–1,500 ms with 50–500 ms ECG-pulsing resulted in a scan acquisition window that was guaranteed to provide the fastest onset of radiation after an R-peak (minimum delay is ± 100 ms, which is 10 % at 60 bpm). Radiation was maintained for 1,500 ms (which is a full heart cycle at 40 bpm) or cut off when the next R-peak occurred. This meant that regardless of the heart rate, a full heart cycle (starting from 100 ms) was guaranteed, which makes this protocol very robust and easy to perform.

The higher dose at 50–500 ms guaranteed high quality systolic images on which pannus, thrombus and leakage can be evaluated. In diastole, dose was reduced to 20 % (with higher noise levels), which is tolerable since this phase is only needed for evaluation of the leaflet motion and confirmation of pathology detected in systole. Moreover, prospective triggering reduced prosthetic heart valve-induced artefacts in comparison with retrospective ECG-gating.⁹ Further development of this protocol could include automatic kV selection for this CTA acquisition in patients with a PHV with a limited amount of metallic components to further lower radiation dose.

The delayed scan comprised the entire chest and thus the full thoracic aorta, at a relatively low radiation cost. The advantages of this 'add-on' scan may be the identification of the extent of disease beyond valves, emphasizing infectious attenuation, better depicting thrombus and differentiating thrombus from flow artefacts (e.g. in the left atrial appendage, since patients with a PHV often have arrhythmias). In five patients (12%) we could thus differentiate between thrombus and flow artefacts (*Figure 7*).

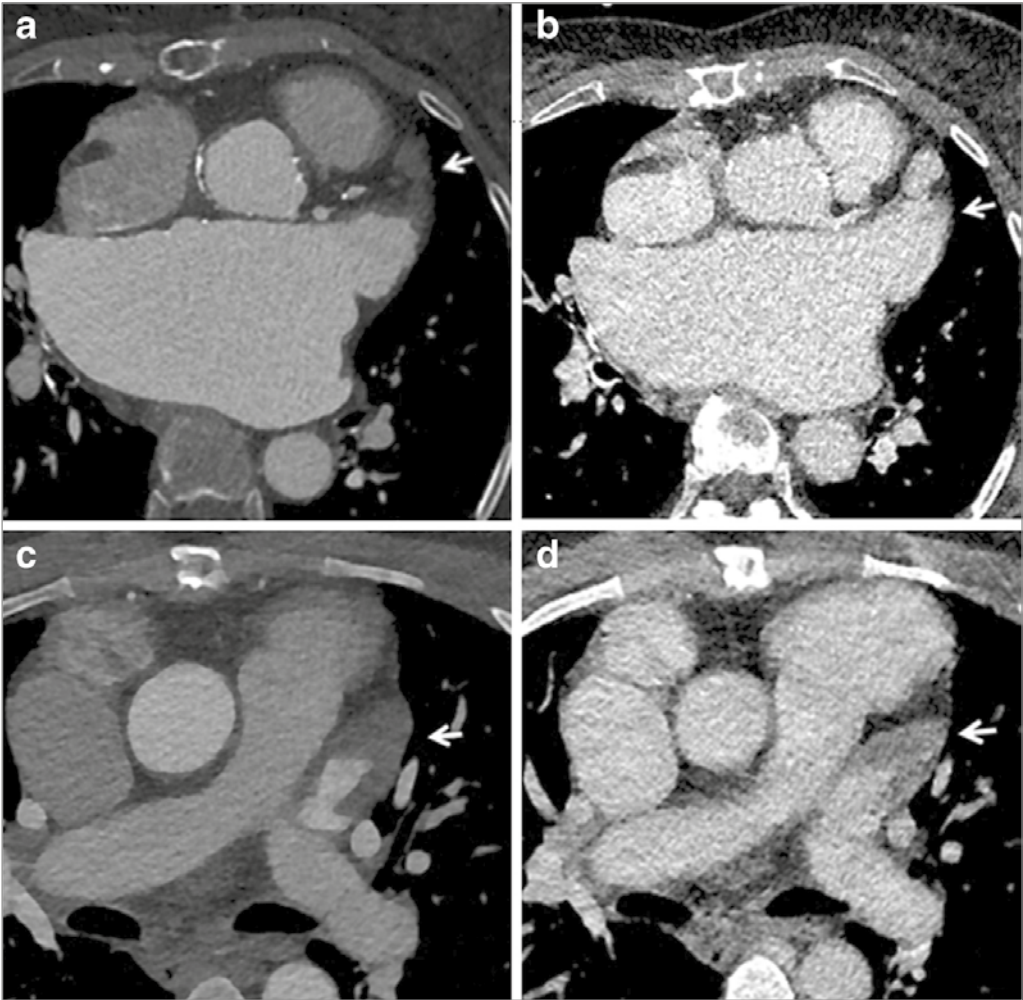


Figure 7 | One of the advantages of the delayed scan acquisition is the ability to better depict thrombus and differentiate thrombus from flow artefacts, since patients with a prosthetic heart valve often have arrhythmias. In the first patient (**A-B**), the arterial CT angiography (CTA) acquisition (**A**) depicts a filling defect in the left atrial appendage (arrow). The delayed scan (**B**) shows that it involved a flow artefact with good filling of the left atrial appendage in this phase (arrows). Thrombus could thus be excluded. In the second patient (**C-D**), the arterial CTA acquisition (**C**) also depicts a filling defect in the left atrial appendage (arrow). However, in this case, the delayed scan (**D**) confirms the presence of a thrombus (arrow).

Besides optimization of CT acquisition parameters, another way to achieve dose reduction is to optimize CT image reconstruction through iterative reconstruction techniques. This alternative image reconstruction method allows imaging at a lower radiation-dose with similar noise levels and image quality compared to routine filtered back-projection (FBP), thus reducing dose without compromising image quality.¹³

Although a mean radiation dose of 8.3 ± 3.0 mSv for all three acquisitions combined is considerably lower than reported previously⁶⁻⁸, it is not minimal. However, one must take into account that this patient population was relatively old and represents a population that often has serious pathology with relatively high morbidity and mortality, e.g. due to endocarditis, with a genuine possibility of needing a high-risk reoperation. This imposes a good balance between lowering the radiation dose as much as possible but still gathering all the information needed for good clinical decision making and preoperative planning.

In follow-up CT examinations, and depending on the clinical question, the non-enhanced or delayed scan can be omitted and the CTA can be obtained using only one stack through the valve, where relevant.

As underlined in several recent studies, another additional benefit of CT is the power to detect leaflet thickening (most likely due to thrombus formation) of biological and transcatheter PHVs that was not detected by TTE.¹⁴⁻¹⁶ The possible addition of CT in the routine work-up early after PHV implantation also necessitates lowering the radiation dose as much as possible.

Our study had some limitations. In this descriptive study of a new CT protocol for the evaluation of PHVs, no comparison with other acquisition protocols in the same or a similar group of patients was made. Furthermore, albeit irrelevant to our main outcome of image quality, no comparison with a reference standard was made regarding pathological findings.

Conclusion

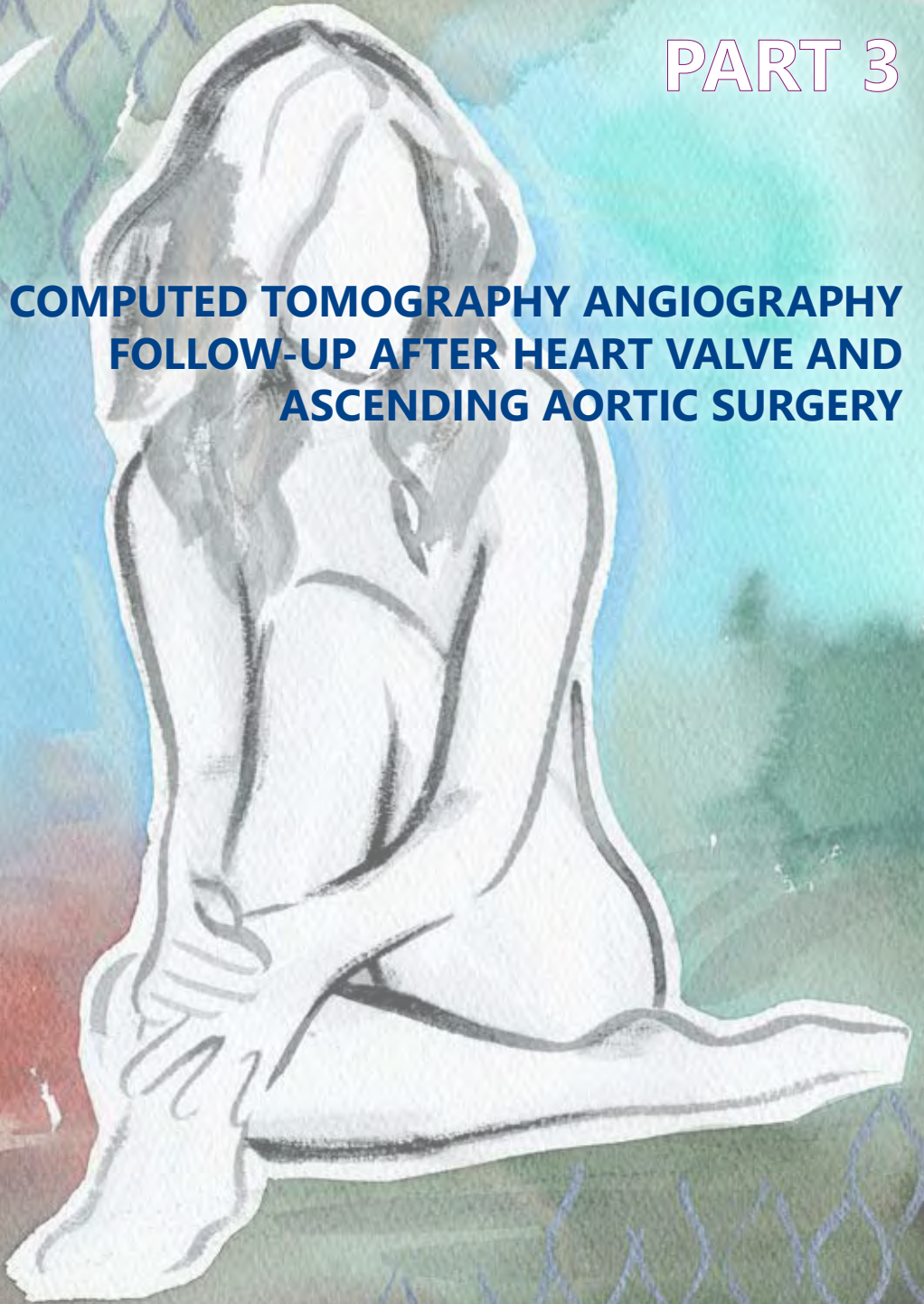
A novel comprehensive CT image acquisition protocol is presented that allows for both dynamic reconstructions to assess PHV leaflet motion and high-resolution anatomical images with good image quality, using third-generation dual-source CT and iterative reconstruction techniques. The moderate radiation dose of 8.3 ± 3.0 mSv for this three-phase acquisition is – albeit not minimal – substantially lower (> 20 % reduction) than previous (usually retrospectively ECG-gated) single-phase image acquisition techniques and can be considered acceptable when seen in relation to the pathology, the risks and possible re-intervention in this patient population.

References

1. Habets J, Budde RPJ, Symersky P, et al. Diagnostic evaluation of left-sided prosthetic heart valve dysfunction. *Nat Rev Cardiol*. 2011;8:466–78.
2. Lancelotti P, Pellikka PA, Budts W, et al. The clinical use of stress echocardiography in non-ischaemic heart disease: recommendations from the European Association of Cardiovascular Imaging and the American Society of Echocardiography. *Eur Heart J Cardiovasc Imaging*. 2016;17:1191–229.
3. Suchá D, Symersky P, Tanis W, et al. Multimodality Imaging Assessment of Prosthetic Heart Valves. *Circ Cardiovasc Imaging*. 2015;8:e003703.
4. Habets J, Symersky P, van Herwerden LA et al. Prosthetic heart valve assessment with multidetector-row CT: imaging characteristics of 91 valves in 83 patients. *Eur Radiol*. 2011;21:1390–6.
5. Gherin E, Martinez CA, Singh V, et al. ECG-gated MDCT after aortic and mitral valve surgery. *AJR Am J Roentgenol*. 2014;203:596–604.
6. Suchá D, Symersky P, van den Brink RB, et al. Diagnostic evaluation and treatment strategy in patients with suspected prosthetic heart valve dysfunction: The incremental value of MDCT. *J Cardiovasc Comput Tomogr*. 2016;10:398–406.
7. Habets J, Tanis W, van Herwerden LA, et al. Cardiac computed tomography angiography results in diagnostic and therapeutic change in prosthetic heart valve endocarditis. *Int J Cardiovasc Imaging*. 2014;30:377–87.
8. Chenot F, Montant P, Goffinet C, et al. Evaluation of anatomic valve opening and leaflet morphology in aortic valve bioprosthesis by using multidetector CT: comparison with transthoracic echocardiography. *Radiology*. 2010;255:377–85.
9. Sympersky P, Habets J, Westers P, et al. Prospective ECG triggering reduces prosthetic heart valve-induced artefacts compared with retrospective ECG gating on 256-slice CT. *Eur Radiol*. 2012;22:1271–7.
10. Deak PD, Smal Y, Kalender WA. Multisection CT protocols: sex- and age-specific conversion factors used to determine effective dose from dose-length product. *Radiology*. 2010;257:158–66.
11. Symersky P, Budde RPJ, Prokop M, de Mol BAJM. Multidetector-Row Computed Tomography Imaging Characteristics of Mechanical Prosthetic Valves. *J Heart Valve Dis*. 2011;20:216–22.
12. Habets J, Meijer TS, Meijer RC, et al. CT attenuation measurements are valuable to discriminate pledgets used in prosthetic heart valve implantation from paravalvular leakage. *Br J Radiol*. 2012;85:e616–21.
13. Willeminck MJ, de Jong PA, Leiner T, et al. Iterative reconstruction techniques for computed tomography. *Eur Radiol*. 2013;23:1623–31.
14. Makkar RR, Fontana G, Jilaihawi H, et al. Possible Subclinical Leaflet Thrombosis in Bioprosthetic Aortic Valves. *N Engl J Med*. 2015;373:2015–24.
15. Leetmaa T, Hansson NC, Leipsic J, et al. Early aortic transcatheter heart valve thrombosis: diagnostic value of contrast-enhanced multidetector computed tomography. *Circ Cardiovasc Interv*. 2015;8:e001596.
16. Pache G, Schoechlin S, Blanke P, et al. Early hypo-attenuated leaflet thickening in balloon-expandable transcatheter aortic heart valves. *Eur Heart J*. 2016;37:2263–71.

PART 3

COMPUTED TOMOGRAPHY ANGIOGRAPHY FOLLOW-UP AFTER HEART VALVE AND ASCENDING AORTIC SURGERY



CHAPTER 9

9

IMPLICATIONS OF PERI-AORTIC FLUID AFTER SURGERY ON THE ASCENDING AORTA

Laurens Swart¹
Sara Boccalini¹
Jos Bekkers
Koen Nieman
Gabriel Krestin
Ad Bogers
Ricardo Budde

Published in: European Journal of Radiology 2017;95:332-41

Abstract

Objective

The Bentall procedure is associated with several complications often accompanied by accumulation of fluid around the aortic graft. CT is the imaging modality of choice to detect these complications. Since these early complications are, however, not easily distinguished from physiological postoperative changes, our aim was to compare the appearance and amount of peri-aortic fluid on early CT scans following Bentall procedures with either an uncomplicated or a complicated course and follow-up.

Methods

Ninety-four scans performed within 3 months of a Bentall procedure were retrospectively included. Patients were divided into either the uncomplicated or the complicated group based on occurrence of Bentall-related complications or death up until 1-year after surgery. Diffuse fluid ("stranding") was distinguished from organized, more clearly delineated fluid collections such as haematomas, and was graded both subjectively and quantitatively.

Results

Forty-seven patients were assigned to each group. Stranding was found on most of the scans, both in the uncomplicated (7.7 ± 3.9 mm, range 0–17 mm) and complicated (6.9 ± 5.5 mm, range 0–19 mm) groups ($p = 0.32$). There were, however, significantly more fluid collections (6 vs. 28; $p < 0.001$), particularly haematomas (1 vs. 17; $p < 0.001$), in the complicated group. When looking at isolated stranding, there was still no significant difference between the two groups (7.8 ± 3.6 mm vs. 9.2 ± 3.7 mm; $p = 0.22$).

Conclusions

Isolated stranding of up to 17 mm is a common finding on postoperative CT within three months of a Bentall procedure, regardless of the occurrence of complications during the procedure or within a 1-year follow-up. Fluid collections are more worrisome indicators of complications that may require closer monitoring.

Introduction

The so-called Bentall procedure consists of the replacement of the aortic valve and ascending aorta in a single operation.¹ The most common pathologies that require this kind of intervention are type A aortic dissections and large ascending aortic aneurysms with associated aortic valve stenosis or insufficiency.

This major intervention may lead to both peri- and post-procedural complications^{2,3}, of which some of the most fearsome and potentially fatal are infection of the aortic prosthesis and endocarditis. The imaging modality of choice to depict their occurrence is CT, which is also preferred for routine follow-up examinations.

Due to the extensive structural changes occurring during surgery, certain postoperative alterations can be expected, such as the presence of fluid and stranding in the adipose and soft tissue surrounding the prosthesis, especially in the earliest time period following the procedure. However, infections may show an analogous radiological appearance, resulting in diagnostic dilemmas. Moreover, in most cases the interpretation of the images cannot be guided by the patients' clinical information/presentation because post-operative CT scans are performed as routine follow-up in asymptomatic patients and, furthermore, complications such as endocarditis often present with no or generic symptoms. It is therefore of paramount importance for the radiologist to be familiar with the normal aspects and their physiological change as time progresses in order to be able to distinguish these from complications that need to be closely observed, treated with medical therapy or even a new intervention. Unfortunately, literature regarding normal postoperative CT features after Bentall procedures and their change over time is still limited.

To determine a normal reference, we have retrospectively assessed the appearance and amount of fluid surrounding the composite graft of the aortic valve and ascending aorta on CT scans performed within the first three months following both uncomplicated procedures and procedures with a complicated course or follow-up.

Materials and methods

Study population

In this single-center retrospective cohort study, for which a waiver was received from the local Medical Ethics Committee, patients were selected from a large database comprising 391 Bentall procedures performed in 388 patients in the period between August 2000 and February 2015. Through a search in their electronic files, 206 patients who had undergone at least one CT scan after the procedure were identified. In total, 417 post-operative scans were performed in these patients. Since most of the early complications of a Bentall procedure occur in the first three months⁴⁻⁶ and this is when a reference of the spectrum of normal findings is most crucial, only patients who had undergone a CT scan during this period were selected for the purpose of this study. For each patient only the first scan performed within these three months was included in the analysis.

Complicated versus uncomplicated procedures

To determine the normal appearance and amount of peri-aortic fluid after a Bentall procedure, healthy patients with an uncomplicated follow-up had to be distinguished from patients who had experienced complications during or after the procedure. To accomplish this, all patient files were carefully analyzed and evaluated for strict criteria which had been postulated beforehand, in order to determine whether the procedure and follow-up had been uneventful: (a) the surgical report of the Bentall procedure itself mentioned no procedural complications, (b) the patient was discharged within 14 days of surgery, and was not reoperated upon (e.g. for bleeding or tamponade, infection, sternal dehiscence or other early complications) during this period, (c) the patient was neither readmitted for Bentall-related complications nor deceased within one year of the procedure, and (d) the CT-scan was not performed for suspicion of Bentall-related complications, but rather only as routine follow-up.

Patients who were reoperated upon were further divided based on whether the CT scan had been performed before or after the second procedure. A separate analysis was performed for the first subgroup but not for the second, due to the impossibility to ascribe the findings to either one of the operations. Unless stated otherwise, time was calculated in relation to the first operation.

CT scan assessment

All selected scans performed at our institution or an affiliated one, of which the images were readily available at our institution's PACS, were then retrieved and reassessed on a dedicated multimodality workstation (iSite Enterprise 4.1, Philips Healthcare, the Netherlands) by a blinded observer with over 4 years of experience in cardiovascular imaging. Firstly, several technical parameters of the scans were evaluated, including the number of detectors of the scanner, the smallest reconstruction slice thickness with vascular or soft tissue kernel, and whether the scan had been gated electrocardiographically. Subsequently, the scans were systematically reviewed and scored with regard to technical image quality and the appearance and amount of fluid surrounding the ascending aorta using a predefined reference sheet. The observer had not been involved in the initial selection of scans and was blinded to the reported CT scan results, the request form and any other clinical data.

Overall scan quality was graded on a 5-point scale as 1. poor, 2. moderate, 3. reasonable, 4. good or 5. excellent, based mostly upon the presence of motion artefacts at the level of the ostium of the coronary arteries and ascending aorta, as well as on the extent of beam hardening and scatter artefacts due to any metallic components of the aortic valve prostheses. Key images exemplifying each quality grade are provided in *Figure 1*.

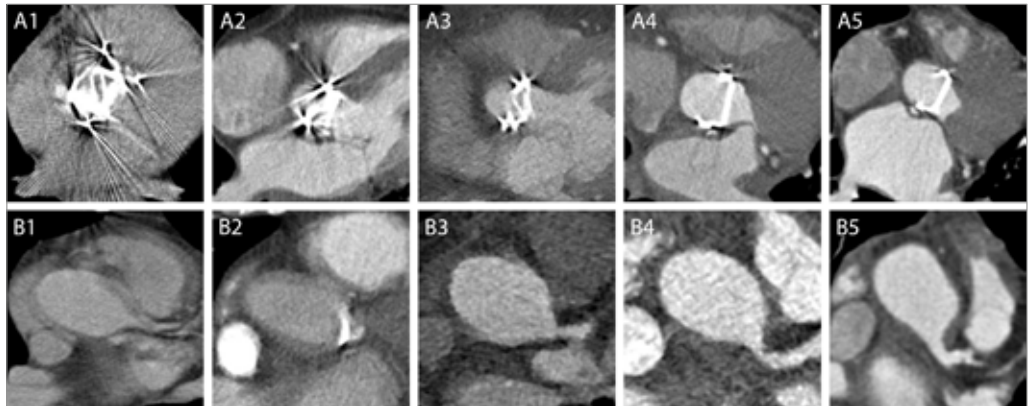


Figure 1 | Rows **A** and **B**: Representative examples for the different CT quality grades, from poor (**A1**, **B1**) to excellent (**A5**, **B5**). The examples show axial images of different patients at the level of two of the most sensitive locations for grading purposes: the aortic valve prosthesis (**A1-5**) with the beam hardening and scattering artefacts, and left coronary artery ostium (**B1-5**) with motion artefacts.

Then, the periaortic fluid was categorized as stranding or a fluid collection based on its appearance. Stranding was defined as an encircling area of increased attenuation of the adipose tissue along the external edge of the aortic lumen, with ill-defined borders and an infiltrating appearance. Fluid collections were distinguished from stranding by their clearer, more regular delineation and their often-incomplete surrounding of the aortic circumference (*Figure 2*).

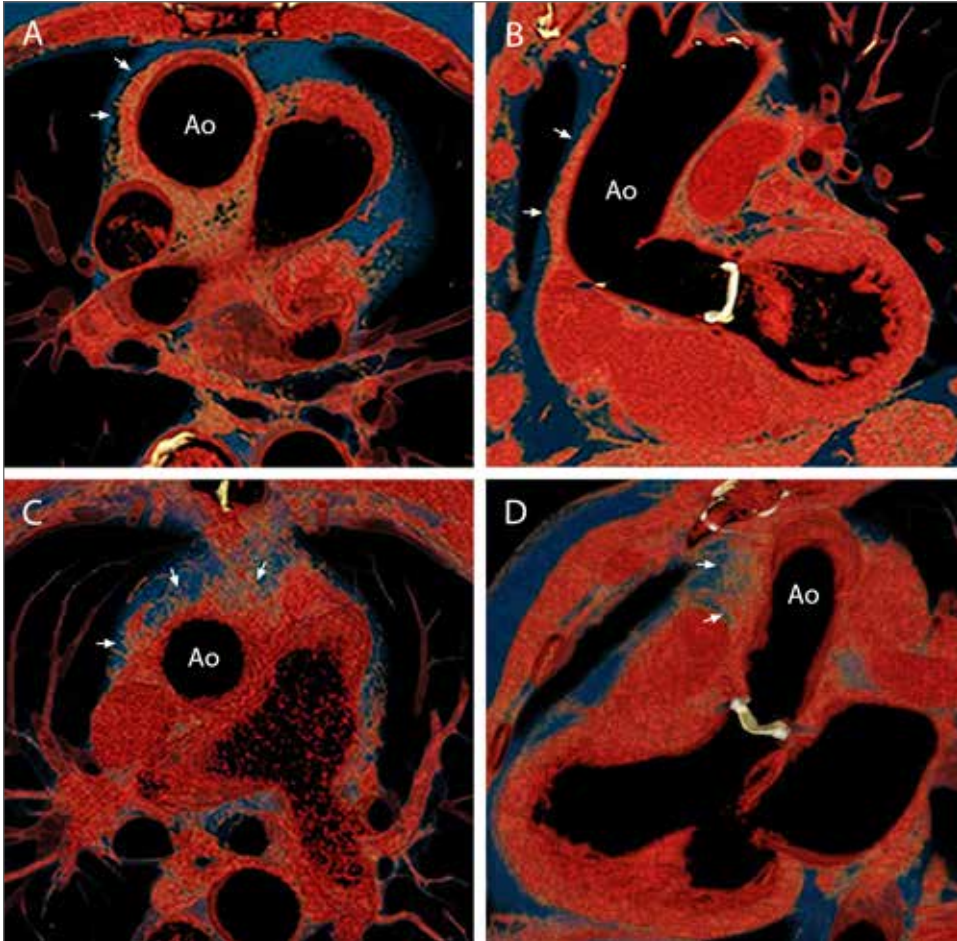


Figure 2 | Distinguishing characteristics of fluid collections and stranding. Thin volume rendering technique (VRT) reconstructions on an axial (**A**) and a modified sagittal view (**B**) of a thin fluid collection localized along the anterolateral wall of the aorta (Ao) and characterized by sharply defined borders with the surrounding adipose and soft tissues (arrows). Thin VRT reconstructions on an axial (**C**) and a modified sagittal view (**D**) of an example of stranding extending along all of the aortic circumference with ill-defined and irregular margins (**arrows**).

Afterwards, we evaluated the amount of stranding, both subjectively and objectively. The overall quantity of the stranding extending in the adipose tissue surrounding the aortic prosthesis was subjectively graded with a 5-point scale as slight, mild, moderate or extensive. The scale was based both on the estimated volume of the stranding (determined by its farthest extension from the aorta at each level) and on the perceived proportion of fluid (vs adipose tissue) inside this volume. *Figure 3* shows the reference sheet (compiled beforehand) based on which the scans were scored at the level of the pulmonary trunk. The thickness of the stranding was also objectively and quantitatively measured at the point of maximum extension from the inner border of the aortic wall on axial images as well as on multi-planar reconstructions (*Figure 4*).



Figure 3 | Reference sheet for the different subjective grades of the amount of stranding. The panels show axial images of different patients at the level of the pulmonary trunk, demonstrating (A) no stranding, (B) slight, (C) mild, (D) moderate and (E) extensive stranding.

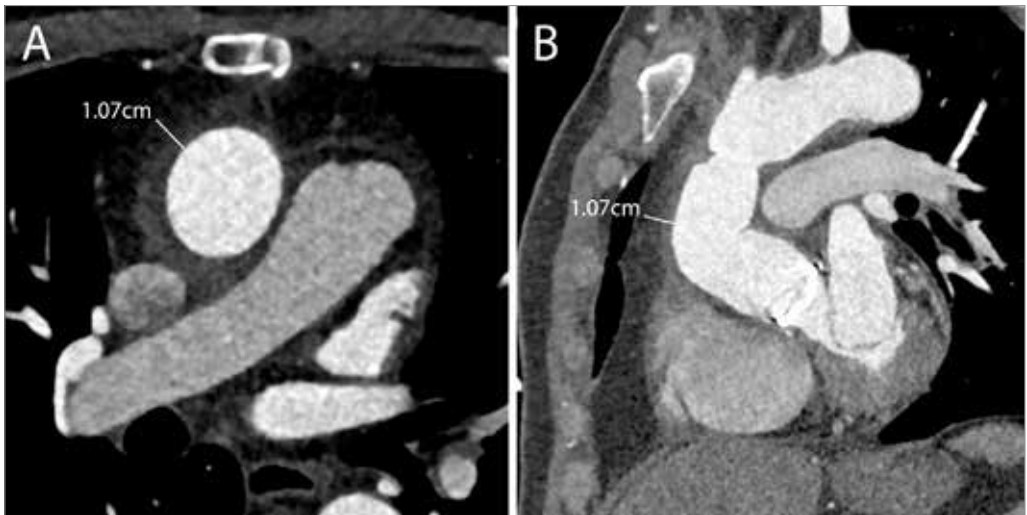


Figure 4 | Quantitative assessment of peri-aortic stranding. Axial (A) and modified sagittal (B) views showing how measurements of stranding were performed at the point of its maximum extension from the inner border of the aortic wall.

The content of the fluid collections was derived from their attenuation and defined as fluid with a water-like density (0–35 HU), hemorrhagic (35–100 HU), contrast leakage (>100 HU) or contrast leakage with associated hemorrhagic content (*Figure 5*). Wall enhancement of the fluid collections was separately scored, as well as whether there were air bubbles inside or other signs that resembled characteristics of an abscess, such as fistulous connections or extensions to adjacent anatomical structures. Fluid collections with a high density due to the presence of contrast were further categorized as suture aneurysms or pseudoaneurysms based on previously published criteria.^{2,7} In case a fluid collection was surrounded by stranding (even if not entirely), they were both scored separately. Furthermore, because stranding surrounding a fluid collection is most likely a different entity, and because its shape and amount may have been influenced by the presence of that fluid collection, scans showing only stranding and no fluid collections (referred to as “isolated stranding”) were also analyzed separately.

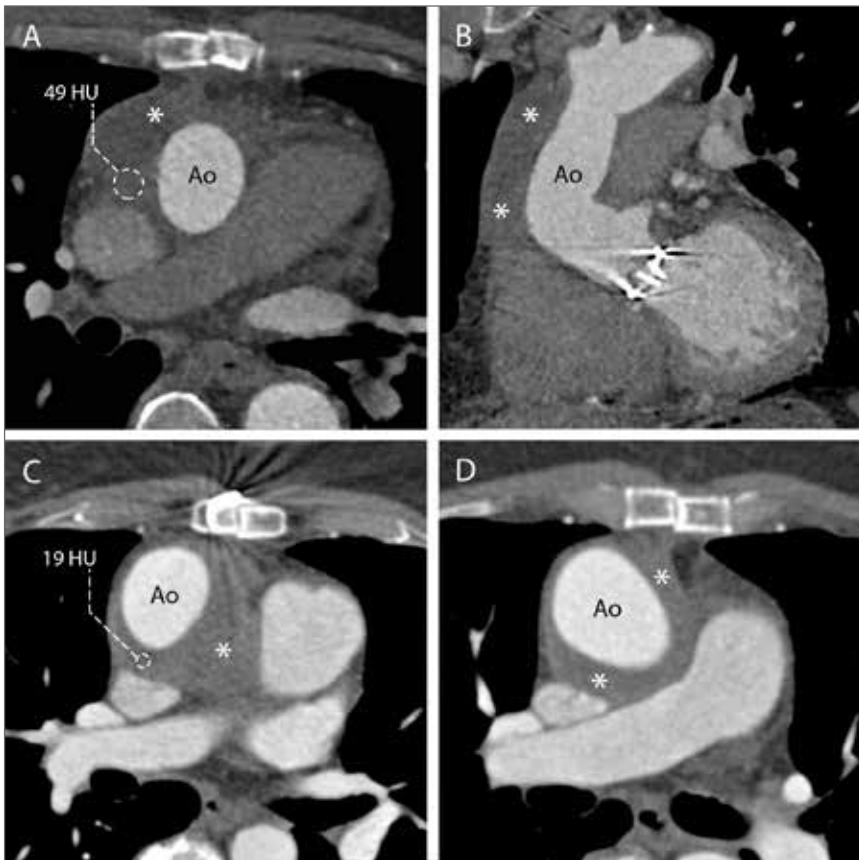


Figure 5 | Differentiation of fluid collections. Axial (**A**) and modified coronal (**B**) views of a fluid collection (**asterisks**) with a high density content (49 HU lateral to the aorta) therefore classified as haematoma. Axial views at different levels (**C**, **D**) of a fluid collection (**asterisks**) with contents of a low water-like density (19 HU posterior to the aorta).

Particular attention was paid to the differentiation of stranding and fluid collections from other possible confounding findings such as residual thymus (especially in young patients), scars from previous surgeries and peri-aortic pericardial recesses filled with pericardial effusion. Furthermore, even in patients who did not undergo any surgical procedure involving the mediastinum, some stranding of the periaortic adipose tissue can be encountered. However, in these CT scans that were performed for unrelated reasons, stranding appears as thin lines and does not encircle the aorta. Exams with the just mentioned characteristics were considered to be without stranding for the purpose of this study.

The presence of other complications involving the prosthetic valve (vegetations and mycotic aneurysms) that could have possibly influenced the presence of fluid surrounding the aortic graft, was assessed as well.

Data collection and statistical analysis

All data retrieved from the surgical database and CT scan analyses were anonymized and registered into a secure online electronic database (MySQL, Oracle, Redwood Shores, CA, USA) that was tailor-made specifically for this study. For every scan inserted into the database, a web-based form was automatically created that comprised several fields for all the appropriate variables and findings.

For statistical analyses, SPSS version 22 (IBM Corp., Arbonk, NY, USA) was used. Besides descriptives, the independent t-test and Mann-Whitney U test were used to compare the complicated and uncomplicated patient groups regarding normally distributed and non-parametric variables and outcomes respectively. The Kolmogorov-Smirnov test was employed to test for normality of all involved continuous variables, including the amount of stranding in millimeters. To compare dichotomous variables such as the presence of fluid collections to the occurrence of complications, the Chi-Square test was employed. Finally, linear regression was used to analyze the course of stranding over time.

Results

Among the 206 patients with 417 postoperative scans in the database, 94 patients, who had been operated upon between March 2003 and February 2015, had received their first postoperative CT scan within three months of surgery (*Table 1*).

	Uncomplicated (n=47)	Complicated (n=47)	Total (n=94)
Male	33 (70%)	36 (77%)	69 (73%)
Age (mean, SD, range) in years	54.2±15.8 (18-80)	55.5±14.9 (22-83)	54.8±15.4 (18-83)
Surgery indication			
- Aneurysm	34 (72%)	24 (51%)	58 (62%)
- Dissection	3 (6%)	11 (23%)	14 (15%)
- Other	10 (21%)	12 (26%)	22 (23%)
Valve			
- Mechanical	41 (87%)	45 (96%)	86 (91%)
- Biological	6 (13%)	2 (4%)	8 (9%)
Postoperative hospitalization (mean, SD, range) in days	7.5±2.8 (4-19)	19.5±20.0 (5-110)	13.5±15.4 (4-110)

Table 1 | Patient population.

Patient classification

The scans of 47 patients were assigned to the complicated group for one or more of the following reasons (*Table 2*): the post-surgical hospitalization period had been complicated by infection or extensive bleeding related to the procedure (n = 29), a re-sternotomy for early bleeding/tamponade or infection (n = 25) or even complete replacement of the Bentall graft (n = 4) had been required due to Bentall-related complications; the patient had been readmitted because of Bentall-related complications (n = 15), the patient had died (n = 3) within 1 year of surgery, or the scan had been performed for clinical suspicion of Bentall-related complications (n = 25). Among the patients who were reoperated, 5 underwent a CT scan before the second procedure (on average 38.25 days prior; in 4 cases within a time span of 6 days), which consisted of a replacement of the Bentall in three cases. The remaining 47 scans had all been acquired as routine clinical follow-up in patients who had experienced an uncomplicated procedure and uneventful 1-year follow-up.

Complication	Occurrence (n=94) ^a
Complicated postoperative hospitalization	29 (31%)
Early re-sternotomy for bleeding or infection	25 (27%)
Reoperation on, or replacement of the Bentall graft	4 (4%)
Readmission within one year of surgery for Bentall-related complications	15 (16%)
Death within one year of surgery	3 (3%)

Table 2 | Occurrence of complications. (a) The occurrence of complications is reported relative to the total number of patients included. It is possible for one patient to have experienced multiple complications (e.g. complicated postoperative hospitalization and early re-sternotomy).

Time distribution and technical parameters

These examinations acquired in the uncomplicated group were mostly obtained in the second and third postoperative months (range 28–89 days, *Figure 6*), as this is when routine follow-up is usually performed in our center. The scans in patients who experienced either a complicated procedure and/or follow-up were obtained at points in time more evenly spread throughout the entire 3-month postoperative period (range 1–90 days, *Figure 6*), most notably because scans performed for suspicion of early Bentall-related complications (i.e. bleeding/tamponade and infection) were often acquired in the first weeks following the procedure.

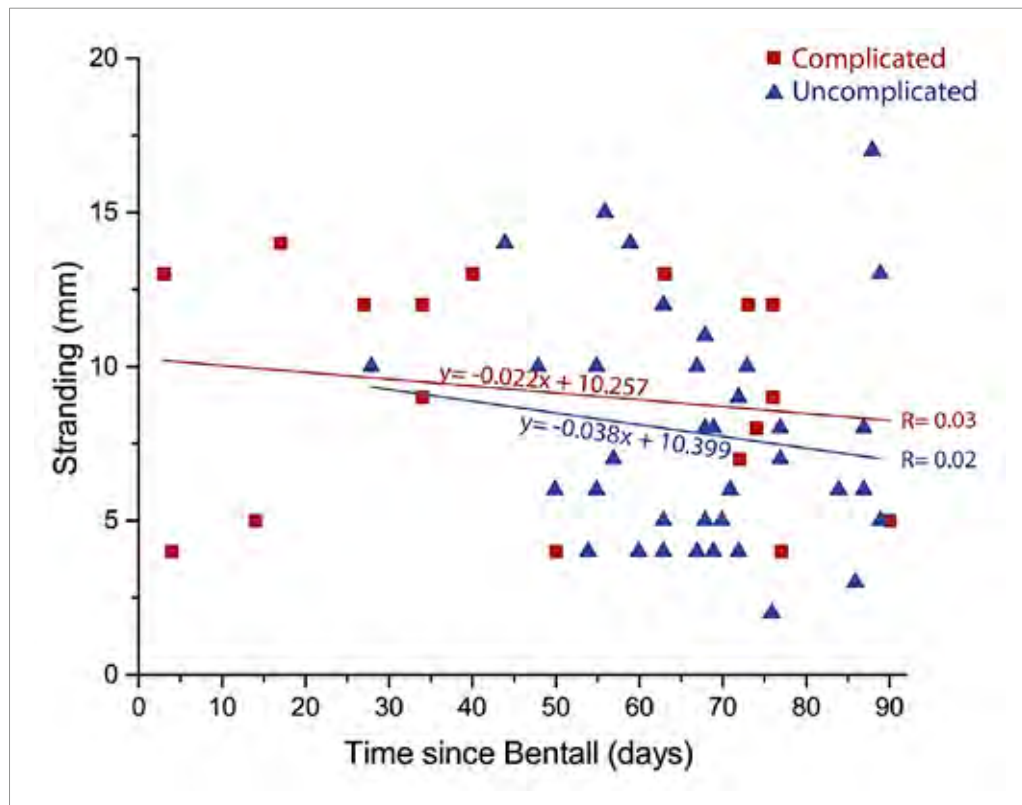


Figure 6 | Distribution of time between scans and surgery (days) and measured stranding over time (mm) in uncomplicated (blue triangles, $R^2=0.02$) and complicated (red squares, $R^2=0.03$) patients. Neither trend was statistically significant.

Fifty-five (59%) scans were ECG-gated, and all scans were contrast-enhanced. Over the years, several scanners with different technical specifications were employed: 4 slice (1 scan, 1%), 16 slice (11 scans, 12%), 40 slice (1 scan, 1%), 64 slice (26 scans, 28%), 128 slice (44 scans, 47%) and 192 slice (11 scans, 12%). Average reconstruction slice thickness was 1.5 ± 1.5 mm (range 0.75–8 mm).

Image quality

Overall image quality was reasonable to good, with an average quality of 3.2 ± 1.0 (scale from 1 to 5). Five (5%) and 22 (23%) scans were graded as poor and moderate quality respectively, mostly due to scatter artefacts and motion of the ascending aorta. The remaining 67 scans were all of reasonable (22 scans, 23%), good (43 scans, 46%) or even excellent quality (2 scans, 2%). The quality score was higher in the uncomplicated group (3.5 ± 0.78 , median 4) than in the complicated (2.8 ± 1 , median 3; $p < 0.001$), most likely due to a more frequent employment of the ECG-gating in the uncomplicated group (37 scans, 79%) than in the complicated group (18 scans, 38%; $p < 0.001$).

Stranding

Stranding was, to some extent, present in all but two of the patients (96%) in the uncomplicated group (Table 3). The subjectively graded amount of stranding in these patients ranged from none (2 scans, 4%) to moderate (6 scans, 13%), with most scans showing only slight (22 scans, 47%) or mild (17 scans, 36%) stranding around the aortic circumference. The maximum measured extent of stranding reaching out from the inner border of the aortic wall in these patients was 17 mm, while on average there was $7.7 \text{ mm} \pm 3.9 \text{ mm}$ of stranding, with 43 scans (91%) showing more than 4 mm and less than 15 mm of stranding. On the two scans that did not show any stranding, a fluid collection was identified (see below).

	Uncomplicated (n=47)	Complicated (n=47)	
Stranding grade			p=0.23
1. None	2 (4%)	12 (26%)	
2. Slight	22 (47%)	15 (32%)	
3. Mild	17 (36%)	12 (26%)	
4. Moderate	6 (13%)	7 (15%)	
5. Extensive	0 (0%)	1 (2%)	
Stranding (mean, SD, range) in mm	7.7 ± 3.9 (0-17)	6.9 ± 5.5 (0-19)	p=0.32
- Isolated stranding ^a	7.8 ± 3.6 (2-17) [n=38]	9.2 ± 3.7 (4-14) [n=17]	p=0.22
Fluid collections	6 (13%)	28 (60%)	p<0.001
- Haematoma	1 (2%)	17 (36%)	p<0.001
- Abscess	0 (0%)	2 (4%)	p=0.25
- Water-like density	5 (11%)	9 (19%)	p=0.19
Other			
- Suture-aneurysms	4 (9%)	2 (4%)	p=0.34
- Pseudo-aneurysms	0 (0%)	2 (4%)	p=0.25

Table 3 | Comparison of findings on CT between patients with uncomplicated and complicated procedure/follow-up. (a) Excluding stranding around fluid collections and pseudo-/suture-aneurysms.

9

In the complicated group on the other hand, no stranding was found in 12 patients (26%). However, in all of these 12 patients a fluid collection was identified. The results of the subjective assessment of the amount of stranding are the following: fifteen scans (32%) showed slight stranding, 12 scans (26%) mild, 7 scans (15%) moderate and 1 scan (2%) showed extensive stranding. No statistically significant difference could be found in the subjectively graded amount of stranding between patients with a complicated and an uncomplicated procedure ($p=0.22$). The maximum measured extent of stranding in these patients was 19 mm, with an average of $6.9 \text{ mm} \pm 5.5 \text{ mm}$ of stranding, which was not significantly different from the uncomplicated group ($p=0.32$).

When excluding all scans with fluid collections (since these may have influenced the amount –and reliability of the measurements– of stranding), 38 scans (81%) in the complicated group and 17 scans (36%) in the uncomplicated group showed isolated stranding. The isolated stranding averaged $7.8 \text{ mm} \pm 3.6 \text{ mm}$ in the uncomplicated group, and $9.2 \text{ mm} \pm 3.7 \text{ mm}$ in the complicated group ($p=0.22$).

Overall, when considering the measurements performed on the scans of all the included patients (in-patient analysis was not possible as only the first scan of each patient was included), there was a non-significant downward trend in the amount of isolated stranding over time, both in the complicated and uncomplicated group (uncomplicated: $R^2=0.02$, $p=0.39$; complicated: $R^2=0.03$, $p=0.51$) (*Figure 6*).

In the five scans performed before a reoperation, stranding was not present in one case (20%), and had an average extension of $12 \pm 4,5 \text{ mm}$ in the remaining four patients. Only in one case (20%) the stranding was isolated.

Fluid collections

In total, 34 fluid collections were identified: 6 in the uncomplicated group (13%) and 28 in the complicated group (60%; $p < 0.001$). Most of these fluid collections (18) could be classified as haematomas, while 14 of them were classified as having contents with a water-like density and 2 collections showed characteristics of an abscess (*Table 3*).

Almost all haematomas were identified in patients in the complicated group (1 vs. 17; $p < 0.001$), whereas fluid collections with a water-like density were found in both groups (5 vs. 9; $p = 0.19$). The one haematoma found in the uncomplicated group was identified on a scan that was acquired 66 days after the Bentall procedure and had a maximum diameter of approximately 26 mm. The reporting radiologist considered it to be a normal residual hematoma at that time, and the patient did not experience any complications during the ensuing 1-year follow-up period, yet no follow-up scans were performed. No abscesses were found in the uncomplicated group (0 vs. 2; $p = 0.25$).

Some suture-aneurysms were found in both groups (4 vs. 2; $p = 0.34$), but only in the complicated group there were 2 pseudo-aneurysms ($p = 0.25$), one of which was reoperated upon shortly after the CT scan, whereas the other one was deemed to be a residual pseudo-aneurysm after extensive *S. aureus* endocarditis.

One of the abscesses involved the valvular plane and was therefore classified also as a mycotic aneurysm. With the limitations inherent to the image quality of the scans and the lack of ECG gating of part of the scans, no vegetations of the aortic valve were found.

Finally, in the group of reoperated patients with a scan performed before the second procedure one collection with water-like density and three hematomas were found. One patient had both a hematoma and a pseudoaneurysm.

More than half of the fluid collections were accompanied by slight to moderate stranding, but in 14 scans no distinct stranding was identified besides or surrounding the fluid collection. There were no scans with neither stranding nor a fluid collection: all 94 scans showed some form of fluid around the Bentall prosthesis.

The principal finding of this study is that peri-aortic stranding is a normal post-operative phenomenon which occurs to some extent in nearly every patient following surgery on the ascending aorta, and does not necessarily warrant clinical vigilance in a patient without symptoms of bleeding or infection. We found that stranding extending up to 17 mm from the aortic circumference is a common finding on CT imaging during the first three postoperative months in both healthy patients who did not experience any complications during a 1-year follow-up period and in patients with a complicated procedure or follow-up. No differences in the amount of isolated stranding were found between the patients who experienced complications and those who did not. On the contrary, fluid collections, while being a relatively common finding on routine CT follow-up after uncomplicated procedures, were more frequently observed and showed more worrisome characteristics in the group of complicated procedures.

Peri- and post-procedural complications may occur after a Bentall procedure. The rate of early post-procedural complications varies greatly depending on the preoperative diagnosis and clinical setting⁵⁻⁸, and can be divided in those related to thoracic surgery in general and those specific to the Bentall procedure. The latter include pseudo-aneurysms, suture aneurysms, leakages, valve regurgitation or obstruction, aortic graft infection and endocarditis. The clinical relevance of these complications may vary, ranging from self-limiting to life-threatening situations that require immediate pharmacological or surgical treatment as in the case of infection and endocarditis. Since clinical presentation and time of onset after surgery are also variable, the diagnosis of complications often relies on imaging findings. Therefore, most related guidelines suggest regular follow-up by means of imaging –even in the absence of symptoms–, although there is no general consensus regarding the most appropriate timing.^{5,9,10} Preceded by transthoracic or transesophageal echocardiography, the method of choice to investigate post-Bentall patients is CT, which allows for a complete assessment of the aorta (along its entire tract, if necessary) as well as of the thorax.

However, due to the complexity of these procedures and the unique anatomical and functional features of the structures involved, morphological changes related to the physiological postoperative inflammatory response, haematoma reabsorption and an immunologic reaction to the aortic graft¹¹ without any pathological meaning can also be expected. The envisioned CT appearance of these post-procedural changes in the adipose and soft tissue surrounding the aorta may mimic that of worrisome complications such as infectious processes. This could result in either overestimation of the severity of the situation –caused in fact by a physiological process– and subsequent unnecessary investigations and therapy, or in misdiagnosis of potentially fatal complications.

These physiological changes due to the operation are expected to diminish over time; therefore, it is in the early postoperative period that the distinction with complications is expected to be more complex and a reference of normal findings is necessary. Thus, we focused our investigation on the first three postoperative months which, moreover, coincide with the time span when most early complications have been reported.⁴⁻⁶ Accordingly, notwithstanding the absence of consensus on the optimal follow-up timing, different guidelines suggest that the first imaging exam should be acquired within the first three months.^{9,10}

Although several investigators have reported the presence of stranding or collections of fluid around the aortic graft, to the best of our knowledge there is still no clear indication of what should be considered to be within acceptable limits. Sundaram et al.¹¹ regarded the presence of low-attenuation material with a thickness greater than 10 mm adjacent to the graft as a complication, despite the fact that, in their study, 10 out of the 20 patients with this finding were completely asymptomatic and demonstrated an otherwise uneventful follow-up. However, since three patients in this series had a proven graft infection and in five cases one was suspected, the presence of low attenuation material surrounding the aortic graft was later considered by others to have the potential to become a site of infection.^{12,13}

In Sundaram's study, low-attenuation material with a thickness of less than 10 mm was considered normal, and these scans were not included in the study. On the other hand, Valente et al.¹⁴ suggested an unsubstantiated upper limit of 15 mm as a normal thickness of peri-aortic fluid. Quint et al.¹⁵ reported on the presence of unspecified material adjacent to or surrounding the aorta in 74 out of 82 patients who had a CT scan in a time period of 6 months after aortic surgery. The maximum diameter of this material ranged from 4 to 80 mm. Unfortunately, the authors did not specify whether any of these patients experienced any symptoms or complications.

Fagman et al.¹⁶ investigated the accuracy of aortic wall thickness as a sign of endocarditis in patients who underwent aortic valve replacement. All dense structures adjacent to the posterior side of the aortic lumen at the level of the left atrium, where measurements were performed, were considered to be constituents of the aortic wall. Their findings showed that, in the first three months after the operation, a cut-off value of 5 mm has a sensitivity of 57% and a specificity of 67% for endocarditis.

Our study was designed to distinguish the scans of patients with relevant complications related to the procedure from those performed in patients with an uneventful follow-up, and to compare the appearance and amount of fluid surrounding the aortic graft between these two groups of patients. Therefore, for the first time, the correlation between the CT characteristics of periaortic fluid in the first three postoperative months and complicated Bentall procedures was systematically investigated based on predefined parameters. In addition, in our study, the scans were not excluded nor assigned to either one of the two groups based on the CT findings.

Criteria for the definition of a complicated procedure did not include symptoms and/or clinical presentation for two main reasons. First, in these patients the absence of a clear correlation between symptoms and complications (and even gravity of complications) is a matter of fact acknowledged by guidelines that, therefore, suggest to perform routine follow-up with imaging techniques in this population.^{9,10} Routinely imaging post-operative patients implies that a large number of scans are performed in asymptomatic patients with no clinical suspicion of complications. Second, endocarditis and leakages can be asymptomatic (especially in the early phases) or manifest with generic symptoms while determining massive structural damages that need to be promptly treated. Hence, the diagnosis of endocarditis is based on the combination of multiple criteria.¹⁷ Therefore, since many CT scans are performed as routine follow-up and the absence of symptoms does not guarantee that the patient is free from complications at the time of the exam, we investigated the correlation between CT findings and complications and not with symptoms.

9

On top of all the scans that were assigned to the complicated group because the patient experienced a complicated procedure or 1-year follow-up, we additionally assigned any scan that was not performed as routine follow-up to the complicated group (i.e. any scan that was performed for suspicion of Bentall-related complications). In our case series, only 25 patients had a suspicion of Bentall-related complications at the moment of the CT examination. Furthermore, scans performed after reoperations (including second Bentall procedures) were also assigned to the complicated group (even if this reoperation had been uneventful) due to the impossibility to ascertain the date of appearance of any findings.

For the same reason and due to the variety of the reoperations with subsequent different degrees of manipulation of the periaortic tissues and aortic graft, the exams performed after a second operation were not analysed separately. The absence of statistically significant difference in the amount of stranding (based on both the subjective and objective scoring) between the uncomplicated and the complicated group, notwithstanding the fact that the latter included patients that were operated upon twice, seems to reinforce our conclusion that stranding is a normal postoperative finding. Patients who experienced a prolonged hospitalization and who died within the first post-operative year were assigned to the complicated group regardless of the specific cause. Apart from this, other events unrelated to the Bentall procedure were not taken into account due to the unlikelihood of their influence on the presence and amount of fluid surrounding the aortic graft. This way, we ensured that the remaining scans would represent a group of patients with a truly uncomplicated procedure, uneventful follow-up and low pre-test risk.

Theoretically, as guidelines and current clinical practice suggest to perform at least one follow-up imaging exam (mainly CT) within the first three months in all operated patients^{9-11,15}, even after uneventful, uncomplicated procedures and even in the absence of symptoms, the vast majority of the low-risk population should have undergone a CT scan in this period. Moreover, since in our study all operations and monitoring were performed at the same institution, the availability of the exam was the same for all patients. Real figures of the present study differ from these expectations. Out of the 388 patients who underwent at least one Bentall procedure, only 206 had a post-operative CT scan, of which 94 were obtained in the first three months. However, half of the patients we included represent the low risk, as well as the uncomplicated, cohort. We therefore believe that our results are representative and allow us to draw conclusions on what can be considered as a normal finding in this population.

Our results suggest that the presence of fluid surrounding the aortic graft is a very common finding in post-Bentall patients. Compared to the papers mentioned above, that reported the presence of material around the aorta in most post-operative patients as well, in the current study a systematic differentiation and classification of the fluid based on its CT characteristics (appearance and amount) was introduced. Thereafter, for the first time, different imaging features were separately correlated to complications allowing identification of the most worrisome CT characteristics and distinguish them from normal findings.

In most patients, this fluid could be classified as stranding (fluid infiltrating the soft and adipose tissue surrounding the aorta), while in 34 patients at least part of the peri-aortic fluid was considered to be a fluid collection. This distinction, while evident in most cases (*Figure 2*), was sometimes very subtle, especially when there was an abun-

dance of fluid completely surrounding the aorta. In the few cases in which a high level of confidence in differentiation could not be achieved, the fluid was classified as stranding. On the contrary, no doubt arose regarding the distinction of the stranding from the thin hyperdense lines that can be found in the periaortic adipose tissue of patients who were not operated upon the ascending aorta. More importantly, isolated stranding was analysed separately from stranding associated with other findings (i.e. stranding around fluid collections, pseudo-aneurysms etc.), since these are most likely two very different entities.

Fourteen of these fluid collections had contents showing attenuation values similar to that of water: 5 in the uncomplicated group and 9 in the complicated group. While fluid collections with hyperdense contents can be ascribed to the presence of blood and/or contrast, the aetiology of the collections with water-like density is still under debate. The occurrence of peri-graft seromas with sterile fluid contents has been described for abdominal aortic grafts following open repair.^{18,19} Although many hypotheses have been postulated, their cause remains unclear but is likely to involve a failure of normal graft healing and incorporation and/or transudation of fluid through graft pores. While the collections in our series showed some compatible features on CT, the reported diagnoses of peri-graft seromas in these studies were reached later on after surgery. For instance, Kadakol et al.¹⁸ employed a cut off time of three months after surgery as a criterion in their definition of a seroma.

Some possibly confounding factors have to be taken into account concerning the definition of the extent of the stranding. Measurements were acquired mainly on the axial plane with the aid of reconstructions on coronal and sagittal planes, but double oblique reconstructions to obtain a plane perpendicular to the aortic axis were not routinely performed. We found that this did not substantially influence measurements because stranding is rarely a perfectly circular entity and the most prominent extension of the fluid is usually located along the anterior border of the aorta at the level of the pulmonary trunk, where the aorta has a course nearly perpendicular to the transverse plane. However, in some of these patients the physiological conformation of the ascending aorta and of the aortic arch is altered with a sharp anterior curvature that can reach as far as few millimetres from the sternum, resulting in the reduction of the normal amount of adipose tissue anterior to the aorta and an underestimation of the stranding at this level. All these reasons prompted us to additionally introduce a subjective grading of the overall quantity of the stranding. The subjective scale was based on the volume of the stranding as well as on the perceived proportion of the fluid in respect to the adipose tissue it was mingled with. However, an objective measure of the HU density of stranding was not feasible due to its irregular borders and different compositions proceeding from the aortic wall. Fluid collections were not measured because they had such an irregular shape that linear measurements would not be representative of the real dimensions.

One of the limitations of the present study is the relatively small number of patients with an uncomplicated procedure who underwent a CT scan in the analysed period. Another limitation which has to be considered, is the inconsistency of the time points at which the CT scans were acquired. The scans were widely spread throughout the second and third post-operative months in the uncomplicated group, while most scans in the complicated group were performed within the first month. Unexpectedly, we did not find any statistically significant reduction in the amount of stranding over time in either

9

of the two groups; however, the short period we analysed, the heterogeneous distribution of exams throughout this period, the choice to include only the first scan of each patient and the fact that some patients underwent two operations before the CT are all variables that might have influenced this result, which therefore has to be interpreted with caution. Furthermore, over the years, several different CT scanners, protocols and acquisition methods were employed, which may have influenced our findings to some extent. Finally, in order to assess normal findings, we separated CT scans that had been performed for indications other than a routine check and assigned them to the complicated group. All scans were re-assessed by an operator blinded to the patient's categorization and to the clinical report. To prevent a selection bias, the CT findings themselves, of both the clinical report and the independent re-assessment, were deliberately not used to distinguish normal from abnormal follow-up. However, due to the retrospective nature of this study, some degree of selection bias could not be avoided since CT findings were likely to have influenced the patients' management. This also implies that some of the findings such as the more extensive fluid collections or haematomas in otherwise uncomplicated patients –although not associated with any complications within a one-year follow-up- may not be representative of a normal healing process. Merely the fact that the patient did not experience any symptoms or adverse clinical outcome, does not mean that the findings on CT can be considered normal.

Conclusions

The presence of fluid around the aortic graft during the first three postoperative months can be found on CT in all patients following a Bentall procedure. This fluid can be classified as stranding or as a fluid collection based on its characteristics on CT. The extent of isolated stranding does not differ between patients who experienced a complicated or an uneventful procedure and follow-up, and can thus be considered a normal finding. Even when extending up to 17 mm from the inner border of the aortic wall, the presence of isolated stranding does not necessitate any management other than the usual follow-up. Fluid collections on the other hand, are more common in patients who experienced complications either during the procedure or in the course of follow-up, and may require closer monitoring.

References

1. Bentall H, de Bono A. A technique for complete replacement of the ascending aorta. *Thorax*. 1968;23:338–9.
2. Chu, LC, Johnson, PT, Cameron, DE, Fishman, EK. MDCT Evaluation of aortic root surgical complications. *Am J Roentgenol*. 2013;201:736–44.
3. Christensen JD, Seaman DM, Washington L. Imaging of complications of thoracic and cardiovascular surgery. *Radiol Clin North Am*. 2014;52:929–59.
4. Hirasawa Y, Aomi S, Saito S, et al. Long-term results of modified Bentall procedure using flanged composite aortic prosthesis and separately interposed coronary graft technique. *Interact Cardiovasc Thorac Surg*. 2006;5:574–7.
5. Svensson LG, Adams DH, Bonow RO, et al. Aortic valve and ascending aorta guidelines for management and quality measures: executive summary. *Ann Thorac Surg*. 2013;95:1491–505.
6. Akins CW, Miller DC, Turina MI, et al. Guidelines for reporting mortality and morbidity after cardiac valve interventions. *J Thorac Cardiovasc Surg*. 2008;135:732–8.
7. Sundaram B, Quint LE, Patel HJ, Deeb DM. CT findings following thoracic aortic surgery. *Radiographics*. 2007;27:1583–94.
8. Zehr KJ, Orszulak TA, Mullany CJ, et al. Surgery for aneurysms of the aortic root: a 30-year experience. *Circulation*. 2004;110:1364–71.
9. Hiratzka LF, Bakris GL, Beckman JA, et al. 2010 ACCF-AHA-AATS-ACR-ASA-SCA-SCAI-SIR-STS-SVM guidelines for the diagnosis and management of patients with thoracic aortic disease. *Circulation*. 2010;121:e266–369.
10. Erbel R, Aboyans V, Boileau C, et al. 2014 ESC guidelines on the diagnosis and treatment of aortic diseases. *Eur Heart J* 2014;35:2873–926.
11. Sundaram B, Quint LE, Patel S, et al. CT appearance of thoracic aortic graft complications. *Am J Roentgenol*. 2007;188:1273–77.
12. Hoang JK, Martinez S, Hurwitz LM. Imaging of the postoperative thoracic aorta: the spectrum of abnormal findings. *Semin Roentgenol*. 2009;44:52–62.
13. Sundaram B, Quint LE, Patel HJ, Deeb GM. CT findings following thoracic aortic surgery. *Radiographics*. 2007;27:1583–94.
14. Valente T, Rossi G, Rea G, et al. Multidetector CT findings of complications of surgical and endovascular treatment of aortic aneurysms. *Radiol Clin North Am*. 2014;52:961–89.
15. Quint LE, Francis IR, Williams DM, et al. Synthetic interposition grafts of the thoracic aorta: postoperative appearance on serial CT studies. *Radiology*. 1999;211:317–24.
16. Fagman E, Bech-Hansen O, Flinck A, et al. Increased aortic wall thickness on CT as a sign of prosthetic valve endocarditis. *Acta Radiol*. 2016;57:1476–82.
17. Habib G, Lancellotti P, Antunes MJ, et al. 2015 ESC Guidelines for the management of infective endocarditis: The Task Force for the Management of Infective Endocarditis of the European Society of Cardiology (ESC). *Eur Heart J*. 2015;36:3075–128.
18. Kadakol AK, Nypaver TJ, Lin JC, et al. Frequency, risk factors and management of perigraft seroma after open abdominal aortic aneurysm repair. *J Vasc Surg*. 2011;54:637–43.
19. Ahn SS, Machleder HI, Gupta R, Moore WS. Perigraft seroma: clinical, histologic and serologic correlates. *Am J Surg*. 1987;154:173–8.



CHAPTER 10

CT ANGIOGRAPHY FOR DEPICTION OF COMPLICATIONS AFTER A BENTALL PROCEDURE

Laurens Swart¹
Sara Boccalini¹
Jos Bekkers
Koen Nieman
Gabriel Krestin
Ad Bogers
Ricardo Budde

10

Published in: British Journal of Radiology 2018

Abstract

Following a Bentall procedure, which comprises a composite replacement of both the aortic valve and the ascending aorta, the imaging modality of choice to depict known or suspected complications is CT angiography. An update and extension of the literature regarding complications after the Bentall procedure is provided. The wider availability of ECG-gating has allowed for a clearer depiction of the aortic valve and ascending aorta. This resulted not only in the identification of previously undetectable complications, but also in a more precise assessment of the pathophysiology and morphology of known ones, reducing the need for additional imaging modalities. Moreover, the possibility to combine positron emission tomography images with CT angiography offers new insights in case of suspected infection. Due to the complexity of the operation itself and concomitant or subsequent additional procedures, as well as the wide spectrum of underlying pathology, new scenarios with multiple complications can be expected.

Introduction

The most common pathologies that involve the ascending aorta, namely large aneurysms and type A dissections, require surgical treatment with aortic replacement mainly in an elective and emergency setting, respectively. This procedure may also involve simultaneous replacement of the aortic valve whenever the aforementioned pathology is accompanied by aortic stenosis or insufficiency. One of the options, representing the procedure of choice at our institution, is the implantation of a single composite graft in a one-step surgery (Bentall procedure).¹

Since its introduction in 1968 different methods to perform this intervention have been practiced.^{1,2} A mechanical or biological aortic valve prosthesis can be employed with the same general indications and limitations as in isolated aortic valve replacements. The aortic valve prosthesis can be sutured to the aortic graft in the operating room by the surgeon or, more commonly, the two components can be manufactured and employed as a single unit. The native aortic wall can be left in place and wrapped around the prosthesis (inclusion technique) although it is generally excised and substituted by the graft (interposition technique, *Figure 1*).

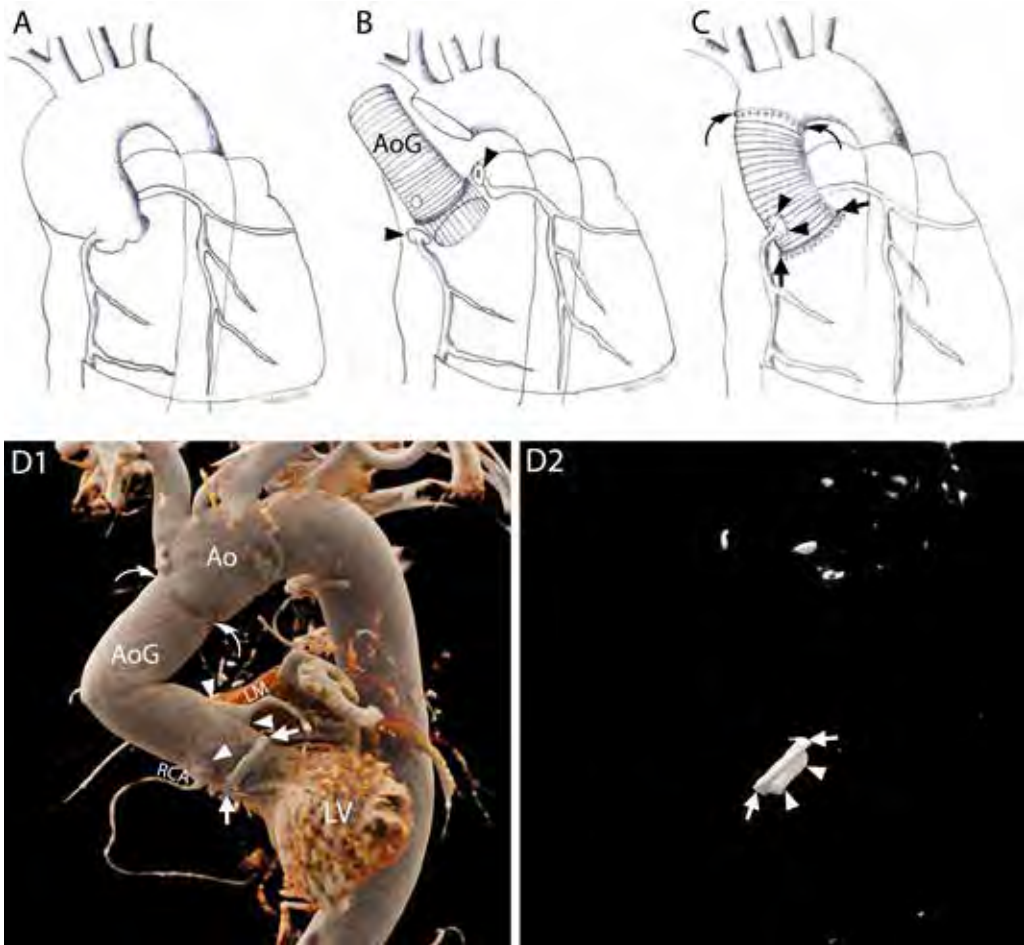


Figure 1 | The Bentall procedure. **A-C** – Schematic representations of the most commonly practiced variation of the Bentall procedure. The native wall of the aneurysmatic (**A**) or dissected ascending aorta is excised together with the stenotic or insufficient aortic valve (interposition technique). The ostia of the coronary arteries are cut out with a button of the native aortic wall attached (button technique) (**B**, **arrowheads**). The aorta and the aortic valve are substituted by one or multiple grafts (**B**, **AoG**) and a prosthetic aortic valve which are sutured to the left ventricle outflow tract (LVOT) (**C**, **arrows**) and the native aorta (**C**, **curved arrows**). The buttons around the coronary ostia are reattached to the aortic graft (**C**, **arrowheads**). **D1-D2** – 3D reconstructions of CTA images of a patient who underwent a Bentall procedure with the implantation of a mechanical aortic valve, performed according to the technique described above, showing the exterior surface of the aortic prosthesis and native aorta (**D1**) and the prosthetic aortic valve within (**D2**), respectively. **D1** – ring of the aortic valve (**arrows**); aortic grafts (**AoG**); anastomosis of the coronary arteries (**arrowheads**); distal suture line with the native aorta (**curved arrows**). **D2** – metallic ring of the aortic valve (**arrows**); leaflet of the mechanical valve (**arrowheads**). Ao – native aorta, LM – left main, LV – left ventricle, RCA – right coronary artery. Sketches drawn by S. Boccalini (2018).

One of the most crucial aspects of the operation is the reattachment of the coronary arteries. The original procedure described by Bentall involved directly suturing the aortic wall around the coronary ostia to the graft. This was complicated by bleeding and pseudoaneurysm formation caused by excessive wall tension and tearing of partial-thickness sutures. In 1981, with the introduction of the Cabrol procedure, a prosthetic conduit was anastomosed to the coronary ostia and side-to-side to the aortic graft. Intrinsic complications of the Cabrol procedure included early postoperative death in patients with aortic dissection, anastomotic leak, coronary graft insufficiency from kinking or intimal hyperplasia, acute coronary graft thrombosis, and endocarditis.³ The modified Bentall procedure addressed these problems by mobilizing the coronary ostia with a button of native aortic wall, thus reducing wall tension and allowing an all-thickness suture to the aortic prosthesis (*Figure 1*).

The Bentall procedure can also be combined with other procedures extending to the aortic arch (such as a partial or complete aortic arch replacement, the Elephant trunk technique, etc.) depending on the extent of the aorta that is affected.⁴

CT scan timing and protocol

After the Bentall procedure, imaging investigations are indicated not only if complications are suspected, but also for routine follow-up in asymptomatic patients. CT is generally the modality of choice.⁵⁻⁸ However, the best timing for routine exams has not been ascertained and different schemes are suggested in guidelines.^{6,7,9} The underlying pathology should also be taken into account to decide the best schedule. Whilst at least one CT scan should be performed within the first three post-operative months in all patients, in case dissection was the cause of the procedure, adding more controls, at 1 and 6 months, is suggested.⁷ Thereafter, a control after the first year should be planned and, if no signs of complications are found, a yearly follow up can be foreseen.

When planning the scan the protocol should be adapted for each case, and tailored to the specific clinical question. Therefore, it is essential that the details of the surgical technique be provided (or searched if not provided) to optimize the acquisition as well as to aid in the successive interpretation.

If the scan is performed in the setting of routine follow-up, an aortic protocol with thin-slice reconstructions ($\leq 1\text{mm}$) can be employed. ECG-gating or triggering is always recommended. However, if no complications are suspected, prospective triggering and especially high-pitch prospectively triggered acquisitions, if available, should be preferred to limit the radiation dose.

Whenever complications involving the valve, either mechanical or infectious, are suspected, an acquisition with retrospective ECG-gating will allow assessment of the motility of the leaflets and the movement of any vegetations or thrombi. If the presence of hemorrhage (including intramural hematoma of the native aortic wall) or leakage is investigated, an unenhanced acquisition will help establishing the nature of any hyperdense areas and, therefore, distinguish surgical material from calcifications, blood and contrast. Reconstructions of both pre- and post-contrast injection acquisitions should be performed with the same thickness to ease comparison. In case coronary artery stenoses have to be ruled out, an appropriate protocol should be adopted.

Although in routine follow up the sole thoracic aorta/thorax can be investigated, in specific scenarios the scan should be extended to include also the abdomen. This is the case for suspected extension of the dissection and/or hematoma and patients presenting increasing aortic diameters on preceding controls. However, since aortic pathology might involve any segment of the vessel, the entire aorta should be included in the scan range and assessed at least once.⁶

Normal findings

The normal post-operative CT appearance of prosthetic aortic valves (*Figure 2*), aortic grafts (*Figure 3*), as well as other surgical materials (*Figure 4*) should be known beforehand to be able to distinguish complications and avoid misdiagnosis.

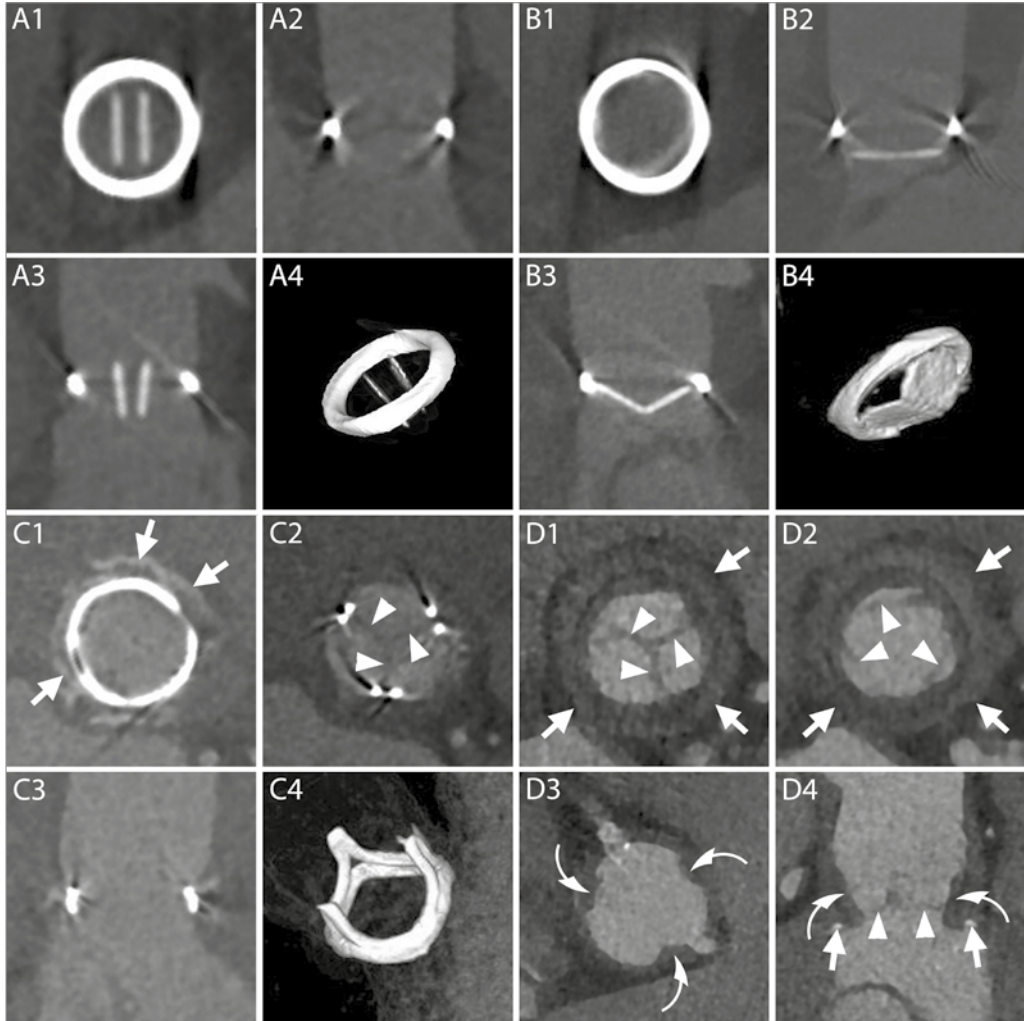


Figure 2 | Normal aspect of prosthetic heart valves. **A1-B4** – CT aspect of the most commonly employed mechanical prosthetic valve (St. Jude, Abbot). The bi-leaflet valve is shown with open and closed leaflets respectively during systole (**A1-A4**) and diastole (**B1-B4**). **A1** and **B1** – multiplanar reconstructions (MPR) on planes perpendicular to the centerline of the aorta at the level of the outer ring of the valve. **A2** and **B2** – MPR parallel to the centerline of the aorta and parallel to the direction of the leaflets. **A3** and **B3** – MPR parallel to the centerline of the aorta and perpendicular to the direction of the leaflets. **A4** and **B4** – volume rendering (VR) of the valve. **C1-C4** – CT aspect of a stented biological valve during diastole. **C1** and **C2** – MPR on planes perpendicular to the centerline of the aorta respectively at the level of the most caudal (**C1**) and most cranial (**C2**) part of the metallic stent. In **C1** the pledgets used to reinforce the sutures on the suture ring are visible

(**arrows**). The biological leaflets are attached to the frame and when closed have an appearance similar to a native tricuspid aortic valve (**C2, arrowheads**). **C3** – MPR parallel to the centerline of the aorta. **C4** - VR of the valve. **D1-D4** – CT aspect of a stentless biological valve. **D1** and **D2** – MPR on planes perpendicular to the centerline of the aorta at the level of the suture ring of the valve (**arrows**) showing the three closed (**D1**) and open (**D2**) leaflets (**arrowheads**). **D3** – More cranially, at the level of the coronary arteries ostia, the outer frame of the valve appears as small hypodense irregularities (**curved arrows**) of the aortic contour protruding in the lumen. **D4** – A MPR parallel to the centerline of the aorta shows the cusps of the leaflets (**arrowheads**), the outer frame of the valve (**curved arrows**) and the pledgets used to reinforce the sutures (**arrows**).

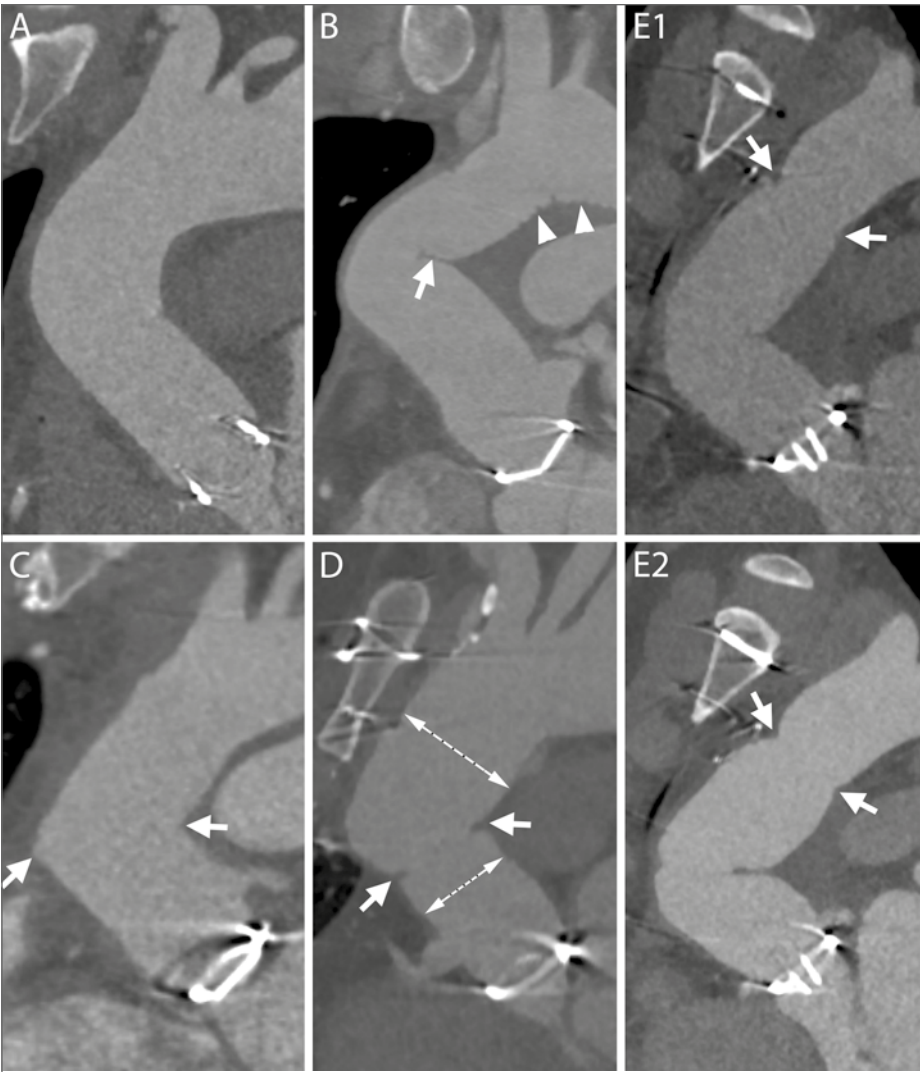


Figure 3 | Normal aspect of aortic grafts. **A** – The aortic graft can present a smooth outer contour and appear similar to a native aorta. **B** – Especially in case of a sharp angulation of the ascending aorta and in case a long graft has been employed, the fabric of the graft can present an inward fold projecting inside the aortic lumen (**arrow**). The small grooves of the outer surface of the graft can also be visible on CT scans (**arrowheads**). **C** – When two grafts are employed, a sharp angle in the contour of the ascending aorta may develop at the level of the connection (**arrows**). **D** – If needed for anatomical reasons, the two employed grafts can have different sizes (**two dashed lines**) and a slight inward fold is seen at the level of the suture (**arrows**). **E1-E2** – Two consecutive scans of the same patient, acquired within less than one year, show a change in angulation and appearance of the aortic grafts. The distal suture of the more caudal of the grafts with the native aorta is evident as it appears as a stricture in the aortic contour (**E1-E2, arrows**).

In particular, since surgical material is generally hyperdense and located at the level of the sutures, it could be confused for extravasated contrast media. The most reliable way to distinguish the two entities is by comparing enhanced and unenhanced images. While on enhanced images their appearance and density might be similar, on unenhanced images only the surgical material will be visible as a hyperdense structure (*Figure 4* and *Figure 5*).

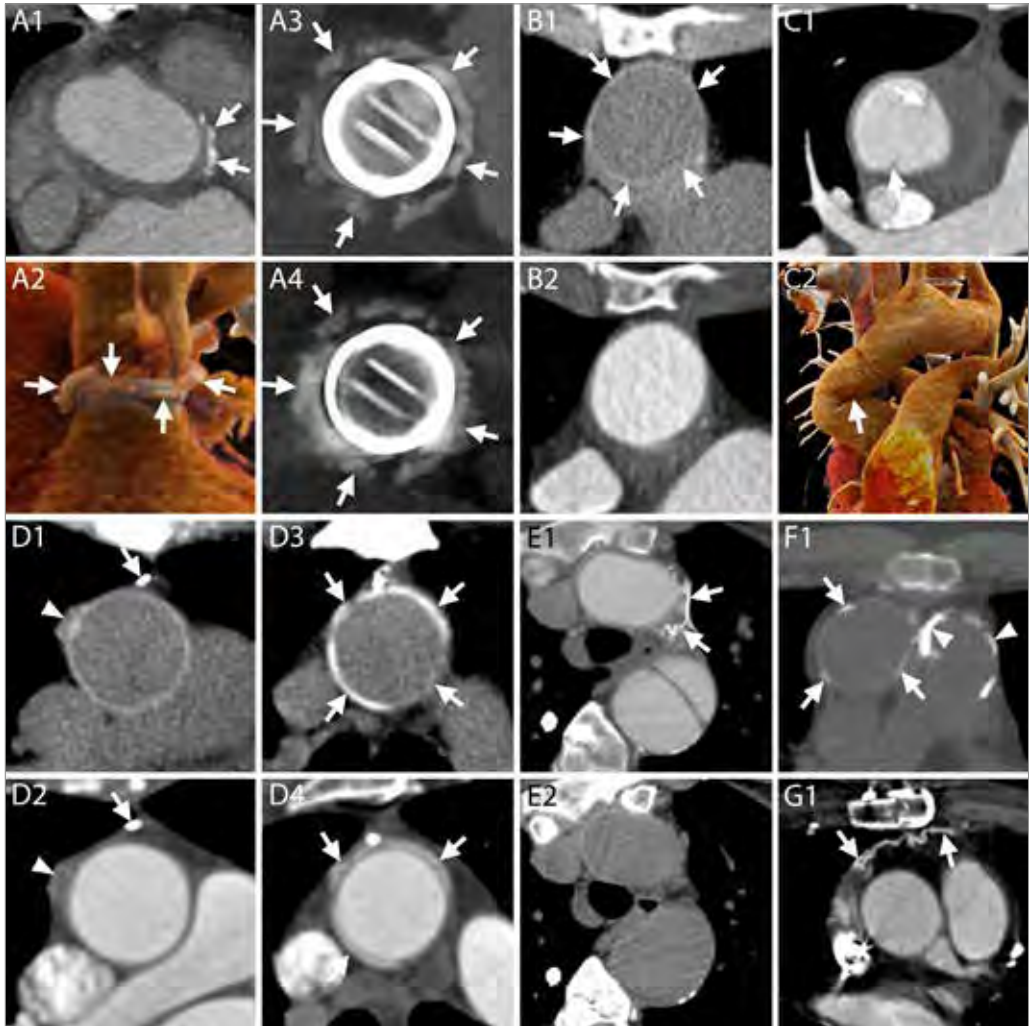


Figure 4 | Surgical material and potential pitfalls. **A1-A4** –CT appearance of pledgets. After a Bentall procedure or surgical aortic valve replacement, hyperdense material can be seen around the aortic root on axial images (**A1**, arrows). These hyperdense images represent pledgets that are employed by surgeons to reinforce the sutures on the suture ring of the valve and should not be mistaken for extravasated contrast. The material can be seen surrounding the junction of the LVOT and the aortic root (**A2**, arrows), at a short distance from the valvular ring (**A3**, arrows), although generally not all on the same plane (**A2**). An un-enhanced acquisition can be useful to assess the presence of the images also before contrast administration and confirm their nature (**A4** arrows). **A1** – Axial image. **A2** - 3D reconstruction. **A3-A4** - MPR with maximum intensity

projection reconstructions on planes perpendicular to the centerline of the aorta of enhanced and unenhanced acquisitions, respectively. **B1-B2** – CT appearance of the aortic graft. **B1** - On unenhanced acquisitions, the aortic graft appears as a thin rim of hyperdense material (**arrows**). **B2** - On contrast-enhanced acquisitions, the graft cannot be distinguished from the contrast in the aortic lumen. **B1-B2** - Axial images. **C1-C2** – At the level of the ascending aorta, one or two hypodense lines can be spotted in the aortic lumen (**C1, arrows**) of some post-Bentall scans. They should not be mistaken for new or residual intimal flaps as they represent an inward fold of the graft that can be more easily identified on VR (**C2, arrow**) or MPR reconstructions (see panel B of **Figure 3**). **C1** - Axial image. **C2** - 3D reconstruction. **D1-D4** – Surgical material adjacent to the aortic graft. **D1-D2** - Surgical material includes metallic clips with very high attenuation values (**D1** and **D2, arrows**) as well as other slightly hyperdense structures (**D1** and **D2, arrowheads**), usually placed at the cannulation sites, which are identifiable on unenhanced acquisitions (**D1**) but can hardly be distinguished from the adjacent periaortic tissue on enhanced acquisitions (**D2**). **D3-D4** – PTFE can be employed to reinforce the distal suture line of the aortic graft and appears as hyperdense material surrounding the aorta (**D3** and **D4, arrows**), on both unenhanced (**D3**) and enhanced acquisitions (**D4**). **D1-D4** – MPR. **E1-E2** – It is not uncommon in these patients to have collateral vessels in the mediastinum that might fill with contrast (**E1, arrows**) and may therefore appear very hyperdense, making them easy to be mistaken for surgical material. Contrary to surgical material, the vessels are not visible on corresponding unenhanced slices (**E2**). **E1-E2, F1, G1** - Axial images. **F1** – Calcifications can appear on aortic grafts (**arrows**) implanted years before (in this case example the Bentall had been performed 12 years prior to the CT scan). Calcifications may also be seen at the level of the pulmonary valve (**arrowheads**) indicating a previous Ross procedure. **G1** – After the procedure the pericardium is generally left open and without sutures. However, in some circumstances, it can be closed with a patch of synthetic material (**arrows**).

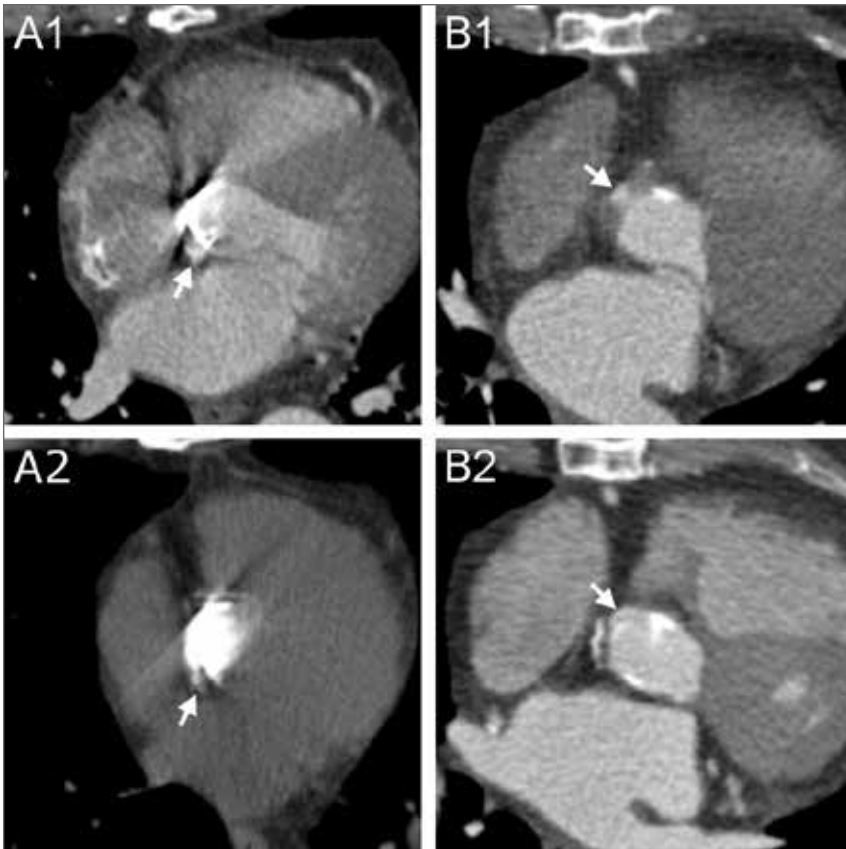


Figure 5 | Differentiation between surgical and contrast material. **A1-A2** – Surgical material adjacent to the prosthetic valve possibly mistaken for contrast medium. On enhanced acquisitions (**A1**), a hyperdense rounded structure situated in the close proximity of proximal (or distal) suture lines (**arrow**) could be interpreted as surgical material, particularly a pledget, or as extravasated contrast medium. However, on unenhanced acquisitions (**A2**) only surgical material is visible (**arrow**) and, therefore, hyperdense structures present in the same location on both acquisitions are attributed to exogenous matter employed during the Bentall procedure. **B1-B2** – Small pseudoaneurysm mistaken for surgical material. On a first postoperative scan (**B1**) an axial image of an enhanced acquisition showed a small hyperdense structure (**arrow**) close to the aortic prosthesis that was not reported as it was mistaken for a pledget. In this case an unenhanced acquisition was not performed. The real etiology of this structure was appreciated on a second enhanced exam (**B2**) where, due to changes in aortic orientation, it was clear that the structure (**arrow**) was in communication with the LVOT and should therefore be referred to a small pseudoaneurysm.

The origin of the coronary arteries after the anastomosis commonly has a peculiar appearance that has been incorrectly referred to as a “pseudoaneurysm” (Figure 6).¹⁰ The aortic arch can be involved in the procedure, thus radiologists should be familiar also with procedures at this level (Figure 7). The native aorta should be assessed for the presence of residual or new complications (Figure 7), including dissections and intramural hematoma.

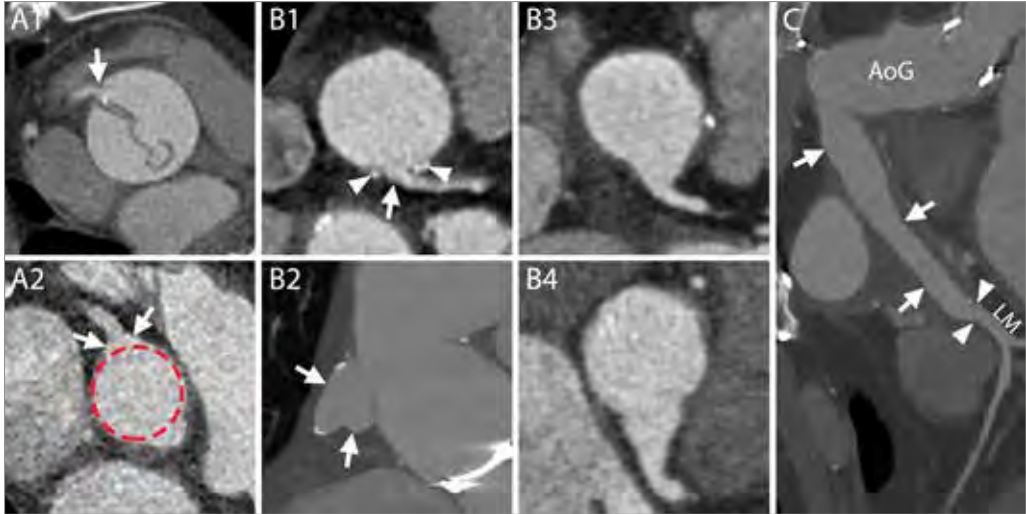


Figure 6 | Normal aspect of coronary artery sutures and origin. **A1-A2** – The most commonly practiced version of the Bentall procedure includes preservation of a “button” of native aortic wall around the coronary ostia that will be sutured to the aortic graft. Therefore, most commonly, even coronaries that before the operation had an abrupt origin from the aortic wall (**A1, arrow**) after the operation will show an enlarged emergence (**A2, arrows**) protruding from the circular profile of the graft (**A2, red line**) due to the additional tissue of the button of the native aorta. **A1-A2** – MPR perpendicular to the centerline of the aorta. **B1** and **B2** – Depending on the extension of the resected native aortic wall, the appearance of the new origin of the coronary artery can be very different, as shown in these two case examples: almost normal (**B1, arrow** at the origin of the left coronary artery) or very enlarged (**B2, arrows** at the origin of the right coronary artery). Surgical material can be seen at the level of the suture lines (**B1, arrowheads**). **B3** and **B4** – The shape of the origin can be different as well, and can have a “trumpet-like” (**B3**) or “flask-like” (**B4**) appearance. **B1, B3, B4** – MPR perpendicular to the centerline of the aorta. **B2** – MPR parallel to the centerline of the aorta. **C** – A graft (**arrows**) can be interposed between the aortic graft (**AoG**) and the native coronary artery (**arrowheads**). In this case the procedure is referred to as “Cabrol procedure”. Curved planar reformation (CPR). AoG – aortic graft, LM – left main.

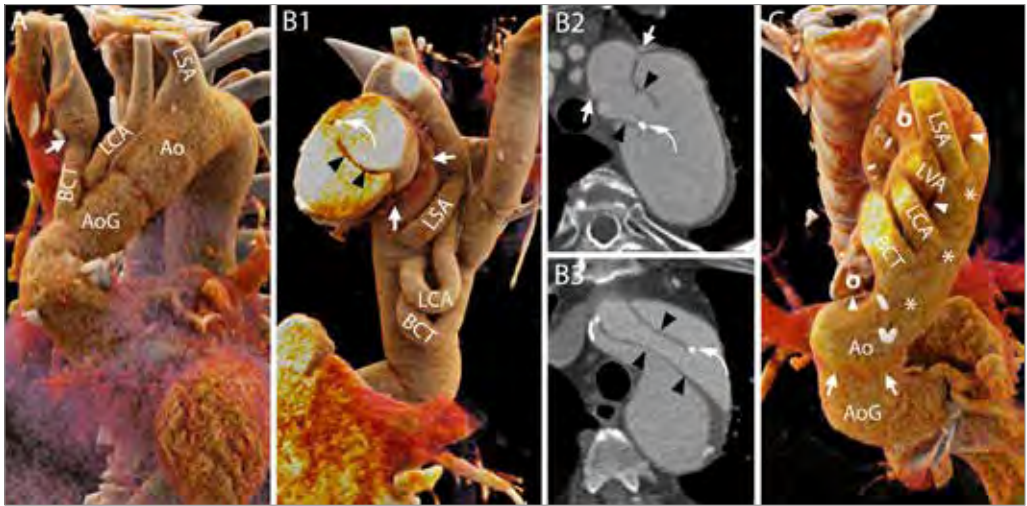


Figure 7 | Normal aspect of the aortic arch and aortic branches. **A** – Hemi-arch replacement. In this patient, the aorta was replaced up to the mid-arch. Therefore, only the brachiocephalic trunk (BCT) and the left carotid artery (LCA) were “debranched” and re-attached to the aortic graft with the interposition of surgical grafts. In some cases, the level of the suture line along the aortic branches can be easily recognized due to the mismatch of caliber between the native vessel and the graft (**arrow**). On the contrary, the left subclavian artery (LSA) was left attached to the native aortic arch. 3D reconstruction. **B1-B2** and **B3** – Elephant trunk (**B1-B2**) and confounders (**B3**). In case the entire arch has to be replaced and the descending aorta is dilated to such an extent that further interventions are required, the “Elephant trunk” technique can be employed. During the first step of this procedure, the aortic arch is replaced and sutured to the native aorta, where the felt used to reinforce the suture can be seen on CT images (**B1** and **B2**, **arrows**), and the BCT, LCA and LSA are re-attached to the graft (**B1**). The most characteristic feature of the procedure is that the aortic graft has some additional fabric attached to the distal edge that is left floating freely in the lumen of the native aorta (thus the name “elephant trunk”) and will guide and ease future interventions on the proximal descending aorta. The fabric appears on CT images as hypodense lines (**B1-B2**, **arrowheads**) that should not be mistaken for intimal flaps that might have an analogous aspect (**B3**, **arrowheads**). Although a metallic component is added to the distal end of the trunk to ease its visualization (**B1** and **B2**, **curved arrows**), intimal flaps can have similar looking calcifications (**B3**, **curved arrows**). **B1** - 3D reconstruction. **B2** and **B3** - axial images. **C** – Residual dissection. Distal to the suture line (**arrows**) of the aortic graft the dissection can be left into place with its true lumen (**asterisks**) in continuity with the lumen of the graft. The aortic branches (including the independent origin of the left vertebral artery, **LVA**) all originated from the true lumen very close to the intimal flap (**arrowheads**) and the false lumen (**circles**). 3D reconstruction seen from above. Ao – native aorta, AoG – aortic graft, BCT – brachiocephalic trunk, LCA – left carotid artery, LSA – left subclavian artery, LVA – left vertebral artery.

Multiplanar reconstructions should be employed to assess the valves in all their parts, on planes perpendicular and parallel to the long axis of the aorta. Three-dimensional reconstructions can also aid in the visualization of anomalies of the components of the valves (*Figure 2*).

Peri-aortic fluid

Postoperative changes can be expected in the tissues surrounding the aorta due to manipulation during the procedure and related healing processes, especially shortly after the operation. In particular, it has been shown that the presence of fluid around the aortic graft can be demonstrated in all patients undergoing a CT scan in the first three post-operative months. However, CT characteristics of the fluid can help establishing its aetiology and potential clinical consequences.¹¹

For instance, the presence of peri-aortic fluid in the form of stranding (fluid mingled with adipose tissue, without clear borders and completely surrounding the aortic graft) in the first three post-operative months can be considered a normal finding, even when extending up to 17 mm from the border of the graft (*Figure 8*).¹¹



Figure 8 | Peri-aortic fluid in the form of stranding and fluid collections. **A-C** – Three different cases showing increasing amounts of peri-aortic fluid in the form of stranding. The scans were performed 55 (**A**), 69 (**B**) and 59 (**C**) days after an uncomplicated operation. In all cases, the patients had undergone an uneventful procedure and did not have any complications within the first year following the operation. **D** – A fluid collection with water-like content (**aster-**

isk) twelve days after a Bentall procedure in an 83-year-old woman. The patient was reoperated nine months later because of progressive dilation of the descending aorta. **E** – The day after a Bentall operation for type A dissection extending to the right carotid artery, this 61-year-old man presented a reduction of hemoglobin levels that prompted to investigate the source of bleeding. A CT scan was performed which highlighted the presence of a hematoma completely surrounding the aorta (**asterisks**). The patient died two days later for neurological complications. **F1-H2** – A 53-year-old woman who had undergone a Bentall and a MAZE procedure four days before started complaining of posterior chest pain at the level of Th7. A CT scan (**F1** and **F2**) performed for the suspicion of spondylodiscitis or mediastinitis demonstrated a fluid collection (**asterisks**) with water-like density surrounding the aortic graft. Three days later, the patient had high fever and a new CT scan was performed to locate the focus of infection. Axial images (**G1** and **G2**) showed an increase in diameter of the previously reported fluid collection (**asterisks**) that had, at that time, clear characteristics of an abscess with air bubbles inside and slight compression of the prosthesis (**arrowheads**). Appropriate antibiotic therapy was started. The day after an unenhanced CT scan (**H1** and **H2**) demonstrated an increase in the air content of the collection (**asterisks**) albeit with an overall reduction in size and a restoration of the normal aortic graft appearance (**arrowheads**). The following day, the patient was re-operated and the collection drained.

On the contrary, fluid with defined and clear borders, not necessarily completely encircling the aortic graft, is referred to as a fluid collection and can be divided into subtypes based on the radiodensity (in HU) of its contents (water-like content, hematoma, contrast, contrast and hematoma together) (*Figure 8*). Although identifiable in the first months after the procedure, even in patients who underwent a successful operation without complications, fluid collections are more often associated with complicated procedures.¹¹

When infected, fluid collections may show CT characteristics of abscesses: wall enhancement, air inside the collection or fistula with other organs (*Figure 8*).

Complications

After Bentall procedures with mechanical valves, a pooled rate of early post-operative mortality of 5.6% and an event rate of reoperation of 1.01% per year have been reported.¹² Data on late mortality and complications are still lacking.

Valve

With an estimated cumulative incidence at 10 years of 26.6%, complications involving mechanical valves are among the most common.¹² Although traditionally investigated with transthoracic or trans-esophageal echocardiography, all complications at the level of the valve can be depicted with CT.¹³

Mechanical causes of valve malfunctioning include the degeneration of the leaflets of biological valves and the presence of pannus/thrombus (*Figure 9*).¹⁴ Evaluation of these alterations is possible with ECG gated or triggered scans that reduce motion artifacts at the level of the valve and surrounding structures (*Figure 10*). Furthermore, ECG-gated acquisitions allow assessment of the dynamics of the valves and, for mechanical valves, the opening and closing angles of the leaflets, which have to be compared to normal values for that specific valve type.¹⁴

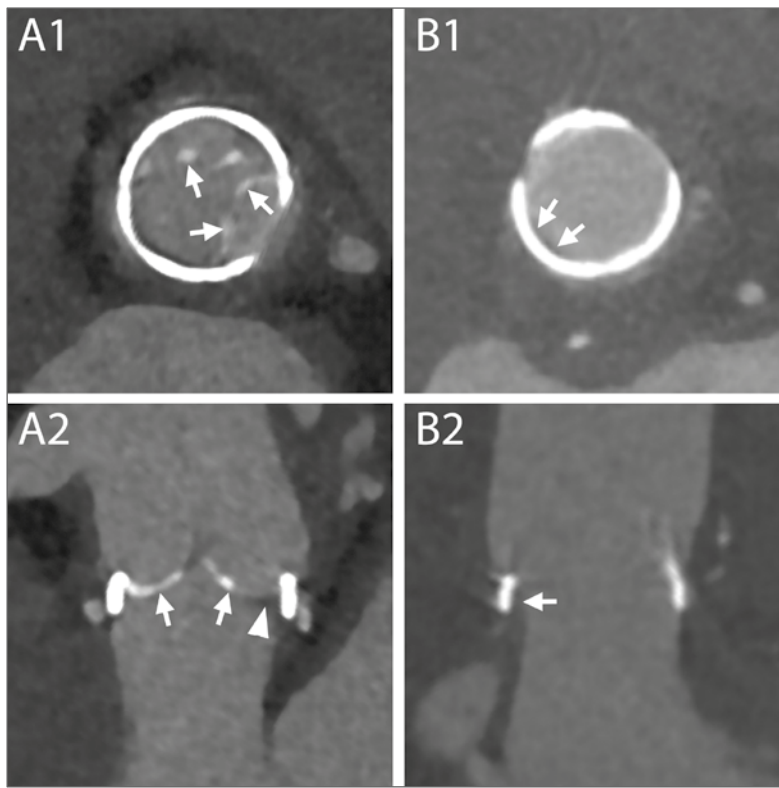


Figure 9 | Mechanical alterations to aortic valve prosthesis function. **A1-A2** – MPR reconstructions perpendicular (**A1**) and parallel (**A2**) to the centerline of the aorta demonstrating calcifications (**arrows**) and thickening (**arrowheads**) of the leaflets of a biological valve implanted 7 years before this scan in a 37-year-old man. The degeneration of the leaflets caused a severe, although asymptomatic, stenosis (4,5m/s at echo) and the valve was replaced a few months later. **B1-B2** – A follow-up CT scan in a 81-year-old woman revealed the presence of a thin rim of hypodense material (**arrows**) adjacent to the ring of this biological valve, which was implanted 4 months before, on both MPR reconstructions perpendicular (**B1**) and parallel (**B2**) to the centerline of the aorta. Although an infectious origin could not be ruled out with certainty based solely on CT characteristics, the laminated and smooth aspect of the material along the contour of the metallic ring indicated that it should more likely be ascribed to thrombus/pannus.

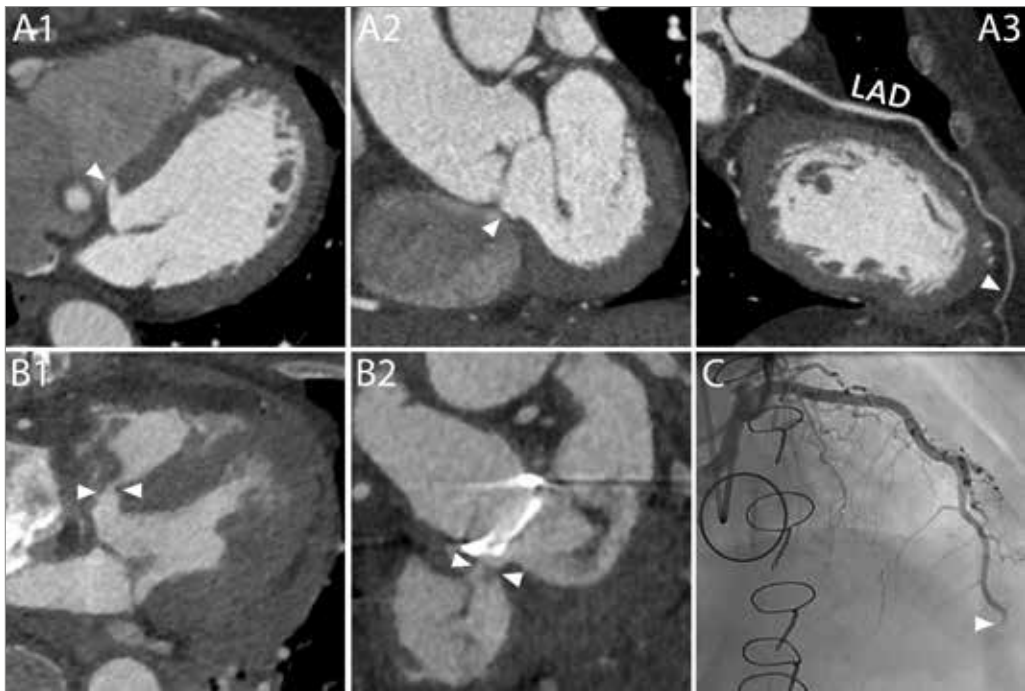


Figure 10 | Small perforation of the membranous ventricular septum after resuscitation of a patient with a Bentall prosthesis due to an acute mid-LAD occlusion approximately 1 month after implantation. This 70-year-old female patient without prior history of coronary artery disease underwent a Bentall procedure for a dilated ascending aorta. At the last follow-up scan prior to the procedure, a distinct thin membranous part of the septum was clearly illustrated (**A1, A2, arrowheads**). No signs of any concomitant coronary artery disease were found (**A3**). One month after Bentall implantation, the patient experienced an acute ST elevated myocardial infarction (STEMI) with ventricular fibrillation, for which she was successfully resuscitated. An emergency CT scan did not show any signs of aortic dissection, but did give the impression of a small perforation (**arrowheads**) of the membranous ventricular septum on the axial images (**B1**), which became even more evident on the multi-planar reconstructions (**B2**), possibly due to either the Bentall implantation or the resuscitation itself. Coronary angiography revealed a new mid-LAD occlusion (**C, arrowhead**) as the probable cause of the STEMI, but ensuing emergency PCI attempts failed. Although it is possible that a high Doppler signal over such a small perforation may have been overlooked, echocardiography did not show any signs of flow over the septum during follow-up, and the patient was discharged later on with good left ventricular function. LAD – left anterior descending artery.

Endocarditis at the level of the valve can cause the formation of vegetations attached to its structure (*Figure 11*) or mycotic pseudoaneurysms (*Figure 11* and *Figure 12*). While identification of voluminous pseudoaneurysms is relatively simple, millimetric ones could be easily missed or misinterpreted for surgical material. As mentioned above, the safest way to distinguish contrast media outside of the aortic lumen from surgical material is by comparing enhanced and unenhanced acquisitions (*Figure 5*). In case an unenhanced acquisition was not available, researching a communication between the vessel or left ventricular outflow tract and the suspected pseudoaneurysm by means of multiplanar reconstructions and comparing successive scans or acquisitions performed at different timing after contrast administration could be decisive (*Figure 5*). The latter can be located cranially or caudally to the plane of the ring or involve both levels and cause paravalvular regurgitation.

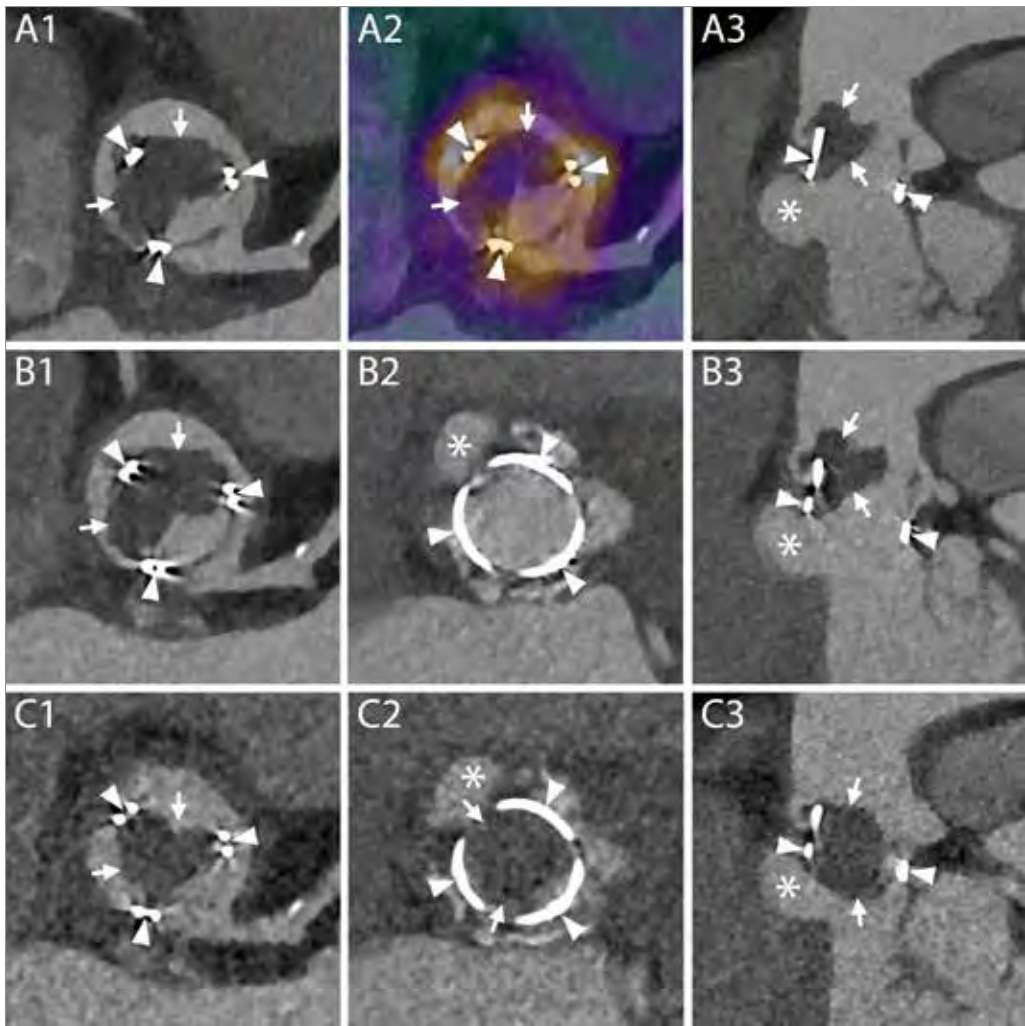


Figure 11 | Endocarditis of a biological valve with a mass obstructing the aortic lumen of uncertain origin and a pseudoaneurysm in the LVOT. One year after having undergone a Bentall procedure for endocarditis, this 80-year-old man presented with fever and blood cultures positive for *S. Aureus* and *Candida parapsilosis*. A CT scan revealed the presence of a big hypodense mass (**A1, arrows**) attached to the structure of the valve (**A1, arrowheads**) and partially occluding the aortic lumen. A PET/CT, the images of which were fused with those of the CTA, demonstrated increased uptake of FDG at the level of the structure of the valve (**A2, arrowheads**) but not of the mass itself (**A2, arrows**). Therefore, doubts arose regarding the aetiology of the mass and whether it should be considered a vegetation (PET-negative because of incarceration of pathogen agents in the midst of fibrotic tissue and consequent lack of inflammatory response), a thrombus or a combination of the two. However, due to the positive PET exam and to the additional presence of a pseudoaneurysm (**A3, asterisk**) just below the valve (**A3, arrowheads**) and the mass (**A3, arrows**), which confirmed the occurrence of a destructive infectious process, the patient was treated with antibiotics and antifungals. Two weeks later a new CT scan was performed (**B1-B3**) with ECG-gating and reconstructions in both systole (**B1-B3**) and diastole (**C1-C3**). The new exam did not reveal any reduction in the size of the mass (**B1, B3, C1-C3, arrows**) which was still attached to the structure of the valve (**B1, B3, C1-C3, arrowheads**) and even appeared slightly bigger.

The pseudoaneurysm remained unchanged in size (**B2-B3, C2-C3, asterisks**). Assessment of the dynamics of the mass during the cardiac cycle demonstrated partial obstruction of the aortic lumen during systole (**B1-B3**) with patent valve opening (**B2, arrows**) that was almost completely occluded during diastole with protrusion of the mass below the level of the metallic ring (**C2-C3**). The patient died 12 days later because of uncontrolled candidemia. **A1-A2, B1, C1** - MPR on planes perpendicular to the centerline of the aorta at the level of the left coronary artery. **B2-C2** - MPR on planes perpendicular to the centerline of the aorta at the level of the metallic ring of the valve. **A3-C3** - MPR on planes parallel to the centerline of the aorta.

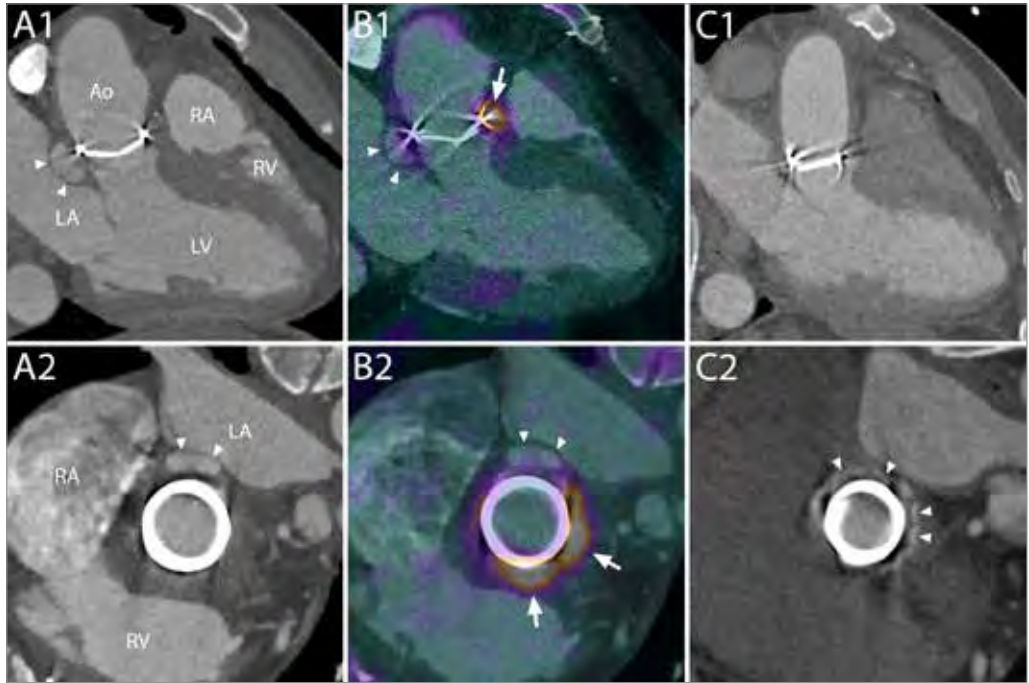


Figure 12 | Endocarditis of a mechanical aortic valve prosthesis after Bentall procedure, with an aseptic perivalvular extension on fused ^{18}F -FDG PET-CT Angiography. A 47-year-old male patient who had undergone a Bentall-procedure for a dilated ascending aorta nine years before, was initially admitted for palpitations due to a new atrial flutter. Upon further questioning, it appeared he had been experiencing intermittent fevers over the previous weeks. Blood cultures were positive for a Gram-positive Streptococcus, and transesophageal echo revealed a small cavity close to the posterior annulus, which was found to be a perivalvular extension (i.e. pseudo-aneurysm) on subsequent CT angiography (**A1, A2, arrowheads**). Interestingly, the ^{18}F -FDG PET/CT scan (**B1, B2**), which is increasingly being used in patients suspected of prosthetic valve endocarditis and is now a new major diagnostic criterion according to the ESC Guidelines for infective endocarditis, revealed intense uptake of FDG around the entire annulus (after 12 days of intravenous antibiotics) (**arrows**), except for the posterior part where the pseudo-aneurysm was located. The patient was electively reoperated, the infected surgical material (including the perivalvular extension) removed, and a new composite valvular and aortic prosthesis was successfully implanted. Swab cultures of the valve and tissue of the pseudo-aneurysm showed no growth of any micro-organisms (after 22 days of intravenous antibiotics), and histopathology revealed only a slight chronic inflammation. Follow-up imaging (**C1, C2**) nicely showed the hyperdense felt pledgets around the new prosthetic valve, without any signs of endocarditis. Ao – aorta, RA – right atrium, RV – right ventricle, LA – left atrium, LV – left ventricle.

The diagnosis of endocarditis, fundamental to avoid lethal consequences, remains difficult and is based on multiple criteria among which CT and ^{18}F -FDG PET are gaining an increasingly important role.¹⁶ Images of ^{18}F -FDG PET can be fused with CTA images and provide information regarding the presence of active inflammatory processes, although results have to be interpreted by an experienced multidisciplinary team to avoid pitfalls including those related to intake of carbohydrates before the examination, insufficient spatial resolution, cardiac motion, inflammation in recently implanted valves and prior use of surgical adhesives.¹⁶

A rare complication after aortic valve replacement is the formation of a ventricular septal defect. Generally the perimembranous portion of the septum is involved. The aetiology of this perforation has been identified in iatrogenic disruption of the structure (*Figure 10*) and endocarditis.^{16,17} Treatment is required only for hemodynamically significant defects.

Coronary arteries

As mentioned, the dilated aspect of the coronary ostia is a normal finding after the operation and are not a complication.¹⁰ The anastomosis of the coronary arteries is prone to leakages with pseudoaneurysms formation (*Figure 13* and *Figure 14*). Other rarer complications include stenosis and dissection of the ostia (*Figure 14*).

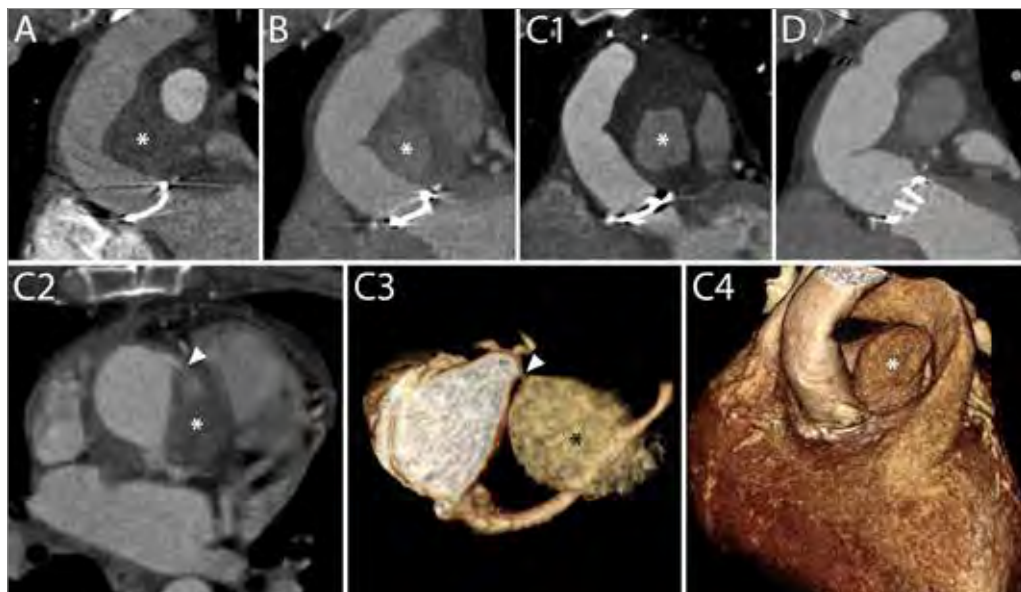


Figure 13 | Gradually changing content of a pseudo-aneurysm after Bentall procedure due to contrast leakage from the right coronary anastomosis. A 30-year-old male patient who had undergone a Bentall procedure for acute Type-A aortic dissection three years before, was readmitted to the ER for acute chest pain. During routine yearly follow-up, a collection of fluid had been identified around the aortic root and ascending aorta, which, although its density had increased, had not changed in size (**A, B, asterisks**). The routine clinical work-up at admission did not show any signs of acute myocardial infarction, but additional CT angiography (**C**) now showed a significant increase in size of the fluid collection, and clearly demonstrated the presence of contrast material inside (**C1, asterisk**). A closer evaluation of the axial images (**C2**) revealed a “puff” of contrast emanating from the anastomosis of the right coronary button (**arrowhead**), and the additional 3D volume rendering reconstructions highlighted this connection (**C3, C4**). The pseudo-aneurysm was successfully removed during reoperation, as shown on a postoperative CT scan (**D**), where-after the leakage was macroscopically confirmed to originate from the anastomosis of the right coronary artery and could successfully be sealed.

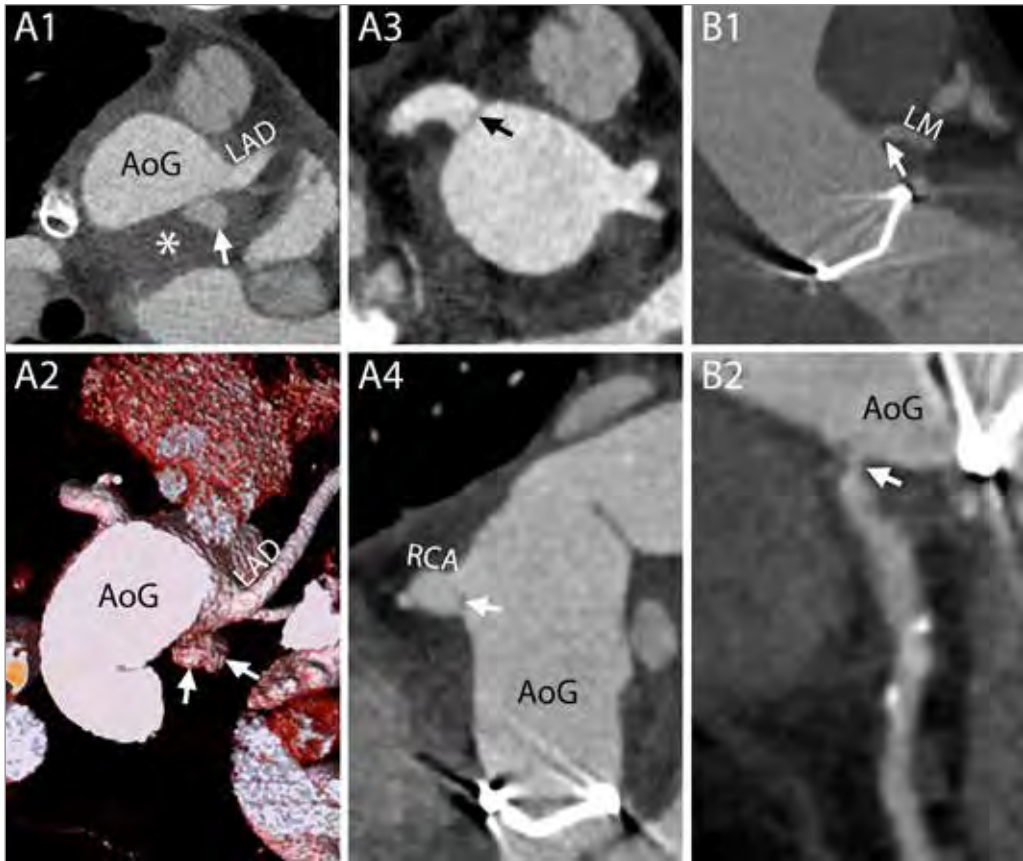


Figure 14 | Complications at the site of coronary arteries anastomosis and ostia. **A1-A4** – Different complications involving the two coronary arteries in the same patient. On a CT scan performed one month after a Bentall procedure, this 27-year-old man showed signs of complications at both coronary arteries. At the level of the suture line of the left main, a small collection of extravasated contrast material (**A1** and **A2**, arrows) surrounded by a hematoma (**A1**, asterisk) was identified. The right coronary artery, that had to be re-attached a second time to the aortic graft due to bleeding from the first suture, presented a hypodense line at the ostium (**A3** and **A4**, arrows) that could be attributed to a small intimal flap or to an inward fold of the graft. No invasive or surgical treatment was undertaken. **A1** - Axial mage. **A2** - VR. **A3** - MPR perpendicular to the centerline of the aorta. **A4** - MPR parallel to the centerline of the aorta. **B1-B2** – Stenosis of the coronary ostium. On a routine follow-up CT scan performed five months after the procedure, this 60-year-old man showed a stenosis of the left coronary artery (**B1** and **B2**, arrows). **B1** - MPR parallel to the centerline of the aorta. **B2** - CPR. AoG – aortic graft, LAD – left anterior descending, LM – left main, RCA – right coronary artery.

Aortic graft

The graft can be involved in (or surrounded by) infectious processes (*Figure 8*), hematomas (*Figure 7*), leakages from the sutures (including proximal and distal sutures and those between grafts) or combinations of the above (*Figure 15*).

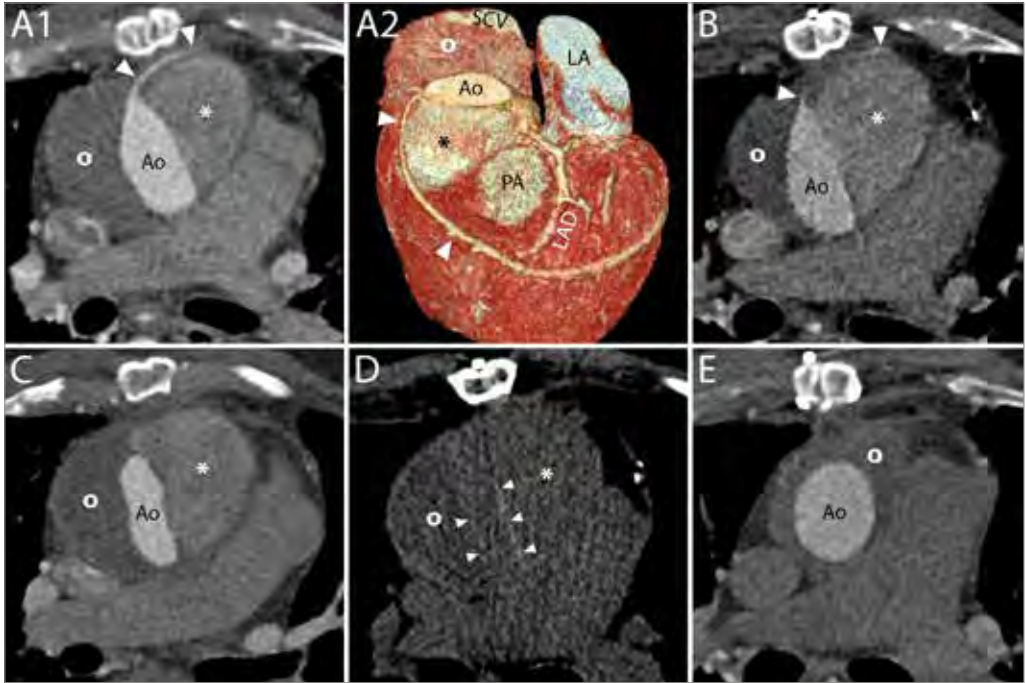


Figure 15 | Loss of vein graft following combined Bentall and coronary artery bypass procedure due to progressive compression by two fluid collections. This 68-year-old male patient underwent a combined Bentall and coronary artery bypass procedure for a severely stenosed bicuspid aortic valve and concomitant three-vessel disease. Like most Bentall procedure performed at our institution, the interposition technique was used, implying that the native ascending aorta was excised and replaced by a vascular prosthesis (as opposed to the inclusion technique by which the aneurysm sac is closed around the vascular graft). Routine follow-up CT two months later (**A1, A2**) showed two fluid collections, one (**asterisk**) denser than the other (**circle**), and both moderately compressed the aortic graft and encompassed but did not compress the vein graft (**arrowheads**). Two follow-up scans were acquired four months (**B**) and 10 months later (**C**), which did not show any distinguishable change in size of both fluid collections, but did reveal that the aortic prosthesis—and now also the vein graft (**arrowheads**)—had become compressed even further (**B, C**), resulting in occlusion of the vein graft (**C**). An additional non-enhanced scan (**D**) did not show any differences in density between the two fluid collections compressing the aortic graft (**arrowheads**), indicating that the denser fluid collection (**asterisk**) had to have been partially filled with contrast on all previous contrast-enhanced scans. The patient was thereupon electively reoperated, the leaking right coronary artery button was resutured and the pseudo-aneurysm successfully removed, restoring normal aortic dimensions (**E**) and leaving only a small hematoma behind (**circle**). Ao – aorta, SCV – superior caval vein, LA – left atrium, PA – pulmonary artery, LAD – left anterior descending artery.

CT is very sensitive for the detection of mediastinal collections and can provide some important elements to define their etiology although with several limitations, especially in the differentiation of infectious processes. An overlap of CT characteristics between normal postoperative findings and endocarditis has to be expected. Clear signs of infection include the presence of a fistulous tract and the appearance or augmentation of wall enhancement and air within the collection. If a preceding scan is not available the latter are impossible to assess. However, as mentioned above, fluid encountered in patients who underwent uncomplicated procedures is usually in the form of stranding and completely surrounds the aorta. Therefore, any other appearance, namely the presence of a defined wall, focal extension around the aorta, wall enhancement and presence of air in the collection, although not pathognomonic by themselves especially in the very early postoperative period, should always warrant further investigation and follow up.¹¹ While decisive in guiding the diagnosis if present, symptoms are often subtle and non-specific or can have a late onset when morphological damage is very advanced. Therefore, the absence of clinical complaints should not rule out the possibility of an ongoing infection. Although an ¹⁸F-FDG PET-CT scan can provide additional information, the surgical adhesives used around the graft during surgery have been reported to be PET-positive and may result in misdiagnosis.¹⁵

Fluid collections can dislocate and/or compress other adjacent structures. The risk is higher in case of collections with progressive increase of volume, such as hematomas, and multiple collections. The aortic graft and venous bypass grafts are particularly prone to this complication as they are completely encircled by the collection more frequently than other organs (*Figure 15*).

Native aorta

The native aorta and aortic branches should always be carefully assessed regarding the progression of the eventual residual dissection (*Figure 16*) and for the occurrence of any new complications such as a rupture, intramural hematoma or dissection. Aortic diameters should be measured on planes perpendicular to the long axis of the aorta and at predefined locations for all examinations.⁶

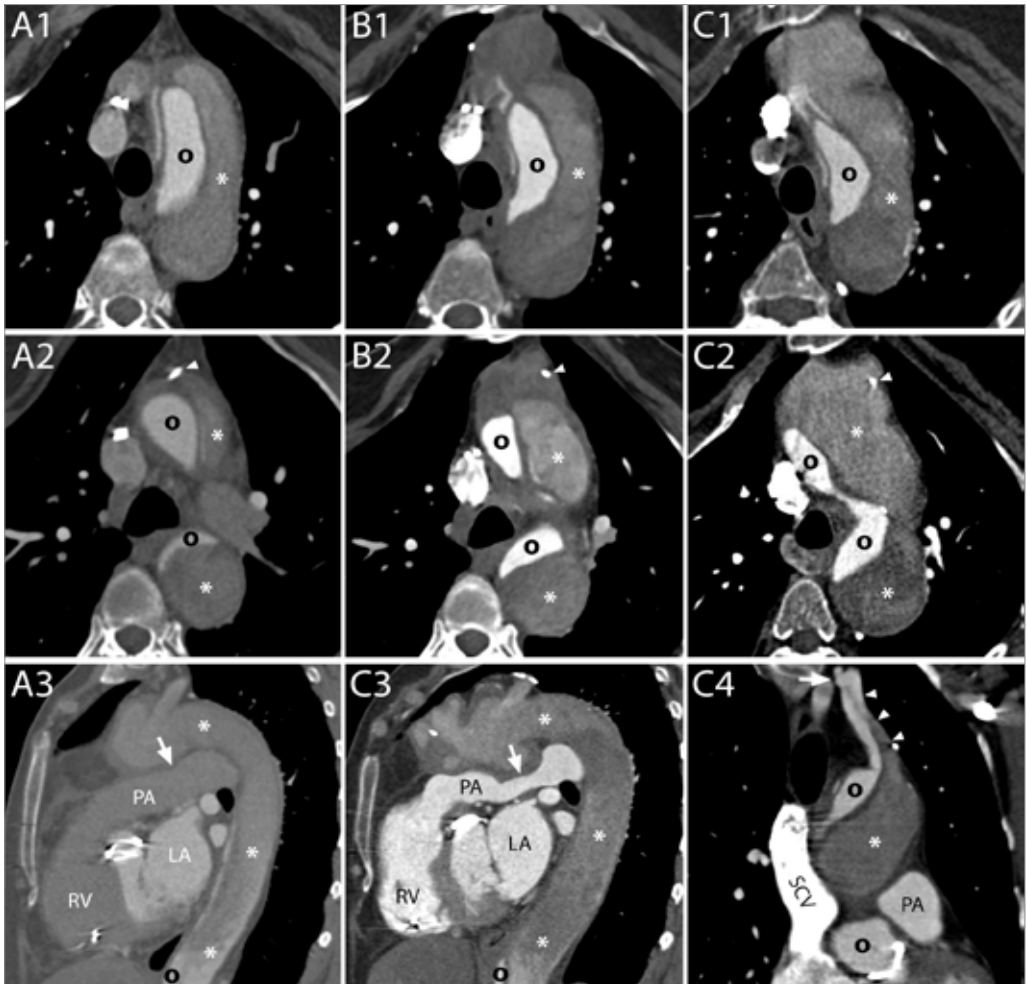


Figure 16 | Natural history of a growing false lumen of a residual dissection after Bentall procedure for acute Type-A aortic dissection in a patient with Marfan's syndrome. This 63-year-old female patient with a family history of Marfan's syndrome underwent a Bentall procedure for acute Type-A aortic dissection at the age of 57 years. The first postoperative follow-up scan depicted a residual dissection of the aortic arch and descending aorta (**A**) with a large false lumen (**asterisk**) and a compressed true lumen (**circle**). Over the ensuing 5 years, follow-up imaging showed a gradual enlargement of the persisting, partially thrombosed aneurysm sac directly distal to the aortic prosthesis, shown here at the level of the distal suture (**A1–C1**) and approximately 15mm below (**A2–C2**, **video 5**), at the level of a metallic surgical clip (**arrowheads**), clearly illustrating the anterolateral expansion of the outer aortic wall. After 5 years, the aneurysm sac had grown to approximately 6cm in diameter, no longer only compressing the true lumen but also the pulmonary artery (**A3**, **C3**). One of the re-entry tears, through which the false lumen had been supplied with blood after surgical repair of the ascending aorta, was clearly depicted on the last scan (**C4**), which distinctly showed a discontinuity of the intimal flap in the left subclavian artery at the level of the vertebral artery ostium (**arrow**), where contrast was passing into the false lumen (**arrowheads**). In the meantime, however, the patient had been diagnosed with a concomitant advanced stage malignancy, and was treated conservatively. PA – pulmonary artery, RV – right ventricle, LA – left atrium, SCV – superior caval vein.

Conclusions

After a Bentall procedure, CT is the imaging modality of choice for routine follow-up and to evaluate all complications. Whilst review of images with the surgeon is useful, it is fundamental for radiologists to be familiar with the surgical technique and materials employed to recognise the normal post-operative appearances and identify complications, thus avoiding misdiagnosis and unnecessary further examinations.

References

1. Bentall H, de Bono A. A technique for complete replacement of the ascending aorta. *Thorax*. 1968;23:338–9.
2. Cherry C, DeBord S, Hickey C. The modified Bentall procedure for aortic root replacement. *AORN*. 2006;84:52–70.
3. Kourliouros A, Soni M, Rasoli S, et al. Evolution and current applications of the Cabrol procedure and its modifications. *Ann Thorac Surg*. 2011;91:1636–41.
4. Sundaram B, Quint LE, Patel HJ, Deeb GM. CT findings following thoracic aortic surgery. *Radiographics*. 2007;27:1583–94.
5. Sundaram B, Quint LE, Patel S, Patel HJ, Deeb GM. CT appearance of thoracic aortic graft complications. *AJR Am J Roentgenol*. 2007;188:1273–7.
6. Erbel R, Aboyans V, Boileau C, et al. 2014 ESC Guidelines on the diagnosis and treatment of aortic diseases. *Eur Heart J*. 2014;35:2873–926.
7. Hiratzka LF, Bakris GL, Beckman JA, et al. 2010 ACCF-AHA-AATS-ACR-ASA-SCAI-SIR-STS-SVM guidelines for the diagnosis and management of patients with thoracic aortic disease. *Circulation*. 2010;121:e266–369.
8. Quint LE, Francis IR, Williams DM, Monaghan HM, Deeb GM. Synthetic interposition grafts of the thoracic aorta: postoperative appearance on serial CT studies. *Radiology*. 1999;211:317–24.
9. Svensson LG, Adams DH, Bonow RO, et al. Aortic valve and ascending aorta guidelines for management and quality measures. *Ann Thorac Surg*. 2013;95:S1–66.
10. Chwan Ng AC, Yiannikas J, Chiang Yong AS, et al. Coronary ostial morphology after modified Bentall operation assessed with dual-source multidetector computed tomography. *J Cardiovasc Comput Tomogr*. 2010;4:206–12.
11. Boccalini S, Swart LE, Bekkers JA, et al. Peri-aortic fluid after surgery on the ascending aorta: Worrisome indicator of complications or innocent postoperative finding? *Eur J Radiol*. 2017;95:332–41.
12. Mookhoek A, Korteland NM, Arabkhani B, et al. Bentall Procedure: a systematic review and meta-analysis. *Ann Thorac Surg*. 2016;101:1684–9.
13. Fagman E, Perrotta S, Bech-Hanssen O, et al. ECG-gated computed tomography: a new role for patients with suspected aortic prosthetic valve endocarditis. *Eur Radiol*. 2012;22:2407–14.
14. Tanis W, Budde RP, van der Bilt IA, et al. Novel imaging strategies for the detection of prosthetic heart valve obstruction and endocarditis. *Neth Heart J*. 2016;24:96–107.
15. Swart LE, Scholtens AM, Tanis W, et al. 18F-fluorodeoxyglucose positron emission/computed tomography and computed tomography angiography in prosthetic heart valve endocarditis: from guidelines to clinical practice. *Eur Heart J*. 2018. doi: 10.1093/eurheartj/ehx784.
16. Ashmeik K, Pai RG. An unusual case of acquired ventricular septal defect as a complication of aortic valve endocarditis: echocardiographic delineation of multiple subvalvular complications in one patient. *J Am Soc Echocardiogr*. 2000;13:693–695.
17. Holzer R, Latson L, Hijazi ZM. Device closure of iatrogenic membranous ventricular septal defects after prosthetic aortic valve replacement using the Amplatzer membranous ventricular septal defect occluder. *Catheter Cardiovasc Interv*. 2004;62:276–80.

EPILOGUE





GENERAL DISCUSSION AND CONCLUSIONS



E

Summary and general discussion

Over 300,000 prosthetic heart valves are implanted every year, and due to the ever-aging population and indications which are continually being expanded with improving replacement techniques, this number is expected to rise rapidly in the next few decades.¹ Prosthetic heart valve endocarditis (PVE), an infection of the prosthetic valve or surrounding structures, is a life-threatening complication of this procedure, which affects up to 5% of patients within the first 5 years following valve implantation.² Its mortality is the highest of all conditions in the field of cardiology, with reported 1-year rates of up to 30-50%.³

Unfortunately, despite rapid advancements in echocardiographic imaging and microbiological technology allowing more rapid and reliable detection of possible causative micro-organisms which facilitates earlier appropriate antibiotic therapy, the timely diagnosis of PVE remains difficult, with a delay in diagnosis being associated with a risk of severe complications such as the formation of abscesses or dehiscence of the prosthetic valve.^{4,5}

In 2015, based on relatively scarce literature on a small number of patients (<300 in total), clinical guidelines were updated to include two additional imaging techniques as new appropriate diagnostics in patients with suspected PVE: ¹⁸F-FDG PET/CT, which aids in the diagnosis of intracardiac and extracardiac infectious foci by visualization of the most metabolically active areas in the body (in this case: areas of inflammation); and cardiac CT angiography, which nowadays allows for highly detailed anatomical depiction of most types of prosthetic heart valves in all phases of the cardiac cycle on the latest-generation CT scanners.⁵ However, knowledge regarding how to acquire and even interpret ¹⁸F-FDG PET/CT and CT angiography in patients with suspected PVE (or a prosthetic valve in general for that matter), was very limited.⁶

In this thesis, we aimed to further investigate the additional value of ¹⁸F-FDG PET/CT and CT angiography in the diagnosis of prosthetic heart valve endocarditis, and how their use and diagnostic accuracy may be improved.

First of all, in *Part I*, we have provided an overview of current literature on ^{18}F -FDG PET/CT and CT angiography in suspected PVE up until the update of the 2015 ESC guidelines (*Chapter 2*). In this review, we have highlighted limitations of previous studies, and put forward our opinion on how the new imaging techniques should be employed in clinical practice (when, and in which patients, to employ which technique, how to visually and quantitatively interpret the images, etc.) based on additional evidence published after the update of the guideline, as the guidelines did not address this. Furthermore, we emphasized the need for standardized acquisition protocols and image interpretation, especially now that these techniques were starting to be widely embraced by the cardiovascular society.

Based on all available literature and our own pioneering clinical experiences, our main recommendations in this review (*Chapter 2*) were the following. While the ESC guidelines only recommended cardiac CTA and ^{18}F -FDG PET/CT to be employed when diagnostic uncertainty remains after the usual diagnostics (echocardiography and blood cultures)⁵, we recommended, in light of the consequential delay of additional imaging and thereby possibly of appropriate therapy (sometimes spanning several weeks of possibly inadequate antibiotics), to perform both PET/CT and CTA *early* in the diagnostic workup. With either technique, but ^{18}F -FDG PET/CT in particular, being able to detect inflammation before structural changes (i.e. vegetations or perivalvular extensions which are required for echocardiographic detection of PVE) ensue, early implementation may allow for initiation of appropriate antibiotic therapy before extensive structural damage (which may require a major reoperation and is associated with extremely high mortality rates) has occurred.

Regarding image acquisition and interpretation, we made several recommendations as well. First of all, in order to suppress myocardial ^{18}F -FDG uptake which may otherwise hamper assessment of the prosthetic heart valve and surrounding tissues, patients should be prepared with extended fasting and a low-carbohydrate diet.^{7,8} Additionally, evidence suggests an intravenous heparin injection 15 minutes prior to FDG administration may reduce the myocardial uptake even further.^{9,10} Second, surgical adhesives used during valve implantation or other cardiothoracic surgery need to be considered when evaluating PET/CT images in suspected PVE, as certain surgical glues can be very FDG-avid and have been reported to result in false-positive misinterpretations.¹¹ Third, as predictors of a false-negative misinterpretation, prolonged antibiotic therapy resulting in lower inflammatory activity needs to be taken into account¹², once more warranting early employment in patients with suspected PVE, while isolated, small or mobile vegetations have also been reported to be missed by ^{18}F -FDG PET/CT.¹³

The complexity of the decision-making process around which patients should undergo additional imaging at what stage, combined with the required expertise, advanced scanning equipment and a broad reference framework required for the interpretation of PET/CT and CTA images in suspected PVE, led us to the final recommendation of emphasizing the need for a multidisciplinary *Endocarditis Team* consisting of cardiologists, cardiothoracic surgeons, infectious disease specialists, radiologists and other involved physicians in every surgical reference centre.^{14,15}

Although several of these factors that ought to be taken into account when acquiring or interpreting PET/CT images had been mentioned in previous studies as factors that could have possibly influenced their results, none of the studies to date had accounted or corrected for them.¹⁶ Moreover, as mentioned, visual image analyses, and quantitative analyses in particular, had been performed in an ill-described, unstandardized manner¹⁷ (*Chapter 5*), making results of previous studies, especially regarding diagnostic cut-offs for quantified FDG uptake, inapplicable to other centres of even other PET/CT scanners. Therefore, we subsequently performed a large, nationwide study (*Chapter 3*) in which we retrospectively included 160 patients who underwent ¹⁸F-FDG PET/CT for suspicion of PVE, while also including a negative control group of 77 patients who had a prosthetic heart valve but underwent PET/CT imaging for other indications.

In this study, we examined the influence of an extensive list of possible confounders, known and unknown (i.e. other patient characteristics or scan parameters), using a logistic regression model, and subsequently excluded these to obtain a more accurate idea of the true diagnostic power of ¹⁸F-FDG PET/CT in suspected PVE. Low inflammatory activity (i.e. C-reactive protein [CRP] levels < 40mg/L) was a statistically significant predictor of a false negative scan, while prior use of certain surgical adhesives was a significant positive confounder. Excluding scans that were affected by these confounders resulted in an increase of sensitivity, specificity, PPV and NPV from 74%/91%/89%/78% to 91%/95%/95%/91%, once more implying that early implementation while inflammatory parameter levels are still high is of paramount importance. Furthermore, with knowledge of the localization of the areas where surgical adhesives had been applied during surgery, a caveat can adequately be added to any uptake that is identified in this area, while experienced nuclear medicine physicians may even be able to distinguish uptake patterns caused by these adhesives from infectious ones.

Since most of the PET/CT scans in this study had been acquired on scanners that provided an additional standardized (according to European Association of Nuclear Medicine Research Ltd., or “EARL”) image construction which, regardless of the scanning protocol or equipment, always yields the exact same quantified amount of FDG uptake (expressed as standardized uptake value, or SUV), for the first time, quantitative analyses that would result in cut-offs applicable to any centre with EARL-accreditation (currently over 150 centres in Europe¹⁸) were finally feasible. After exclusion of scans affected by the previously mentioned confounders, in our study, a standardized uptake value ratio (SUV_{ratio}) of ≥ 2.0 was found to be a 100% sensitive and 91% specific cut-off for PVE. Moreover, because we employed a standardized measuring method involving a software-generated automatic isocontour around the area of increased FDG uptake surrounding the prosthetic heart valve, the inter-observer agreeability was excellent in scans of patients that had adequately been prepared with an extended fasting period and a 24-h low-carbohydrate diet (intra-class correlation coefficient 0.95).

Interestingly, although the ESC guidelines recommended not to perform ¹⁸F-FDG PET/CT imaging in patients who had recently (<3 months before) undergone valve replacement surgery due to the possibility of either post-operative inflammation or an early foreign-body reaction resulting in physiological FDG uptake around the prosthetic valve⁵, recent valve implantation (within 90 or even 30 days prior to PET/CT imaging) was not a significant predictor of false-positive scan. This was in concordance with another study by Mathieu et al.¹⁹, in which the mean amount of FDG uptake in a cohort of 51 patients without any suspicion of PVE was found not to be different between pa-

tients scanned within 3 months of implantation or thereafter. Furthermore, they found that slightly elevated FDG uptake may occur as late as 8 years after valve implantation without any clinical suspicion of PVE, exemplifying that, although the more diffusely distributed pattern of FDG uptake may indicate a physiological process rather than an infectious one¹⁹, caution regarding the possibility of slight physiological FDG uptake is warranted.

To conclude this chapter, we presented a flowchart for the proposed diagnostic work-up of suspected PVE, with emphasis on preventing both unnecessary delays in diagnosis and negative influences by possible confounders.

Finally, in *Chapter 4*, we present two unique case reports: one of a patient with a transcatheter-implanted prosthetic aortic valve (TAVI), and one of a patient with a percutaneously implanted prosthetic pulmonary valve (Melody), both of whom were suspected of prosthetic heart valve endocarditis and underwent combined PET/CT and CT angiography. These case reports are the first to describe the use of these new imaging techniques in patients with these kind of heart valves, and demonstrate that they can most accurately depict inflammation and even the tiniest structural defects caused by the infection. Moreover, the case report of the TAVI endocarditis illustrated that, although the patient was successfully conservatively treated with 6 weeks of antibiotics as illustrated by an uneventful 1-year follow-up, repeated PET/CT imaging as a means of follow-up proved to be difficult. On one hand, there is the negative confounding effect of prolonged antibiotic therapy, in which absence of FDG uptake does not necessarily imply complete eradication of the causative micro-organism, while on the other hand, greatly diminished but still slightly present FDG uptake around the prosthetic valve does not seem to imply unsuccessful conservative treatment.

Part II: Technical aspects and considerations

In *Part II*, we dive deeper into some of the technical aspects of ^{18}F -FDG PET/CT and CT angiography, while also presenting some of our more detailed work on potential confounders and the importance of standardized quantitative FDG measurements which all contributed to the foundation of our multicentre trial described in *Chapter 3*.

First off, in *Chapter 5* an overview of all studies which included a (semi-)quantitative analysis of FDG uptake in suspected PVE is provided. As stated in our larger review of literature (*Chapter 2*), the acquisition and measuring methods varied widely between the included studies, as did their cut-offs and reported standardized uptake values for patients with and without PVE.¹⁶ Moreover, as mentioned above, barely any of these reported values had been acquired on EARL-standardized reconstructions, rendering them inapplicable in any other centre and on any other scanner, even of the same vendor. Therefore, we called for standardization of image acquisition and quantitative interpretation methods.

Second, in *Chapter 6* we move on to a small prospective study in which we looked at the acquisition protocol of the PET/CT, which, besides the previously mentioned preparatory fasting and low-carbohydrate diet, was almost directly taken from the standard oncological acquisition protocol. In this standard protocol, ^{18}F -FDG is administered to the patient, followed by a 60-minute resting period to achieve optimal FDG distribution throughout the body, after which the images are acquired. However, several authors of some of the more early studies on PET/CT in suspected PVE suggested that an earlier or later acquisition timing may be more appropriate for the detection of infection and inflammation: the former based on the fast influx of radiolabeled glucose into inflammatory cells followed by efflux due to activated glucose-t-phosphatase²⁰; the latter based on persistent influx in inflammatory cells and further clearance of the radiolabeled glucose from the blood pool, resulting in a higher contrast between activity in infectious foci and the so-called 'background'.^{21,22} In our study, in which we *added* a delayed acquisition at 150 minutes post-injection of the radiotracer (dual-time-point acquisition²³), 14 scans acquired for suspicion of PVE were included. Although in one case, a false-negative PET/CT scan turned true positive on the late acquisition, as it did in a previous case report²¹, overall the late images proved to be more prone to false-positive interpretation for both the visual and semi-quantitative analyses, leading to our recommendation to interpret these images with caution.

Third, *Chapter 7* presents one of our earlier studies on the possible confounders in ^{18}F -FDG PET/CT imaging for suspected PVE, which laid the foundation for several studies thereafter including our own multicentre trial (*Chapter 3*) in which we based our confounder analysis on the potential factors we first identified in this pictorial case series. As the boundaries between normal and abnormal findings were, and still are, relatively undefined at that time, we presented a number of variations that could lead to misdiagnosis, such as unsuppressed myocardial FDG uptake, infectious versus inflammatory uptake intensity and uptake patterns, other causes of FDG uptake in areas close to prosthetic heart valves such as atrial fibrillation or lipomatous hypertrophy of the interatrial septum, as well as the negative confounding effect of prolonged antibiotic therapy and the possibility of false-negative misinterpretations in isolated vegetations.

To conclude this part, in *Chapter 8* we evaluated a novel 'home-made' CT acquisition protocol for comprehensive prosthetic heart valve assessment at a limited radiation

dose. In this study, 43 consecutive patients who underwent CT angiography for assessment of prosthetic heart valve dysfunction or infection were prospectively included. Three acquisitions were obtained: a non-enhanced scan, a contrast-enhanced arterial CT angiography scan with reconstructions at every 5% of the R-R interval, and a delayed high-pitch CTA of the entire chest. The non-enhanced scan was of particular use in the identification of valvular calcifications and suture pledgets (and the distinction of these from contrast-enhancing peri-annular extensions), while the delayed-phase acquisition of the entire chest allowed for depiction of abscesses, septic pulmonary emboli and overall thoracic anatomy.

For the contrast-enhanced scan, in order to reduce radiation dose, we opted to use prospective ECG-triggering as opposed to retrospective ECG-gating which most previous studies had employed.²⁴ Using several dose-reduction strategies nowadays available on third-generation dual-source CT scanners, including iterative reconstruction²⁵, we were able to significantly reduce the mean total radiation dose of the CTA acquisition while still allowing for dynamic assessment of prosthetic heart valve leaflet motion: compared to mean radiation doses ranging from 11.6 to 18.8 mSv reported in previous studies, the mean radiation dose of our contrast-enhanced ECG-triggered acquisition was 6.7 mSv. Our mean image quality score was good-to-excellent (4.1 out of 5 for the non-enhanced scan, 4.7 out of 5 for the arterial acquisition and 4.2 out of 5 for the delayed acquisition), with a total mean image quality score of 4.3 out of 5. The mean total radiation dose of this comprehensive three-phase acquisition was 8.3 mSv, which in light of the risks of the possible underlying pathology and conceivable major therapeutic consequences, could be considered acceptable.

Finally, in *Part III* we have looked at the role of CT angiography in the routine follow-up of prosthetic heart valve and ascending aortic surgery, including a definition of the spectrum of normal findings that may be seen shortly and late after replacement of the aortic valve and ascending aorta. Furthermore, we have looked at its potential in the evaluation of several possible complications.

In *Chapter 9*, we present the results of our study on a phenomenon best described as 'stranding' or 'induration' of the adipose tissue around the prosthetic heart valve and ascending aortic graft, which is usually caused by sterile inflammation and oedema but can be a sign of graft infection. The aim of our study was to compare the appearance and amount of this peri-aortic fluid on early CT scans following a combined replacement of the aortic valve and ascending aorta (the so-called Bentall procedure) between patients with either an uneventful or a complicated course and follow-up.

Ninety-four scans performed within 3 months of a Bentall-procedure were retrospectively included, and patients were divided into the uncomplicated or the complicated group based on the occurrence of Bentall-related complications or death within one year of surgery. We found that diffuse stranding, as opposed to organized, more clearly delineated fluid collections which are often hematomas, was present on almost all of the scans. In patients with an uneventful procedure and 1-year follow-up, this fluid spanned an average 7.7mm from the aortic circumference in the second and third postoperative months. When there were no signs of concomitant fluid collections such as hematomas or abscesses, the amount of isolated stranding did not significantly differ between the complicated and the uncomplicated group, with up to 17mm of standing seen in the uncomplicated group.

These results are of particular importance in the assessment of patients with recently implanted composite ascending aortic graft who are suspected of an early graft infection, as the diffuse circular oedema previously deemed a sign of infection needs to be interpreted with caution. While our results suggested a gradual decrease in stranding over time (-0.038mm per day of stranding from the aortic circumference, $R=0.02$), this trend was not statistically significant and was not based on sequential data acquired in the same patient.

Lastly, in *Chapter 10*, we start off by providing an extensive overview of the spectrum of normal findings that may be seen on post-operative CT images of prosthetic aortic valves, aortic grafts and other surgical materials, of which knowledge is of the greatest importance in order to be able to distinguish complications and avoid misdiagnosis. We then present real case examples of several potential complications including but not limited to degeneration or obstruction of mechanical valve leaflets due to thrombus or pannus, perforations and fistula, lesions of the coronary arteries or bypass grafts and ensuing myocardial infarction, fluid collections such as hematomas or abscesses with their potential dislocation of adjacent structures, abnormalities of the native aorta including eventual residual dissections, and, naturally, prosthetic heart valve endocarditis and all its subsequent complications.

Conclusions

To conclude, ^{18}F -FDG PET/CT and CT angiography are both equally important new additions to the diagnostic work-up of patients with suspected prosthetic heart valve endocarditis. The diagnostic accuracy of ^{18}F -FDG PET/CT for the detection of inflammation, even before structural damage occurs, is very high, provided it is employed in the early stages of the disease, allowing timely initiation of antibiotic treatment and possibly saving patients from extremely high-risk reoperations.

In this thesis, we have identified some factors that need to be taken into account when acquiring and interpreting ^{18}F -FDG PET/CT and CT angiography images in patients with suspected PVE, of which low inflammatory activity due to prolonged antibiotic therapy and prior use of certain surgical adhesives are the most important. We could not corroborate the guidelines' recommendation not to perform ^{18}F -FDG PET/CT within 3 months of prosthetic heart valve implantation –due to the possible confounding effect of postoperative inflammation–, as we did not find that recent surgery caused more false-positive interpretations. Furthermore, we have shown that quantitative ^{18}F -FDG PET/CT has the advantage of being less observer-dependant, and should be performed in every scan acquired for suspicion of PVE provided the uptake is measured on calibrated reconstructions in a standardized manner. Accounting for the aforementioned confounders, we found that a ratio of uptake around the prosthetic valve divided by the background activity in the blood pool ($\text{SUV}_{\text{ratio}}$) of ≥ 2.0 was a 100% sensitive and 91% specific predictor of PVE.

Finally, cardiac CT angiography is an indispensable tool in the assessment of patients with suspected (or confirmed) PVE. Although it cannot (and should not) replace echocardiography, with knowledge of the distinction between normal postoperative findings and signs of pathology, many of that modality's shortcomings in the assessment of prosthetic heart valves are covered by CT angiography, warranting a more prompt and frequent use in daily clinical practice, particularly now that comprehensive assessment of prosthetic heart valves is possible at an acceptable radiation dose.

Future perspectives

While this thesis provides some important new pieces of the puzzle, confirming that ^{18}F -FDG PET/CT and CT angiography are of additional value in the early and accurate diagnosis of PVE while further emphasizing the need for a generalized, standardized approach to patients with suspected PVE and particularly the imaging modalities used in this intricate disease, several questions remain unanswered which future studies will have to further assess in order to elucidate the exact role these imaging techniques have to play.

First of all, clinical guidelines (particularly those in the field of nuclear medicine) will have to be updated further to include a framework which, based on current literature, guides visual and quantitative ^{18}F -FDG PET/CT interpretation in suspected prosthetic heart valve endocarditis (Figure 1) and ensures a uniform image analysis which will enable larger multicentre trials to take place and meta-analyses to compare results of different studies from different centres.

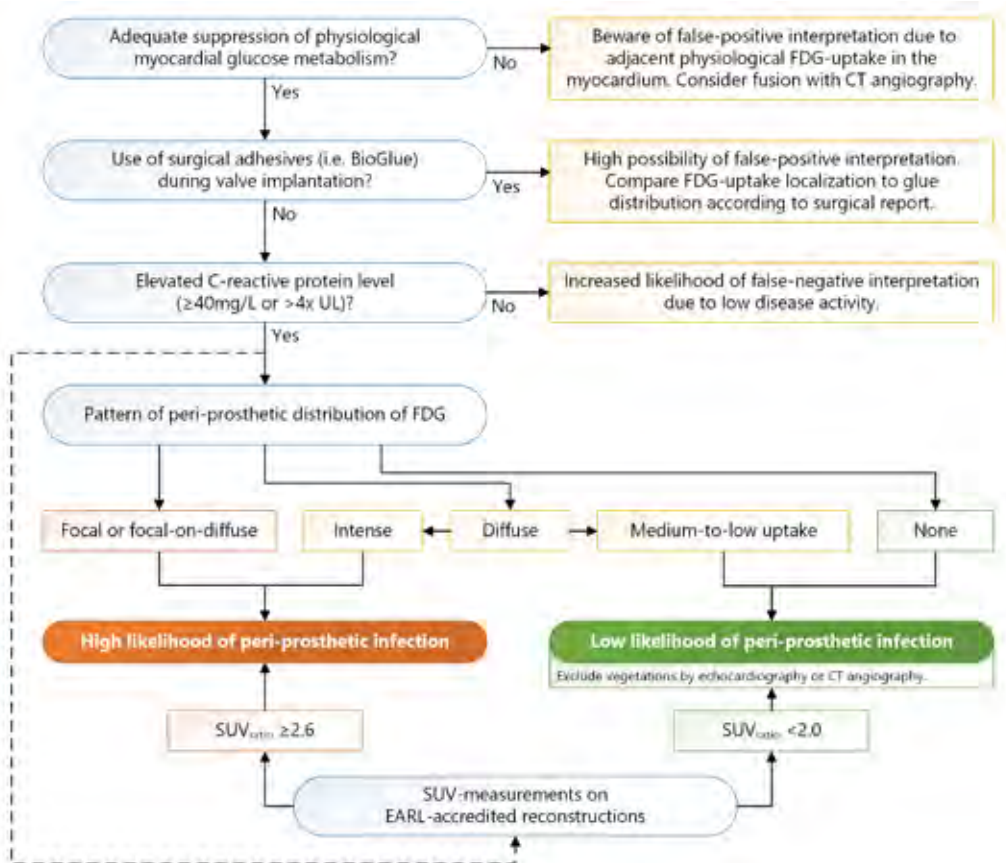


Figure 1 | Flowchart for the suggested interpretation of ^{18}F -FDG PET/CT findings in suspected prosthetic heart valve endocarditis. Adapted with permission from Scholtens et al.

Second, as with CT, knowledge of normal variations in periprosthetic uptake on ^{18}F -FDG PET/CT, particularly shortly after valve implantation, is of paramount importance, yet currently largely lacking. While a recent study by Mathieu et al.¹⁹, in which they describe that non-infected prosthetic heart valves generally display a slight degree of homogeneous FDG uptake which remains steady over time, provides some insight into the different patterns of FDG uptake in infection versus inflammation (*Figure 2*), a clear definition of when a certain degree of perivalvular uptake can be regarded normal is still unclear.

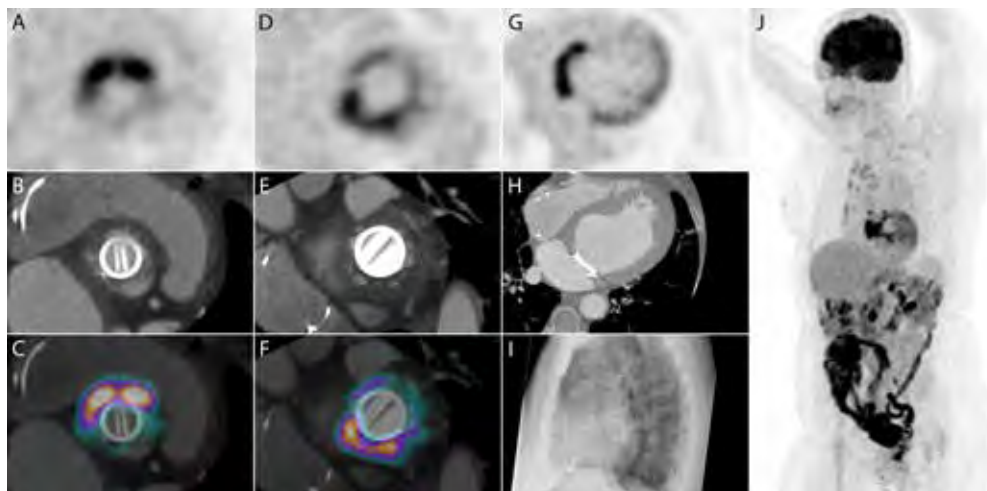


Figure 2 | Infection versus inflammation. Images of a patient with both a prosthetic aortic and mitral valve, as well as two pacemaker wires in situ (plain X-ray, **I**). The PET, CTA and fused images (**A-F**) of the aortic (**A-C**) and mitral (**D-F**) valves showed increased FDG uptake near both valves, while PET and CTA images in the transaxial plane (**G-H**) showed that the entire basal septal wall between the valves was hyperactive. The minor uptake in the lateral wall is likely due to physiological myocardial FDG-uptake as a result of incomplete suppression. Finally, the MIP image (**J**) demonstrated the extent of pathological uptake. Combined, the images show a large metabolic lesion in the entire basal septum, reaching out to both PHVs. Blood cultures were negative, and inflammation parameters were relatively low for such a large lesion. Initial biopsy of the lesion was difficult to interpret, with suspicion of infection. However, antibiotics did not change the clinical presentation, and re-evaluation of the biopsy samples led to the diagnosis of a sterile granuloma, possibly sarcoidosis. Symptoms diminished under corticosteroid therapy.

In one of our ongoing studies (the *PROSPECTA* trial), patients without any suspicion of endocarditis who underwent aortic valve replacement surgery 1, 3 or 12 months ago, are currently prospectively being included to undergo combined ^{18}F -FDG PET/CT and CT angiography. The results of this trial will most likely provide conclusive information on what can be considered normal uptake of FDG around aortic prosthetic heart valves and what a normal appearance of recently implanted prosthetic aortic valves is in the early, late, and chronic post-operative phase.

Third, the role of ^{18}F -FDG PET/CT in follow-up of conservative treatment needs to be investigated. Where we stand right now, the role of FDG PET herein seems limited due to the fact that suppressed inflammatory activity cannot readily be distinguished from completely eradicated infection (*Figure 3*)²⁶, while on the other hand diminished yet residual FDG uptake after an antibiotic-free grace period following prolonged antibiotic therapy does not necessarily indicate unsuccessful treatment (*Chapter 4*).

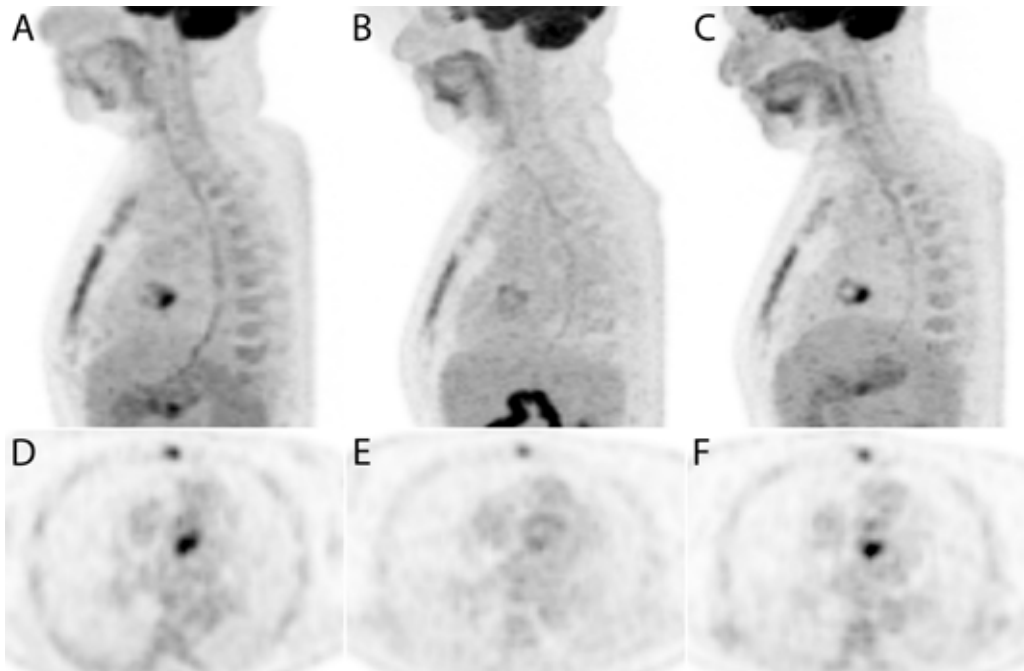


Figure 3 | Sagittally oriented MIP and transaxial PET images before, during and after antibiotic therapy. (**A, D**) Initially, focal activity at the dorsal side of the implanted aortic PHV is observed. After 6 weeks of antibiotic therapy (**B, E**), the diffuse activity around the PHV is minimal, suggesting the infection has been treated. Three weeks later (**C, F**), focal activity has returned which subsequent surgery showed to be due to a persistent focal *P. aeruginosa* infection. Although the second scan could arguably be false negative, it is probably true negative with regard to disease activity, as all clinical and laboratory parameters had also normalized. As this case shows, this does not necessarily imply the complete eradication of pathogens. Adapted with permission from Scholtens et al.

In a recent study by Husmann et al.²⁷, FDG PET/CT was used in long-term monitoring of patients with aortic graft infection, a disease entity not unlike PVE. Although the study mostly reports on the therapeutic impact of clinical markers (i.e. CRP levels, fever) combined with the focality and amount of FDG uptake, in a select number of patients

the impact of a follow-up PET/CT scan after completion of antibiotic therapy was assessed. While the authors state that higher SUV values and a more focal pattern of FDG uptake were associated with continuation of antibiotic therapy, regrettably, this does not provide us with additional evidence as to whether this is in fact the right approach. Moreover, due to the not-entirely-prospective nature of the study and the PET/CT not being the exclusive decisive factor, it is hard to draw any sound conclusions, which leaves a lot of room for future prospective studies. For example, treating physicians may be initially blinded to the follow-up PET/CT findings in order to evaluate the predictive value regarding a potential relapse (e.g. if the quantified FDG uptake diminishes less than a certain percentage). Hopefully, we can then establish the exact role ^{18}F -FDG PET/CT may or may not have to play in treatment monitoring and clinical decision-making.

Likewise, prospective studies on the outcomes of patients in whom a conservative treatment was chosen based on normal echocardiography and CT angiography findings, such as the patients described in *Chapter 4*, would be of most interest. Currently, the decision not to reoperate is based on expert opinion which, in our case, although surgery is generally recommended in any case of prosthetic heart valve infection according to previous guidelines, a more patient-tailored approach considering signs of structural damage, vegetational growth, recurrent emboli and the virulence of the causative micro-organism (basically: following guidelines for surgical therapy in *native* valve endocarditis), is that patients with structurally normal valvular and perivalvular anatomy can generally be treated conservatively with close imaging follow-up.

As something that may help us overcome the issue of distinguishing infection from inflammation, another interesting possible future development may be the use of more specific tracers that, for example, target specific micro-organisms. This *targeted imaging*, which is based on the coupling of a radionuclide to an antibody, antibiotic, antimicrobial peptide, a bacteriophage or DNA/RNA-binding compound, has gained an increasing interest over the past decade.^{28,29} Currently, the most knowledge in targeted imaging described is of experiments using ^{99}Tc -ciprofloxacin, which was shown to have decent sensitivity (85.4% in one large multi-centre study³⁰) but lacked specificity, possibly because, while ciprofloxacin does target the bacteria specifically, they do not retain it any longer than healthy tissue.³¹ Other antibiotic-based tracers such as radiolabeled ceftriaxone or fleroxacin have also been successfully used in patients, but studies to date are too small to draw conclusions about their diagnostic value.^{32,33} Alternatively, radiolabeled synthetic fragments of an antimicrobial peptide called ubiquicidin, which was first isolated from murine macrophages and was found to bind to both Gram-positive and Gram-negative bacteria as well as to fungi, may be used for the localization of bacterial infections, with several clinical studies having found high sensitivity (97.5% [94.9–99.0%]) and specificity rates (88.8% [83.8–92.7%]).³⁴ So far, no immunological side effects have been observed, yet the use of $^{99\text{m}}\text{Tc}$ -ubiquicidin in suspected infectious endocarditis currently doesn't span more than a few animal studies and case reports.³⁵

Altogether, keeping in mind that the goal of new diagnostic studies should never be to replace –but rather to assess the additional value on top of– existing diagnostic tests, each with their specific strengths and weaknesses, to obtain a composite test with optimal diagnostic accuracy, the future for novel imaging techniques in prosthetic heart valve infections looks bright.²⁹

References

1. Butchart EG, Gohlke-Bärwolf C, Antunes MJ, et al. Recommendations for the management of patients after heart valve surgery. *Eur Heart J*. 2005;26:2463–71.
2. Lalani T, Chu VH, Park LP, et al. In-hospital and 1-year mortality in patients undergoing early surgery for prosthetic valve endocarditis. *JAMA Intern Med*. 2013;173:1495–504.
3. Baddour LM, Wilson WR, Bayer AS, et al. Infective endocarditis: diagnosis, antimicrobial therapy, and management of complications. *Circulation* 2005;111:e394–e434.
4. Dilsizian V, Achenbach S, Narula J. Adding or selecting imaging modalities for incremental diagnosis: a case study of 18FDG PET/CT in prosthetic valve endocarditis. *JACC Cardiovasc Imaging* 2013;6:1020–1021.
5. Habib G, Lancellotti P, Antunes MJ, et al. 2015 ESC Guidelines for the management of infective endocarditis: The Task Force for the Management of Infective Endocarditis of the European Society of Cardiology (ESC). *Eur Heart J*. 2015;36:3075–128.
6. Gomes A, Glaudemans AW, Touw DJ, et al. Diagnostic value of imaging in infective endocarditis: a systematic review. *Lancet Infect Dis*. 2017;17:e1–e14.
7. Tiwari B, Kand P. Myocardial uptake of F-18-fluorodeoxyglucose in whole body positron emission tomography studies. *Indian J Nucl Med*. 2012;27:69.
8. Harisankar CNB, Mittal BR, Agrawal KL, et al. Utility of high fat and low carbohydrate diet in suppressing myocardial FDG uptake. *J Nucl Cardiol*. 2011;18:926–936.
9. Morooka M, Moroi M, Uno K, et al. Long fasting is effective in inhibiting physiological myocardial 18F-FDG uptake and for evaluating active lesions of cardiac sarcoidosis. *EJNMMI Res*. 2014;4:1.
10. Scholtens AM, Verberne HJ, Budde RPJ, Lam M. Additional heparin preadministration improves cardiac glucose metabolism suppression over low carbohydrate diet alone in 18F-FDG-PET imaging. *J Nucl Med*. 2016;57:568–74.
11. Schouten LR, Verberne HJ, Bouma BJ, et al. Surgical glue for repair of the aortic root as a possible explanation for increased F-18 FDG uptake. *J Nucl Cardiol*. 2008;15:146–7.
12. Scholtens AM, van Aarnhem EE, Budde RP. Effect of antibiotics on FDG-PET/CT imaging of prosthetic heart valve endocarditis. *Eur Heart J Cardiovasc Imaging*. 2015;16:1223.
13. Tanis W, Scholtens AM, Habets J, et al. CT angiography and ¹⁸F-FDG-PET fusion imaging for prosthetic heart valve endocarditis. *JACC Cardiovasc Imaging*. 2013;6:1008–13.
14. Botelho-Nevers E, Thuny F, Casalta JP, et al. Dramatic reduction in infective endocarditis-related mortality with a management-based approach. *Arch Intern Med*. 2009;169:1290–8.
15. Chirillo F, Scotton P, Rocco F, et al. Impact of a multidisciplinary management strategy on the outcome of patients with native valve infective endocarditis. *Am J Cardiol*. 2013;112:1171–6.
16. Swart LE, Scholtens AM, Tanis W, et al. 18F-fluorodeoxyglucose positron emission/computed tomography and computed tomography angiography in prosthetic heart valve endocarditis: from guidelines to clinical practice. *Eur Heart J*. 2018. doi: 10.1093/eurheartj/ehx784.
17. Scholtens AM, Swart LE, Kolste HJ, et al. Standardized uptake values in FDG PET/CT for prosthetic heart valve endocarditis: a call for standardization. *J Nucl Cardiol*. 2017. doi: 10.1007/s12350-017-0932-x.

18. Kaalep A, Sera T, Oyen W, et al. EANM/EARL FDG-PET/CT accreditation - summary results from the first 200 accredited imaging systems. *Eur J Nucl Med Mol Imaging*. 2018;45:412–22.
19. Mathieu C, Mikail N, Benali K, et al. Characterization of 18F-fluorodeoxyglucose uptake pattern in noninfected prosthetic heart valves. *Circ Cardiovasc Imaging*. 2017;10:e005585.
20. Van Riet J, Hill EE, Gheysens O, et al. (18)F-FDG PET/CT for early detection of embolism and metastatic infection in patients with infective endocarditis. *Eur J Nucl Med Mol Imaging*. 2010;37:1189–97.
21. Caldarella C, Leccisotti L, Treglia G, Giordano A. Which is the optimal acquisition time for FDG PET/CT imaging in patients with infective endocarditis? *J Nucl Cardiol*. 2013;20:307–9.
22. Leccisotti L, Perna F, Lago M, et al. Cardiovascular implantable electronic device infection: delayed vs standard FDG PET-CT imaging. *J Nucl Cardiol*. 2014;21:622–32.
23. Jamar F, Buscombe J, Chiti A, et al. EANM/SNMMI guideline for 18F-FDG use in inflammation and infection. *J Nucl Med*. 2013;54:647–58.
24. Suchá D, Symersky P, van den Brink RB, et al. Diagnostic evaluation and treatment strategy in patients with suspected prosthetic heart valve dysfunction: The incremental value of MDCT. *J Cardiovasc Comput Tomogr*. 2016;10:398–406.
25. Habets J, Symersky P, de Mol BA, et al. A novel iterative reconstruction algorithm allows reduced dose multidetector-row CT imaging of mechanical prosthetic heart valves. *Int J Cardiovasc Imaging*. 2012;28:1567–75.
26. Glaudemans AW, de Vries EF, Galli F, et al. The use of ¹⁸F-FDG-PET/CT for diagnosis and treatment monitoring of inflammatory and infectious diseases. *Clin Dev Immunol*. 2013.
27. Husmann L, Ledergerber B, Anagnostopoulos A, et al. The role of FDG PET/CT in therapy control of aortic graft infection. *Eur J Nucl Med Mol Imaging*. 2018;45:1987–97.
28. Van Oosten M, Hahn M, Crane LM, et al. Targeted imaging of bacterial infections: advances, hurdles and hopes. *FEMS Microbiol Rev*. 2015;39:892–916.
29. Heuker M, Gomes A, van Dijk JM, et al. Preclinical studies and prospective clinical applications for bacteria-targeted imaging: the future is bright. *Clin Transl Imaging*. 2016;4:253–64.
30. Britton KE, Wareham DW, Das SS, et al. Imaging bacterial infection with 99mTc-ciprofloxacin (Infecton®). *J Clin Pathol*. 2002;55:817–23.
31. Langer O, Brunner M, Zeitlinger M, et al. In vitro and in vivo evaluation of 18F-ciprofloxacin for the imaging of bacterial infections with PET. *Eur J Nucl Med Mol Imaging*. 2004;32:143–150.
32. Kaul A, Hazari PP, Rawat H, et al. Preliminary evaluation of Technetium-99m-labeled ceftriaxone: infection imaging agent for the clinical diagnosis of orthopedic infection. *Int J Infect Dis*. 2013;17:263–70.
33. Fischman AJ, Livni E, Babich JW, et al. Pharmacokinetics of ¹⁸F-fleroxacin in patients with acute exacerbations of chronic bronchitis and complicated urinary tract infection studied by PET. *Antimicrob Agents Chemother*. 1996;40:659–64.
34. Ostovar A, Mahsan Assadi M, Vahdat K, et al. A pooled analysis of diagnostic value of 99mTc-ubiquidicin scintigraphy in detection of infectious process. *Clin Nucl Med*. 2013;38:413–6.
35. Taghizadeh Asl M, Mandegar MH, Assadi M. Technetium-99m-ubiquidicin scintigraphy in the detection of infective endocarditis. *Hell J Nucl Med*. 2014;17:47–8.



SUMMARY IN DUTCH

Nederlandse samenvatting



E

Samenvatting en algemene discussie

Jaarlijks worden er wereldwijd meer dan 300.000 kunsthartkleppen geïmplanteerd, en met oog op de vergrijzing en de steeds breder wordende indicaties voor hartklepvervanging dankzij continu verbeterende technieken is de verwachting dat dit aantal snel verder zal stijgen de komende decennia.¹ Kunstklependocarditis, een infectie van de kunstklep of omliggende weke delen, is een levensbedreigende complicatie van deze procedure, die tot wel 5% van de patiënten per jaar na klepimplantatie aandoet² met een 1-jaars mortaliteit van tot wel 50%³, het hoogst van alle cardiovasculaire aandoeningen.

Ondanks snelle ontwikkelingen op het gebied van echocardiografische beeldvorming en microbiologische onderzoeken die het mogelijk hebben gemaakt steeds sneller en betrouwbaarder de mogelijke veroorzakende micro-organismen te detecteren waardoor tijdige antibiotische behandeling vaker kan worden gestart, blijft de tijdige diagnose van kunstklependocarditis moeilijk, waarbij een latere diagnose geassocieerd is met een verhoogd risico op ernstige complicaties zoals de vorming van abscessen of (gedeeltelijke) loslating van de kunstklep.^{4,5}

In 2015 zijn de richtlijnen op basis van op dat moment vrij beperkte literatuur over een klein aantal patiënten (in totaal <300) uitgebreid met twee additionele beeldvormingstechnieken die gebruikt kunnen worden als diagnosticum bij patiënten die verdacht worden van kunstklependocarditis: ¹⁸F-FDG PET/CT, een techniek die helpt bij het identificeren van zowel intracardiale als extracardiale infectieuze foci door middel van het afbeelden van de meest metabool actieve gebieden in het lichaam (in dit geval gebieden van ontsteking); en cardiale CT angiografie, wat met de laatste generatie CT-scanners uiterst gedetailleerde afbeelding van de meeste tegenwoordig gebruikte kunstkleppen in alle fasen van de cardiale cyclus mogelijk maakt. Echter, kennis over hoe beide technieken precies moesten worden toegepast en hoe de verkregen beelden moesten worden geïnterpreteerd in het kader van een patiënt met een kunstklep, laat staan een patiënt die verdacht werd van kunstklependocarditis, was erg beperkt.⁶

Met dit proefschrift hebben wij geprobeerd de toegevoegde waarde van ¹⁸F-FDG PET/CT en CT angiografie bij de diagnose van kunstklependocarditis beter in kaart te brengen, als ook hoe hun gebruik en diagnostische accuratesse kunnen worden verbeterd.

Allereerst hebben wij in *Deel 1* van dit proefschrift een overzicht gemaakt van alle literatuur over ^{18}F -FDG PET/CT en CTA bij de diagnose van kunstklependocarditis tot aan de update van de ESC richtlijnen van 2015 (*Hoofdstuk 2*). In deze literatuurstudie hebben we de beperkingen van voorgaande onderzoeken uitgestippeld en onze inzichten ten aanzien van hoe deze nieuwe beeldvormingstechnieken toegepast zouden moeten worden in de klinische praktijk (zoals wanneer, welke techniek bij welke patiënten, hoe de verkregen beelden visueel danwel kwantitatief te interpreteren, etc.) weergegeven. Hierbij hebben wij ons gebaseerd op de nieuwe bewijslast die sinds de update van de richtlijnen beschikbaar is geworden, aangezien de richtlijnen hier zelf niet op in gingen. Bovendien benadrukt deze literatuurstudie dat standaardisering van beeldacquisitie- en interpretatieprotocollen noodzakelijk is, vooral omdat deze nieuwe technieken nu steeds meer gebruikt gaan worden binnen de cardiovasculaire gemeenschap.

Op basis van alle beschikbare literatuur en onze eigen klinische pionierservaringen waren onze belangrijkste aanbevelingen uit deze literatuurstudie (*Hoofdstuk 2*) de volgende. Hoewel de ESC richtlijnen enkel aanraadden om cardiale CT angiografie en ^{18}F -FDG PET/CT toe te passen wanneer de gebruikelijke diagnostische middelen (echocardiografie en bloedkweken) niet tot een zekere diagnose hebben geleid⁵, adviseren wij, met het oog op de vertraging in het verrichten van additionele beeldvorming en de daarbij mogelijke vertraging in het starten van adequate behandeling die dientengevolge kan ontstaan en soms kan oplopen tot meerdere weken, om zowel PET/CT als CT angiografie *vroegtijdig* in de diagnostische work-up toe te passen. Aangezien beide technieken, maar ^{18}F -FDG PET/CT in het bijzonder, in staat zijn om een ontsteking te detecteren voordat er structurele veranderingen (zoals vegetaties of perivalvulaire uitbreidingen, welke wel vereist zijn voor echocardiografische detectie van kunstklependocarditis) moeten zijn opgetreden, kan vroege implementatie het mogelijk maken dat de juiste antibiotische behandeling tijdig wordt gestart, voordat er uitgebreide structurele schade is ontstaan (waarvoor misschien een grote heroperatie noodzakelijk is wat geassocieerd is met een zeer hoog mortaliteitsrisico).

Ten aanzien van de beeldvergarings- en -interpretatie hebben we ook enkele aanbevelingen gedaan. Ten eerste is het, om eventuele myocardiale opname van ^{18}F -FDG wat de beoordeling van de kunstklep en omliggende weefsels zou kunnen belemmeren te onderdrukken, van belang om patiënten voor te bereiden met een langdurige periode van vasten en een dieet laag in koolhydraten.^{7,8} Daarnaast is aangetoond dat toevoeging van een intraveneuze heparine-injectie 15 minuten voorafgaand aan FDG-toediening de myocardiale FDG opname nog verder zou kunnen onderdrukken.^{9,10} Ten tweede moet het eventuele gebruik van chirurgische lijmstoffen tijdens de klepimplantatie in acht genomen worden aangezien bepaalde lijmstoffen zeer FDG-avide kunnen zijn en kunnen leiden tot fout-positieve misinterpretaties¹¹. Ten derde moeten, als voorspellers van fout-negatieve misinterpretaties, langdurige antibiotische behandeling, wat resulteert in verlaagde ontstekingsactiviteit¹², als ook kleine of mobiele geïsoleerde vegetaties die gemist kunnen worden op ^{18}F -FDG PET/CT, worden overwogen.¹³

De complexiteit van het besluitvormingsproces met betrekking tot welke patiënten wel of niet aanvullende beeldvorming moeten ondergaan in welk stadium gecombineerd met de vereiste expertise, geavanceerde scanapparatuur en een breed referentiekader voor de interpretatie van PET/CT- en CT angiografie-beelden bij een verdenking

op kunstklependocarditis, maakt dat wij als laatste willen benadrukken dat een multidisciplinair *Endocarditis Team* van cardiologen, cardiothoracaal chirurgen, infectieziekten-specialisten, radiologen en andere betrokken specialismen een must is in elk chirurgisch referentiecentrum.^{14,15}

Hoewel veel van deze factoren waar rekening mee moet worden gehouden bij het vergaren of interpreteren van PET/CT beelden wel genoemd zijn in eerdere studies als mogelijke negatieve invloeden op hun resultaten, hebben geen van deze studies tot op heden de invloed hiervan geanalyseerd of hun resultaten hiervoor gecorrigeerd.¹⁶ Bovendien zijn, zoals genoemd, de visuele en in het bijzonder de eventuele kwantitatieve analyses uitgevoerd op een slecht beschreven, niet gestandaardiseerde manier¹⁷ (*Hoofdstuk 5*), wat maakt dat resultaten van voorgaande onderzoeken, met name met betrekking tot diagnostische afkapwaarden voor gekwantificeerde FDG-opname, onbruikbaar zijn in andere centra, of zelfs op andere PET/CT-scanners. Om die reden hebben wij vervolgens een grote, landelijke studie opgezet (*Hoofdstuk 3*) waarin we retrospectief 160 patiënten hebben geïncludeerd die een ¹⁸F-FDG PET/CT hebben ondergaan voor verdenking van kunstklependocarditis, waarbij tevens een controle-groep van 77 patiënten die wel een kunstklep maar geen enkele verdenking op kunstklependocarditis hadden en de ¹⁸F-FDG PET/CT om andere redenen hadden ondergaan is geïncludeerd.

In dit onderzoek hebben wij de invloed van een uitgebreid aantal bekende en onbekende (zoals overige patiëntkarakteristieken of scan parameters) mogelijke factoren onderzocht met behulp van een logistisch regressiemodel, waarop wij deze hebben geëxcludeerd om een beter beeld te krijgen van de daadwerkelijke diagnostische nauwkeurigheid van ¹⁸F-FDG PET/CT bij een verdenking op kunstklependocarditis. Lage ontstekingsactiviteit (d.w.z. C-reactief proteïne [CRP] concentraties < 40 mg/L) bleek hierbij een statistisch significante voorspeller van een fout-negatieve scan, terwijl eerder gebruik van bepaalde chirurgische lijmiddelen een significante fout-positieve verstoorder bleek. Exclusie van alle scans die beïnvloed waren door deze verstoorders resulteerde in een verhoging van de sensitiviteit, specificiteit en positief en negatief voorspellende waarden van 74%/91%/89%/78% naar 91%/95%/95%/91%, waaruit opnieuw blijkt dat vroege implementatie, wanneer de concentratie van ontstekingsparameters nog hoog is, van enorm belang is. Bovendien kan, met kennis van de locatie van eerder tijdens de implantatie gebruikte lijmiddelen, een duidelijke kanttekening worden geplaatst bij eventuele verhoogde opname in dit gebied, waarbij ervaren nucleair geneeskundigen mogelijk zelfs patronen van opname ten gevolge van lijmiddelen zullen kunnen onderscheiden van die met infectieuze karakteristieken.

Aangezien de meeste PET/CT-scans in dit onderzoek verkregen waren op scanners die naast de standaard beeldreconstructies een (volgens de European Association of Nuclear Medicine Research Ltd., oftewel "EARL"-)gestandaardiseerde beeldreconstructie meeleverden welke, ongeacht de apparatuur of het scanprotocol altijd exact dezelfde gemeten hoeveelheid FDG uptake bepaalt (uitgedrukt in *standardized uptake value*, oftewel SUV), konden voor het eerst kwantitatieve analyses worden verricht die resulteren in een afkapwaarde die toepasbaar zou zijn in elk centrum met EARL-accreditatie (op dit moment meer dan 150 centra in Europa¹⁸). Bovendien was, aangezien wij een gestandaardiseerde meetmethode hadden toegepast waarin een door software gegenereerde automatische isocontour rond de verhoogde FDG opname rond de klep wordt benut, de inter-observer overeenstemming uitstekend wanneer de scan was gemaakt bij een patiënt die goed was voorbereid met een langdurige vastperiode en een koolhydraatarm dieet (intra-class correlatie-coëfficiënt 0.95).

Wat verder opviel is dat, hoewel de ESC richtlijnen afraden om ^{18}F -FDG PET/CT beeldvorming te verrichten bij patiënten die recent (<3 maanden geleden) hun klepvervanging hebben ondergaan (in verband met de mogelijkheid van postoperatieve ontsteking of een vroege vreemdlichaamreactie welke resulteert in verhoogde fysiologische FDG opname rond de kunstklep)⁵, recente klepimplantatie (binnen 90 of zelfs binnen 30 dagen voorafgaand aan PET/CT beeldvorming) geen significante voorspeller was van een fout-positieve scan. Deze resultaten waren in samenspraak met die van een andere studie door Mathieu e.a.¹⁹, waarin de gemiddelde hoeveelheid FDG opname in een cohort van 51 patiënten zonder enige verdenking op kunstklependocarditis niet hoger was bevonden tussen patiënten die binnen 3 maanden na implantatie waren gescand of daarna. Bovendien vonden zij dat licht verhoogde FDG opname tot wel 8 jaar na klepimplantatie kan vóórkomen zonder enige klinische verdenking op kunstklependocarditis, nogmaals illustrerend dat, hoewel een meer diffuus verdeeld opnamepatroon van FDG een indicatie kan zijn van een fysiologisch proces in tegenstelling tot een infectieus proces, bedachtzaamheid van de mogelijkheid van licht verhoogde fysiologische FDG opname noodzakelijk is.

Ter afsluiting van dit hoofdstuk hebben wij een stroomdiagram voor de diagnostische work-up bij een verdenking op kunstklependocarditis voorgesteld, waarin de nadruk ligt op het voorkomen van onnodige vertragingen in de diagnose en de negatieve invloed van mogelijke versturende factoren.

Tenslotte presenteren wij in *Hoofdstuk 4* twee unieke casusbeschrijvingen: één van een patiënt met een via een katheter ingebrachte aortakunstklep (TAVI) en één van een patiënt met een percutaan ingebrachte pulmonalisklep (Melody) die beiden verdacht werden van kunstklependocarditis en een gecombineerde PET/CT met CT angiografie ondergingen. Dit zijn de eerste beschrijvingen van het gebruik van deze nieuwe beeldvormingstechnieken bij patiënten met dit type hartkleppen, waarin wij demonstreren dat deze technieken zeer betrouwbaar de ontsteking en zelfs de kleinste structurele afwijkingen aan de klep ten gevolge van de infectie kunnen afbeelden. Bovendien illustreerde de casusbeschrijving van de TAVI-endocarditis dat, hoewel de patiënt succesvol conservatief behandeld was met antibiotica gedurende 6 weken zoals bleek uit een onbewogen follow-up nadien gedurende meer dan een jaar, interpretatie van herhaalde PET/CT beeldvorming bij wijze van follow-up erg lastig was. Aan de ene kant bestaat er namelijk het fout-negatieve versturende effect van langdurige antibiotische behandeling, waarbij afwezigheid van opname van FDG niet per sé betekent dat de infectie volledig is uitgeroeid, terwijl aan de andere kant een duidelijke maar onvolledige afname van FDG opname rond de kunstklep niet per sé betekent dat de conservatieve behandeling heeft gefaald.

In *Deel II* presenteren wij, naast dieper in te gaan op sommige van de technische aspecten van ^{18}F -FDG PET/CT en CT angiografie, de resultaten van wat meer gedetailleerde onderzoeken naar potentiële versturende factoren en de noodzaak van gestandaardiseerde kwantitatieve analyses van FDG opname, welke allen hebben bijgedragen aan de grondlegging van onze multicenterstudie die beschreven is in *Hoofdstuk 3*.

Allereerst toont *Hoofdstuk 5* een overzicht van alle studies waarin een (semi-)kwantitatieve analyse van FDG opname bij verdenking op kunstklependocarditis is verricht. Zoals genoemd in onze grootschaligere literatuurstudie (*Hoofdstuk 2*) varieerden de acquisitie- en meetmethoden enorm tussen de geïnccludeerde onderzoeken, net zoals de gerapporteerde afkapwaarden en SUV waarden van patiënten met en zonder kunstklependocarditis.¹⁶ Bovendien waren, zoals genoemd, bijna geen van deze gerapporteerde waarden verkregen uit EARL-gestandaardiseerde reconstructies, waardoor ze praktisch ontoepasbaar zijn in enig ander centrum en op enige andere scanner, zelfs als deze van dezelfde fabrikant is.

Als tweede gaan wij in *Hoofdstuk 6* in op een kleiner prospectief onderzoek waarin we hebben gekeken naar het acquisitieprotocol van de PET/CT welke eigenlijk, behoudens de eerdergenoemde patiëntvoorbereidingen, direct is overgenomen van het standaard oncologische scanprotocol. In dit standaardprotocol wordt ^{18}F -FDG toegediend aan de patiënt, waarna eerst een rustperiode van 60 minuten in acht wordt genomen om optimale verdeling van het FDG door het lichaam te waarborgen om vervolgens de scan te maken. Echter is door enkele auteurs van eerdere onderzoeken naar PET/CT bij mogelijke kunstklependocarditis gesuggereerd dat een vroegere of juist latere acquisitietiming beter zou kunnen zijn voor de detectie van infectie en ontsteking, waarbij de theorie van een eventuele vroegere acquisitie gebaseerd is op de mogelijke snellere instroom van radioactief gelabeld glucose in ontstekingscellen welke gevolgd wordt door een uitstroom die gemedieerd wordt door geactiveerde glucose-t-fosfatase, terwijl de theorie van een latere acquisitie gebaseerd is op de blijvende continue instroom in ontstekingscellen en verdere klaring van het radio-actieve glucose uit de bloedbaan wat resulteert in een hoger contrast tussen activiteit in infectieuze foci en de zogenoemde 'achtergrond'.^{21,22} In ons onderzoek, waarin we een late opname 150 minuten na toediening van de radioactieve tracer hebben *toegevoegd* (dual-time-point acquisitie²³), werden 14 scans die verricht werden voor verdenking van kunstklependocarditis geïnccludeerd. Hoewel in één geval een fout-negatieve vroege scan correct positief werd bij de late acquisitie, waren de laat verkregen beelden over het algemeen meer vatbaar voor fout-positieve misinterpretatie bij zowel visuele als semi-kwantitatieve analyse, wat resulteerde in onze aanbeveling om deze beelden bedachtzaam te interpreteren.

Als derde presenteren wij in *Hoofdstuk 7* een van onze eerdere onderzoeken naar mogelijke versturende factoren bij ^{18}F -FDG PET/CT beeldvorming van kunstklependocarditis, welke de fundering hebben gelegd voor verscheidene studies nadien, waaronder onze eigen multicenter studie (*Hoofdstuk 3*) waarin onze analyse naar versturende factoren was gebaseerd op de potentiële confounders die wij in deze serie van casus voor het eerst hebben beschreven. Aangezien de grenzen tussen wat als normaal en abnormaal moest worden beschouwd destijds, en nu nog steeds, relatief ongedefinieerd waren (en zijn), hebben wij in dit artikel een aantal bijzonderheden gepresenteerd die zouden kunnen leiden tot een foutieve diagnose, zoals bijvoorbeeld niet-onderdrukte

myocardiale FDG opname, bepaalde inflammatoire maar niet infectieuze vormen van FDG opname, andere oorzaken van verhoogde FDG opname in de regio van kunstkleppen zoals bijvoorbeeld boezemfibrilleren of lipomateuze atriumseptumhypertrofie, als ook het negatieve versturende effect van langdurige antibiotische behandeling en een mogelijke fout-negatieve beoordeling ten gevolge van geïsoleerde vegetaties.

Ter afsluiting van dit deel hebben wij in **Hoofdstuk 8** een nieuw zelf-ontwikkeld CT acquisitieprotocol voor een uitgebreide beoordeling van kunstkleppen met een relatief beperkte stralingsdosis gepresenteerd. In dit onderzoek werden 43 opeenvolgende patiënten die een CT angiografie ondergingen voor beoordeling van kunstklepdysfunctie of -infectie prospectief geïnccludeerd. Drie acquisities werden vergaard: een scan zonder contrast, een scan met contrast in de arteriële fase met reconstructies van elke 5% van het R-R interval, en een late hoge-snelheidsscan met contrast van de gehele borstkas. De scan zonder contrast was vooral nuttig bij het identificeren van calcificaties op de kleppen en bepaalde hechtingsmaterialen (en het onderscheid hiervan maken met bepaalde contrasthoudende perivalvulaire uitbreidingen), terwijl de late-fase acquisitie van de gehele thorax het mogelijk maakte om abscessen en septische longembolieën, als ook de algehele anatomie van de thorax af te beelden.

In tegenstelling tot retrospectieve ECG-*gating* wat door de meeste voorgaande studies werd gebruikt voor de scan met contrast in de arteriële fase, hebben wij ervoor gekozen om prospectieve ECG-*triggering* te gebruiken.²⁴ Met behulp van verscheidende stralingsdosisreducerende technieken die tegenwoordig beschikbaar zijn op de derde generatie van dual-source CT-scanners, waaronder iteratieve reconstructie²⁵, waren wij in staat om de gemiddelde totale stralingsdosis van de acquisitie met contrast hiermee significant te verlagen terwijl de mogelijkheid van een dynamische beoordeling van de kunstklep en klepbladbewegingen behouden werd: in vergelijking met de gemiddelde stralingsdosis in voorgaande studies reikend van 11.6 tot 18.8 mSv was de gemiddelde stralingsdosis van onze ECG-*triggered* scan met contrast 6.7 mSv. Onze gemiddelde beeldkwaliteitsscore was daarbij goed tot uitstekend (4.1 uit 5 voor de scan zonder contrast, 4.7 uit 5 voor de scan met arterieel contrast en 4.2 uit 5 voor de late acquisitie), met een totale gemiddelde beeldkwaliteitsscore van 4.3 uit 5. De gemiddelde totale stralingsdosis van de gehele drie-fasen acquisitie was 8.3 mSv, wat met het oog op de risico's van de mogelijke onderliggende pathologie en de omvang van niet onwaarschijnlijke behandelconsequenties acceptabel zou kunnen worden geacht.

Tenslotte hebben wij in *Deel III* gekeken naar de rol van CT angiografie bij de routine follow-up na hartklep- en aorta ascendenschirurgie, met name wat betreft de definiëring van het spectrum van wat normale bevindingen kunnen zijn kort en langere tijd na vervanging van de aortaklep en aorta ascendens. Daarnaast hebben we gekeken naar de mogelijkheden van deze beeldvormingstechniek om verscheidene mogelijke complicaties van deze operatie in beeld te brengen.

In *Hoofdstuk 9* presenteren wij de resultaten van ons onderzoek omtrent een fenomeen wat beschreven wordt als 'induratie' of 'aankleuring' van het omliggende vetweefsel rondom de aortakunstklep en aorta ascendens, wat meestal veroorzaakt wordt door een steriele ontsteking met oedeem maar ook een teken kan zijn van prothese-infectie. Het doel van deze studie was om de hoeveelheid en het uiterlijk van dit peri-aortale vocht op CT vroeg na gecombineerde aortaklep- en aorta ascendensvervanging (de zogenoemde Bentall-procedure) te vergelijken tussen patiënten met ofwel een ongecompliceerde danwel een gecompliceerde procedure en verder beloop.

Vierennegentig scans die verricht waren binnen 3 maanden na een Bentall-procedure hebben we retrospectief geïnccludeerd, waarna we de patiënten hebben onderverdeeld in de ongecompliceerde of gecompliceerde groep op basis van het optreden van Bentall-gerelateerde complicaties of overlijden binnen 1 jaar na operatie. Hierbij vonden we dat diffuse aankleuring, in tegenstelling tot meer georganiseerde en duidelijker begrensde vochtophopingen welke vaak berusten op hematomen, op bijna alle scans aanwezig was. Bij de patiënten met een ongecompliceerde procedure en 1-jaars beloop, bedroeg de gemiddelde omvang van dit vocht in de tweede en derde postoperatieve maand 7.7mm vanaf de omtrek van de aorta. Wanneer er geen tekenen waren van bijkomende vochtcollecties zoals hematomen of abscessen, was de hoeveelheid geïsoleerde induratie niet significant verschillend tussen de gecompliceerde en de ongecompliceerde, met een maximum gemeten aankleuring tot 17mm in de ongecompliceerde groep.

Deze resultaten zijn voornamelijk van belang bij de beoordeling van patiënten met recent geïmplanteerde volledige aorta ascendensprothesen die verdacht worden van een vroege prothese-infectie, omdat diffuus cirkelvormig oedeem wat voorheen vaak als teken van infectie werd gezien dus met voorzichtigheid moet worden geïnterpreteerd. Hoewel onze resultaten suggereerden dat er een geleidelijke afname van deze aankleuring optrad (-0.038mm induratie vanaf de omtrek van de aorta per dag, $R=0.02$), was deze trend niet statistisch significant en helaas ook niet gebaseerd op sequentiële metingen binnen dezelfde patiënt.

Als afsluiting laten we in *Hoofdstuk 10* een uitgebreid overzicht zien van het spectrum van mogelijke normale varianten die kunnen worden gezien op postoperatieve CT-beelden van aortakunstkleppen, aortaprothesen en andere chirurgische materialen, waarvan kennis van groot belang is om deze goed van complicaties te kunnen onderscheiden en een foutieve diagnose te voorkomen. Daarna presenteren wij voorbeelden van echte casuïstiek van verscheidene mogelijke complicaties zoals: degeneratie of obstructie van mechanische klepbladen door trombus of pannus; perforaties en fistelvorming; laesies aan de kransslagaders of eventuele omleidingen met myocardinfarcten tot gevolg; vochtcollecties zoals hematomen of abscessen en de mogelijke verdrinking van omliggende structuren hierdoor; afwijkingen aan de native aorta zoals eventuele residuële dissecties; en uiteraard kunstklependocarditis en al diens mogelijke complicaties.

Conclusies

Concluderend zijn ^{18}F -FDG PET/CT en CT angiografie beiden zeer belangrijke toevoegingen aan de diagnostische work-up van patiënten die verdacht worden van kunstklependocarditis. De diagnostische nauwkeurigheid van ^{18}F -FDG PET/CT voor het detecteren van ontsteking, zelfs vóórdat structurele schade optreedt, is zeer hoog, mits het wordt ingezet in een vroeg stadium van het ziektebeeld, waardoor tijdig met antibiotische behandeling kan worden gestart en patiënten mogelijk een zeer hoog-risico heroperatie kan worden bespaard.

In dit proefschrift hebben we enkele factoren gevonden die mee moeten worden genomen bij de vergaring en beoordeling van ^{18}F -FDG PET/CT en CT angiografie beelden bij patiënten met een verdenking op kunstklependocarditis, waarvan lage ontstekingsactiviteit ten gevolge van langdurige antibiotische behandeling en het gebruik van bepaalde chirurgische lijmstoffen de belangrijkste zijn. We konden de aanbeveling van de richtlijnen om geen ^{18}F -FDG PET/CT te verrichten binnen 3 maanden na klepimplantatie –in verband met het mogelijke versturende effect van postoperatieve ontsteking– echter niet ondersteunen, daar wij geen aanwijzingen hebben gevonden dat recente klepchirurgie meer fout-positieve scan interpretaties veroorzaakte.

Daarnaast hebben we laten zien dat kwantitatieve beoordeling van ^{18}F -FDG PET/CT het voordeel heeft minder beoordelaarsafhankelijk te zijn, en dat dit bij elke scan die verkregen wordt voor verdenking op kunstklependocarditis zou moeten worden verricht, mits de opname van FDG op een gestandaardiseerde manier gemeten wordt op gekalibreerde reconstructies. Met in acht neming van de bovengenoemde confounders, vonden we dat een verhouding tussen de opname rond de kunstklep en de achtergrond opname in de bloedbaan (de $\text{SUV}_{\text{ratio}}$) van ≥ 2.0 een 100% sensitieve en 91% specifieke voorspeller was van kunstklependocarditis.

Tenslotte hebben we laten zien dat cardiale CT angiografie een onmisbaar middel is bij de beoordeling van patiënten met mogelijke (of zelfs bewezen) kunstklependocarditis. En hoewel het echocardiografie niet kan (en ook niet zou moeten) vervangen vangt CT angiografie, wetende wat het onderscheid is tussen normale postoperatieve bevindingen en tekenen van pathologie, veel van de tekortkomingen van echocardiografie bij de beoordeling van kunstkleppen op, wat maakt dat het veel laagdrempeliger zou moeten worden ingezet in de dagelijkse klinische praktijk, zeker nu dat volledige beoordeling van kunstkleppen mogelijk is voor een acceptabele stralingsdosis.

Referenties

1. Butchart EG, Gohlke-Bärwolf C, Antunes MJ, et al. Recommendations for the management of patients after heart valve surgery. *Eur Heart J*. 2005;26:2463–71.
2. Lalani T, Chu VH, Park LP, et al. In-hospital and 1-year mortality in patients undergoing early surgery for prosthetic valve endocarditis. *JAMA Intern Med*. 2013;173:1495–504.
3. Baddour LM, Wilson WR, Bayer AS, et al. Infective endocarditis: diagnosis, antimicrobial therapy, and management of complications. *Circulation* 2005;111:e394–e434.
4. Dilsizian V, Achenbach S, Narula J. Adding or selecting imaging modalities for incremental diagnosis: a case study of 18FDG PET/CT in prosthetic valve endocarditis. *JACC Cardiovasc Imaging* 2013;6:1020–1021.
5. Habib G, Lancellotti P, Antunes MJ, et al. 2015 ESC Guidelines for the management of infective endocarditis: The Task Force for the Management of Infective Endocarditis of the European Society of Cardiology (ESC). *Eur Heart J*. 2015;36:3075–128.
6. Gomes A, Glaudemans AW, Touw DJ, et al. Diagnostic value of imaging in infective endocarditis: a systematic review. *Lancet Infect Dis*. 2017;17:e1–e14.
7. Tiwari B, Kand P. Myocardial uptake of F-18-fluorodeoxyglucose in whole body positron emission tomography studies. *Indian J Nucl Med*. 2012;27:69.
8. Harisankar CNB, Mittal BR, Agrawal KL, et al. Utility of high fat and low carbohydrate diet in suppressing myocardial FDG uptake. *J Nucl Cardiol*. 2011;18:926–936.
9. Morooka M, Moroi M, Uno K, et al. Long fasting is effective in inhibiting physiological myocardial 18F-FDG uptake and for evaluating active lesions of cardiac sarcoidosis. *EJNMMI Res*. 2014;4:1.
10. Scholtens AM, Verberne HJ, Budde RPJ, Lam M. Additional heparin preadministration improves cardiac glucose metabolism suppression over low carbohydrate diet alone in 18F-FDG-PET imaging. *J Nucl Med*. 2016;57:568–74.
11. Schouten LR, Verberne HJ, Bouma BJ, et al. Surgical glue for repair of the aortic root as a possible explanation for increased F-18 FDG uptake. *J Nucl Cardiol*. 2008;15:146–7.
12. Scholtens AM, van Aarnhem EE, Budde RP. Effect of antibiotics on FDG-PET/CT imaging of prosthetic heart valve endocarditis. *Eur Heart J Cardiovasc Imaging*. 2015;16:1223.
13. Tanis W, Scholtens AM, Habets J, et al. CT angiography and ¹⁸F-FDG-PET fusion imaging for prosthetic heart valve endocarditis. *JACC Cardiovasc Imaging*. 2013;6:1008–13.
14. Botelho-Nevers E, Thuny F, Casalta JP, et al. Dramatic reduction in infective endocarditis-related mortality with a management-based approach. *Arch Intern Med*. 2009;169:1290–8.
15. Chirillo F, Scotton P, Rocco F, et al. Impact of a multidisciplinary management strategy on the outcome of patients with native valve infective endocarditis. *Am J Cardiol*. 2013;112:1171–6.
16. Swart LE, Scholtens AM, Tanis W, et al. 18F-fluorodeoxyglucose positron emission/computed tomography and computed tomography angiography in prosthetic heart valve endocarditis: from guidelines to clinical practice. *Eur Heart J*. 2018. doi: 10.1093/eurheartj/ehx784.

17. Scholtens AM, Swart LE, Kolste HJ, et al. Standardized uptake values in FDG PET/CT for prosthetic heart valve endocarditis: a call for standardization. *J Nucl Cardiol*. 2017. doi: 10.1007/s12350-017-0932-x.
18. Kaalep A, Sera T, Oyen W, et al. EANM/EARL FDG-PET/CT accreditation - summary results from the first 200 accredited imaging systems. *Eur J Nucl Med Mol Imaging*. 2018;45:412–22.
19. Mathieu C, Mikail N, Benali K, et al. Characterization of 18F-fluorodeoxyglucose uptake pattern in noninfected prosthetic heart valves. *Circ Cardiovasc Imaging*. 2017;10:e005585.
20. Van Riet J, Hill EE, Gheysens O, et al. (18)F-FDG PET/CT for early detection of embolism and metastatic infection in patients with infective endocarditis. *Eur J Nucl Med Mol Imaging*. 2010;37:1189–97.
21. Caldarella C, Leccisotti L, Treglia G, Giordano A. Which is the optimal acquisition time for FDG PET/CT imaging in patients with infective endocarditis? *J Nucl Cardiol*. 2013;20:307–9.
22. Leccisotti L, Perna F, Lago M, et al. Cardiovascular implantable electronic device infection: delayed vs standard FDG PET-CT imaging. *J Nucl Cardiol*. 2014;21:622–32.
23. Jamar F, Buscombe J, Chiti A, et al. EANM/SNMMI guideline for 18F-FDG use in inflammation and infection. *J Nucl Med*. 2013;54:647–58.
24. Suchá D, Symersky P, van den Brink RB, et al. Diagnostic evaluation and treatment strategy in patients with suspected prosthetic heart valve dysfunction: The incremental value of MDCT. *J Cardiovasc Comput Tomogr*. 2016;10:398–406.
25. Habets J, Symersky P, de Mol BA, et al. A novel iterative reconstruction algorithm allows reduced dose multidetector-row CT imaging of mechanical prosthetic heart valves. *Int J Cardiovasc Imaging*. 2012;28:1567–75.



PORTFOLIO



List of publications

Thesis-related publications

- ◆ Scholtens AM, **Swart LE**, Verberne HJ, Tanis W, Lam MG, Budde RP. Confounders in FDG-PET/CT Imaging of Suspected Prosthetic Valve Endocarditis. *JACC Cardiovasc Imaging*. 2016;9:1462-5.
- ◆ **Swart LE**, Scholtens AM, Liesting C, van Mieghem NM, Krestin GP, Roos-Hesselink JW, Budde RPJ. Serial ¹⁸F-fluorodeoxyglucose positron emission tomography/CT angiography in transcatheter-implanted aortic valve endocarditis. *Eur Heart J*. 2016;37:3059.
- ◆ Scholtens AM, **Swart LE**, Verberne HJ, Budde RP, Lam MG. Dual-time-point FDG PET/CT imaging in prosthetic heart valve endocarditis. *J Nucl Cardiol*. 2018;25:1960-7.
- ◆ Scholtens AM, **Swart LE**, Kolste HJ, Budde RP, Lam MG, Verberne HJ. Standardized uptake values in FDG PET/CT for prosthetic heart valve endocarditis: a call for standardization. *J Nucl Cardiol*. 2018;25:2084-91.
- ◆ **Swart LE**¹, Boccacini S¹, Bekkers JA, Nieman K, Krestin GP, Bogers AJ, Budde RP. Peri-aortic fluid after surgery on the ascending aorta: Worrisome indicator of complications or innocent postoperative finding? *Eur J Radiol*. 2017;95:332-41.
- ◆ Faure ME, **Swart LE**, Dijkshoorn ML, Bekkers JA, van Straten M, Nieman K, Parizel PM, Krestin GP, Budde RP. Advanced CT acquisition protocol with a third-generation dual-source CT scanner and iterative reconstruction technique for comprehensive prosthetic heart valve assessment. *Eur Radiol*. 2018;28:2159-68.
- ◆ **Swart LE**, Scholtens AM, Tanis W, Nieman K, Bogers AJ, Verzijlbergen FJ, Krestin GP, Roos-Hesselink JW, Budde RP. ¹⁸F-fluorodeoxyglucose positron emission/computed tomography and computed tomography angiography in prosthetic heart valve endocarditis: from guidelines to clinical practice. *Eur Heart J*. 2018;39:3739-49.
- ◆ **Swart LE**, Roos-Hesselink JW, Valkema R, Schurink CA, Budde RP. Hybrid ¹⁸F-fluorodeoxyglucose positron emission tomography/CT angiography in percutaneous pulmonary prosthetic valve endocarditis. *Eur Heart J Cardiovasc Imaging*. 2018;19:1188-9.
- ◆ **Swart LE**¹, Gomes A¹, Scholtens AM¹, Sinha B, Tanis W, Lam MG, van der Vlugt MJ, Streukens SA, Aarntzen EH, Bucerius J, van Assen S, Bleeker-Rovers CP, van Geel PP, Krestin GP, van Melle JP, Roos-Hesselink JW, Slart RH², Glaudemans AW², Budde RP². Improving the Diagnostic Performance of ¹⁸F-FDG PET/CT in Prosthetic Heart Valve Endocarditis. *Circulation*. 2018;138:1412-27.

- ◆ **Swart LE**¹, Boccalini S¹, Bekkers JA, Nieman K, Krestin GP, Bogers AJ, Budde RP. CT angiography for depiction of complications after the Bentall procedure. *Br J Radiol.* 2018. doi: 10.1259/bjr.20180226.

Other publications

- ◆ **Swart LE**, Tuininga YS. A rare case of narrow QRS complex tachycardia. *Neth Heart J.* 2014;22:573-4.
- ◆ Chelu RG, van den Bosch AE, van Kranenburg M, Hsiao A, van den Hoven AT, Ouhlous M, Budde RP, Beniast KM, **Swart LE**, Coenen A, Lubbers MM, Wielopolski PA, Vasanawala SS, Roos-Hesselink JW, Nieman K. Qualitative grading of aortic regurgitation: a pilot study comparing CMR 4D flow and echocardiography. *Int J Cardiovasc Imaging.* 2016;32:301-7.
- ◆ **Swart LE**, Koster K, Torn M, Budde RP, Uijlings R. Clozapine-induced myocarditis. *Schizophr Res.* 2016;174:161-4.
- ◆ Chelu RG, Wanambiro KW, Hsiao A, **Swart LE**, Voogd T, van den Hoven AT, van Kranenburg M, Coenen A, Boccalini S, Wielopolski PA, Vogel MW, Krestin GP, Vasanawala SS, Budde RPJ, Roos-Hesselink JW, Nieman K. Cloud-processed 4D CMR flow imaging for pulmonary flow quantification. *Eur J Radiol.* 2016;85:1849-56.

PhD portfolio

Summary of PhD training and teaching activities

Name of PhD student:	L.E. Swart	PhD period:	Sep. 2014 – Mar. 2018
Erasmus MC dept.:	Radiology/Cardiology	Promotor(s):	G.P. Krestin
Research school:	COEUR		J.W. Roos-Hesselink
		Co-promotor(s):	R.P.J. Budde

PhD training

General academic skills	Year	ECTS
- Biomedical English Writing and Communication (Graduate school), Sally Hill, Erasmus MC, Rotterdam, NL	2015	3.0
- Research Integrity	2016	0.4
- BROK	2017	2.1
Research skills		
- Statistics (private sessions for COEUR students) dr. van Domburg, Erasmus MC, Rotterdam, NL	2015	1.2
In-depth courses (e.g. Research school, Medical Training)		
- Basic and Advanced Cardiac CT Course (5 day course) dr. Nieman, Erasmus MC, Rotterdam, NL	2014	3.7
- COEUR Course Cardiovascular Imaging and Diagnostics prof. dr. van der Lugt, Erasmus MC, Rotterdam, NL	2015	1.5
- COEUR Course Congenital Heart Disease prof. dr. Roos-Hesselink, Erasmus MC, Rotterdam, NL	2015	1.5
- COEUR Course Arrhythmia dr. N.M. de Groot, Erasmus MC, Rotterdam, NL	2016	1.5
- Advanced Life Support Opleidingsinstituut Spoedeisende Geneeskunde, Houten, NL	2018	4.0
- Fundamental Critical Care Support (NVIC) Opleidingsinstituut Spoedeisende Geneeskunde, Houten, NL	2018	4.0

Presentations

- Assessment of PHV by PET/CT in patients without PVE. ESCR Cardiac Imaging 2015, Vienna, Austria (scientific)	2015	0.4
- ¹⁸ F-FDG PET/CT for Prosthetic Heart Valve Endocarditis: Surmounting the insurmountable diagnostic difficulties. RSNA 2015, Chicago, USA (educational)	2015	0.4
- "The PROSPECTA study", UMCU, Utrecht, NL (January 18 th)	2016	0.4
- Educational at the "Wetenschapsavond" of the department of cardiothoracic surgery, AMC, Amsterdam, NL (March 9 th)	2016	0.4
- Educational at the "Echo-avond" of the department of cardiology, Albert Schweitzer Hospital, Dordrecht, NL (May 19 th)	2016	0.4
- Educational at the "Regionale refereeravond cardiale beeldvorming", Diaconessenhuis, Utrecht, NL (June 29 th)	2016	0.4
- Educational at the "WES symposium 'are you sepsis-proof?'" , De Doelen, Rotterdam, NL (March 10 th)	2017	0.4
- Peri-aortic fluid on CTA after Bentall. ECR 2017, Vienna, Austria (educational)	2017	0.4
- Educational at the "Beeldvormingsavond Multi-modality Imaging", CVOI, Utrecht, NL (June 7 th)	2017	0.4
- Educational at the "Endocarditis symposium" in honor of the Ph.D. graduation of dr. van Valen, Erasmus MC, Rotterdam, NL (October 25 th)	2017	0.4
- "The Endocarditis Team", UMCG, Groningen, NL (November 27 th)	2017	0.4
- Improving the diagnostic performance of PET/CT in suspected PVE. Refereeravond CCR, Rotterdam, NL (October 4 th)	2018	0.4
- Results of the first 100 patients referred to the Endocarditis Team. Refereeravond MMB, Rotterdam, NL (October 11 th)	2018	0.4
- Earl-standardized PETCT in suspected Prosthetic Heart Valve Endocarditis. EANM 2018, Düsseldorf, Germany (scientific)	2018	0.4
- Improving the diagnostic performance of PET/CT in suspected PVE. RSNA 2018, Chicago, USA (scientific)	2018	0.4

International conferences

- ESCR Cardiac Imaging 2015, Vienna, Austria	2015	0.9
- RSNA 2015, Chicago, USA	2015	1.8
- ECR 2017, Vienna, Austria	2017	1.5

Seminars and workshops

- | | | |
|--|------|-----|
| - New imaging strategies for the detection of atherosclerosis, prof. dr. M. de Jong, Erasmus MC, Rotterdam, NL | 2014 | 0.2 |
| - Symposium aortic imaging
dr. Cozijnsen, Gelre Ziekenhuizen, Apeldoorn, NL | 2015 | 0.2 |
| - CVOI Symposium Cardiovascular Imaging, CVOI, Utrecht, NL | 2015 | 0.2 |
| - Secondary prevention with anti-thrombotics Seminar
prof. dr. van Geuns, Erasmus MC, Rotterdam, NL | 2015 | 0.2 |
| - Symposium ultra-low dose cardiopulmonary CT with Iterative Reconstruction, dr. Willeminck, UMCU, Utrecht, NL | 2015 | 0.2 |

Didactic skills

- | | | |
|---|------|-----|
| - Course "omgaan met groepen" for tutors of 1 st year medical students, G. Jansen, Erasmus MC, Rotterdam, NL | 2016 | 0.4 |
|---|------|-----|

Other

- | | | |
|---|--------------|-----|
| - Member of the scientific editorial board, European Radiology, (18 external reviews) | 2015
2018 | 3.2 |
|---|--------------|-----|

Teaching activities

Lecturing	Year	ECTS
- Education for residents in cardiology, Erasmus MC, Rotterdam, NL (staflunch, May 23 rd)	2016	0.4
- Education for residents in radiology, Erasmus MC, Rotterdam, NL (2x, Sept. 5 th and 6 th)	2016	0.4
- Education for 2 nd year cardiology ("keuzeproject") students (Cardiac MRI), Erasmus MC, Rotterdam, NL	2016	0.4
- Education for 2 nd year cardiology ("keuzeproject") students (Cardiac MRI), Erasmus MC, Rotterdam, NL	2017	0.4
- Education for 3 rd year cardiology minor students (Endocarditis), Erasmus MC, Rotterdam, NL	2016	0.4
- Education for 3 rd year cardiology minor students (Endocarditis), Erasmus MC, Rotterdam, NL	2017	0.4
- Education for 3 rd year cardiology minor students (Endocarditis), Erasmus MC, Rotterdam, NL	2018	0.4
Supervising practicals and excursions		
- Cardiac CT Course, 2h case-reading workshop on Cardiac CT, <i>dr. Nieman</i> , Erasmus MC, Rotterdam, NL	2015	1.5
- Cardiac CT Course, 2h case-reading workshop on Cardiac CT, <i>dr. Nieman</i> , Erasmus MC, Rotterdam, NL (2 sessions)	2016	3.0
- Cardiac CT Course, 2h case-reading workshop on Cardiac CT, <i>dr. Budde</i> , Erasmus MC, Rotterdam, NL (3 sessions)	2017	4.5
- Cardiac CT Course, 2h case-reading workshop on Cardiac CT, <i>dr. Budde</i> , Erasmus MC, Rotterdam, NL (2 sessions, February)	2018	3.0
- Cardiac CT Course, 2h case-reading workshop on Cardiac CT, <i>dr. Budde</i> , Erasmus MC, Rotterdam, NL (2 sessions, October)	2018	3.0
Other		
- Supervising 2nd year medicine students ("keuzeproject cardiologie") in writing a systematic review	2016	0.9
- Supervising (tutoring) 1st year medicine students during the first 6 months of their freshman year.	2016	2.8
- Supervising 2nd year medicine students ("keuzeproject cardiologie") in writing a systematic review	2017	0.9
- Supervising (tutoring) 1st year medicine students during the first 6 months of their freshman year.	2017	2.8
Total ECTS		62.9



ABOUT THE AUTHOR

Curriculum vitae



About the author

Laurens Emile Swart was born on March 12th, 1990 in Deventer, the Netherlands. After graduating from high school cum laude (Ettly Hillesum Lyceum, Deventer), he studied medicine at the University of Groningen. In the last year of his medical training, he followed a research internship at the department of cardiology of the Deventer Ziekenhuis, during which he investigated the reliability of adenosine-stress perfusion cardiac MRI. After acquiring his degree, he started working as a resident in cardiology at the same hospital. In 2014, he moved to pursue a Ph.D. in the field of imaging of prosthetic heart valve endocarditis at the Erasmus University, Rotterdam. Under supervision of dr. Ricardo Budde, prof. Jolien Roos-Hesselink and prof. Gabriel Krestin, he had the opportunity to investigate the value and possible improvement of new imaging techniques in this intricate disease and to present his work, put forward in this thesis, at several international conferences and publish it in internationally peer-reviewed journals. Following the completion of his thesis, he has been working as a resident at the department of cardiology of the Erasmus Medical Center and is currently in training to become a cardiologist.

